Angel Serrano Aroca

Dr. Eng. Sci. Thesis

Synthesis and characterisation of macroporous poly(methyl methacrylate) with plasma-polymerised hydrophilic coating

Valencia, Spain, 2005

Synthesis and characterisation of macroporous poly(methyl methacrylate) with plasma-polymerised hydrophilic coating

Thesis submitted by

Angel Serrano Aroca

to obtain the degree of Dr. Eng. Sci.
at the Polytechnic University of Valencia

Valencia, Spain, 2005

Thesis supervisors:
Dr. M. Monleón Pradas
Dr. J. Luis Gómez Ribelles

Thesis reporters

Dr. Jacques Rault
Université de Paris-Sud XI, CNRS (*member of the jury*)

Dr. Polykarpos Pissis
National Technical University of Athens (*member of the jury*)

Dr. Gloria Gallego Ferrer
Universidad Politécnica de Valencia (*member of the jury*)

Dr. Julio Suay Antón
Universidad Jaume I (*member of the jury*)

Dr. Manuel Salmerón Sánchez
Universidad Politécnica de Valencia (*member of the jury*)

Dr. João Mano
Universidade do Minho

Dr. José María Meseguer Dueñas
Universidad Politécnica de Valencia.

Acknowledgements:

To my thesis supervisors: Manuel Monleón Pradas and José Luis Gómez Ribelles for all their dedication and friendship.

To Ana Vidaurre Garayo, Julio Suay Anton, Manuel Salmerón Sánchez, Gloria Gallego Ferrer, Isabel Castilla Cortázar, José María Meseguer Dueñas, Jorge Más Estellés, Raúl Brígido Diego and the rest of my workmates at the Center for Biomaterials at the Polytechnic University of Valencia for their continued help and support.

To Jacques Rault for his direction and kindness at the Laboratoire de Physique des Solides, Université de Paris-Sud XI, CNRS, Orsay, France where I performed most of the DSC measurements of this thesis as an European Marie Curie fellow during the last 4 months of the year 2003.

To professors Hynek Biederman and Miroslava Trchova at Charles University in Prague for their help with some FTIR results.

To the Electronic Microscopy Service at the Polytechnic University of Valencia where the SEM micrographs were taken.

To my family and friends for their support and love.

Financial support from the Spanish Government's CICyT under projects MAT2002-04239-C03-03 and MAT2001-2678-C02-01 is acknowledged and appreciated.

Contents

Summary

In the last decades, *tissue engineering* has become one of the most promising application fields for macroporous polymers as scaffolds or three-dimensional porous matrices where cells can be cultivated. Tissue engineering is a relatively young discipline that combines materials science, biology, engineering and medicine.

The optimal chemical or physical configurations of new biomaterials as they interact with living cells to produce tissue-engineered constructs are under study by many research groups. These biomaterials can be permanent or biodegradable. They can be naturally occurring materials, synthetic materials, or hybrid materials. They need to be developed to be compatible with living systems or with living cells *in vitro* and *in vivo*.

Their design characteristics are major challenges for the field, and should be considered at a molecular chemical level. Scaffold materials must have a highly porous structure with a high surface/volume ratio to allow cell attachment. They must be stiff enough to assume and retain a given shape while retaining some pliability. They must also resist the applied tension *in vivo* while the repaired tissue is developing.

One of the ways to obtain a porous polymer is by polymerisation in the presence of a diluent. In this way, pores are formed due to the segregation of solvent from the polymer network during the polymerisation process. In this work, macroporous polymer networks of poly(methyl methacrylate) (PMMA) were synthesised by polymerisation in the presence of ethanol. In this case, in comparison with porous poly(2-hydroxyethyl acrylate) (PHEA) synthesised in the same way, pores do not collapse during the drying process and they are much larger. A series of porous and non-porous PMMA networks with different degrees of porosity and cross-linker contents were synthesised by free radical polymerisation.

Scaffolds made out of a combination of hydrophobic and hydrophilic materials seem to be more promising for tissue engineering applications. For this reason, macroporous PMMA, which is very hydrophobic, was coated with a hydrophilic polymer by plasma polymerisation. Thus, this thesis focuses on the synthesis and characterisation of a new macroporous biomaterial, which could be successfully used as scaffold for cell culture.

Macroporous PMMA was allowed to adsorb 2-hydroxyethyl acrylate monomer vapour. The absence of thermal or photoinitiators makes difficult the

initiation of the polymerisation process of the adsorbed monomer. However, by plasma treatment this problem can be solved. This method of forming a pure hydrophilic coating by plasma polymerisation is very interesting because the porosity of the scaffold hardly changes at the end of the process. Some samples can even increase its porosity because of the swelling produced after adsorbing HEA vapour. This fact is very important in cell culture where the porosity of the scaffold is essential. This plasma-polymerised poly(2-hydroxyethyl acrylate) coatings make these materials even more promising for tissue engineering due to the mechanical reinforcement and the combination of hydrophilic and hydrophobic groups in the material. It has been reported that hydrophobic groups are necessary for cell anchor and hydrophilic groups for diffusion of water.

Dynamic-Mechanical Spectroscopy (DMS) was performed in order to study the mechanical properties of these new materials and measure the reinforcement produced by the hydrophilic coating. These results show a typical biphasic system with two main relaxation transitions due to the PHEA and PMMA domains. The dynamic-mechanical spectrum shows that the materials synthesised in this work are a new kind of macroporous hydrogel with a high mechanical modulus at room temperature and able to adsorb water while keeping their mechanical properties. Takayanagi's block model was applied to these dynamic-mechanical results to characterise the biphasic behaviour of these systems.

Porosity measurements were performed to determine the volume fraction of pores in the samples before and after the plasma treatment. These results showed that macroporous PMMA with plasma-polymerised hydrophilic coating increases or decreases its porosity after the plasma treatment depending on the amount of cross-linker used in the polymerisation process. The structure and morphology of these macroporous systems were observed by Scanning Electron Microscope (SEM). The plasma-polymerised PHEA coating could also be clearly observed by this Technique.

The nature and the homogeneity of the *pl*PHEA coating was studied by Attenuated Total Reflectance Fourier Transform Infrared Spectroscopy (ATR FTIR) and Thermogravimetry Analysis (TGA). The stability of the hydrophilic coating was studied by Differential Scanning Calorimetry (DSC), ATR FTIR, TGA and immersion in water. It was found that the *pl*PHEA is very stable and only in very drastic conditions (boiling water) can suffer hydrolytic degradation.

The water sorption and diffusion properties of these biomaterials were studied by dynamic desorption, contact angle, equilibrium sorption isotherms

and immersion experiments. Thermal analysis of water in the hydrophilic layer was performed by DSC. Bulk PHEA and *pl*PHEA with different water mass fractions were studied. Crystallisation of water in *pl*PHEA was found to be faster because of having different chemical nature and being interpenetrated with the hydrophobic PMMA matrix.

All these experimental techniques suggested that the plasma-polymerised PHEA is more homogeneously interpenetrated with macroporous PMMA polymerised with 5 wt.% of ethylene glycol dimethacrylate (EGDMA).

These porous systems have been designed with the aim of finding application in biomedical engineering but there is also a broad range of fields (dialysis, seawater desalting, etc.) in which they could be very useful as well due to their large specific area and water diffusion properties.

Resumen

En estas últimas décadas, la ingeniería tisular ha llegado a ser uno de los campos de aplicación más prometedores de los polímeros macroporosos para soportes o matrices porosas tridimensionales donde las células se pueden cultivar. La ingeniería tisular es una disciplina relativamente joven que combina la ciencia de materiales, la biología, la ingeniería y la medicina.

Hay muchos grupos de investigación estudiando la óptima configuración química y física de nuevos biomateriales que interactúen con células vivas para reconstruir tejidos. Estos biomateriales pueden ser permanentes o biodegradables. También pueden ser materiales de origen natural, sintéticos o híbridos. Es necesario desarrollar estos materiales de forma que sean compatibles con los sistemas vivos o con las células vivas *in vitro* e *in vivo*.

Los mayores retos de este campo son las características de diseño que deben ser consideradas a nivel químico molecular. Los materiales soporte para cultivo celular deben de tener una estructura altamente porosa con una relación superficie/volumen que permita el anclaje celular. Deben de ser suficientemente rígidos para mantener una forma dada pero también tener flexibilidad. Deben también resistir la tensión aplicada *in vivo* mientras el tejido reparado se desarrolla.

Una de las formas de obtener un polímero poroso es mediante la polimerización en disolución. De esta forma, los poros se forman debido a la segregación de disolvente de la red polimérica durante el proceso de polimerización. En esta tesis, se han sintetizado redes poliméricas de polimetacrilato de metilo (PMMA) por polimerización en presencia de etanol. En este caso, en comparación con poliacrilato de hidroxietilo (PHEA) polimerizado de la misma forma, los poros no se colapsan durante el proceso de secado y son mucho más grandes. Se han sintetizado una serie de redes de PMMA poroso y no poroso con diferentes porosidades y contenidos de entrecruzador por polimerización radical.

Parece ser que los soportes poliméricos que están hechos a partir de una combinación de materiales hidrófilos e hidrófobos son más prometedores para las aplicaciones en ingeniería tisular. Por este motivo, PMMA macroporoso, que es muy hidrófobo, fue recubierto con un polímero hidrófilo mediante polimerización por plasma. De este modo, esta tesis se basa en la síntesis y caracterización de un nuevo biomaterial macroporoso que podría utilizarse con éxito como soporte para cultivo celular.

El PMMA macroporoso se coloca en una atmósfera saturada de vapor de monómero de acrilato de hidroxietilo. La ausencia de iniciador térmico o fotosensible hace difícil el inicio del proceso de polimerización del monómero adsorbido. Sin embargo, este problema se puede resolver mediante la polimerización por plasma. Este método en el que se forma un recubrimiento hidrófilo puro mediante polimerización por plasma es muy interesante porque la porosidad del soporte polimérico apenas cambia al final del proceso. Algunas muestras pueden incluso aumentar la porosidad debido al hinchamiento producido después de adsorber vapor de HEA. Este hecho es muy importante en cultivo celular donde la porosidad del soporte es esencial. Estos recubrimientos de poliacrilato de hidroxietilo hacen estos materiales incluso más prometedores en ingeniería tisular debido al refuerzo mecánico producido y la combinación de grupos hidrófilos e hidrófobos en el material. Se ha publicado que los grupos hidrófobos son necesarios para el anclaje de las células y los grupos hidrófilos para la difusión de agua.

Se estudia las propiedades mecánicas de estos nuevos materiales mediante espectroscopía dinámico-mecánica (DMS) para así poder medir el refuerzo producido por el recubrimiento hidrófilo. Estos resultados muestran un típico sistema bifásico con dos relajaciones principales debido a los dominios de PHEA y de PMMA. El espectro dinámico-mecánico muestra que los materiales sintetizados en esta tesis son un nuevo tipo de hidrogel macroporoso con un alto módulo mecánico a temperatura ambiente y capaz de adsorber agua manteniendo sus propiedades mecánicas. Se ha aplicado el modelo de bloques de Takayanagi a estos resultados dinámico-mecánicos para caracterizar el comportamiento bifásico de estos sistemas.

Mediante medidas de porosidad se determina la fracción en volumen de poros en las muestras antes y después del tratamiento de plasma. Estos resultados muestran que el PMMA macroporoso con recubrimiento hidrófilo aumenta o disminuye su porosidad después del tratamiento de plasma dependiendo de la cantidad de entrecruzador utilizado en el proceso de polimerización. La estructura y morfología de estos sistemas macroporosos se ha observado mediante microscopía electrónica de barrido (SEM). El recubrimiento de PHEA polimerizado por plasma puede también verse claramente con esta técnica.

Se estudia la naturaleza y homogeneidad del recubrimiento de *pl*PHEA mediante espectroscopía infrarroja ATR FTIR y análisis termogravimétrico TGA. La estabilidad de este recubrimiento hidrófilo se ha analizado mediante calorimetría diferencial de barrido (DSC), ATR FTIR, TGA e inmersión en agua. Estos resultados demuestran que el *pl*PHEA es muy estable y solo en condiciones muy drásticas como en agua hirviendo puede

sufrir degradación hidrolítica.

Se ha estudiado la absorción de agua y propiedades de difusión de estos biomateriales mediante desorción dinámica, ángulo de contacto, isotermas de adsorción de agua en equilibrio y experimentos de inmersión. Se ha medido PHEA en bloque y *pl*PHEA con diferentes contenidos de agua mediante DSC para realizar el análisis térmico del agua en el recubrimiento hidrófilo. La cristalización de agua en el *pl*PHEA es mas rápida debido a tener diferente naturaleza química y estar interpenetrada en con la matriz hidrófoba de PMMA.

Todas estas técnicas experimentales sugieren que el PHEA polimerizado por plasma está mas homogéneamente interpenetrado con el PMMA macroporoso polimerizado con 5% en peso de etilenglicol dimetacrilato (EGDMA).

Se han diseñado estos sistemas porosos con el objetivo de encontrar aplicaciones en ingeniería biomédica pero hay también otros muchos campos (diálisis, desalinización de agua de mar, etc.) donde estos materiales podrían emplearse con mucho éxito, debido a su gran área específica y propiedades de difusión.

Resum

En aquestes últimes dècades, l'enginyeria de teixits ha arribat a éser uns dels camps d'aplicació amb més futur per als polímers macroporosos utilizats com a bastides o matrius poroses tridimensionals on les cèl·lules es poden cultivar. L'enginyeria de teixits és una branca relativament jove que barreja la ciència de materials, biologia, enginyeria i medicina.

Hi ha molts grups d'investigació estudiant l'òptima configuració química i física de nous biomaterials que interactuen amb cèl·lules vives per reconstruir teixits. Aquestos biomaterials poden ser permanents o biodegradables. També poden ser materials d'origen natural, sintètics o híbrids. És necessari desenvolupar aquestos materials perquè siguen compatibles amb els sistemes vius o amb les cèl·lules vives *in vitro* e *in vivo.*

Els majors reptes d'aquest camp són les característiques de disseny que cal considerar a nivell molecular. Els materials bastides per a cultiu cel·lular han de tenir una estructura altament porosa amb una relació superfície/volum que permeta l'ancoratge cel·lular. Han de ser suficientment rígids per mantenir una forma donada però també tenir flexibilitat. Han de resistir la tensió aplicada *in vivo* mentre el teixit reparat es desenvolupa.

Una de les formes d'obtenir un polímer porós és mitjançant la polimerització en dissolució. D'aquesta manera, els porus es formen com a conseqüència de la segregació del dissolvent de la xarxa polimèrica durant el procés de polimerització. En aquesta tesi, s'han sintetitzat xarxes polimèriques de polimetacrilat de metil (PMMA) per polimerització en presència d'etanol. En aquest cas, comparant-ho amb el poliacrilat d'hidroxietil (PHEA) polimeritzat de la mateixa forma, els porus no es col·lapsen durant el procés de secat i són molt més grans. S'han sintetitzat una serie de xarxes de PMMA porós i no porós amb diferents porositats i continguts d'entrecreuador per polimerització radical.

Sembla que les bastides polimèriques que estan fets amb una combinació de materials hidròfils e hidròfobs són més interessants per a les aplicacions d'enginyeria de teixits. És per aquest motiu, que el PMMA macroporós hidròfob, és recobreix amb un polímer hidròfil mitjançant polimerització per plasma. Amb aquests antecedents, podem dir que aquesta tesi es basa en la síntesi i caracterització d'un nou biomaterial macroporós que podria emprar-se amb èxit com a suport per a cultiu cel·lular.

El PMMA macroporos es col·loca en atmòsfera saturada de vapor de monòmer d'acrilat d'hidroxietil. L'absència d'iniciador tèrmic o fotosensible fa difícil l'inici del procés de polimerització del monòmer adsorbit. Tanmateix,

aquest problema es pot resoldre mitjançant la polimerització per plasma. Aquest mètode amb el qual es forma un recobriment hidròfil pur mitjançant polimerització per plasma és molt interessant perquè la porositat del suport polimèric no canvia gaire al final del procés. Algunes mostres poden inclús augmentar la porositat degut a l'unflament produït després d'adsorbir vapor de HEA. Aquest fet és molt important en cultius cel·lulars on la porositat de la bastida és essencial. Aquestos recobriments de poliacrilat de hidroxietil li donen un valor afegit als materials degut al reforçament mecànic produït i a la combinació de grups hidròfils i hidròfobs. S'ha publicat que els grups hidròfobs són necessaris per l'ancoratge de les cèl·lules i els grups hidròfils per la difusió de l'aigua.

S'estudia les propietats mecàniques d'aquestos nous materials mitjançant espectroscòpia dinàmica-mecànica (DMS) per a així poder mesurar el reforçament produït pel recobriment hidròfil. Estos resultats mostren un típic sistema bifàsic amb dues relaxacions principals, degut als dominis de PHEA i PMMA. L'espectre dinàmic-mecànic, mostra que els materials sintetitzats en aquesta tesi son uns nous tipus d'hidrogels macroporosos amb un alt mòdul mecànic a temperatura ambient i amb la capacitat d'absorbir aigua, tot mantenint les seues propietats mecàniques. S'aplica el model de blocs de Takayanagi a aquests resultats dinàmic-mecànics per a caracteritzar el comportament bifàsic d'aquests sistemes.

Es realitza mesures de porositat per determinar la fracció en volum de porus en la mostra, abans i després del tractament de plasma. Aquestos resultats mostren que el PMMA macroporós amb recobriment hidròfil, augmenta o disminueix la seua porositat després del seu tractament de plasma, depenent de la quantitat d'entrecreuador utilitzat en el procés de polimerització. S'observa l'estructura i morfología d'aquestos sistemes macroporosos mitjançant microscòpia electrònica d'escombrada (SEM). El recobriment de PHEA polimeritzat per plasma pot veure's també clarament amb aquesta tècnica.

Mitjançant espectroscòpia infrarroja ATR FTIR i anàlisi termogravimètric (TGA), s'estudia la naturalesa i homogeneïtat del recobriment de *pl*PHEA. L'estabilitat d'aquest recobriment hidròfil s'analitza mitjançant calorimetria diferencial d'escombrada (DSC), ATR-FTIR, TGA i immersió en aigua. Es demostra que el *pl*PHEA és molt estable i solament en condicions molt dràstiques, com en aigua bollint, poden sofrir degradació hidrolítica.

S'estudia l'absorció d'aigua i propietats de difusió d'aquestos biomateriales mitjançant desorció dinámica, angle de contacte, isotermes d'adsorció d'aigua en equilibri i experiments d'immersió. Es mesura PHEA en bloc i *pl*PHEA amb diferents continguts d'aigua mitjançant DSC per realitzar

l'analisi tèrmic de l'aigua al recobriment hidròfil. La cristal·lització en el *pl*PHEA és més ràpida degut a la diferent naturalesa química i al fet d'estar interpenetrada amb la matriu hidròfoba de PMMA.

Totes aquestes tècniques experimentals suggereixen que el PHEA polimeritzat per plasma està més homogèniament interpenetrat amb el PMMA macroporós polimeritzat amb un 5% en pes d'etilenglicol dimetacrilat (EGDMA).

S'han dissenyat aquestos sistemes porosos amb l'objectiu de trobar aplicacions en enginyeria biomèdica, però hi ha també molts altres camps (diàlisi, desalinització d'aigua de mar, etc.) on estos materials podrien emprar-se amb molt d'èxit, degut a la seua gran àrea específica i propietats de difusió.

1. Introduction.

1.1. Objective.

The objective of this thesis is to develop a new macroporous material which combines the elastic properties of a hydrophobic polymer and the water sorption and diffusion of a hydrophilic coating.

These new materials have been designed with the purpose of being used in biomedical engineering as scaffolds for cell culture. Developing a polymeric scaffold is a really difficult task because many requirements have to be accomplished. They must be highly porous and have an interconnected pore structure with enough mechanical resistance at the same time. Thus, the synthesis of macroporous poly(methyl methacrylate) (PMMA) networks with different degrees of porosity and cross-linker contents with plasma-polymerised poly(2-hydroxyethyl acrylate) (*pl*PHEA) was the first goal to achieve. The characterisation of these new biomaterials was the following objective. Therefore, several experimental techniques were carried out in order to study their porosity, specific volumes, dynamic-mechanical and thermal properties, water sorption and diffusion, contact angle, thermogravimetric analysis, infrared spectroscopy and the thermal transitions of water in the hydrophilic part of these materials. Their different morphologies were observed by scanning electron microscopy.

Because of the large specific area and water diffusion properties of these biomaterials, there are other fields where this material could also be successfully employed as dialysis, seawater desalting, etc.

1.2. Poly(methyl methacrylate) as biomaterial.

In the last decade, biomaterials are an extremely attractive subject of study for chemists, physicians, biologists, pharmacists, engineers and others. This fact is due to the extension of their use to the most varied fields of medicine, biotechnology, and pharmacy. Numerous faculties of biomedical engineering are emerging in most universities around the world. Forty years ago polymers were only applied in medicine to make syringes and transfusion tubes; today they are irreplaceable in the manufacture of artificial heart valves, blood vessels, and kidney membranes.

Biomaterials are natural or synthetic materials that can be implanted in a living organism, and are used for repairing or substituting a damaged tissue. In this sense, they should mimic tissue properties as much as possible and be biocompatible at the same time. Moreover, they must not be either toxic or carcinogenic, they must be chemically stable and inert, susceptible of sterilisation and have adequate mechanical properties. Synthetic materials used for implants can be classified into metallic, ceramic, polymeric and composites. Different applications and information about biocompatibility can be found in references [1-3]

In this work, a new biomaterial made of PMMA and PHEA is studied. PMMA is a clear, colourless polymer with a glass transition temperature above 100°C. Due to its optical properties (exceptional transparency), remarkable behaviour in time, brilliance, easy thermoformation and easy welding, is extensively used as biomaterial in stomatology, bone cementation, intraocular lenses, contact lenses and in fixation of articular prostheses. [1]. PHEA is a polymer hydrogel (see section 1.3).

1.3. Polymer Hydrogels.

Polymer hydrogels are hydrophilic polymer networks that are able to absorb large amounts of water, which can exceed their own weight. However, they are insoluble in water due to chemical or physical cross-links between polymer chains. Synthetic polymer hydrogels have been proposed for many biomedical applications [4-9] due to their good biocompatibility and water permeation properties. Biocompatibility is mainly due to the great sorption of water, which acts as a medium for transport of gases and nutrients and gives similar surface properties to those of the living tissue minimising surface energy differences. Hydrophilicity is due to the presence of molecular groups able to form hydrogen bonds with water: –OH, –COOH, –CONH, $–CONH_2$, $–SO_3H$, etc.

Hydrogels are non-toxic materials, chemically stable, with a low surface tension in aqueous or biological media. Sterilisation before implanting is an easy task due to their high water permeability.

Poly(2-hydroxyethyl methacrylate) (PHEMA) is probably the most studied of all the hydrophilic polymers employed in the biomedical industry. This hydrogel has many biomedical applications: contact lenses, biosensor coating, controlled drug delivery, blood vessel replacement, wound drainage, soft tissue replacements, cell culture, etc. PHEMA is only one of several acrylic type polymers used to produce hydrogels for biomedical devices. Some other

examples of hydrophilic polymers similar in general structure to PHEMA are poly(hydroxyethoxyethyl methacrylate) (PHEEMA), poly(hydroxydiethoxyethyl methacrylate) (PHDEEMA), poly(methoxyethyl methacrylate) (PMEMA), poly(methoxyethoxyethyl methacrylate) (PMEEMA), poly(methoxydiethoxyethyl methacrylate) (PMDEEMA), poly(ethylene glycol dimethacrylate) (PEGDMA) and poly(2-hydroxyethyl acrylate) (PHEA). The hydrogel used in this work (PHEA) is able to absorb more water than PHEMA but its mechanical properties are worse. The water sorption and dynamic-mechanical properties of bulk PHEA with different cross-linking densities were studied in reference [10].

Other common hydrophilic polymers used in biomedical engineering are poly(vinyl alcohol) (PVA), poly(ethylene oxide) (PEO), poly(carboxylic acids) as poly(acrylic acid) (PAA) and poly(methacrylic acid) (PMAA), and Poly(*N*-vinyl-2-pyrollidone) (PNVP). PVA is employed in controlled drug delivery, degradable suture threads, modifying contact lenses surfaces, artificial cartilage, artificial skin, dialysis membranes, etc. PEO is utilised in vascular grafts, contraceptive devices, controlled drug delivery, membranes, surface modifiers to improve biocompatibility, etc. Poly(carboxylic acids) are employed as part of spermicide gels, laxative systems and as dispersing agents in several pharmaceutical products. PNVP is used as coating in implants, in controlled drug delivery and immobilisation of enzymes.

The preceding examples are, by far, the most commonly encountered hydrophilic polymers in the biomedical industry. However, there are a number of other hydrophilic materials that have been under research for possible use in the manufacture of medical devices. For instance, poly(sulfonic acids), which exhibit a high degree of solubility, can be made to be superabsorbent. Examples include poly(acrylamidemethylpropane sulfonic acid), poly(styrene sulfonic acid), and poly(vinyl sulfonic acid). Poly(acrylonitrile) (PAN) is employed to form hydrogels and IPNs for drug delivery and immobilisation of other materials (synthetic and naturally occurring hydrophilic polymers, enzymes, etc.). Some general types include poly(acrylamide), poly(N-alkylacrylamides) and poly(methacrylamide). Polyuretahanes find extensive use in the production of hydrophilic microporous gel systems. These systems contain large amounts of PEO (i.e., a polyether) in their matrix structure, which imparts hydrophilicity to the gels thus formed. By varying the types of the ether glycols used to form the final cross-linked system, the desirable balance of hydrophilic and mechanical properties can be obtained. More information about hydrogels (chemistry, preparation techniques, types, physic properties, etc.) can be found in references [4, 11, 12].

1.4. Porous polymers.

Porous polymers have many applications and they have received increasing attention in the last years. Macroporous hydrogels are used as superabsorbent materials with applications in wound dressing, diapers and sanitary towels [13, 14], and in agriculture as controllers of ground humidity [15]. Polymers utilised as cell microcarriers to segregate therapeutic substances [16] and systems for controlled drug delivery [17] are also in need of a porous structure to allow the interchange of segregated substances. Porous polymers are also used as semipermeable membranes in dialysis, seawater desalting, etc [18].

Macroporous polymers, employed as scaffolds in cell culture, are a very promising application field of biomedical engineering. The most common polymers used in this kind of applications are the poly(α-hydroxy esters) as polylactic acid (PLA) and polyglycolic acid (PGA), polycaprolactone (PCL) and naturally occurring polymers as chitosane [19] and alginate [20]. Poly(α-hydroxy esters) are able to biodegrade in the living organism [21]. PCL has a much slower degradation rate than the poly(α-hydroxy esters) and is used as pure polymer or copolymerised with PLA or PGA. Hydrogels also find application in this field and much research has been done about porous PHEMA by Chirila and his research group. A PHEMA sponge for axonal regeneration was prepared in reference [22]. This material is also proposed as anchorage ring of a cornea prosthesis in references [23, 24] where ingrowth and colonisation of cells from the surrounding tissue is required to obtain an adequate fixation. Porous PHEMA as scaffold for cartilage regeneration have been also studied by Corkhill *et al.* [25]. Poly(*N*-(2-hydroxypropyl) methacrylamide)) (PHPMA), agarose hydrogel [26] and PEO [27] have been proposed for axonal regeneration. Gelatine has good properties for bone regeneration [26, 28]. Other non-degradable polymers have been utilised as scaffolds for cell culture [29-31].

Scaffolds made of a combination of hydrophobic and hydrophilic materials seem to be more suitable in cell culture [32-36]. Hydrophobic groups improve cell anchor and hydrophilic groups make easier water diffusion. For this reason, in this work, macroporous PMMA, which is very hydrophobous, was coated with a plasma-polymerised hydrophilic layer of PHEA. This coating was formed following a particular method of plasma polymerisation.

Porous polymers can be prepared with the use of sparkling agents [37], fibres joined together forming a mesh [38], salt particles or glass microspheres as porogen agent [39], the solvent exchange method [40, 41], the

freeze thaw technique [42, 43], thermally induced phase separation [44], microemulsion continuous phase polymerisation [45], fused deposition modelling [46] and polymerisation in the presence of solvents [47], which is the technique used in this thesis and is described in detail in the following paragraph.

By polymerisation in the presence of a diluent, pores are formed due to the segregation of solvent from the polymer network during the polymerisation process. After this phase separation, the solvent is evaporated and a porous polymer network is obtained. Formation mechanisms of porous polymers are not completely understood and their explanations are qualitative. In 1967 a theoretical approach to the problem based on the Flory-Huggins theory and rubber elasticity was published by Dušek [48, 49]. According to Dušek [49], phase separation occurring during the polymerisation process is called 'syneresis'. In the presence of a good solvent of the polymer, one phase consists of the swollen polymer network with equilibrium solvent content and the other phase of pure solvent that has been segregated from the network. The solvent is segregated because the cross-linked polymer has an equilibrium maximum expansion degree determined by the number of monomeric units between cross-links. In the presence of a bad solvent of the polymer, phase separation happens due to a change in the nature of the interaction among the system species (from monomer-solvent to polymer-solvent). The Flory-Huggins parameter χ, which changes as the polymer is formed, is determinant in this phenomenon. Whatever the mechanism is, phase separation can happen as 'macrosyneresis' or as 'microsyneresis'. *Macrosyneresis* is related to the unswelling of the growing polymer network when phase separation occurs. The system is transformed into a suspension of polymer spherical particles diffused in a liquid phase formed by unreacted monomer and solvent. When polymerisation progresses, new particles are generated and tend to join together with those formed before. Cross-linking between particles can also be produced. Finally, two continuous phases exist, one of them formed by connected polymer spherical particles and the other by solvent. An example of macrosyneresis with a macroporous PMMA sample synthesised in this work is shown in Figure 1.1.

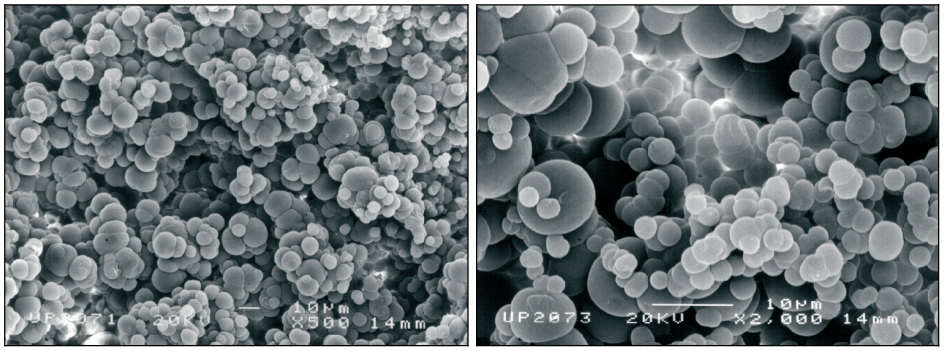

x500 x2000

Figure 1.1. Example of macrosyneresis. Scanning electron micrograph of a PMMA sponge polymerised with 70 wt.% of ethanol and 1 wt.% of EGDMA at two different magnifications (500 and 2000).

The SEM micrographs of Figure 1.1 show that there are two phases: the polymer as interconnected spherical particles (clear phase) and the pores, the space occupied by the solvent at the end of the polymerisation and that was eliminated afterwards by evaporation (dark phase).

On the other hand, *microsyneresis* consists of a separation of solvent forming disperse domains inside the growing network. When polymerisation goes on, if the amount of solvent is enough, the domains can increase in size. Pores are not interconnected for low solvent contents used in the polymerisation process (see Figure 1.2). However, for high solvent contents, the pore sizes increase so much that they connect with the others obtaining the typical structure known in the porous material literature as 'honeycomb' structure, where all the pores are interconnected. An example of microsyneresis with a porous hydrogel with interconnected porosity also synthesised in our laboratory can be seen in Figure 1.3.

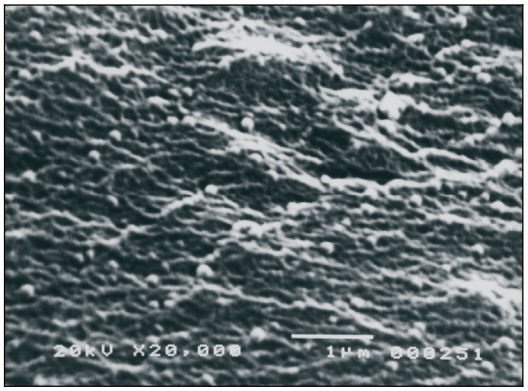

x20000

Figure 1.2 Example of microsyneresis for low solvent contents. Scanning electron micrograph of a PHEA sponge polymerised with 20 wt.% of methanol and 1 wt.% of EGDMA at 20000 of magnification. SEM micrograph taken from reference [118].

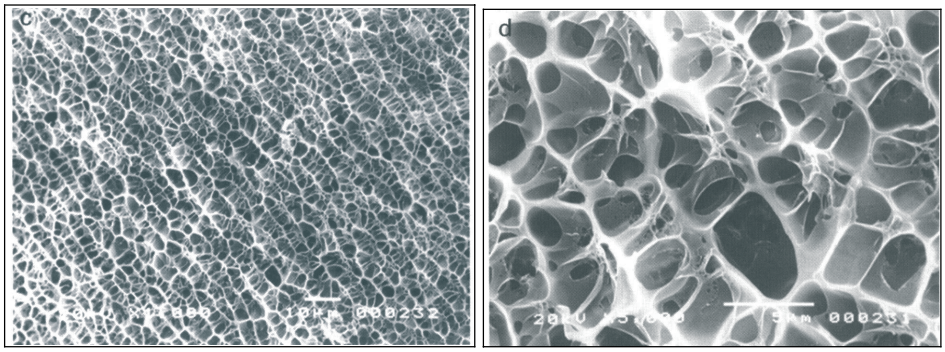

x1000 x5000

Figure 1.3. Example of 'honeycomb' structure for high solvent contents in microsyneresis. Scanning electron micrograph of a PHEA sponge polymerised with 60 wt.% of ethanol. SEM micrograph taken from [50].

These mechanisms show that once the solvent has been chosen, the situation of either macrosyneresis or microsyneresis depends on the solvent content added in the reactive mixture. The morphology of the porous polymer network differs very much from one situation to the other. When phase separation occurs as macrosyneresis, the morphology of the sponges consists of interconnected spheres with pores in between them. Nevertheless, microsyneresis gives rise to interconnected porosity or the 'honeycomb' structure in the limit. Their sizes and interconnection degrees depend, among other parameters, on crosslinking density, chain flexibility and solubility

parameters of polymer and solvent. These mechanisms suggest that beyond a certain amount of solvent it is possible to pass from microsyneresis to macrosyneresis.

In this work, macroporous polymer networks of poly(methyl methacrylate) (PMMA) were synthesised by polymerisation in the presence of ethanol. For high solvent contents, this PMMA sponge presents a typical macrosyneresis structure as it was shown in Figure 1.1.

1.5. Plasma treatment and plasma polymerisation.

Plasma contains activated species able to initiate chemical or physical reactions at the solid surface of polymers. As a result, modification reactions at the surface occur and cause alteration of surface properties and surface morphology. This process is called *plasma treatment*. On the other hand, when plasma interacts with organic molecules in a vapour phase, polymerisation is produced, and all surfaces of substrates inside the plasma chamber are coated with the polymers formed. This process is called *plasma polymerisation*. Plasma is an initiator of these processes and the interaction with plasma plays an important role. The species in plasma that lead to the process of plasma treatment and plasma polymerisation are electrons, ions and radicals. The species, with the exception of electrons, are generated by the collision between electrons and gas molecules existing in the plasma zone. In a chemical sense, the interaction with electrons, ions, and radicals are implantation reactions of atoms, radical generation, and polymer-forming reactions, and, in a physical sense, the interaction is an etching reaction. Which reaction is initiated by these species depends mainly on the nature of the plasma gases, as well as the energy level of the plasma and nature of the polymeric materials. The plasma composed of inorganic gases such as argon, helium, hydrogen, nitrogen, and oxygen leads to implantation of atoms, radical generation, and etching reactions, and the plasma composed of organic gases such as hydrocarbons and alkylsilanes leads to polymer-forming reactions. Plasma can be classified into two categories: non-polymer-forming plasma and polymer-forming plasma.

In this section, only the polymer-forming plasma type will be explained because it is the kind of plasma more similar to the method for plasma polymerisation used in this thesis. However, more information about the other kind of plasmas and all which concerned with plasma surface modification and plasma polymerisation can be found in [51].

When organic gases are introduced into plasma, polymer-like products deposit on the surfaces of all substrates in the reaction chamber. In this

sense, the process is called plasma polymerisation and the product formed is called plasma polymer. The polymer properties of the plasma polymers are strongly dependent on the plasma conditions (power, gas flow rates, time of treatment and base pressure in the reaction chamber).

The concept of the atomic polymerisation points out that elemental reactions occurring in plasma polymerisation are the fragmentation of monomer molecules, the formation of active sites (radicals), and recombination of the activated fragments. If fragmentation and recombination operate in plasma, starting molecules for plasma polymerisation will not be restricted to unsaturated compounds such as vinyl compounds, and saturated compounds can also deposit polymers.

Plasma polymers are different in chemical composition from conventional polymers polymerised via radical and ionic reactions, even if the same monomers are used in the two kinds of polymerisation.

In conventional polymerisation, when starting molecules with polymerisable groups such as vinyl groups are polymerised by a chain reaction mechanism or radical or ionic polymerisation, the formed polymers will have the same elemental composition of the starting molecules, assuming that the degree of polymerisation of the formed polymers is very high, because the effect of the chain-end groups are very small. If the starting molecule with CH_2=CHX is polymerised by conventional methods, the formed polymer will have a repeating unit of –[CH_2–CHX]– . Therefore, the elemental composition of the polymers (H/C = 3/2 and X/C = 1/2) is equal to that of the starting molecule of monomer CH_2=CHX (H/C = 3/2 and X/C = 1/2). However, plasma polymers are different in elemental composition from the corresponding monomers. The hydrogen concentration for the plasma polymers is lower than that for the corresponding monomer, and a small amount of oxygen is usually incorporated from the residual air in the plasma polymers. Thus, for instance, the plasma polymerisation of ethylene deposits a hydrophilic polymer similar in physical properties to polyethylene. However, the elemental composition of this plasma polyethylene ($C_2H_{2.6}O_{0.4}$) is different from that of polyethylene (C_2H_4) [51]. Therefore, the polymer-forming process in plasma polymerisation is never as simple as a chain reaction via polymerisable groups such as vinyl groups. This is a distinguishing feature of plasma polymerisation. Plasma polymers are not composed of repeating monomer units, but of complicated units containing cross-linked units and units fragmented or rearranged from the monomers. Therefore, plasma polymers are expected to be essentially different in chemical and mechanical properties than conventional ones, even if the same monomer is used for both plasma and conventional polymerisations. In addition, it is well

known that plasma polymers are always cross-linked in some extent [62, 51] and for this reason generally exhibit superior stability to chemical, thermal, and mechanical stress than conventional polymers. Their partial or total insolubility has made plasma polymers rather difficult to characterise.

The activation of monomers and reactivation of the recombined molecules by plasma, as described before, are essentially due to fragmentation (hydrogen abstraction and bond scission) by plasma. The fragmentation process depends on the supplied power to maintain the plasma, how much the monomers were introduced into plasma and where the monomer molecules interacted with activated species of the plasma.

1.6. Dynamic mechanical properties.

Dynamic mechanical spectroscopy is performed in order to measure the mechanical properties of materials as they are deformed under periodic forces. The dynamic modulus, the loss modulus, and a mechanical damping or internal friction express these properties. The dynamic modulus indicates stiffness of polymeric material under the dynamic stress and strain condition. It depends upon the type of polymer, temperature, and frequency. This value is related to the Young modulus of polymers. The dynamic loss modulus, related to the internal friction, is sensitive to many kinds of molecular motion, transitions, relaxation processes, structural heterogeneities and the morphology of multiphase systems (crystalline polymers, polymer blends, and copolymers). Therefore, interpretations of the dynamic mechanical properties at the molecular level are of great scientific and practical importance in understanding the mechanical behaviour of polymers. The mechanical damping or internal friction indicates the amount of energy dissipated as heat during the deformation of the material.

The dynamic mechanical properties of polymers are usually studied over a wide temperature range (-150 to 300ºC). In the region where the dynamic-modulus-temperature curve has an inflection point, the loss tangent ($tan\ \delta$) curve goes through a maximum. This relaxation is called the glass transition region where the dynamic modulus E' changes from approximately 1 *GPa* in the glassy state to about 1 *MPa* in the soft rubbery state. In the transition region, the damping is high owing to the initiation of conformational motion in molecular chains. This kind of motion is concerned with the co-operative diffusional motion of main-chain segments.

In the region of the glass transition of an amorphous polymer, *E'* drops while the loss tangent goes through a maximum. This relaxation process

is called α relaxation or the main dynamic-mechanical relaxation process. Other relaxation transitions can be found in a glassy state at temperatures lower than the α relaxation. These are called secondary relaxations and are usually designated as β, γ, etc., in order of decreasing temperature. Determination of the relaxation spectra of polymers is very useful for understanding the molecular motion in the structure. More information about dynamic mechanical properties can be found in [52].

The dynamic-mechanical properties of bulk PMMA polymerised under UV light with 10 wt.% of EGDMA was measured in reference [53] (see Figure 1.4).

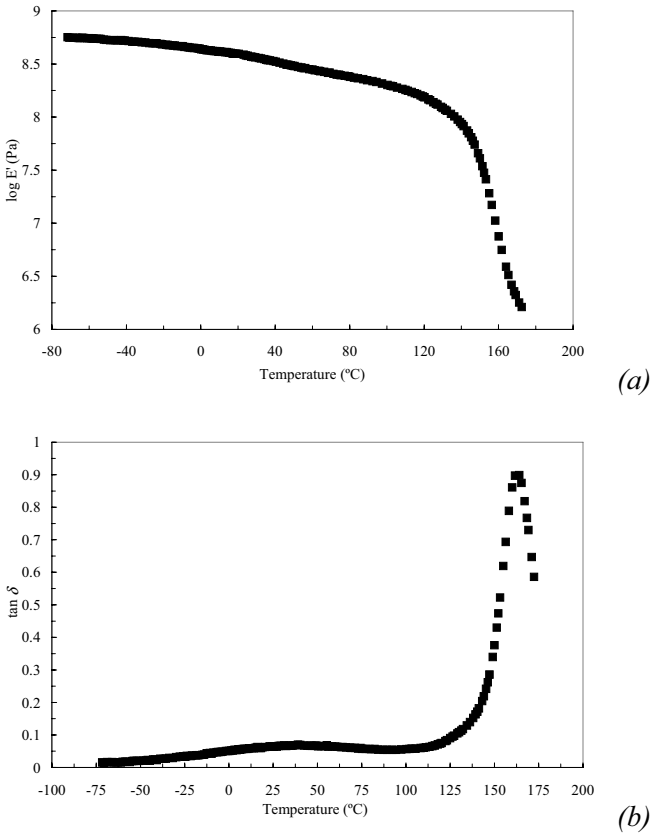

Figure 1.4. Temperature dependence of the storage modulus *(a)* and loss tangent *(b)* of bulk PMMA polymerised under UV light with 10 wt.% of EGDMA. These measurements were conducted at 1 *Hz*. DMS results taken from reference [53].

The storage modulus falls drastically from the glassy to the rubbery state (see Figure 1.4 *(a)*). The maximum of the main relaxation (α *peak*) appear

around 160ºC (see Figure 1.4 *(b)*). The secondary β relaxation of PMMA, due to side-chain motion of the ester group, appears around 40ºC.

In this work, bulk PMMA polymerised with EGDMA as cross-linker and benzoin as photoinitiator was also measured and it is not expected to be very different from these results, although the cross-linker content usually has a strong effect on the dynamic-mechanical properties of polymers.

The DMS spectra of PMMA polymerised in the presence of different solvent and cross-linker contents were also measured with this technique and a strong decrease of the storage modulus is expected due to porosity. However, the storage modulus of bulk PHEA and PHEA polymerised in the presence of different ethanol contents has approximately the same value in the glassy state independently of the amount of solvent used in the polymerisation process [50] (see Figure 1.5) because all the pores collapse in the drying process.

In the rubbery state, the storage modulus decreases with increasing the solvent content due to the presence of discontinuities in these materials with collapsed pores. However, the pores of macroporous PMMA polymerised with high ethanol contents do not collapse in the drying process. Therefore, the elastic modulus must fall in the glassy state due to the presence of open pores in the dry state.

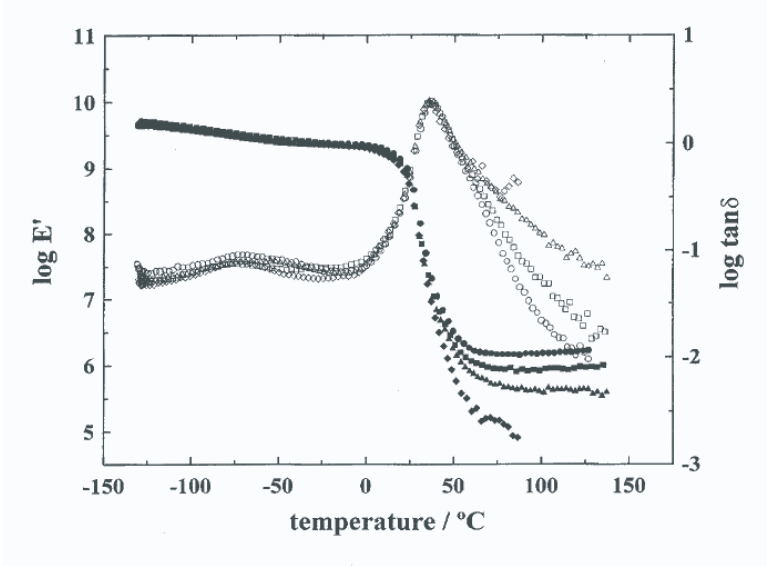

Figure 1.5. Temperature dependence of the real part of the elastic modulus (full symbols) and the loss tangent (open symbols) of bulk PHEA (●). PHEA polymerised in the presence of 20 (■), 40 (▲) and 60 (◆) wt.% of ethanol. All the samples polymerised with 1 wt.% of EGDMA. These measurements were conducted at 1 *Hz*. Figure taken from reference [50].

The main relaxation (α peak) of bulk PHEA, polymerised with 1 wt.% of EGDMA, appears with its maximum around 35ºC (see Figure 1.5). A secondary relaxation, which is usually called γ in the literature, appears at lower temperatures in the glassy state around -75ºC. This relaxation process is associated to local motions within the side-chain group. The presence of very small amounts of water absorbed produces a new relaxation peak, β_{sw}, at temperatures higher than those of the γ relaxation, due to the link of two side-chain groups by a water molecule through hydrogen bonding producing a bulkier molecular group of reduced mobility, whose relaxation takes place at a higher temperature [50 and the references cited therein].

The dynamic mechanical behaviour of heterogeneous systems depends on a variety of factors such as composition, phase morphology, adhesion between phases (i.e. properties of the interfaces), individual properties of the pure phases, and eventual formation of interphases. This complex behaviour is better analysed against the predictions of a simple model relating the overall properties of the blend with those of the individual pure phases in a known way. Takayanagi's block model has been proved to be useful in the analysis of heterogeneous media as diverse as semicrystalline polymers [54], incompatibles blends [55-57], fibre reinforced polymer composites [58-60] and particle filled polymers [61].

The experimentally measured dynamic-mechanical spectra of the blends can be compared with those predicted by a two phase, three block model, in which two blocks in series model the continuous phase, whereas the disperse phase is modelled by the block in parallel.

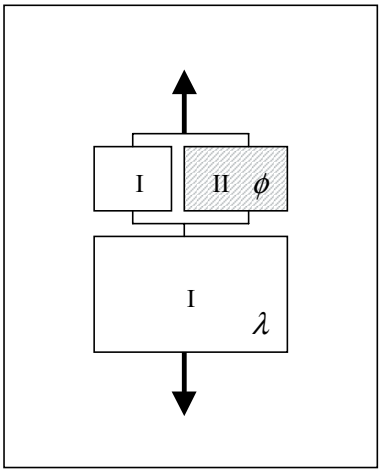

Figure 1.6. Takayanagi's block model. Two phases (I and II) with λ and ϕ as adjustable parameters.

In this three-block model, the parameter ϕ is the volume fraction of the disperse phase (II) and λ ($0 \leq \lambda \leq 1$) is the volume fraction of the continuous phase (I) in series, i.e. $\lambda(1-\phi) \equiv \xi$ is the total volume fraction in series. Therefore, when $\lambda = 1$, the load is the same for both phases and the deformation is the addition of the deformation of each phase. However, when $\lambda = 0$, the load is supported by the two phases and the deformation is the same for both phases.

The storage modulus and the tangent of the loss angle in this three-block arrangement are given by equations (1.1) and (1.2) [60].

$$E' = \frac{(M'E'_m - M''E''_m)(\xi M' + \bar{\xi}E'_m) + (M'E'_m + M''E''_m)(\xi M'' + \bar{\xi}E''_m)}{(\xi M' + \bar{\xi}E'_m)^2 + (\xi M'' + \bar{\xi}E''_m)^2} \tag{1.1}$$

$$\tan\delta = \frac{(M'E'_m + M''E''_m)(\xi M' + \bar{\xi}E'_m) - (M''E'_m - M'E''_m)(\xi M'' + \bar{\xi}E''_m)}{(M''E'_m - M'E''_m)(\xi M' + \bar{\xi}E'_m) + (M'E'_m + M''E''_m)(\xi M'' + \bar{\xi}E''_m)} \tag{1.2}$$

where $E'' = E' \cdot \tan\delta$ is the imaginary part of the complex Young modulus and

$$M' = \psi E'_d + \bar{\psi} E'_m \tag{1.3}$$

$$M'' = \psi E''_d + \bar{\psi} E''_m \tag{1.4}$$

$$\psi = \phi/(1-\xi) \tag{1.5}$$

$$\bar{\xi} = 1 - \xi \tag{1.6}$$

$$\bar{\psi} = 1 - \psi \tag{1.7}$$

where the subindex *m* refers to the properties of the pure copolymer acting as a matrix in the blend (continuous phase) and the subindex *d* refers to the properties of the pure copolymer acting as disperse phase in the blend. The experimentally determined values of these properties for the pure phases serve as input for the model calculations.

1.7. Infrared Spectroscopy.

Infrared spectroscopy is one of the most often used spectroscopic tools for the study of polymers. Poly(methyl methacrylate) is a well known polymer and much information can be found in the literature about its FTIR spectrum. However, the infrared spectroscopy of PMMA polymerised in the presence of ethanol has never been published but it is not expected to be very different from conventional PMMA. In this work, the spectrum of macroporous PMMA polymerised in the presence of a diluent with and without plasma-polymerised coating was measured.

The spectrum of conventional PMMA is shown in Figure 1.7. The CH_2 and CH_3 stretching vibrations in the region of 2800-3000 cm^{-1}, the carbonyl (C=O) band at 1720 cm^{-1}, the ester peaks at 1140 cm^{-1} to 1450 cm^{-1}, the α-CH_3 deformation peak at 970 cm^{-1} and the intense CH_2 rocking modes coupled with C–C stretching at 750 cm^{-1} can be identify in this spectrum [62].

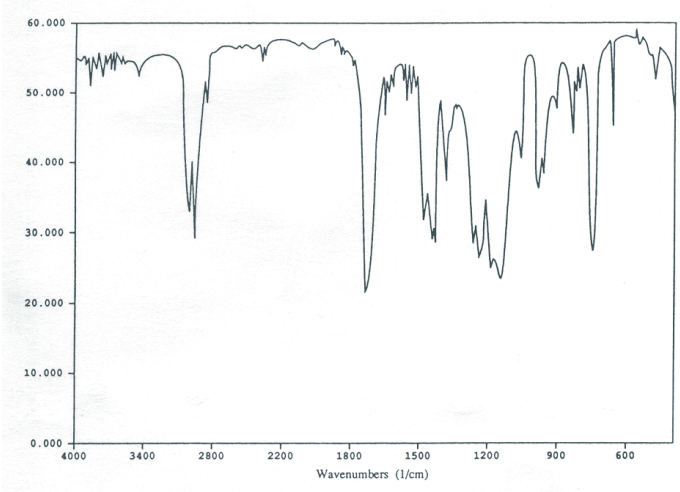

Figure 1.7. FTIR spectrum of conventional poly(methyl methacrylate) (PMMA). Figure taken from reference [62].

There is not much information in the literature about poly(2-hydroxyethyl acrylate). However, the FTIR spectrum of a PHEA gel was measure in reference [63] (see Figure 1.8). This FTIR spectrum shows a broad absorption around 3400 cm^{-1} (O–H stretching) and a strong absorption at 1740 cm^{-1} (C=O). The CH_2 and CH_3 stretching vibrations in the region of 2800-3000 cm^{-1} can also be seen [63].

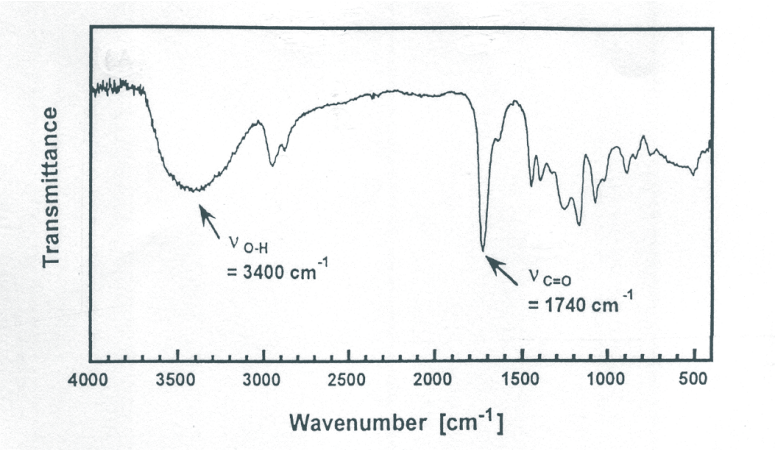

Figure 1.8. IR spectrum (KBr) of poly(2-hydroxyethyl acrylate) (PHEA). Spectrum taken from reference [63].

In this work, the FTIR spectrum of bulk PHEA was also measured for comparison with that of *pl*PHEA. The FTIR spectra of plasma-polymerised PMMA and conventional PMMA were compared in reference [62] and it was found that the PMMA films formed under RF cold plasma conditions were substantially modified and cross-linked in nature and do not retain many of the structural characteristics of conventional PMMA.

Poly(2-hydroxyethyl methacrylate) (PHEMA) is the most studied of all the hydrophilic polymers used in biomedical engineering as contact lenses, controlled drug delivery, etc. This polymer has the same chemical structure than PHEA but the substitution of the hydrogen atom attached to the chiral carbon atom in the PHEA repeat unit by a methyl group.

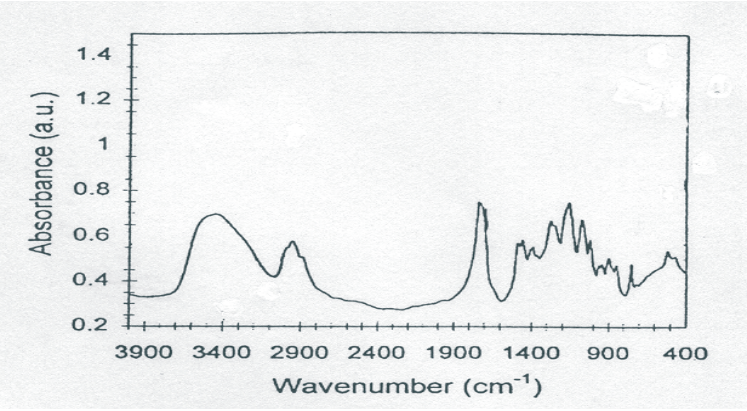

Figure 1.9. FTIR spectrum of pure PHEMA. Spectrum taken from [64].

Figure 1.9 shows the FTIR spectrum of PHEMA with a broad absorption around 3400 cm^{-1} due to the O–H stretching vibration, the CH_2 and CH_3 stretching vibrations in the region of 2800-3000 cm^{-1} and a strong absorption at 1740 cm^{-1} due to the presence of the carbonyl group[64, 65]. It is difficult to differentiate both spectra since both polymers are very similar and have the same functional groups.

More information about the principles and the application of FTIR spectroscopy in polymers can be found in references [66, 67]

1.8. Thermogravimetry.

Thermogravimetric analysis (TGA) or thermogravimetry (TG) is an experimental technique in which the mass of a sample located in a specified atmosphere is monitored against time or temperature while the temperature of the sample is programmed. This technique is broadly used to study thermal degradation of polymers. The thermal degradation on polymeric materials varies greatly with the nature of the polymer. For example, natural polymers like cellulose starts to decompose below 100ºC. Nevertheless, polyimides are stable up to 400ºC. This is the usual range of degradation temperatures for polymers. There are other factors that affect the changes greatly like the presence of additives and the atmosphere used. When heated in an inert atmosphere, polymeric materials react by two general routes, often related to their mode of polymerisation and the heat of polymerisation. They may either *depolymerise* back to the monomer like polymers such as poly(methyl methacrylate) (PMMA) and polystyrene (PS) or *carbonise* [68, 69]. These polymers have a low enthalpy increment of polymerisation. Random scission of poly(alkenes) like poly(ethylene) (PE) will produce unsaturated hydrocarbons from chain fragments of varying lengths like butenes, hexenes and dienes. The temperature of degradation is much affected by substitutions. For example, poly(tetrafluoroethylene) (PTFE) decomposes at a much higher temperature than PE due to the fluorine substitution. Nevertheless, with methyl substitution, poly(propylene) (PP) degrades at a lower temperature than PE. Poly(vinyl chloride) (PVC) and poly(acrylonitrile) (PAN) may eliminate small molecules in the beginning and form unsaturated links and cross-links before finally degrading by complex reactions to a char, which will oxidise in air. Polymers with polar groups, such as polyamides (e.g. nylon 66), may absorb moisture, which is usually lost below 100ºC. Cellulose polymers, polyester resins and phenol-formaldehyde polymers have extremely complex decomposition schemes, eliminating small molecules, often flammable or toxic, and eventually leaving a charred mass. More information about the thermogravimetric technique and its applications can be found in reference [70].

PMMA is a very studied polymer and it is well know that pure PMMA decomposes in two stages. In the first stage, the thermal stability of PMMA is related to the *weak links* in the radical-polymerised PMMA as the principal initiation sites of degradation. The second steps in degradation of PMMA are attributed to the presence of head-to-head linkages, the lack of saturation of the end groups related to the combination and termination of two radicals and random scission [71]. In the endothermic decomposition process, the methyl methacrylate monomer (MMA≥90%) and CO_2(≤10%) are the only pyrolisis products detected [72]. The thermal degradation of bulk poly(methyl methacrylate) with different ethyleneglycol dimethacrylate contents was studied in reference [127]. It was also found two degradation stages as pure PMMA. These results are shown in Figure 1.10.

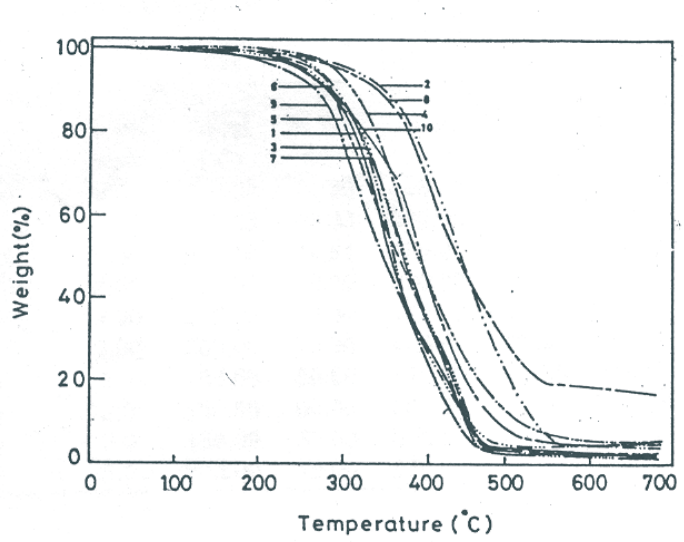

Figure 1.10. TGA of PMMA with different EGDMA contents: (1) 50% (-), (2) 25% (..-), (3) 20% (…-), (4) 9% (….-), (5) 4.8% (--), (6) 3.2% (…….-), (7) 2.4% (-..-), (8) 1.6% (--), (9) 1.2% (-.-), (10) 0.99%(- - -). TGA carried out under a nitrogen atmosphere at a heating rate of 10ºC/min. Figure taken from reference [127].

PMMA with EGDMA as cross-linker agent begins to degrade between 166 to 235ºC depending on the amount of EGDMA. Finally, when the PMMA samples reach between 435 and 494ºC, the degradation process is over.

The thermal degradation of poly(2-hydroxyethyl acrylate) has never been published in the literature because this PHEA polymer is not so studied as other polymers like PHEMA. A detailed study of thermal degradation of

poly(2-hydroxyethyl methacrylate) can be found in reference [73]. The TGA thermogram of this polymer is shown in Figure 1.11. The mass loss of PHEMA begins at ~322ºC and reaches its maximum at 361ºC. The TG curve of PHEMA indicates one reaction stage (Figure 1.11 *(a)*), which is reflected as a single peak in the derivative curve (Figure 1.11 *(b)*). The initial degradation temperature of PHEMA showed that the degradation was due to random chain scission. This polymer starts degrading at a temperature around 100ºC higher than PMMA with EGDMA due to the presence of OH groups in the PHEMA polymer, which produce degradation resistance because of hydrogen bonding. PHEMA and PHEA have quite similar chemical structures. Therefore, the degradation behaviour of PHEA cannot be very different from that of PHEMA.

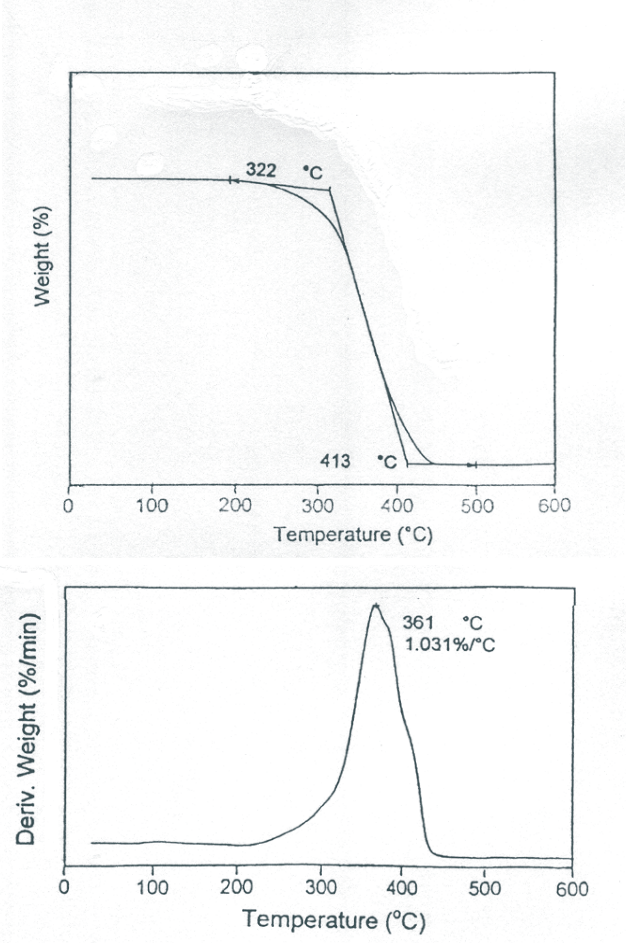

Figure 1.11. TGA thermograms of PHEMA. Weight loss *(a)* and derivative weight *(b).* TGA carried out under a nitrogen atmosphere at a heating rate of 10ºC/min. Figures taken from reference [74].

1.9. Equilibrium water sorption isotherms.

Water sorption is a very complex phenomenon. The equilibrium states corresponding to low water contents can be well described by the equations of adsorption theories. States with higher water contents share more features with polymer solutions and can be well described, for instance, by solutions theories such as Flory-Huggin's.

Sorption isotherms in polymers fit into Brunauer's classification scheme [75] (types II and III mainly). The equations of adsorption are the ones which best describe the phenomenon [90], even when sorption takes place in the whole volume of the system. The adsorption equations are so successful in describing the sorption equilibrium of hydrophilic polymers that it suggests indirectly that sorption is indeed a localised process and underlines the importance of the specific interactions in this type of system between the hydroxyl groups and water molecules as shown in Figure 1.12.

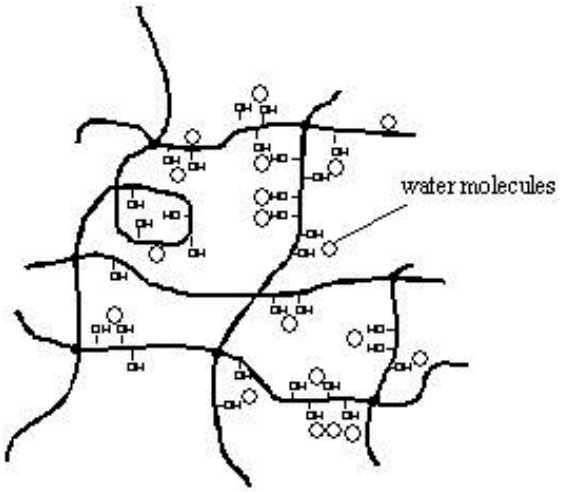

Figure 1.12. Water adsorption in a hydrophilic polymer.

The well known adsorption equations of Langmuir, Brunauer-Emmett-Teller (BET) and Guggenheim-Anderson-de Boer (GAB) were originally deduced from kinetic considerations. These equations characterise equilibrium states and relate some measure of the system composition with the activity or fugacity of the adsorbed gas. This feature introduces a first parameter of these models , the *monolayer sorption capacity* w_m, which is a measure (mole number, mass fraction, volume or normalised volume, concentration) of the

amount of adsorbate that saturates the available sorption sites, an adsorbed molecule *per* each sorption site. However, the equations, which account only for this feature (such as Langmuir's), cannot describe all types of adsorption curves found experimentally. The Brunauer-Emmett-Teller (BET) equation introduces a second fundamental notion in the theories of adsorption: the concept of *multilayer adsorption*, which consists of the idea that the molecules can be adsorbed as piles of more than one unity at each sorption site. Thus, the BET equation contains besides w_m , a second parameter $\bar{c}$ related to the difference between the enthalpy ascribed to the molecules adsorbed in the first layer, h^{l1}, and the enthalpy of the molecules adsorbed in layers two, three, four, etc., which are supposed to be all of them equal to the enthalpy of saturated liquid water h_l^L ($h^{l2} = h^{l3} = h^{l4} = \cdots = h_l^L$).

$$w = w_m \frac{\bar{c}\, a}{(1 - a)(1 + (\bar{c} - 1)a)} \equiv w^{BET}(a, w_m, \bar{c}) \qquad (1.8)$$

where w is water content and a water activity.

The temperature dependence of the new term $\bar{c}$ introduced in the BET equation can be expressed as

$$\bar{c} = \alpha \exp\left(\frac{h_l^L - h^{l1}}{RT}\right) \qquad (1.9)$$

The concept of multilayer adsorption turned out to be so successful that only on its basis became possible to account for the wide phenomenology of adsorption, to the point that calculations of porosity and specific surface area of porous materials follow a norm based on it [76, 77]. However, the BET equation predicts an infinite value of w at activity one. This is incompatible with the finite swelling degrees attained by polymer hydrogels in immersion.

The correction of modifying the BET hypothesis that the enthalpies of adsorbed molecules are those of the saturated condensed pure adsorbate, leads to the Guggenheim- Anderson-de Boer (GAB) equation [78-80],

$$w = w_m \frac{cfa}{(1 - fa)(1 + (c - 1)fa)} \equiv w^{GAB}(a, w_m, c, f) \qquad (1.10)$$

where a denotes the activity of water in the hydrogel and (w_m, c, f) are the so-called GAB parameters. These parameters depend on the temperature and they can be fitted to the experimental data. The parameter f is the new parameter introduce in GAB's equation and it is related to the enthalpies of the molecules

adsorbed in layer two, three, four, etc., which are assumed to be all of them equal as it was for BET's equation, but different from the enthalpy of saturated liquid adsorbate ($h^{l2} = h^{l3} = h^{l4} = \cdots \neq h_1^L$). The w_m parameter is the monolayer capacity ($w_m = m_{1m} / m_2$) where m_{1m} is the mass of water in the completed first layer. This parameter is the same as that of BET's equation. Parameter c as well as f is related to the enthalpy parameters of the molecules adsorbed in the subsequent layers by

$$c = \alpha \exp\left(\frac{h^{l2} - h^{l1}}{RT} \right), \quad f = \beta \exp\left(\frac{h_1^L - h^{l2}}{RT} \right) \tag{1.11}$$

where α, β are preexponential factors usually assumed to be close to unity without sufficient justification [81]. The BET equation can be obtained from GAB's equation for $f = 1$ and $\bar{c} = cf$ when $\alpha \approx \beta \approx 1$. The GAB equation describes correctly the sorption isotherms in macromolecular systems of synthetic [80, 82-84] and biological nature [85]. It has been even recommended by the COST90 project to describe water sorption in food [86].

1.10. Water diffusion in polymer hydrogels.

Water diffusion in polymers is highly dependent on the physical state of the polymer (glassy or rubbery). Most of the time, diffusion is found to be fickian for rubbery polymers [87, 88]. The hydrogel studied in this work (PHEA) is in the rubbery state at room temperature. Therefore, only this case will be explained [87-91].

In this study, the experiments were performed in conditions close to unidirectional diffusion. For time $t = 0$, the concentration c_1^0 of water at the faces of a specimen plate of thickness l along axis x, $-l/2 \leq x \leq l/2$, experience a sudden change of concentration Δc_1 (an increase for sorption and a decrease for desorption),

$$c_1(x=\pm\frac{l}{2},t)=c_1^0+\Delta c_1 \cdot H(t) \tag{1.12}$$

where $H(t)$ is the Heaviside unit step function and $c_1(x,t)$ is the time evolution of the concentration inside the plate. The continuity equation,

$$\frac{\partial c_1}{\partial t}=-\frac{\partial J_1}{\partial x} \tag{1.13}$$

where $J_1(x, t)$ is the water flux at point x and time t. In a first approximation, the water flux can be considered to vary linearly with the spatial gradient of the chemical potential of the diffusing species,

$$J_1(x,t)=-B\frac{\partial\hat{\mu}_1}{\partial x}=-BRT\frac{\partial\ln\hat{a}_1}{\partial x}=-BRT\frac{\partial\ln\hat{a}_1}{\partial c_1}\frac{\partial c_1}{\partial x}=-D(c_1,T)\frac{\partial c_1}{\partial x} \qquad (1.14)$$

where $D(c_1, T)$ is the diffusion coefficient of water in the polymer. Introducing this last equation in the continuity equation,

$$\frac{\partial c_1}{\partial t}=\frac{\partial}{\partial x}\left(D\frac{\partial c_1}{\partial x}\right) \qquad (1.15)$$

assuming D independent of c_1,

$$\frac{\partial c_1}{\partial t}=D\frac{\partial^2 c_1}{\partial x^2} \qquad (1.16)$$

which is *Fick's diffusion equation*. Its solution under boundary initial conditions ($c_1(x=\pm\frac{l}{2},t)=c_1^0+\Delta c_1\cdot H(t)$) is well known [89] and can be expressed in terms of the mass of water $m_1(t)$ in the plate as

$$\frac{\Delta m_{1,t}}{\Delta m_{1,\infty}}=4\left(\frac{Dt}{l^2}\right)^{\frac{1}{2}}\left(\frac{1}{\sqrt{\pi}}+2\sum_{n=1}^{\infty}(-1)^n\, ierfc\left(\frac{nl}{2\sqrt{Dt}}\right)\right) \qquad (1.17)$$

$$\frac{\Delta m_{1,t}}{\Delta m_{1,\infty}}\approx 4\left(\frac{Dt}{\pi\cdot l^2}\right)^{\frac{1}{2}} \; for \; \frac{\Delta m_{1,t}}{\Delta m_{1,\infty}}\le 0.6 \qquad (1.18)$$

where l is the thickness. The function $ierfc(x)$, $\Delta m_{1,t}$ and $\Delta m_{1,\infty}$,

$$\Delta m_{1,t}\equiv m_1(t)-m_1(0) \qquad (1.19)$$

$$\Delta m_{1,\infty}\equiv m_1(\infty)-m_1(0) \qquad (1.20)$$

$$ierfc(x) \equiv \frac{e^{-x^2}}{\sqrt{\pi}} - x + \frac{2x}{\sqrt{\pi}} \int_0^x e^{-u^2} du \qquad (1.21)$$

Since the plot '$\Delta m_{1,t} / \Delta m_{1,\infty}$' *vs* '$t^{1/2}/l$' must be linear for $\Delta m_{1,t}/\Delta m_{1,\infty} \leq 0.6$, the diffusion coefficient of a sorption process (D) can be calculated with equation (1.18) as

$$D = \frac{\pi}{16} K^2 \qquad (1.22)$$

where K denotes the slope of this linear plot.

1.11. Wettability and contact angle.

Zisman defines wettability as the ability of a liquid to adhere to a solid and spread over its surface to varying degrees [92]. Wettability is considered to be a surface property of a material. The degree to which wettability is desired in a material depends on the system design being considered. For example, in adhesive applications it is desirable to maximise wettability. Nevertheless, for applications in which moisture resistance is desired, such as water-repellent fabrics, the objective is to minimise wettability as much as possible.

For the fabrication of medical devices that come into contact with blood and tissue, it is usually desirable to utilise materials that exhibit very high degrees of wettability or hydrophilicity. The reason for this is that most of the internal biological environment is hydrophilic in nature and biocompatibility appears to correlate directly with the degree of hydrophilicity that a surface exhibits [93-95]. A caveat to this design criterion is the fact that most medical devices incorporate polymer materials extensively in their construction, and polymers are generally hydrophobic (non-wettable) in nature. Hence, the practice of incorporating hydrophilic materials into the design of these devices to enhance wetting characteristics has arisen. Because of their limited mechanical properties, however, hydrophilic polymers are often applied to medical devices in the form of coating. In this work, *pl*PHEA is also applied in the form of coating grafted onto macroporous PMMA by plasma polymerisation.

According to the classical model of Thomas Young at the beginning of the 19th century [96] and considering a drop of liquid in equilibrium on a solid surface as shown in Figure 1.13, the tendency of the droplet in

equilibrium is to minimise surface free energy *(G)* so that

$$G = \gamma_{SV} A_{SV} + \gamma_{LV} A_{LV} + \gamma_{SL} A_{SL} \tag{1.23}$$

where γ_{SV} is the surface tension of the solid in contact with air and its corresponding surface area A_{LV} and the interfacial tension (γ_{SL}) between the solid and the liquid with a corresponding contact area (A_{SL}).

If the droplet spreads an infinitesimal amount so that the interfacial area increases by *dA*, then there is a corresponding decrease in the surface area of solid in contact with the air, and an increase in the surface area of liquid in contact with the air equal to $dA\cos\theta$ (Figure 1.13). The corresponding change in surface free energy is

$$dG = -\gamma_{SV} dA + \gamma_{LV} dA \cos\theta + \gamma_{SL} dA \tag{1.24}$$

where θ is the contact angle that the liquid has with the solid surface.

Since $dG=0$ because the droplet is in equilibrium, the previous equation becomes

$$\gamma_{LV} \cos\theta + \gamma_{SL} - \gamma_{SV} = 0 \tag{1.25}$$

which is the well known Young equation relating surface tension and contact angle.

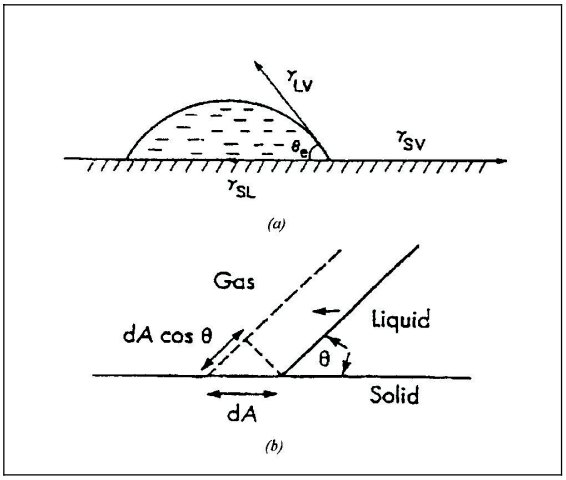

Figure 1.13. Contact angle of a sessile drop on a solid surface *(a)*. Contact angle at the solid-liquid-gas interface *(b)*. Figures reprinted from reference [11].

1.12. Thermal analysis of water in polymer hydrogels.

Thermal analysis of water in polymer hydrogels can be carried out by means of Differential Scanning Calorimetry (DSC). This technique consists of monitoring the heat-flow rate (power) to the sample against time or temperature while the temperature of the sample is programmed. More information about the basic principles of this technique and its application in polymer research can be found in references [97, 98].

The 'state' of water in a swollen hydrogel has been frequently classified into *free*, *freezable bound* and *non-freezing water*. *Free water* and *non-freezing water* are the two extremes of the continuum water 'states' in a hydrogel [99]. *Free or freezing water* is defined as the water which has the same phase transition temperature as bulk water [100]. *Freezable bound water* is the water having a phase transition temperature lower than 273 K. This depression is usually ascribed to the weak interaction of the water with the polymer chains and/or the capillary condensation in the hydrogel [101,102]. *Bound or non-freezing water* is defined as the water, which has no detectable phase transition from 273 to 200K [103]. These water molecules would be strongly associated with the polymer network through hydrogen bonding. Specific strong interactions do not allow the migration of water molecules to the growing crystal phase. Thus, a certain amount of water remains homogeneously mixed with the polymer chains. The term 'state' of water is usually used in the literature of hydrogels. Nevertheless, if one considers a hydrogel as an homogeneous polymer-solvent mixture, the word 'state' itself is not correct. What can be in a state are the whole hydrogel, the mixture itself, and not its components. There is no precise way to single out a state of a component in a mixture independently of the rest of the components. This is reflected, for example, because the properties which characterise the components are partial properties, whose state variables include parameters describing the complete mixture, not only the state parameters of a single substance.

Thermal transitions in the polymer hydrogels studied in this work are explained in a simple thermodynamic framework based on a temperature-composition diagram where the temperature of the transitions is plotted versus water content. Many thermal analysis of water in hydrophilic polymers have been done in the same way [104-108].

The existence of *non-freezable water* can be due to a diffusion problem: as the system approaches the glass transition, the viscosity of the medium increases and water molecules cannot diffuse through the hydrogel phase. Therefore, they cannot contribute to the continuous crystal growth and

become *non-freezable*. Recent studies have demonstrated that the polar interaction between water molecules and polymer chains cannot be the sole factor responsible for the existence of amounts of *non-freezable water* [109].

Melting of water in a hydrogel presents a phenomenology that differs from that of a solvent alone. In particular, the existence of either several endothermic peaks or a broad one is a common feature. On heating in a DSC scan, melting of water in a hydrogel starts a few degrees above the glass transition of the swollen polymer and it continues up to values near the melting temperature of the pure solvent. There are also processes of recrystallisation and reorganisation.

Water partially crystallises below 0ºC in hydrophilic polymers only if its concentration is greater than a critical value (ω'^{**}, see Figure 1.15) .When crystallisation occurs, the glass transition temperature *(T_g)* of the polymer solvent matrix remains constant. This T_g *regulation effect* is broadly explained in references [106, 110] by Jacques Rault *et al*.

If the amount of solvent does not exceed a certain limit, a polymer hydrogel can be considered as an homogeneous mixture of two molecular species at room temperature: the dry polymer and the solvent. The transition diagram of this mixture can be represented by a temperature-composition diagram where there are three curves: T_m, T_c and T_g. The first two curves T_m and T_c define the melting and crystallisation processes of the solvent in the mixture respectively. The curve T_g indicates the composition dependence of the glass transition of the swollen polymer hydrogel.

When the temperature of the liquid state of an amorphous polymer is lowered, molecular mobility is reduced and in a certain temperature interval takes place the glass transition leading to states where the mobility of the molecules is almost negligible as in the solid state but without crystalline order. It is said that the material is in the glassy state. The glass transition temperature can be clearly seen in Figure 1.14 as a change in the slope of the specific volume, specific entropy or specific enthalpy as a function of temperature.

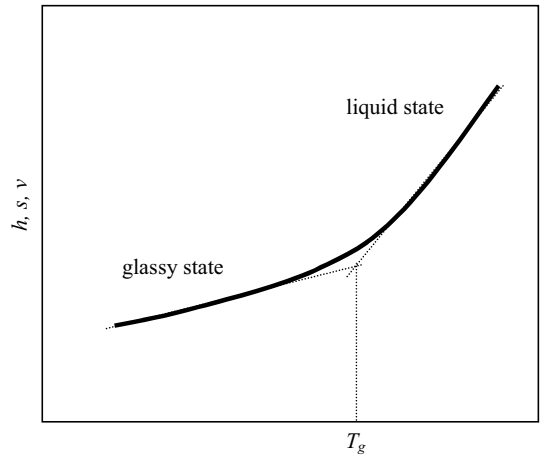

Figure 1.14. Glass transition temperature. Figure taken from reference [109].

The glass transition temperature (T_g) is a very important characteristic of many materials, especially polymers because their properties change dramatically. Much effort has been made to understand the composition dependence of the glass transition temperature of a binary glass-forming system [111-113]. These ideas can be applied to the polymer-water mixture in a PHEA hydrogel. The glass transition temperature curve of a hydrogel (T_{gh}) can be described by the Fox equation [111],

$$\frac{1}{T_{gh}} = \frac{1-\omega'}{T_{g0}} + \frac{\omega'}{T_{gw}} \tag{1.26}$$

or the Couchman-Karasz equation [112],

$$T_{gh} = \frac{(1-\omega')\cdot\Delta c_{p0}\cdot T_{g0} + \omega'\cdot\Delta c_{pw}\cdot T_{gw}}{(1-\omega')\cdot\Delta c_{p0} + \omega'\cdot\Delta c_{pw}} \tag{1.27}$$

where ω' is the weight fraction of water in the hydrogel, T_{g0} and T_{gw} are the glass transition temperatures of the dry polymer and water respectively. Δc_{pw} and Δc_{p0} are the heat capacity increments at the glass transition of water and the dry polymer respectively at T_g.

The Thermodynamics of binary systems predicts that the melting temperature of the solvent will experience a decrease, the so-called cryoscopic depression, with respect to the melting temperature of the pure component. A transition diagram (T_m, T_c and T_g vs ω') can be used to explain the thermal transitions seen in polymer hydrogels subjecting the samples to DSC heating and cooling scans. It is well known that, upon cooling, water does not crystallise until it reaches a temperature T_c that is significantly lower than the melting temperature of water (T_m). Supercooling of 10-20 degrees is often observed in pure water even for cooling rates as low as 0.2 ºC/min. This happens because crystallisation needs the occurrence of two processes: the formation of crystal *nuclei* (germs) on the one hand and their growth on the other. Although a rate of cooling high enough can even prevent crystallisation and result in glassy water [133], for the experimentally common cooling rates in DSC from 1 to 20 ºC/min, a T_c = *-21ºC* is obtained [104]. Upon cooling the hydrogel at a given rate, then, we expect to have a crystallisation curve $T_c=T_c(\omega')$ different from the liquidus curve, with $T_c(\omega') < T_m(\omega')$ for each ω' value.

A typical transition diagram of a swollen hydrogel taking into account the undercooling of water crystallisation is shown in the Figure 1.15.

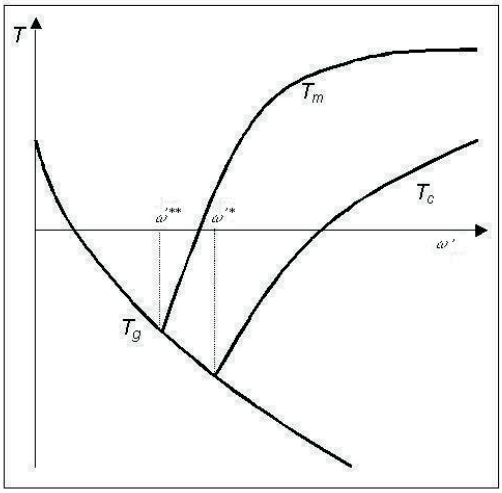

Figure 1.15 Transition diagram of a swollen hydrogel taking into account the undercooling of water crystallisation. Melting and crystallisation temperature of the solvent (T_m and T_c respectively). Glass transition temperature of the swollen polymer (T_g). Figure taken from reference [109]

The intersection of T_g with T_m and T_c defines the compositions ω'^{**} and ω'^{*} respectively. These two values divide the transition diagram in three

concentration domains, which are explained in Figure 1.16.

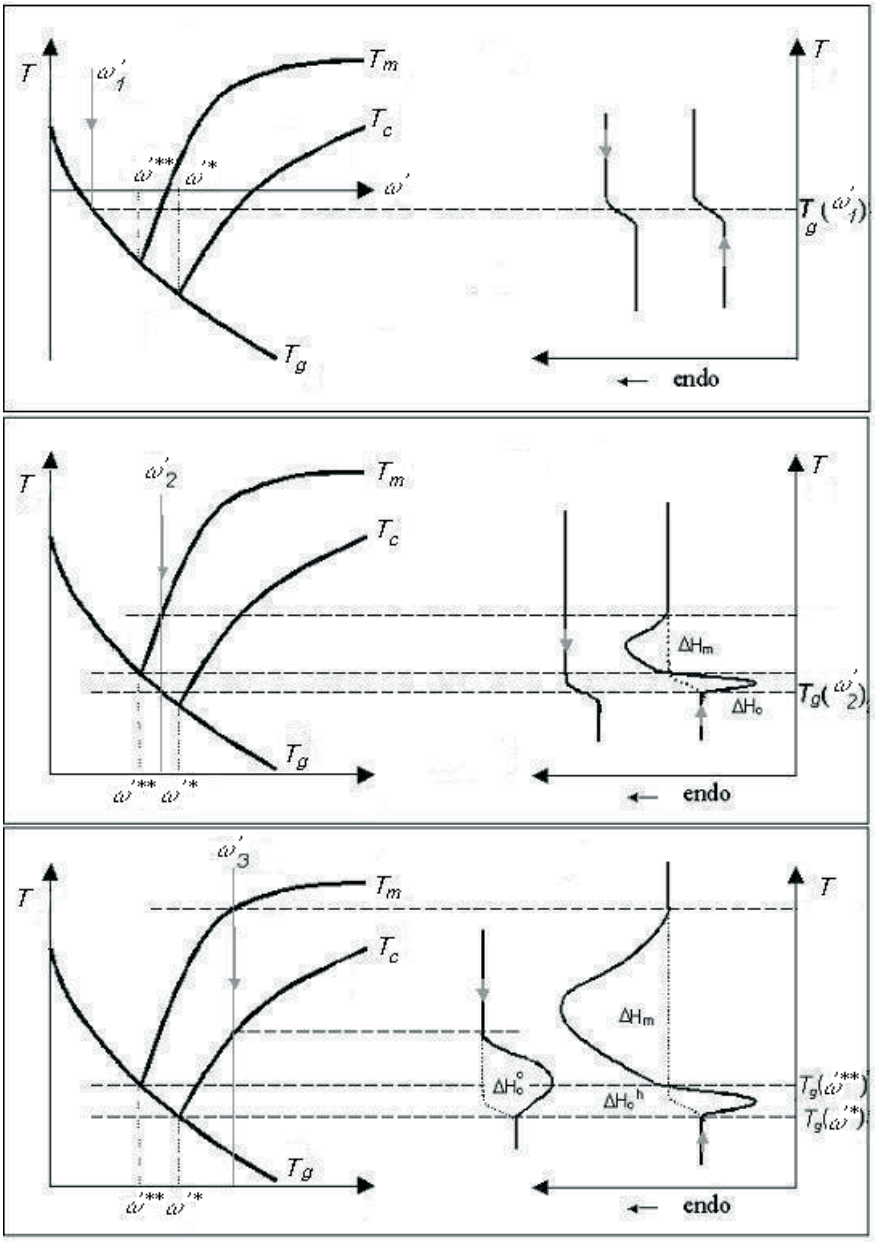

Figure 1.16 Expected shapes of the cooling and heating scans for polymer-water systems with compositions ω'_1, ω'_2 and ω'_3 belonging to the three different concentration domains. Figure taken from reference [109].

Concentration domain $\omega' < \omega'^{**}$: for a solvent concentration $\omega'_1 < \omega'^{**}$ at a temperature $T_g(\omega'_1)$ on cooling, the hydrogel would traverse its glass transition temperature before taking place any crystallisation. Only the glass transition of an amorphous polymer-solvent system occurs. Once the glass transition region has been reached, the mobility of the hydrogel kinetic units almost disappears and the homogeneous material remains as a glass. Physically there is no chance for solvent molecules to migrate from the vitrified polymer to form a new phase. Thus, in the low concentration domain, the solvent does not crystallise.

Concentration domain $\omega'^{**} < \omega' < \omega'^{*}$: for a solvent concentration $\omega'^{**} < \omega'_2 < \omega'^{*}$, the glass transition curve is reached on cooling before crystallisation can take place and all the solvent remains *non-crystallisable* again. This can be explained by the fact that crystallisation involves the formation of a nucleus of a critical size and its subsequent growth. This second stage of growth can solely take place if the nucleus is formed. Upon cooling, nucleation of crystalline germs can occur, but growth of these germs is not possible.

At $T_g(\omega'_2)$, the system is frozen as an homogeneous phase as a consequence of its glass transition, and no further thermal transitions can take place for temperatures lower than $T_g(\omega'_2)$. Then, as temperature increases, viscosity decreases and the crystal growth rate increases allowing the migration of solvent molecules from the swollen network to the embryos formed on cooling, and the solvent will crystallise on heating while still under T_m. Crystallisation causes a decrease in the solvent content present in the polymer phase.

At any temperature T_t , between $T_g(\omega'_2)$ and $T_g(\omega'^{**})$, the solvent migrates from the gel to the growing crystal phase until the composition of the gel reaches a value ω'_t when crystallisation becomes impeded by the glass transition. As temperature increases, this process takes place during the heating process while $T_g(\omega'_2) < T < T_g(\omega'^{**})$ and crystallisation of the solvent occurs between these two temperatures while the gel changes its composition and glass transition temperature continuously.

At ω'^{**} , $T_g(\omega'^{**}) = T_m(\omega'^{**})$ and when the temperature T^{**} is passed, the phase equilibrium of solid water and the hydrogel phase of composition ω'^{**} becomes unstable with respect to an equilibrium of solid water and a hydrogel

phase of composition $\omega' > \omega'^{**}$ on the T_m curve. Crystalline solvent thus begins to melt and diffuses into the hydrogel phase, increasing the latter composition until the starting ω'. Since the temperature is continuously increased, the process can be drawn following the curve T_m from $T_g(\omega'^{**})$ to $T_m(\omega'_2)$ until the starting composition ω'_2. A melting endotherm appears on the heating thermogram.

Summarising, for hydrogel compositions belonging to the interval $[\omega'^{**}, \omega'^{*}]$, no crystallisation is expected on cooling, but crystallisation and subsequent melting of water must be expected upon heating. Still, an amount of water will not crystallise $(m\cdot\omega'^{**})$. The trace of the process on the heating thermogram should thus include a first crystallisation exothermal peak followed by the melting endotherm, and the baseline jump from the beginning to the end should correspond to the heat capacity jump at the glass transition found on the cooling thermogram.

Concentration domain $\omega' > \omega'^{*}$: for a solvent concentration $\omega'_3 > \omega'^{*}$, after a certain supercooling, the solvent crystallises on cooling. Crystallisation is arrested by the glass transition of the system. As the solvent segregates from the gel phase to form a crystal, the composition of the gel decreases continuously following the T_c curve until $T_g(\omega'^{*})$ is reached and a dramatic loss of mobility of the polymer chains of the gel of composition ω'^{*} takes place. The crystal phase is not able to continue growing and both phases become frozen at lower temperatures. The amount of crystal phase will be $m\cdot(\omega'_3 - \omega'^{*})$, where m is the mass of the gel of composition ω'_3. On the subsequent heating scan, the solvent will crystallise as explained before, from $T_g(\omega'^{*})$ to $T_g(\omega'^{**})$ while the composition and glass transition temperature of the gel changes continuously. The amount of crystal solvent formed during heating will be $m\cdot(\omega'^{*} - \omega'^{**})$ independently of ω'_3. At T^{**}, the amount of ice is maximum, and the water concentration in the remaining polymer-water phase is ω'^{**}. From $T_g(\omega'^{**})$ on, the solvent will melt and diffuse following the T_m curve until the initial composition is reached.

From the above discussion, it follows that the interplay of thermodynamic equilibrium and nonequilibrium considerations determine a complex sequence of transitions in polymer hydrogels during constant rate in cooling and heating thermal histories. These are reflected by very specific features of the experimental thermograms, which may serve to support the explanation of their origin here advanced. They include the existence of

different quantities of non-crystallisable water upon cooling $(m \cdot \omega'^{*})$ and upon heating $(m \cdot \omega'^{**})$ and the existence of three qualitatively different concentration regimes, characterised by the presence or absence of crystallisation and melting during cooling and heating.

When cooling a polymer hydrogel, a certain amount of solvent does not crystallise and becomes non-crystallisable or non-freezable. The fraction of solvent, which is able to crystallise, can be calculated by means of DSC measurements.

There are several ways to express the amount of solvent sorbed in a hydrogel. In this work, all of them are referred to the mass of the polymer and can be easily determined gravimetrically.

$$w = \frac{m_{water}}{m_{polymer}} \tag{1.28}$$

where m_{water} is the mass of sorbed water in the sample and $m_{polymer}$ is the mass of dry polymer. It is convenient to normalise sometimes this magnitude between 0 and 1 and it will be transformed into the mass fraction of water in the swollen polymer

$$\omega = \frac{m_{water}}{m_{polymer} + m_{water}} \tag{1.29}$$

When we have a composite material (IPN, hydrophobic material with a plasma-polymerised hydrophilic coating, etc.), the mass of water absorbed can be referred to the mass of the hydrophilic component

$$w' = \frac{m_{water}}{m_{hydrophilic}} \tag{1.30}$$

where $m_{hydrophilic}$ is the mass of the hydrophilic component in the polymer system. In the same way, to normalise this magnitude, the water mass fraction in the hydrophilic component

$$\omega' = \frac{m_{water}}{m_{hydrophilic} + m_{water}} \tag{1.31}$$

The last two definitions assume that all of the sorbed water is located in the hydrophilic component. This assumption is usually valid since the water mass absorbed in the hydrophobic component is negligible most of the times.

The amount of crystallised water in a DSC scan ($m_{watercryst}$) can be determined from the area of the crystallisation peak in the DSC thermogram.

$$m_{watercryst} = \frac{1}{\Delta H} \int \dot{Q}_{exo} dt \tag{1.32}$$

where $\dot{Q}_{exo}$ is the exothermic DSC heat flow, ΔH is the melting heat of water per unit mass and t is time.

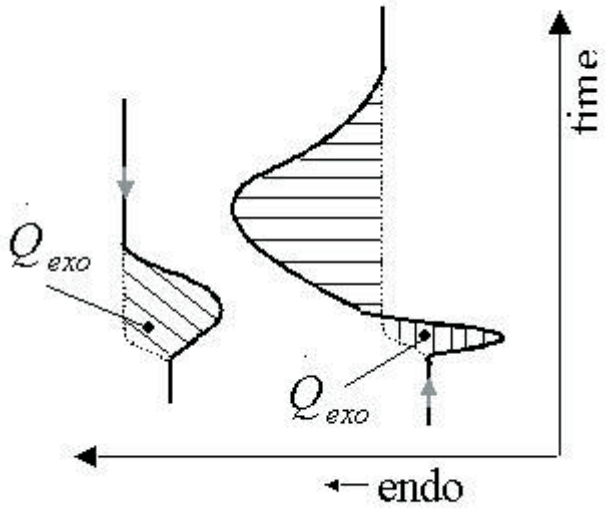

Figure 1.17. DSC thermogram with the cooling and heating scans. The exothermic heat flow on cooling and heating has been marked. Figure taken from reference [109]

Let $m_{totalwater}$ be the mass of water in the hydrogel before starting the DSC measurements. Part of this water crystallises after performing the cooling scan and the mass of water that remains in the polymer network ($m_{watercooling}$) can be calculated as

$$m_{watercooling} = m_{totalwater} - \frac{1}{\Delta H} \int_{cooling} \dot{Q}_{exo} dt \tag{1.33}$$

On the subsequent heating scan, the solvent is able to crystallise and the final mass of water remaining in the polymer ($m_{watercooling\&heating}$) can be determined by

$$m_{watercooling\&heating} = m_{totalwater} - \frac{1}{\Delta H}\left(\int_{cooling} \dot{Q}_{exo}\, dt + \int_{heating} \dot{Q}_{exo}\, dt \right) \qquad (1.34)$$

The thermal events measured in a DSC scan during the crystallisation and melting of water in a hydrogel include, besides the phase transition heat, the heat of demixing and mixing of the solvent in the polymer [114]. Nevertheless, these heats can be neglected compared with the phase-change enthalpies. It has been reported that the enthalpy of mixing is roughly 1/65th of that of crystallisation (melting) [115, 116]. In addition, the above equations assume the constancy of the heat of melting of the solvent with temperature and that the specific latent heat of melting of the solvent in the hydrogel is not different from that of the pure solvent.

2. Materials and experimental methods.

The materials and the experimental techniques employed in this thesis are presented in this chapter. The experimental techniques were carried out to characterise the materials synthesised in this work: dynamic-mechanical spectroscopy (DMS) to study their mechanical properties, porosimetry analysis by swelling in ethyl acetate and water, specific volume determination, scanning electron microscopy (SEM) to observe the morphology of these macroporous structures, differential scanning calorimetry (DSC) to study the thermal transitions of water in the hydrophilic coating, thermogavimetry analysis (TGA) to analyse the degradation of these materials, Fourier Transform Infrared Spectroscopy (FTIR) was perform to study the nature of plasma-polymerised PHEA and water sorption experiments to study the influence of the hydrophilic layer.

2.1. Materials and systems.

2.1.1. Materials.

The objective of this thesis is focused on the synthesis of a new macroporous material, which consists of a macroporous poly(methyl methacrylate) (PMMA) network, obtained by polymerisation in the presence of a solvent, and a plasma-polymerised coating of poly(2-hydroxyethyl acrylate) (PHEA) hydrogel. However, bulk PMMA, macroporous PMMA without hydrophilic coating and bulk PHEA were also synthesised in order to characterise this composite material.

Thus, a series of poly(methyl methacrylate) (PMMA) networks with different porosities and cross-linking densities were synthesised by bulk polymerisation and polymerisation in the presence of ethanol. The polymerisation took place under UV light with benzoin (from Scharlau 98% pure) as photoinitiator and ethylene glycol dimethacrylate (EGDMA, from Aldrich 98% pure) as cross-linker. The monomer (methyl methacrylate, MMA, from Aldrich 99% pure) and the cross-linking agent were purified by vacuum distillation. The chemical structures of benzoin, MMA, EGDMA chemicals and PMMA are shown in Figures 2.1 to 2.4 respectively.

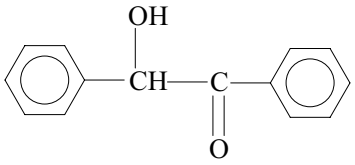

Figure 2.1. Benzoin photo initiator.

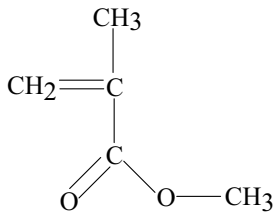

Figure 2.2. MMA monomer.

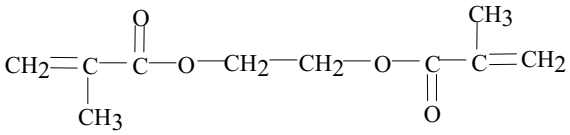

Figure 2.3. Ethylene glycol dimethacrylate cross-linker.

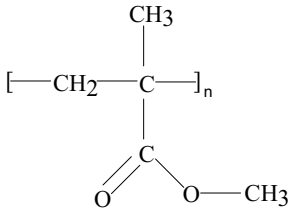

Figure 2.4. Poly(methyl methacrylate).

When the MMA monomer is polymerised with a certain amount of EGDMA, a cross-linked network is obtained as shown in Figure 2.5. In this work, three different EGDMA cross-linker contents were added in the PMMA polymerisation (1, 5 and 10 wt.%).

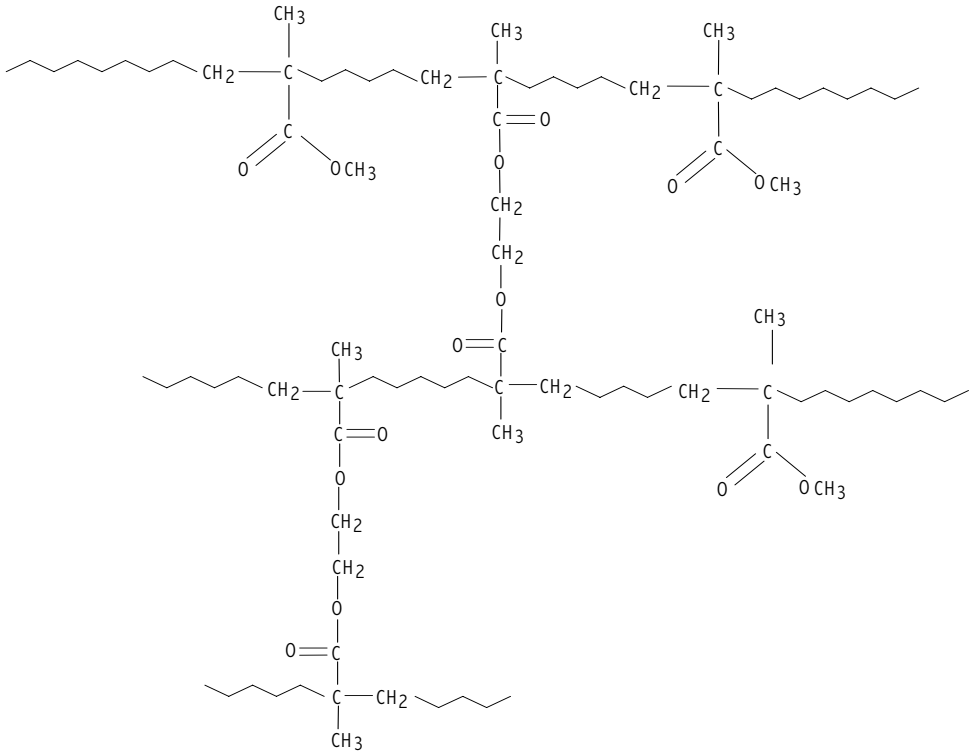

Figure 2.5. PMMA network cross-linked with EGDMA.

Poly(2-hydroxyethyl acrylate) (PHEA) networks were also bulk polymerised under UV light with benzoin as photoinitiator but without EGDMA cross-linker agent in this case in order to make it to be as similar as possible to the plasma-polymerised PHEA coating. The monomer 2-hydroxyethyl acrylate (HEA, from Aldrich 96% pure, stabilised with 200 to 600 ppm of monomethyl ether hydroquinone) was used without further purification. The chemical structures of HEA monomer and PHEA polymer are shown in Figures 2.6 and 2.7 respectively.

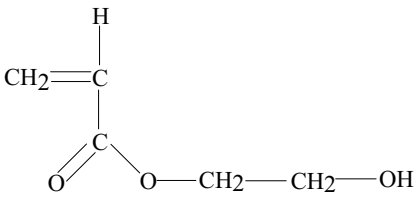

Figure 2.6. HEA monomer.

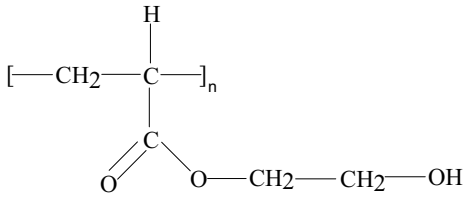

Figure 2.7. PHEA polymer.

The synthesis of these materials by bulk polymerisation and polymerisation in the presence of ethanol are explained in 2.1.2 and 2.1.3 respectively.

Macroporous PMMA obtained by polymerisation in the presence of ethanol was coated with plasma-polymerised PHEA (*pl*PHEA). This *pl*PHEA is a plasma polymer. Therefore, it is supposed to be different in chemical composition from conventional polymers polymerised via radical reactions, even though the same monomer was used in both cases. The method followed to perform the surface grafting of *pl*PHEA onto macroporous PMMA is explained in 2.1.4.

Summarising, four kinds of materials are characterised in this work: bulk PMMA, PMMA polymerised in the presence of ethanol, macroporous PMMA coated with *pl*PHEA and bulk PHEA.

Ethyl acetate (0.9 g/cm^3 at 25ºC, synthesis grade from Scharlau), ethanol absolute (0.79 g/cm^3 at 25ºC, synthesis grade from Scharlau), n-octane (0.703 g/cm^3 at 25ºC, 99(+)% pure from Acros organics) and distilled water were also used in this work.

2.1.2. Bulk polymers.

PMMA networks were bulk polymerised at room temperature under ultraviolet light for 24 hours with 0.2 wt.% of benzoin as photoinitiator and EGDMA as cross-linker. Polymerisation took place between glass plates to form sheets between 1 to 3 mm thick. The low molecular weight substances remaining in the samples after polymerisation were extracted with boiling ethanol for 24 hours. Afterwards, the solvent was allowed to evaporate partially from the samples at room temperature and atmospheric pressure. This step is necessary in order to avoid sample cracking during the drying process. Finally, the samples were dried at 160ºC in vacuo to constant weight.

Thus, a series of PMMA samples with different cross-linking densities was synthesised starting from a mixture of MMA and EGDMA monomers in 99/1, 95/5 and 90/10 weight ratios, which will be called hereafter as PMMAB1, PMMAB5 and PMMAB10.

Following a similar procedure, poly(2-hydroxyethyl acrylate) (PHEA) networks were bulk polymerised between glass plates to form sheets approximately 1 mm thick. Polymerisation took place under UV light for 24 hours with 0.2 wt.% of benzoin as photoinitiator. Samples were washed with boiling water for 24 hours and dried at 90 ºC in vacuo for three days. No cross-linker agent was added in this case.

2.1.3. Porous PMMA.

Macroporous PMMA networks were prepared by polymerisation in the presence of a solvent. Due to its good miscibility with the methacrylic monomers, ethanol was chosen as solvent. Different degrees of porosity were obtained varying the solvent content in the initial reactive mixture. Thus, the solvent weight ratios chosen in the monomers/solvent initial blends were 80/20, 50/50, 40/60, 30/70 and 20/80, in which the monomers (MMA/EGDMA) weight ratios were 99/1, 95/5 and 90/10 for each solvent content. Hereafter these porous samples will be designated by PMMA followed by the cross-linker content, the bar /, solvent content and the first letter of the solvent name (ethanol). For example, PMMA1/60E designates the PMMA sample synthesised with MMA/EGDMA weight ratio 99/1 and monomers/ethanol weight ratio 40/60.

2.1.4. Surface grafted systems.

Poly(2-hydroxyethyl acrylate) hydrophilic coatings were obtained by means of a particular method for surface grafting of plasma-polymerised PHEA described in this work. Porous PMMA networks with different porosity and cross-linker ratios were used to be coated by this hydrogel.

A Piccolo plasma chamber from Plasma-electronic GmbH (Germany) was used to obtain the plasma-polymerised coatings. This stainless steel vacuum chamber of 45 litres is evacuated to a base pressure lower than 100 Pa without any gas injection before the plasma treatment. The plasma is generated by a 2.45 GHz generator (quartz cylinder) which produces up to 600 Watt.

Hereafter these porous PMMA samples with hydrophilic coating will

be designated generically by the name "PMMA-*gr-pl*PHEA", where the letters *gr* mean grafted and *pl* plasma. These PMMA-*gr-pl*-PHEA samples are designated specifically by the name of the respective porous PMMA followed by "-*gr-pl*PHEA(wt.%)". For example, sample PMMA1/60E-*gr-pl*PHEA(12%) designates the PMMA1/60E sample with 12 wt.% of *pl*PHEA. The nomenclature of all the materials synthesised in this work is also shown at the end of the glossary.

2.2. Methods.

2.2.1. Specific volumes and porosities.

A METTLER TOLEDO AX205 balance (sensitivity of 0.01 mg) with density accessory kit was employed to measure the specific volumes at 25±0.5ºC.

The specific volumes of the dry bulk polymers (v_b) was determined through the weight of a sample, around 0.1g, in air (m_{air}) and immersed in n-octane ($m_{n\text{-}octane}$). The density of n-octane ($\rho_{n\text{-}octane}$) is known (0.703 g/cm^3 at 25ºC). Thus, the specific volumes can be calculated by Archimedes' principle as

$$v_b = \frac{m_{air} - m_{n-octane}}{m_{air} \cdot \rho_{n-octane}} \qquad (2.1)$$

The specific volume of sample PMMA1/20E was also determined with this method since it is non-porous. The result obtained for a series of pieces of the same polymer sample was reproducible within 0.002 cm^3g^{-1}.

The specific volumes of the porous polymers cannot be determined with the same method as bulk polymers due to their porosity. Nevertheless, their apparent specific volumes (v_{app}) can be calculated after measuring their three linear dimensions with a micrometer and then weighing the sample. The porous samples were cut with a metal cutter with approximately dimensions: 1x0.5x0.2 *cm*. Four pieces of each porous polymer were measured in order to obtain a more accurate value of v_{app} with the mean and the standard deviation for each sample.

The porosity of the dry porous polymers (P_{dl}) can be determined from their apparent specific volumes ($v_{app}=(V_{pores}+V_b)/m_b$) and the specific volumes of the same bulk polymers (v_b) as

$$P_{d1} = \frac{V_{pores}}{V} = \frac{v_{app} \cdot m_b - V_b}{v_{app} \cdot m_b} \tag{2.2}$$

where V_b and m_b are the volume and the mass of the bulk polymers. Thus,

$$P_{d1} = \frac{v_{app} - v_b}{v_{app}} \tag{2.3}$$

The porosity of the dry porous polymers with hydrophilic coating can also be determined from their apparent specific volumes and the specific volumes of the two pure bulk polymers in the same way but considering in equation (2.3) that $v_b = v_{b1} \cdot X_1 + v_{b2} \cdot (1 - X_1)$. Thus,

$$P_{d1} = \frac{v_{app} - v_{b2}(1 - X_1) - v_{b1} \cdot X_1}{v_{app}} \tag{2.4}$$

where v_{b1} is the specific volume of bulk PHEA, X_1 is the mass fraction of *pl*PHEA and v_{b2} the specific volume of bulk PMMA.

The volume fraction of pores was also gravimetrically determined by swelling the porous polymers in liquid ethyl acetate and water for 48 hours at 25ºC. Ethyl acetate is a good solvent of PMMA and is able to swell this polymer network. Therefore, the fraction of pores determined with this solvent is the porosity of the swollen polymer (P_s). Nevertheless, water is a bad solvent of PMMA and its capacity of swelling this polymer is practically negligible. Therefore, the porosity determined with this solvent (P_{d2}) is very close to the porosity of the dry polymer.

The volume fraction of pores filled with ethyl acetate in the swollen porous samples was estimated considering that the swollen porous materials consisted of two phases. One phase is formed by the polymer network with absorbed solvent, whose behaviour can be assumed equal to the bulk polymer with the same cross-linking density, occupying a volume $V_{swollenb}$. The other phase is formed by pure liquid ethyl acetate occupying the volume of pores V_{pores}.

The equilibrium solvent uptake is usually calculated as

$$w = \frac{m_{solvent}}{m_{drypolymer}} \tag{2.5}$$

This amount of absorbed solvent can also be used as the mass fraction of solvent in the sample,

$$\omega = \frac{m_{solvent}}{m_{drypolymer} + m_{solvent}} \tag{2.6}$$

Thus, the volume fraction of pores in the swollen porous polymer can be calculated as

$$P_s = \frac{V_{pores}}{V_{swollenb} + V_{pores}} = \frac{v_{eacetate} \cdot (w - w_b)}{v_{swollenb} \cdot (1 + w_b) + v_{eacetate} \cdot (w - w_b)} \tag{2.7}$$

where w is the equilibrium solvent uptake of the porous sample after immersion for 48 hours, $v_{eacetate}$ is the specific volume of ethyl acetate (*1.11 cm^3/g* at 25ºC), $v_{swollenb}$ and w_b are the specific volume and the equilibrium solvent uptake ($w_b = m_{eacetate}/m_{polymer}$) after immersion for 48 hours of the swollen bulk sample with the same cross-linking density. The $v_{swollenb}$ was estimated assuming null excess volume in the polymer/ethyl acetate blend. Thus

$$v_{swollenb} = v_{eacetate} \cdot \omega_b + v_b \cdot (1 - \omega_b) \tag{2.8}$$

where v_b is the specific volume of the non-porous sample with the same cross-linking density in the dry state and ω_b is the mass fraction of ethyl acetate in the sample, calculated as $\omega_b = w_b/(1+w_b)$.

The volume fraction of pores filled with water was calculated in the same way. In this case, the hydrophobic behaviour of the PMMA network and the air located in the pores impede water to fill completely the holes. For this reason, it was necessary to extract the air in the pores with a vacuum pump before immersion. A special glass key was used to allow the pass of water right after the air extraction. Thus, the volume fraction of pores can be calculated as

$$P_{d2} = \frac{V_{pores}}{V_{swollenb} + V_{pores}} = \frac{v_{water} \cdot (w - w_b)}{v_{swollenb} \cdot (1 + w_b) + v_{water} \cdot (w - w_b)} \tag{2.9}$$

where v_{water} is the specific volume of pure water at 25ºC, $v_{swollenb}$ and w_b are the specific volume and the equilibrium water uptake after immersion in water for 48 hours of the swollen bulk sample with the same cross-linking density and w is the equilibrium water uptake of the porous sample after immersion in water for 48 hours. The $v_{swollenb}$ was estimated assuming null excess volume in the

polymer/water blend,

$$v_{swollenb} = v_{water} \cdot \omega_b + v_b \cdot (1 - \omega_b) \tag{2.10}$$

where v_b is the specific volume of the non-porous sample with the same cross-linking density in the dry state and ω_b is the mass fraction of water in this sample, calculated as $\omega_b = w_b/(1+w_b)$.

2.2.2. Scanning Electron Microscopy (SEM).

Scanning electron micrographs were taken in an ISIDS-130 microscope at an accelerating voltage ranging from 15 to 20 *kV*. The cryogenic fractures of the samples were sputtered with gold previous to observation.

2.2.3. Dynamic-Mechanical Spectroscopy (DMS).

Dynamic-mechanical spectroscopy (DMS) was performed in a Seiko DMS 210 dynamic-mechanical analyser at a frequency of 1*Hz* in the tension mode. The temperature dependence of storage modulus (*E'*), loss modulus (*E''*), and loss tangent (*tan* δ) was measured in the appropriated temperature range for each sample with a heating rate of 1*K/min*. DMS experiments were conducted on dry samples of prismatic shape.

2.2.4. Differential Scanning Calorimetry (DSC).

Differential scanning calorimetry experiments were performed in a Mettler TA 3000 and a Perkim-Elmer (Pyris 1) apparatus. The temperature of the calorimeter was calibrated with water, cyclohexane and n-octadecane. The melting heat of indium was used to calibrate the heat flow output.

A cryogenic accessory with liquid nitrogen was used to cool down at low temperature. DSC measurements were performed on dry and swollen samples to study the thermal transitions in the hydrophilic coating. The three characteristic temperatures T_g, T_m and T_c were determined from the DSC thermograms. The glass transition temperature was taken from the inflexion point of the heating scan. The melting and crystallisation temperature values were taken from the maxima of the endothermic and exothermic peaks respectively of the thermograms.

2.2.5. Fourier Transform Infrared Spectroscopy (FTIR).

The FTIR spectra shown in this work were taken with a Thermo Nicolet NEXUS spectrometer in the wavenumber region between 400 and 4000 cm^{-1} at room temperature. All measurements were performed by Attenuated Total Reflectance Spectroscopy (ATR) with the Smart Mullti-Bounce HATR accessory for solids with a ZnSe crystal. The spectra shown in this work were the result of 32 scans at the speed of 1 scan per second. The resolution of the spectrometer was 4 cm^{-1}. The spectra were corrected for the presence of water and carbon dioxide in the optical path.

2.2.6. Thermogravimetric Analysis (TGA).

Thermogravimetry Analysis was performed in a TGA92 SETARAN instrument with an Argon flux of 55 *mmHg* and water cooling flow of 3 *l/min*. All experiments were carried out at a heating rate of 10 *K/min*.

2.2.7. Equilibrium sorption isotherms.

Equilibrium water sorption isotherms were measured at 50ºC. The samples were allowed to equilibrate to constant weight (weight change less than 10^{-4} g) in various desiccators where the relative humidity (*rh*) was maintained between 0.06 and 0.96 using different saturated salt solutions (see Table 2.1) [117]. The water content (*w*), defined as *g water/g dry sample*, was determined by weighing.

Table 2.1. Saturated salt solutions used to provide different relative humidities at 50ºC.

Salt	***rh***
LiBr	*0.0553*
LiCl	*0.111*
KF	*0.208*
NaI	*0.2921*
$Mg(NO_3)_2$	*0.4544*
NaBr	*0.5093*
KI	*0.6449*
NaCl	*0.7443*
KCl	*0.812*
K_2SO_3	*0.9582*

2.2.8. Immersion experiments.

This kind of experiments consisted in placing the dried bulk polymers in liquid water and allowed them to equilibrate to constant weight at 25±0.5ºC (until the sample weight change was less than 10^{-4}g). The surface of the samples was dried with filter paper before weighing. However, the water immersion experiments of macroporous PMMA cannot be performed in the same way because of the presence of air inside the pores, which impedes the water filling. In order to avoid this problem, the air present in the pores was evacuated with the help of a vacuum pump before the water filling as explained in section 2.2.1. A vacuum glass key was used to allow the pass of water right after the air extraction. Samples were allowed to equilibrate to constant weight at 25±0.5ºC during a long time to ensure this equilibrium weight (3 days). This experiment was also used to determine the volume fraction of pores.

2.2.9. Dynamic desorption experiments.

Dynamic desorption experiments were performed after equilibrating a sample in an atmosphere with a relative humidity of 97% (obtained with a saturated salt solution of potassium sulphate) and after being saturated in liquid water. Both experiments were performed with an experimental set-up built in our laboratory (Figure 2.8). It consists of a Sartorius BP2110 balance with a container inside which has a double wall to have relative humidity and temperature under control. The humidity is adjusted with an air compressor, which let air pass through a saturated salt solution of lithium chloride providing a relative humidity of 19%. The temperature is fixed (25ºC in this case) with a water bath with thermostat. The experimental set-up has a thermometer and a hygrometer to control these parameters.

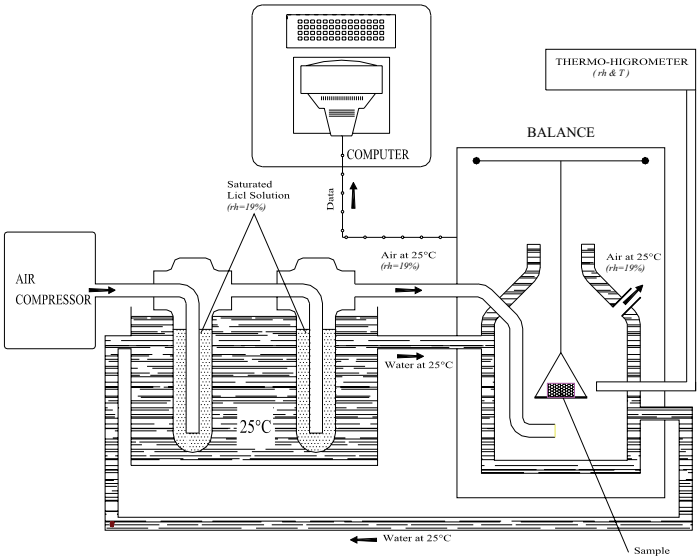

Figure 2.8. Experimental set-up for dynamic desorption experiments with temperature and relative humidity under control. System composed of air compressor, thermal bath, thermo-hygrometer, balance and computer.

The experimental procedure consisted of leaving the samples inside a desiccator to equilibrate to constant weight at 25ºC in an atmosphere with a relative humidity of 97%. After that, they were placed on the stage of the balance of our experimental set-up, where temperature (25ºC) and relative humidity (19%) were under control. Finally, the weight loss of the sample was continuously recorded with the help of a computer.

The second experiment was desorption after equilibrium in liquid water at 25ºC. A sample was immersed in liquid water to equilibrate to constant weight and then, after drying its surface with filter paper, the sample was placed on the stage of the balance of our experimental set-up with a relative humidity of 19% at 25ºC to record continuously its weight in a computer. In this case, evaporation takes an important role in the desorption process because these samples have many pores filled with water.

2.2.10. Contact angle measurements.

Contact angle measurements were performed with an optical contact angle measuring device DataPhysics OCA 10. The contact angle of water on the porous polymers was determined as a function of time in order to study the influence of the hydrophilic coating on these porous materials. The so-called

sessile drop method was used to determine the static contact angle. The movie function of the software was used to take pictures every 1 to 2 seconds and determine a contact angle value for every time. All measurements were performed at room conditions (approximately 25ºC and 60% of relative humidity).

3. Results and discussion.

The purpose of this chapter is to show and discuss the results obtained for the synthesis and characterisation of PMMA-*gr*-*pl*PHEA and its pure phases : macroporous PMMA and *pl*PHEA. The behaviour in water of these hydrophilic-hydrophobic materials is also analysed in the last section of this chapter.

3.1. Macroporous PMMA.

Macroporous poly(methyl methacrylate) networks with different porosities and cross-linking densities were synthesised in this work by polymerisation in the presence of ethanol. In this section, the specific volumes, porosities, dynamical-mechanical properties and glass transition of these porous polymers are shown. The morphology of these porous materials was observed by Scanning Electron Microscopy. Bulk PMMA (non-porous) with different cross-linker contents was also synthesised and studied.

3.1.1. Morphology.

Scanning Electron Microscopy was used in order to study the morphology of these porous materials in the dry state. From Figure 3.1 to 3.3, several SEM micrographs are shown in order to observe the influence of the solvent content used in the polymerisation process. The porosity of the samples in the dry state, determined from the apparent specific volumes (P_{d1}, shown in Table 3.3), and the magnification are indicated in each micrograph.

Figure 3.1 shows that an apparent non-porous polymer is obtained for a low concentration of ethanol (20 wt.%). However, this is a porous polymer with its pores collapsed from the drying process. When this polymer is swollen in a good solvent (ethyl acetate), the pores re-open and a porosity of 14 % is obtained (see P_s results in Table 3.3). The same behaviour was found in references [50, 118] where porous PHEA sponges are non-porous in the dry state. When these sponges are swollen in water, the pores open and the porosity of the samples increased up to 60 %.

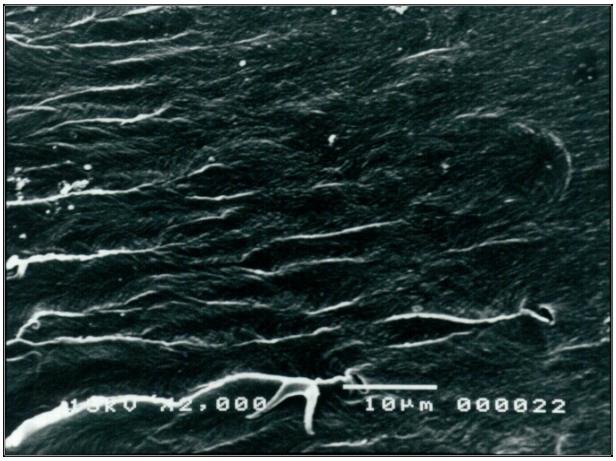

(a)

PMMA1/20E x 2000

Porosity: 0%

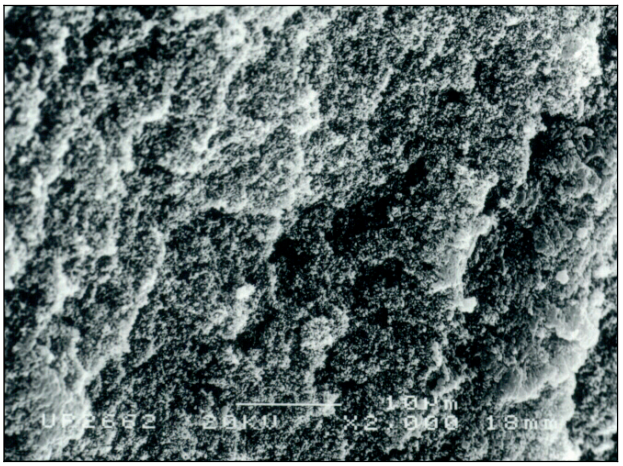

(b)

PMMA1/50E x 2000

Porosity: 8%

Figure 3.1. Influence of the solvent content on the morphology. SEM micrographs of PMMA polymerised in the presence of 20 *(a)* and 50 *(b)* wt.% of ethanol. PMMA samples with 1 wt.% of EGDMA.

A porous polymer is obtained for a 50 wt.% of ethanol (see Figure 3.1). This sample has a porosity of 45 % in the swollen state, 6 times higher than in the dry state (8%). Therefore, many pores are also collapsed in the drying process. For these solvent contents, there are unconnected pores formed by microsyneresis for low concentrations.

Nevertheless, for higher solvent contents (60 wt.%), the transition from microsyneresis to macrosyneresis is produced. A typical structure with spherical polymer particles joined together is formed (see Figure 3.2). For a 60 wt.% of ethanol content, the porosity of the samples increases up to 69% in the dry state. This porosity, on the contrary, decreases down to 61% in the swollen state because the polymeric microspheres swell occupying part of the volume of pores.

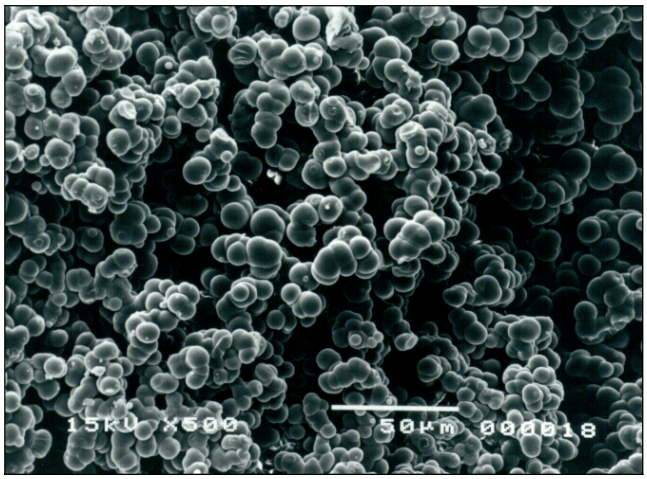

(a)

PMMA1/60E x 500

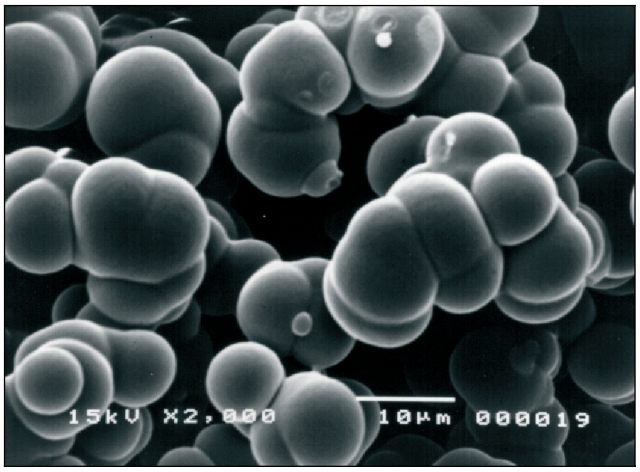

(b)

PMMA1/60E x 2000

Porosity: 69%

Figure 3.2. Influence of the solvent content on the morphology. SEM micrographs of porous PMMA polymerised with 60 wt.% of ethanol and 1wt.% of EGDMA at two different magnifications: 500 *(a)* and 2000 *(b)*.

There is a critical concentration of solvent lower than 60 wt.% from which on a macroporous structure with microspheres joined together and interconnected pores is formed. These PMMA microspheres are all connected and it is possible to measure the mechanical modulus of these samples (see section 3.1.2). For higher solvent contents, a similar morphology is obtained but with larger interconnected pores and more porosity.

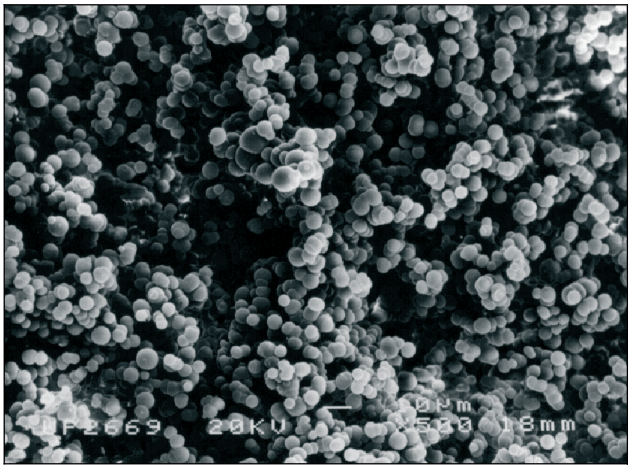

(a)

PMMA1/70E x 500

Porosity: 70%

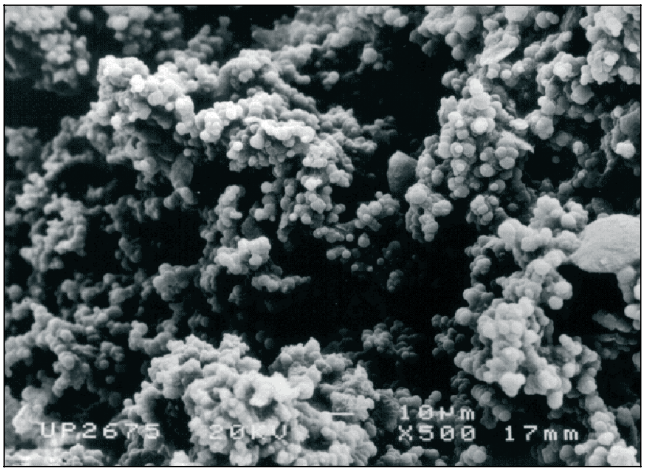

(b)

PMMA1/80E x 500

Porosity: 80%

Figure 3.3. Influence of the solvent content on the morphology. SEM micrographs of porous PMMA polymerised with 1 wt.% of EGDMA and large amounts of ethanol:70 *(a)* and 80 *(b)* wt.%.

The pores of these samples polymerised with 60, 70 and 80 wt.% of ethanol are interconnected and the pore sizes are very irregular ranging from 10 to 100 μm. The porosity of macroporous PMMA polymerised with 70 and 80 wt.% of ethanol is 70 and 80% respectively in the dry state. The porosity of these samples decreases down to 61 and 66% respectively in the swollen state because the microspheres swell occupying volume of pores as happened in sample PMMA1/60E.

It seems that the PMMA microsphere diameter decreases with increasing solvent content. For that reason, these SEM micrographs were analysed measuring around 50 microsphere diameters of each picture in order to have an approximated value of the microsphere diameter for each sample. A size distribution bar graph, the mean, and the standard deviation were determined from these measurements for each sample. The number of microspheres of a given size divided by the total number of measured microspheres is represented against microsphere diameter in this size distribution bar graph. All these results are shown in Table 3.1 and Figure 3.4.

In conclusion, the effect of the solvent content is very strong on the synthesis of macroporous PMMA. The increase of the ethanol content in the polymerisation process of macroporous PMMA produces smaller microspheres with narrower diameter dispersion and higher porosity.

Table 3.1. Mean microsphere diameters of PMMA polymerised with 60, 70 and 80 wt.% of ethanol (mean microsphere diameter ±standard deviation (ϕ_m)). PMMA samples with 1 wt.% of EGDMA.

Sample	ϕ_m **(**μm**)**
PMMA1/60E	7±2
PMMA1/70E	4±1
PMMA1/80E	3±1

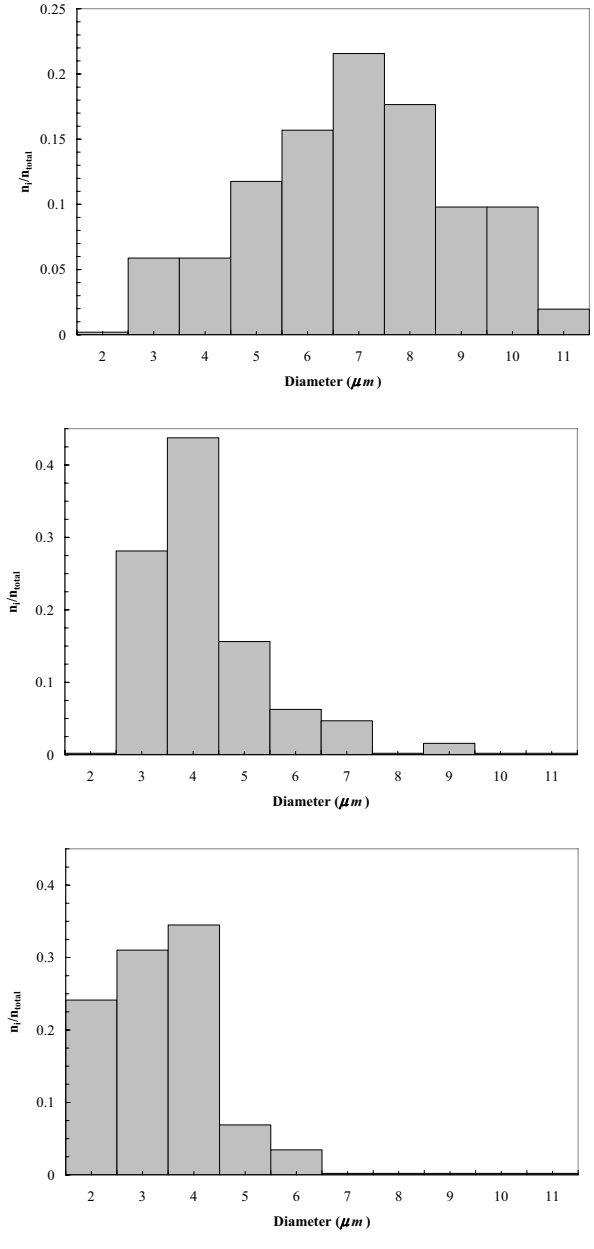

Figure 3.4. Microsphere diameter distribution bar graph of porous PMMA polymerised with 60 *(a)*, 70 *(b)* and 80 wt.% *(c)* of ethanol. PMMA samples with 1 wt.% of EGDMA.

Figures 3.5 and 3.6 are shown in order to observe the influence of the cross-linker content used in the polymerisation process. The porosity of the

samples in the dry state and the magnification are indicated in each micrograph.

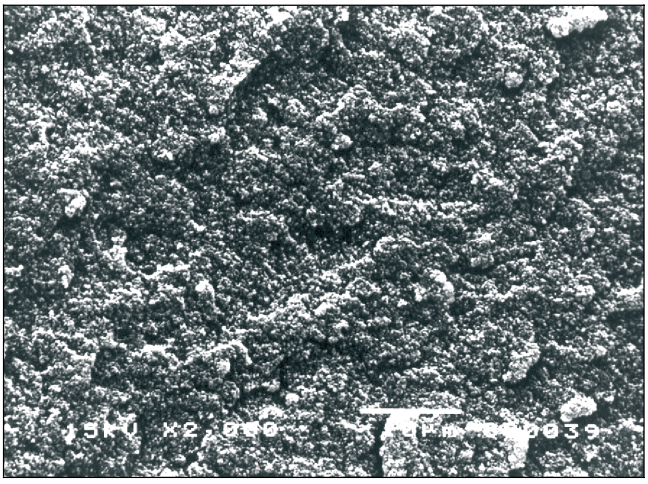

(a)

PMMA5/50E x 2000

Porosity: 26%

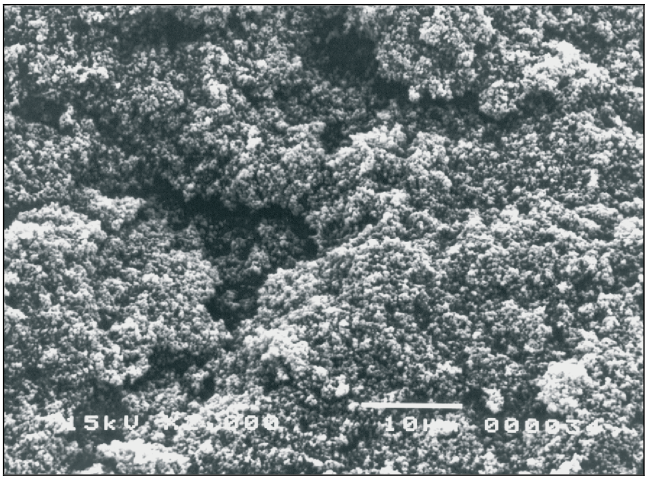

(b)

PMMA10/50E x 2000

Porosity: 52%

Figure 3.5. Influence of the cross-linker content on the morphology. SEM micrographs of porous PMMA polymerised with 50 wt.% of ethanol and two different cross-linker contents: 5 (a) and 10 (b) wt.% of EGDMA.

Cross-linking density has a very strong effect on the morphology of porous PMMA. Thus, sample PMMA10/50E is much more porous than samples PMMA1/50E and PMMA5/50E. The SEM micrograph of sample

PMMA10/50E shows irregular pore sizes ranging from 10 to 30 μm wide. The SEM micrograph of sample PMMA1/50E was shown in Figure 3.1.

Sample PMMA1/50E has a porosity of 8% in the dry state. Nevertheless, this porosity increases up to 26% and 52% when the cross-linker content is increased up to 5 and 10 wt.% respectively. The more cross-linker used in polymerisation process, the larger is the porosity obtained in the dry state.

The cross-linker content has a strong influence in the transition from microsyneresis to macrosyneresis. The SEM micrograph of sample PMMA10/50E shows the previous stage to the transition. Most of the pores of this sample are not collapsed because the porosity only increases from 52 in the dry state up to 55% in the swollen state. However, in microsyneresis the porosity increases very much from the dry to the swollen state because the pores are collapsed and they re-open in the swelling process. Thus, the porosity of samples PMMA1/50E and PMMA5/50 increased very much from the dry state to the swollen state (from 8 to 45% and from 26 to 51% respectively).

The PMMA particles of sample PMMA10/50E start getting spherical shape typical of macrosyneresis but not so well defined like the microspheres observed in sample PMMA1/60E (see Figure 3.2).

The storage modulus of sample PMMA10/50E is considerably lower than that of bulk PMMAB10 in the glassy state (shown in section 3.1.2). Nevertheless, the storage modulus of PMMA1/50E and PMMA5/50E are very close to bulk PMMA polymerised with the same cross-linker content.

It seems that once phase separation occurs as macrosyneresis, the effect of cross-linking on the morphology is not so strong as seen in microsyneresis. The SEM micrographs of macroporous PMMA polymerised with 70 wt.% of ethanol and two different cross-linker contents (5 and 10 wt.%) are shown in Figure 3.6. The SEM micrograph of sample PMMA1/70E can be seen in Figure 3.3.

The SEM micrographs of the three samples with different EGDMA content were analysed (as explained before in this section) in order to have an approximate value of the microsphere diameter for each sample. A size distribution bar graph, the mean and the standard deviation were determined in the same way for each sample. The size distribution plot of sample PMMA1/70E was shown in Figure 3.4.

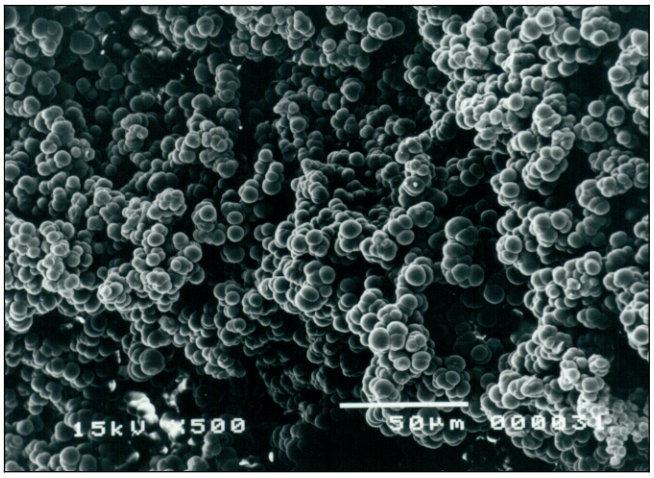

(a)

PMMA5/70E x 500

Porosity: 76%

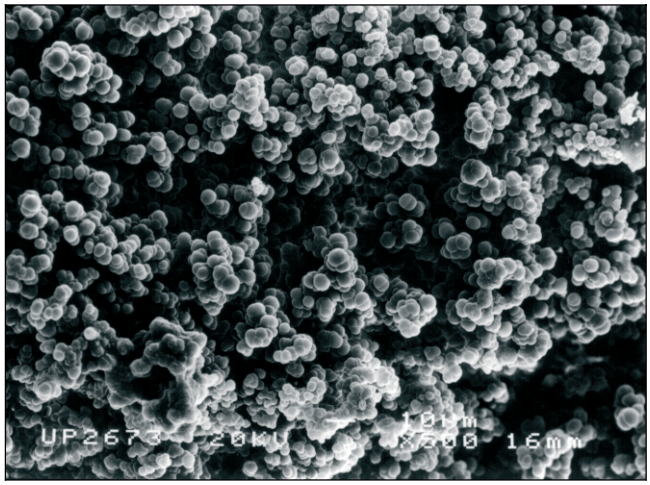

(b)

PMMA10/70E x 500

Porosity: 77%

Figure 3.6. Influence of the cross-linker content on the morphology. SEM micrographs of macroporous PMMA polymerised with the same solvent content (70 wt.% of ethanol) but different cross-linking density: 5 *(a)* and 10 *(b)* wt.% of EGDMA.

Table 3.2. Mean microsphere diameters of PMMA polymerised with the same solvent content (70 wt.% of ethanol) but different cross-linker content: 1, 5 and 10 wt.% of EGDMA (mean microsphere diameter ±standard deviation (ϕ_m)).

Sample	ϕ_m (μm)
PMMA1/70E	4±1
PMMA5/70E	5±1
PMMA10/70E	4±1

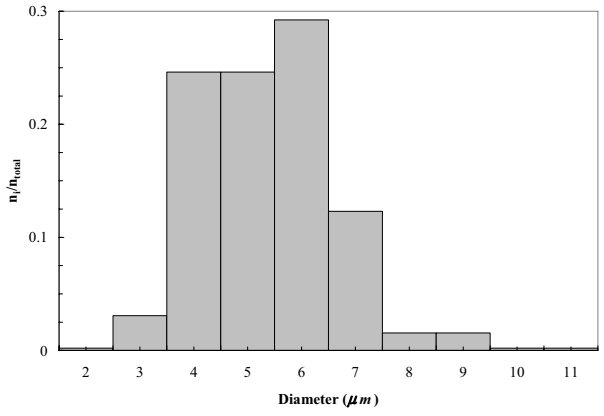

(a)

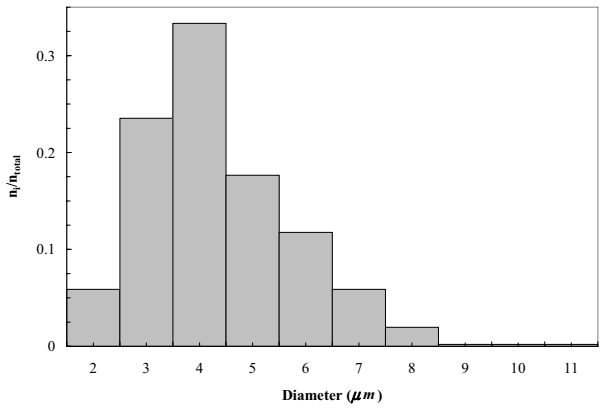

(b)

Figure 3.7. Microsphere diameter distribution bar graph of porous PMMA polymerised with 70 wt.% of ethanol and different cross-linker contents (5 *(a)* and 10 *(b)* wt.%).

When the cross-linker content is increased from 1 to 5 wt.% in PMMA polymerised with 70 wt.% of ethanol, the mean microsphere diameter increases and the microsphere diameter distribution broadens. In addition, the porosity increases from 70 to 76% in the dry state with increasing cross-linking

density. However, the cross-linking density seems not to have much influence on the morphology when the cross-linker content is increased up to 10 wt.%. The PMMA microsphere sizes are similar to PMMA1/70E and its porosity similar to PMMA5/70E. (see Table 3.3).

Therefore, the effect of cross-linking is more important when low solvent contents are added in the polymerisation process of porous PMMA. Increasing the amount of cross-linker implies to increase the porosity very much in microsyneresis. However, for high solvent contents, in macrosyneresis, this effect of cross-linking is smaller. The same effect of cross-linking on the morphology of hydrophilic sponges based on 2-hydroxyethyl methacrylate polymerised in water was found in reference [119].

The specific volumes (v) of bulk PMMA (non-porous) with different cross-linking densities at 25±0.5 ºC are shown in Table 3.3. These results show that the specific volumes of bulk PMMA with three different EGDMA contents (1, 5 and 10 wt.%) are practically equal within the experimental uncertainty ($v \approx 0.860$ cm^3/g).

The apparent specific volumes of macroporous PMMA are also shown in Table 3.3. The apparent specific volume of PMMA polymerised with 50 wt.% of ethanol increases very sharply with increasing cross-linking density.

The porosities in the swollen state (P_s) and in the dry state (P_{d1} and P_{d2}) are shown in Table 3.3 as well. The more ethanol used in the reactive mixture, the more porosity is obtained in the dry state for every cross-linker content. Comparing porosity in the dry state with porosity in the swollen state is a way to know whether the phase separation occurred as 'macrosyneresis' or as 'microsyneresis'. For a low concentration of solvent (microsyneresis), pores are collapsed in the dry state and the samples have less porosity than in the swollen state. These collapsed pores open when the sample is immersed in a good solvent as ethyl acetate and porosity increases. Nevertheless, for a large amount of solvent used in the sample preparation (macrosyneresis), pores are not collapsed. When these samples are swollen in ethyl acetate, the microspheres swell decreasing slightly the porosity in comparison with the dry state.

From the porosity results and from the SEM micrographs, it can be concluded that macrosyneresis starts taking over for a 60 wt.% of ethanol content and 1 wt.% of EGDMA. In addition, porous PMMA polymerised with 50 wt.% of ethanol and 10 wt.% of cross-linker content is the previous stage to the transition from microsyneresis to macrosyneresis. These results show that the situation of either macrosyneresis or microsyneresis depends on the amount of solvent and cross-linker used in the reactive mixture.

In general, the porosity of the samples in the dry state determined from swelling in water (P_{d2}) is smaller than the porosity values determined from the apparent specific volumes (P_{d1}). This fact could be due to water not being able to penetrate in all the pores present in the sample because of the presence of a few non-interconnected pores. This difference between P_{d1} and P_{d2} could also be due to the experimental uncertainty.

There is no value of porosity in the dry state (P_{d2}) for PMMA polymerised with low ethanol contents (20 and 50 wt.%) because water is not able to penetrate in these samples.

Table 3.3. Characteristic parameters of the PMMA networks: specific volumes of bulk PMMA and apparent specific volumes of porous PMMA with different cross-linking densities and porosities at 25ºC±0.5 (v), porosities in the swollen state determined from swelling in ethyl acetate (P_s) and porosities in the dry state determined from the apparent specific volumes (P_{d1}) and from swelling in water (P_{d2}).

Sample	***v* (cm^3/g)**	**P_s (%)**	**P_{d1} (%)**	**P_{d2} (%)**
PMMAB1	0.862±0.002	0	0	0
PMMAB5	0.858±0.002	0	0	0
PMMAB10	0.861±0.002	0	0	0
PMMA1/20E	0.860±0.002	14	0	-
PMMA1/50E	0.933±0.008	45	8	-
PMMA1/60E	2.807±0.011	61	69	63
PMMA1/70E	2.880±0.157	61	70	70
PMMA1/80E	4.272±0.105	66	80	75
PMMA5/50E	1.160±0.029	51	26	-
PMMA5/60E	2.418±0.047	62	65	60
PMMA5/70E	3.569±0.081	66	76	68
PMMA5/80E	4.374±0.121	68	80	81
PMMA10/50E	1.802±0.056	55	52	-
PMMA10/60E	2.826±0.050	61	70	72
PMMA10/70E	3.719±0.095	71	77	72
PMMA10/80E	4.567±0.161	75	81	83

After the phase separation, the solvent suffers evaporation and a porous polymer network is obtained. These porous materials were synthesised with several porosities varying the solvent and cross-linker content. Representing the porosities of the samples as a function of the solvent volume fraction ($\phi_{solvent}$) added in the reactive mixture, this phase separation can be studied.

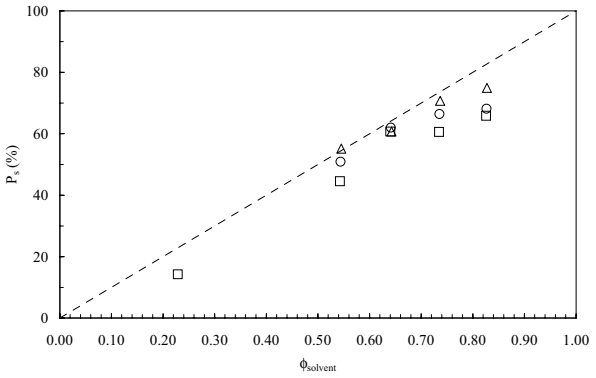

(a)

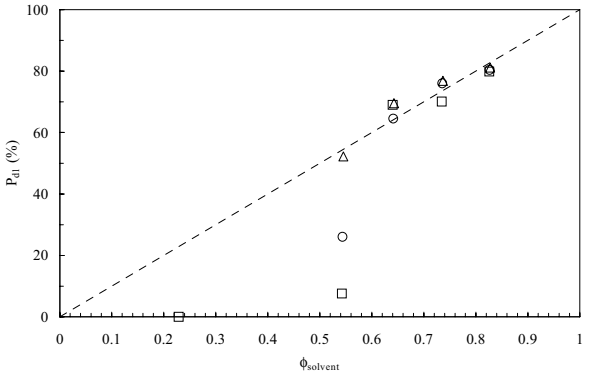

(b)

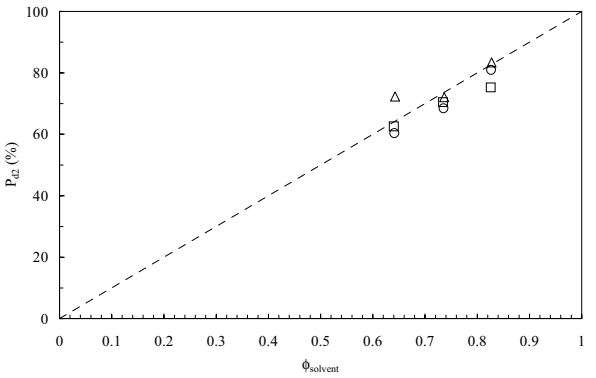

(c)

Figure 3.8. Porosity in the swollen state (P_s *(a)*) and in the dry state determined from the apparent specific volumes (P_{d1} *(b)*) and from swelling in water (P_{d2} *(c)*) as a function of the solvent volume fraction ($\phi_{solvent}$) of porous PMMA with 1 (□), 5 (○) and 10 (△) wt.% of EGDMA cross-linker. Discontinuous straight line indicating P_s, P_{d1} *or* $P_{d2} = \phi_{solvent}$ (---).

All samples have less porosity in the swollen state (P_s) than the solvent volume fraction used in the reactive mixture ($\phi_{solvent}$) except sample PMMA10/50E. The more ethanol used in the reactive mixture, the further the situation is in the swollen state from the ideal value predicted by the equation $P_s = \phi_{solvent}$ (discontinuous straight line in Figure 3.8 *(a)*). However, the more cross-linker used in the polymerisation process, the closer is the situation in the swollen state from the ideal value because increasing cross-linker produces a lower swelling degree and therefore more amount of segregated solvent from the polymer network.

The porosity of the samples polymerised with high ethanol contents decreases after the swelling in ethyl acetate. However, the porosity of the samples polymerised with lower amounts of ethanol increases in the swollen state but always lower than the solvent volume fraction. Sample PMMA10/50E is the only one situated exactly on the ideal straight line $P_s = \phi_{solvent}$, which is in good agreement with the idea of this sample as the previous stage to the transition from microsyneresis to macrosyneresis.

For a solvent volume fraction higher than the critical value ($\phi_{solvent} = 0.6$), all the samples have more or less the same porosity in the dry state as the solvent volume fraction used to prepare each sample (see that P_{d1} and $P_{d2} \approx \phi_{solvent}$ in Figures 3.8 *(b, c)* for high solvent volume fractions). For a solvent volume fraction lower than the critical value, the porosity in the dry state is lower than $\phi_{solvent}$. The transition from microsyneresis to macrosynerises can clearly seen in Figure 3.8 *(b)* in the $\phi_{solvent}$ range from 0.5 to 0.6. The porosity of sample PMMA10/50E is slightly lower than the solvent volume fraction used in the sample preparation because it is the previous stage in the transition from microsyneresis to macrosyneresis.

There are no experimental points for solvent concentrations lower than the critical value in Figure 3.8 *(c)* because these porosity results were determined by swelling in water, which is not able to penetrate the samples with less porosity.

For every solvent volume fraction, the porosity in the swollen state increases with increasing cross-linker content because the swelling degree decreases (see Figure 3.8 *(a)*). Therefore, the microspheres swell less and the porosity decreases less with increasing cross-linker content. Nevertheless, the porosity in the dry state does not follow the same pattern because the samples are dried in one case or water does not swell the PMMA microspheres in the other case (see Figures 3.8 *(b, c)*).

3.1.2. Glass transition and dynamic-mechanical relaxation.

Differential Scanning Calorimetry was performed on bulk PMMA and PMMA polymerised in the presence of different ethanol and cross-linker contents in order to determine the glass transition temperature of these materials at a heating rate of 10ºC/min. These results are shown in Table 3.4.

The heating scans from 80 to 180ºC of bulk PMMA polymerised with three different cross-linker contents are shown in Figure 3.9.

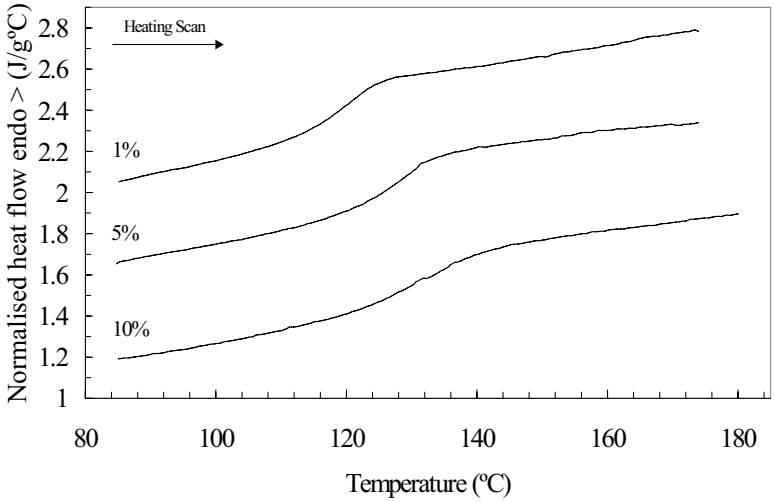

Figure 3.9. DSC heating scans from 80 to 180ºC at a heating rate of 10ºC/min of bulk PMMA polymerised with three different EGDMA cross-linker contents (1, 5 and 10 wt.%).

The glass transition temperature clearly increases with increasing cross-linking density. This is expected because the co-operative conformational rearrangements of the main chains become more difficult as the cross-linking density increases. The glass transition increases 8ºC when increasing cross-linking density from 1 to 5 wt.% (see Table 3.4). However, the T_g only increases 3ºC when increasing cross-linking from 5 to 10 wt.%.

The DSC heating scans of porous PMMA polymerised with different ethanol contents but the same cross-linker content are shown in order to study the glass transition of these materials with different porosities.

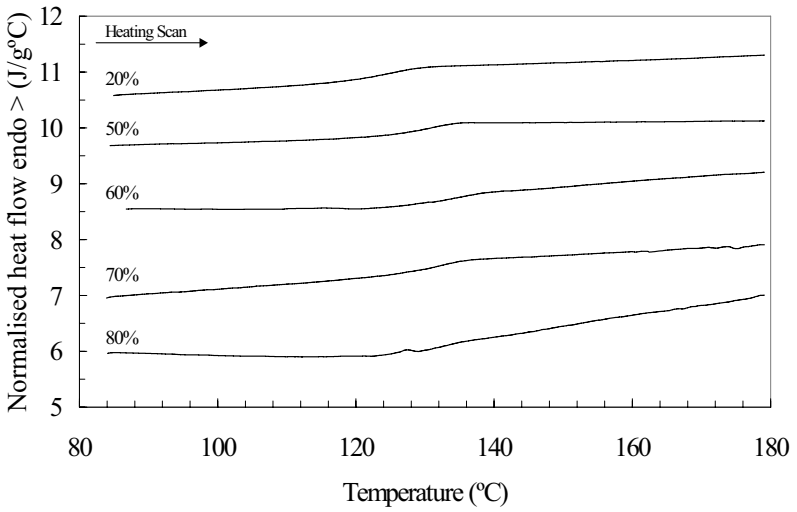

Figure 3.10. DSC heating scans from 80 to 180ºC at a heating rate of 10ºC/min of PMMA polymerised in the presence of different ethanol contents (20, 50, 60, 70 and 80 wt.%) with 1 wt.% of EGDMA.

PMMA polymerised in the presence of ethanol has a glass transition temperature higher than bulk PMMA polymerised with the same cross-linker content (see Table 3.4). The same effect was found in the DMS measurements where the maximum temperature of the α peak was higher for PMMA polymerised in the presence of ethanol than for bulk PMMA (see Figure 3.14 and Table 3.7). The DSC results show that the T_g of PMMA polymerised with 50 wt.% or more ethanol is approximately from 10 to 11ºC higher than bulk PMMA for 1 wt.% of EGDMA. The DMS results show that the maximum temperature of the α peak of PMMA polymerised with 50 or more wt.% of ethanol appears 8ºC higher than for bulk PMMA for 1 wt.% of EGDMA. These differences found in the glass transition temperature between bulk PMMA and porous PMMA must be due to the presence of ethanol in the polymerisation process.

However, the glass transition temperature of sample PMMA1/20E is only approximately 4.5ºC higher. The DMS results of this sample also showed similar α peak than bulk PMMA.

Similar behaviours of increasing the glass transition temperature for PMMA polymerised in the presence of 50 or more wt.% of ethanol were found for PMMA polymerised with 5 wt.% of EGDMA (see Figure 3.11 and Table 3.4).

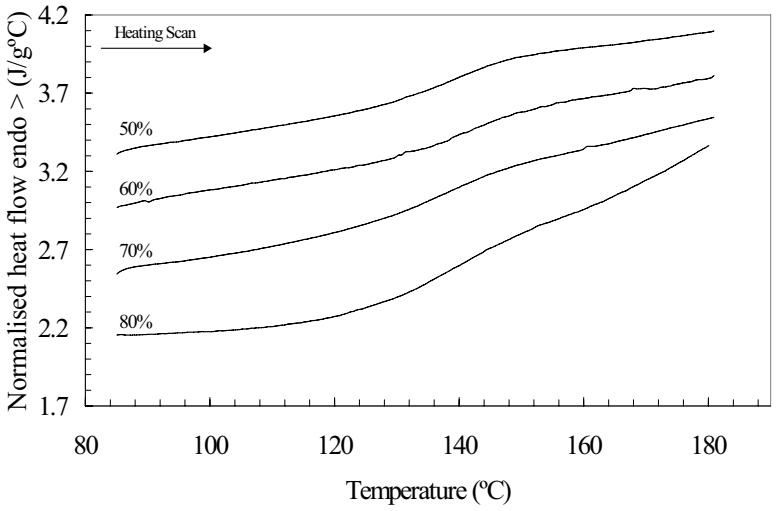

Figure 3.11. DSC heating scans from 80 to 180ºC at a heating rate of 10ºC/min of PMMA polymerised in the presence of different ethanol contents (50, 60, 70 and 80 wt.%) with 5 wt.% of EGDMA cross-linker.

PMMA polymerised with 5 wt.% of EGDMA in the presence of 50 wt.% or more ethanol has a glass transition temperature from approximately 7 to 11ºC (depending on the amount of ethanol) higher than bulk PMMA polymerised with the same cross-linker content. Nevertheless, this increase of T_g is much higher (from 15 to 24ºC depending on the amount of solvent) in porous PMMA polymerised with 10 wt.% of EGDMA (see Figure 3.12 and Table 3.4).

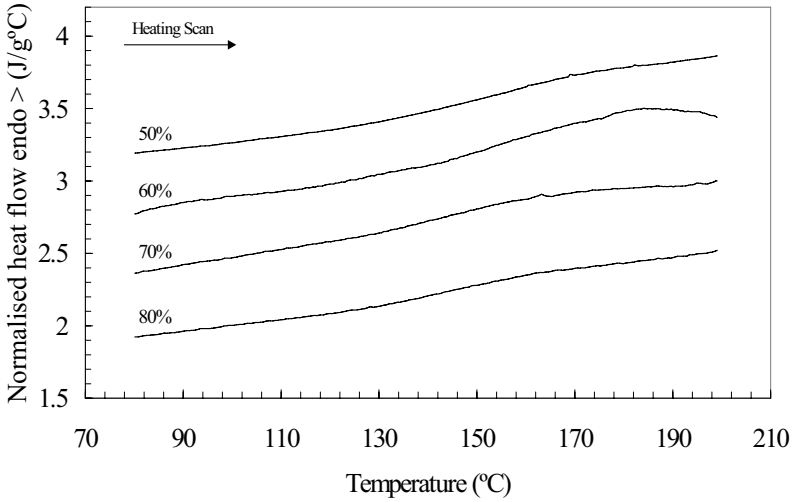

Figure 3.12. DSC heating scans from 80 to 200ºC at a heating rate of 10ºC/min of PMMA polymerised in the presence of different ethanol contents (50, 60, 70 and 80 wt.%) with 10 wt.% of EGDMA cross-linker.

Table 3.4. DSC glass transition temperature of bulk PMMA and PMMA polymerised in the presence of ethanol with different cross-linking densities in the dry state.

Sample	Tg (ºC)
PMMAB1	119.6
PMMAB5	127.5
PMMAB10	130.5
PMMA1/20E	124.0
PMMA1/50E	129.9
PMMA1/60E	130.2
PMMA1/70E	130.8
PMMA1/80E	131.1
PMMA5/50E	138.4
PMMA5/60E	138.8
PMMA5/70E	134.8
PMMA5/80E	134.2
PMMA10/50E	152.0
PMMA10/60E	151.0
PMMA10/70E	154.6
PMMA10/80E	145.5

The dynamic-mechanical properties of bulk PMMA are well known [53] (see DMS spectra of bulk PMMA in Figure 1.4).

The storage modulus and the loss tangent of bulk PMMA synthesised in this work with 1 wt.% of EGDMA as a function of temperature are shown in Figure 3.13. The internal friction (tan δ) curve goes through a maximum (α peak) at approximately 140ºC, which corresponds to the glass transition region. In this region, the damping is high owing to the initiation of segmental motion in molecular chains. This is the main relaxation. The storage modulus starts falling from the lowest temperature of the experiment because of another relaxation transition in the glassy state, the β relaxation, which is associated with side-chain motion of the ester group. In this experimental spectrum the γ relaxation cannot be seen because it appears at lower temperatures. That relaxation involves motion of the methyl groups attached to the main chain.

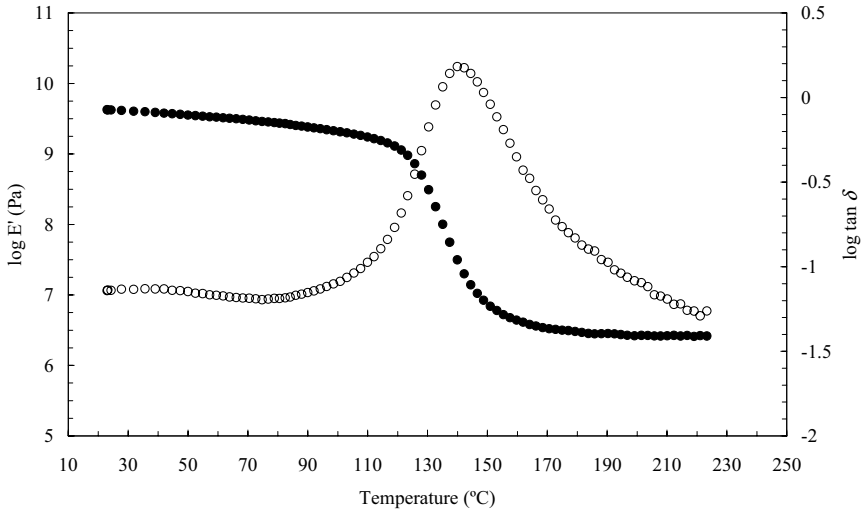

Figure 3.13. Temperature dependence of the real part of the elastic modulus (solid symbols) and the loss tangent (open symbols) of PMMA polymerised with 1 wt.% of EGDMA. Only one point out of ten is plotted to obtain a clearer representation.

The effect of the solvent content used in the polymerisation process on the dynamic-mechanical properties of PMMA with 1 wt.% of EGDMA was studied comparing the relaxation spectra of bulk PMMA and PMMA polymerised in the presence of different amounts of ethanol (see Figure 3.14).

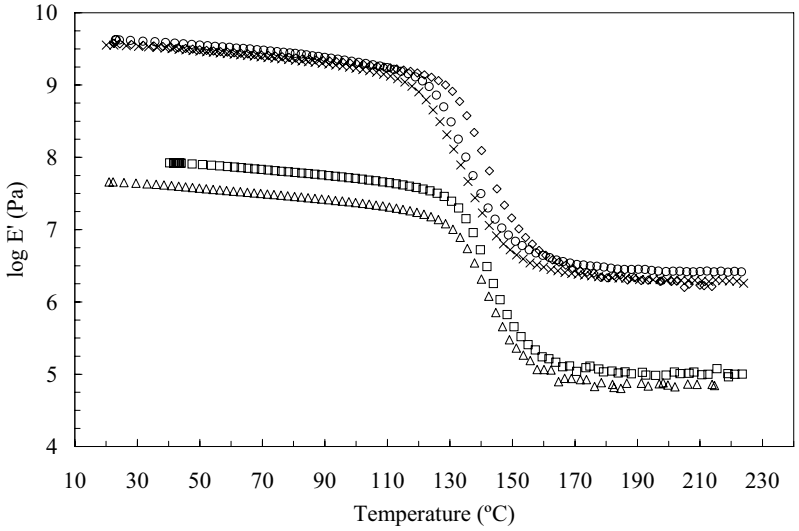

(a)

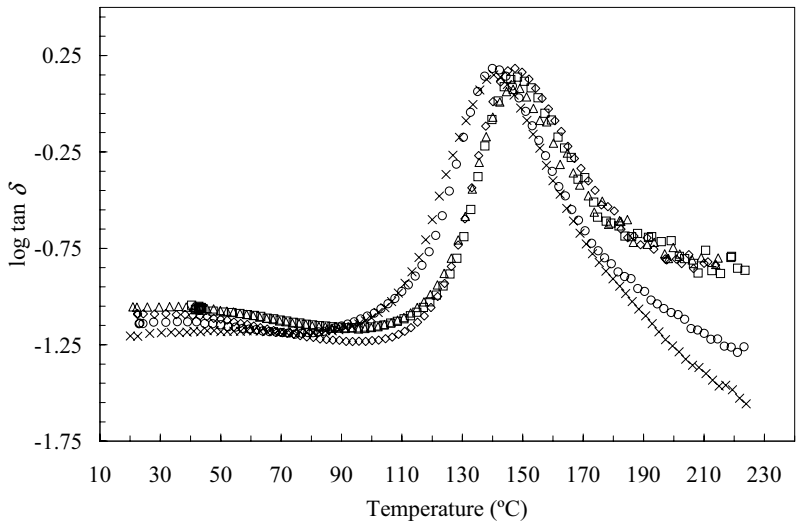

(b)

Figure 3.14. Temperature dependence of the real part of the elastic modulus (a) and the loss tangent (b) of bulk PMMA (○) and porous PMMA polymerised with 20 (X), 50 (◇), 60(□) and 70 (△) wt.% of ethanol. All of the samples polymerised with 1 wt.% of EGDMA. Only one point out of ten is plotted to obtain a clearer representation.

The storage modulus of all the PMMA samples polymerised in the presence of ethanol starts falling from the lowest temperature of the experiment because of the β relaxation.

For low ethanol contents, the relaxation spectrum of porous PMMA are very close to bulk PMMA. Both PMMA polymerised with 20 and 50 wt.% of ethanol have the storage modulus slightly lower than bulk PMMA in both glassy and rubbery state. Bulk PMMA and PMMA polymerised with 20 wt.% of ethanol have similar storage modulus in the glassy state because PMMA1/20 is non-porous in the dry state (collapsed porosity).

The main relaxation peak appears at the same temperature for bulk PMMA and PMMA1/20E. Nevertheless, the α peak of sample PMMA1/50E appears at approximately 8ºC higher. The α peak of porous PMMA polymerised with 60 and 70 wt.% also appears 8ºC higher than bulk PMMA (see Figure 3.14). The samples were drastically dried at 180ºC in vacuo until constant weight to be sure that this shift of 8ºC did not happen due to the presence of solvent remaining from the washing process, however, still the same results were found. Bulk PMMA samples with lower thickness were also prepared so that they were easier to dry but their α peak still appeared at 8ºC lower than the porous PMMA samples. Finally, another set of bulk samples was directly dried without being washed in a solvent but the same result was obtained.

This increase of the maximum temperature of the main relaxation in the PMMA samples polymerised in the presence of 50 or higher wt.% of solvent also happened for PMMA polymerised with 5 and 10 wt.% of EGDMA (see Figures 3.15 and 3.16). The α peak of porous PMMA polymerised with 5 and 10 wt.% of cross-linker is for all the samples around 12ºC and 14 ºC higher than bulk PMMA polymerised with the same cross-linker content respectively. There is a critic amount of solvent (50 wt.%) from which on the α peak increases around 8, 12 or 14ºC depending on the amount of cross-linker used in the polymerisation process (1, 5 or 10 wt.% respectively). All the α peaks appear around the same temperature. These small differences of *tan* δ must be due to the presence of ethanol in the polymerisation process.

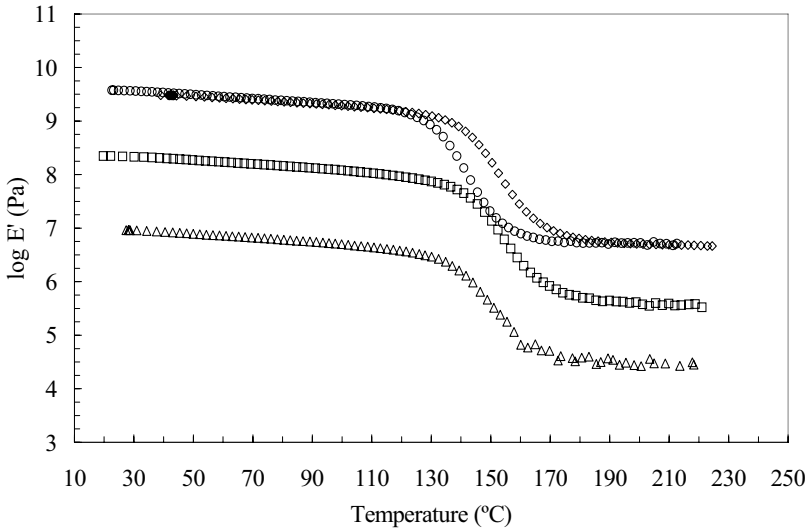

(a)

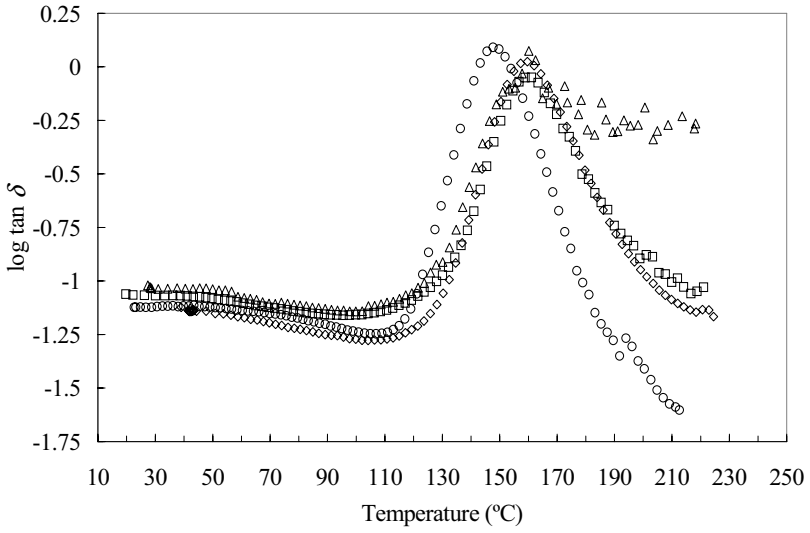

(b)

Figure 3.15. Temperature dependence of the real part of the elastic modulus *(a)* and the loss tangent *(b)* of PMMA polymerised with 5 wt.% of EGDMA: bulk PMMA (○) and PMMA polymerised with 50 (◇), 60 (□) and 70 (△) wt.% of ethanol. Only one point out of ten is plotted to obtain a clearer representation.

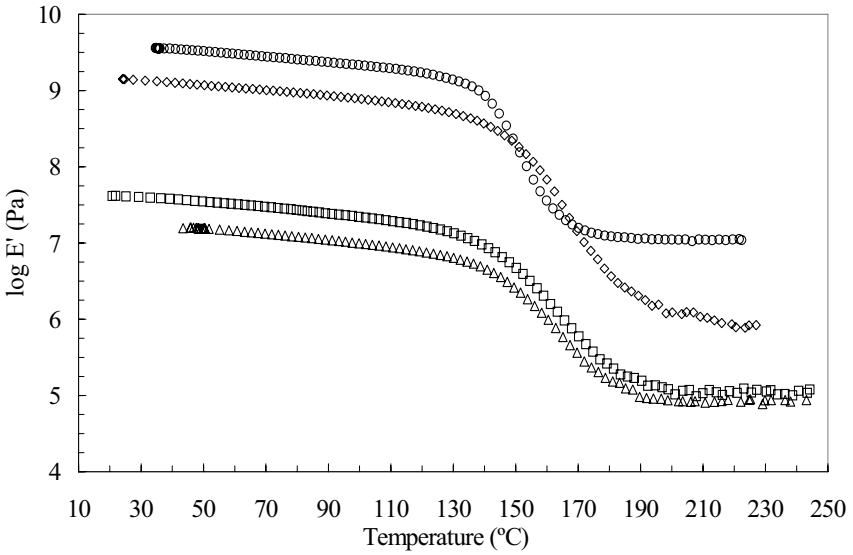

(a)

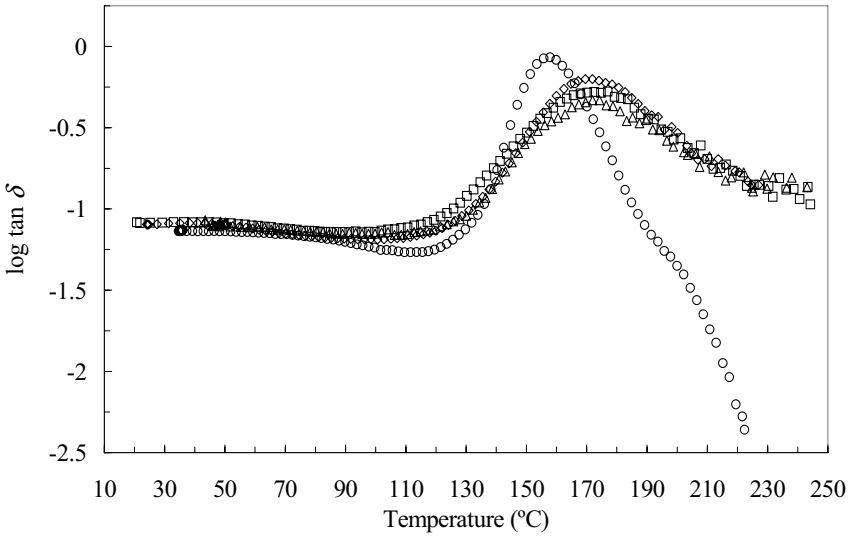

(b)

Figure 3.16. Temperature dependence of the real part of the elastic modulus *(a)* and the loss tangent *(b)* of PMMA polymerised with 10 wt.% of EGDMA: bulk PMMA (○) and PMMA polymerised with 50 (◇), 60 (□) and 70 (△) wt.% of ethanol. Only one point out of ten is plotted to obtain a clearer representation.

The loss tangent of the bulk PMMA polymerised with the highest EGDMA content (sample PMMAB10) shows a shoulder at high temperatures probably due to the presence of aggregates with crosslinking density higher than average (see Figure 3.16 (*b*)).

It was seen in section 3.1.1 that PMMA polymerised in the presence of a high concentration of ethanol has the typical structure of macrosyneresis with microspheres joined together with large interconnected pores. This sample has a much lower storage modulus than bulk PMMA. The storage modulus decreases with increasing the amount of solvent added in the reactive mixture and once phase separation occurs as macrosyneresis, the storage modulus falls to a much lower value both in the glassy and in the rubbery state.

Sample PMMA1/50E (8 % of porosity) and PMMA5/50E (26% of porosity) has a slightly lower storage modulus than PMMAB1 and PMMAB5 respectively. Nevertheless, sample PMMA10/50E, that is much more porous (52%), shows a much lower storage modulus than PMMAB10. The storage modulus of this sample is lower in the glassy state and even lower in the rubbery state than the bulk sample.

In conclusion, porosity plays a very important role in the dynamic-mechanical properties of these materials. In comparison with bulk PMMA, the storage modulus decreases very sharply with increasing porosity for solvent concentrations from the critical one (60 wt.%) because the microspheres are more and more separated and the effective cross-section decreases. The main relaxation (α peak) seems not to be influenced by the porosity appearing always at the same temperature for 50, 60, 70 wt.% of ethanol. However, comparing samples with the same cross-linking density, bulk PMMA has the main relaxation always at approximately 8, 12, 14ºC lower than macroporous PMMA depending on the amount of cross-linker (1, 5 or 10 wt.% respectively). This feature must be due to the presence of ethanol in the polymerisation process, which helps cyclation producing a different structure of the network. It was seen before in this section that the glass transition temperature measured by DSC is also higher for PMMA polymerised in the presence of ethanol than for bulk PMMA (see Table 3.4). Another explanation of this feature could be the effect of the surface energy due to the increase of specific area.

The relaxation spectra of bulk PMMA with three different cross-linker contents (1, 5 and 10 wt.%) are plotted all together in Figure 3.17 in order to study the effect of cross-linking.

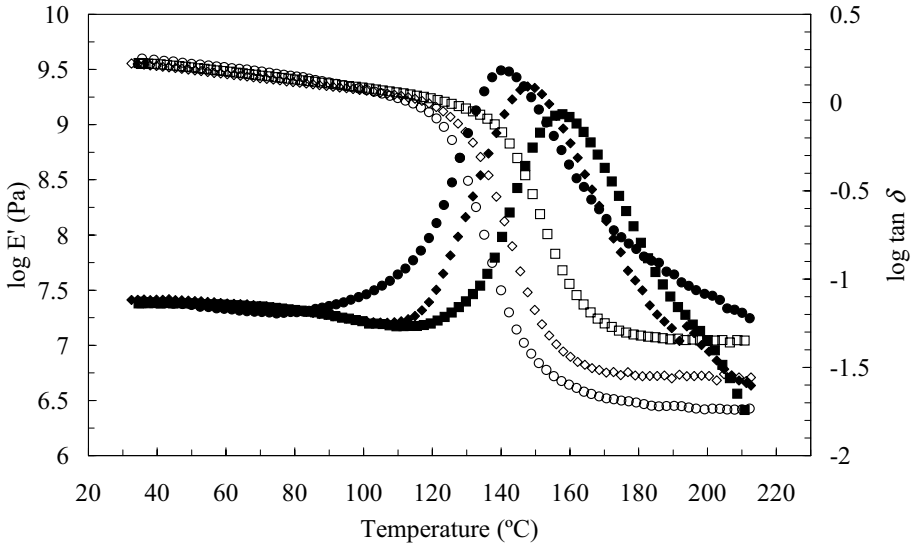

Figure 3.17. Temperature dependence of the storage modulus (open symbols) and the loss tangent (solid symbols) of bulk PMMA with 1 (○), 5 (◇) and 10 (□) wt.% of EGDMA. Only one point out of ten is plotted to obtain a clearer representation.

The effect of cross-linking on the dynamic-mechanical properties of bulk PMMA is evident above T_g. The α peak shifts to higher temperatures with increasing cross-linking. This result is expected since the co-operative conformational rearrangements of the main chains become more difficult as the cross-linking density increases.

The storage modulus in the rubbery state is a sensitive indicator of cross-linking. According to the theory of rubber elasticity, using the affine network model, the mean molecular weight between cross-links of the elastically active chains ($\overline{M_e}$) can be determined from the elastic modulus in the plateau region corresponding to the rubberlike behaviour (E_r') as

$$\overline{M_e} = \frac{\rho RT}{G_e} \tag{3.1}$$

where G_e is the shear modulus in the elastomeric region, which can be estimated as $G_e = E_r'/3$, ρ is the density and R is the universal gas constant.

Thus, the $\overline{M_e}$ values of bulk PMMA with three different cross-linker contents were calculated with the elastic modulus in the rubberlike region and the densities at 200ºC (see Table 3.6). The specific volumes (v) of bulk PMMA were experimentally measured at 25ºC (see Table 3.3) and they were calculated at 200ºC using the expansion coefficients of PMMA (α_g =2.55·10^{-4}K^{-1} ($T<T_g$) and α_r =5.75·10^{-4}K^{-1} ($T>T_g$) taken from [120]) as

$$\ln v(T) = \ln v(298\ K) + \int_{298}^{T_g} \alpha_g \cdot dT + \int_{T_g}^{T} \alpha_r \cdot dT \qquad (3.2)$$

where T_g is the glass transition temperature determined by DSC (Table 3.4). Thus, the specific volumes and the elastic modulus at 200ºC of bulk PMMA with three different cross-linker contents are shown in Table 3.5.

Table 3.5. Specific volumes (v) and storage modulus (E_r') at 200ºC of bulk PMMA with different cross-linker contents.

EGDMA content (wt.%)	*v at 200ºC (cm^3/g)*	*E_r' at 200ºC (MPa)*
1	0.925	2.711
5	0.918	5.201
10	0.921	11.129

The mean number of monomeric units between cross-links of the elastically active strands ($\bar{n}_e$), calculated as $\overline{M_e} / \overline{M_{MMA}}$ ($\overline{M_{MMA}}$ =100 g/mol), decreases as the EGDMA content in the initial mixture of monomers increases. For a perfect network, the number of monomers between cross-linking points expected from stoichiometry ($\bar{n}_{st}$) is half the ration of the MMA and EGDMA mole numbers because the cross-linker is tetrafunctional.

$$\bar{n}_{st} = \frac{\overline{M_{EGDMA}}}{2 \cdot \overline{M_{MMA}} \cdot \dfrac{m_{EGDMA}}{m_{MMA}}} \qquad (3.3)$$

where $\overline{M_{EGDMA}}$ = 198 g/mol.

These results of $\bar{n}_e$ and $\bar{n}_{st}$ are shown in Table 3.6. For a cross-linker content of 1 wt.%, $\bar{n}_e < \bar{n}_{st}$, which means that entanglements contribute to the elastic response. For PMMA with 5 and 10 wt.% of EGDMA, however, the situation is $\bar{n}_e > \bar{n}_{st}$, which means that the number of cross-linker molecules lost in inelastic joints increases rapidly with cross-linker concentration in the reactive mixture [121].

Table 3.6. Characteristic parameters of PMMA as a function of the EGDMA content: molar ratio of MMA to EGDMA monomers in the polymerisation mixture (n_{MMA}/n_{EGDMA}), average molecular weight between cross-links of elastically active chains ($\overline{M_e}$), average number of MMA between cross-links in elastically active chains ($\bar{n}_e$) and average number of MMA monomers between cross-links according to stoichiometry in a perfect network ($\bar{n}_{st}$).

EGDMA content (wt.%)	n_{MMA}/n_{EGDMA}	$\overline{M_e}$ *(g/mol)*	$\bar{n}_e$	$\bar{n}_{st}$
1	196.0	4702.6	47.0	98.0
5	37.6	2468.8	24.7	18.8
10	17.8	1150.8	11.5	8.9

The relaxation spectra of PMMA polymerised with 50 wt.% of ethanol and three different cross-linker contents (1, 5 and 10 wt.%) are shown in Figure 3.18 in order to study the effect of cross-linking in microsyneresis.

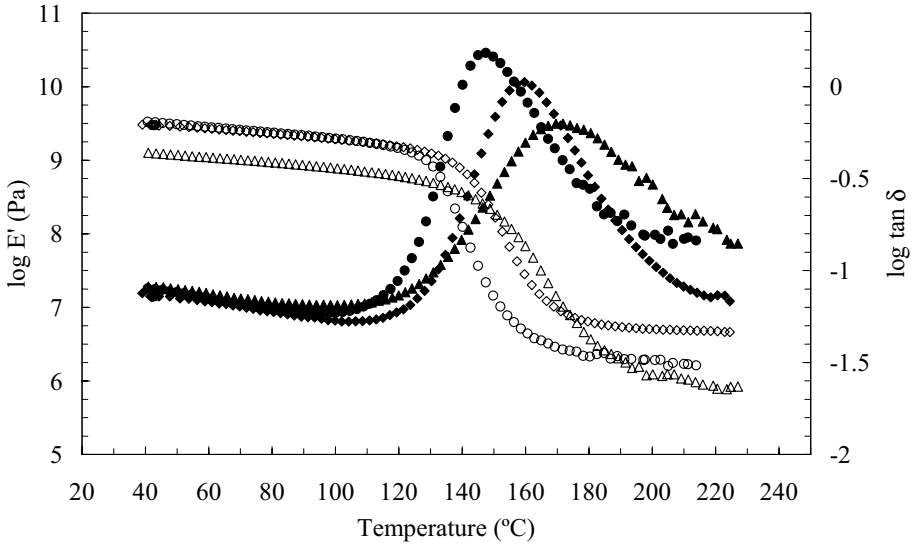

Figure 3.18. Temperature dependence of the storage modulus (open symbols) and the loss tangent (solid symbols) of MMA polymerised with 50 wt.% of ethanol and 1 (○) (P_{dl} = 8%), 5 (◇) (P_{dl} = 26%) and 10 (△) (P_{dl} = 52%) wt.% of EGDMA. Only one point out of ten is plotted to obtain a clearer representation.

The α peak of the main relaxation shifts to higher temperatures with increasing cross-linking as expected. Even though porosity increases from 8 to 26 when the cross-linking density is increased from 1 to 5 wt.%, the storage modulus increases only in the rubbery state. Nevertheless, for a cross-linker content of 10 wt.%, the storage modulus decreases in the glassy and rubbery state due to the big increase of porosity (52%).

The relaxation spectra of PMMA polymerised with 60 wt.% of ethanol and three different cross-linker contents (1, 5 and 10 wt.%) are shown in Figure 3.19 in order to study the effect of cross-linking in macrosyneresis.

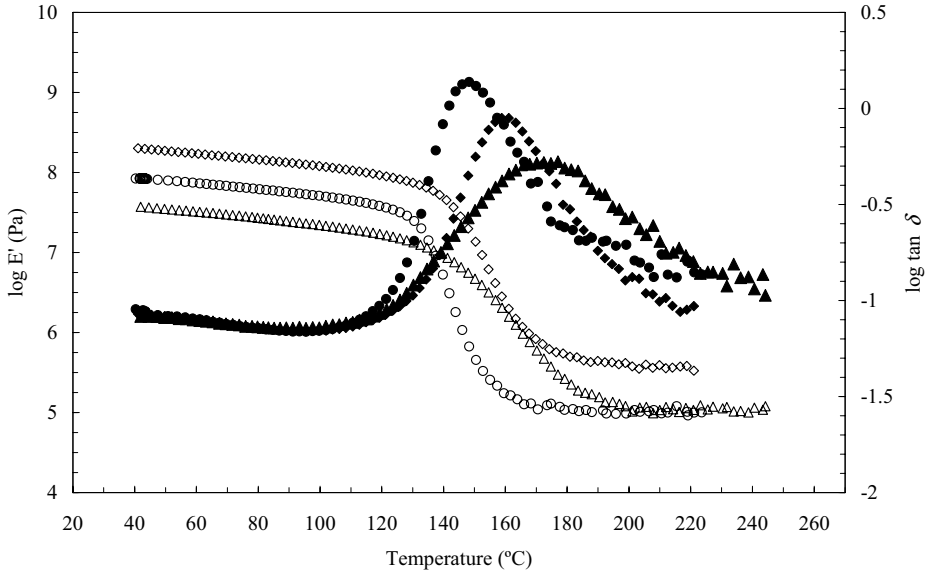

Figure 3.19. Temperature dependence of the storage modulus (open symbols) and the loss tangent (solid symbols) of PMMA polymerised with 60 wt.% of ethanol and 1 (○) (P_{dl} = 69%), 5 (◇) (P_{dl} = 65%) and 10 (△)(P_{dl} = 70%) wt.% of EGDMA. Only one point out of ten is plotted to obtain a clearer representation.

The main relaxation peak also shifts to higher temperatures with increasing cross-linking density as expected. The storage modulus of sample PMMA5/60E is higher than PMMA1/60E in the glassy and rubbery state because the sample polymerised with 5 wt.% of EGDMA is less porous. Nevertheless, PMMA polymerised with 1 and 10 wt.% have similar porosities and the storage modulus falls in the glassy state with increasing cross-linker content. In the rubbery state, both samples with similar porosities have similar mechanical behaviour. Porosity has more effect than cross-linking density

because only 5% less of pores produces a considerable improvement in the dynamic-mechanical properties.

The maximum temperature of the loss tangent (T^{α}), the storage modulus in the glassy state at 40ºC (E'_g) and in the rubbery state at 210ºC (E'_r) for all the PMMA samples are summarised in Table 3.7. Cross-linking has a strong effect on the loss tangent of macroporous PMMA. The main relaxation (α peak) always broadens and shifts to higher temperatures with increasing cross-linking density. However, there is not a clear effect of cross-linking on the storage modulus.

The storage modulus in the glassy state at 40ºC and in the rubbery state at 210ºC as a function of porosity in the dry state (P_{dl}) for macroporous PMMA polymerised with 1, 5 and 10 wt.% of EGDMA are shown in Figure 3.20.

Table 3.7 Maximum temperature of the loss tangent (T^{α}), storage modulus in the glassy state at 40ºC (E'_g) and in the rubbery state at 210ºC (E'_r) of bulk PMMA and PMMA polymerised in the presence of different ethanol and cross-linker contents.

SAMPLE	T^{α} (ºC)	Log E'_g (Pa) at 40ºC	Log E'_r (Pa) at 210ºC
PMMAB1	140.6	9.59	6.42
PMMAB5	148.1	9.53	6.74
PMMAB10	157.0	9.55	7.03
PMMA1/20E	140.8	9.50	6.30
PMMA1/50E	147.0	9.53	6.23
PMMA1/60E	147.8	7.92	5.02
PMMA1/70E	147.5	7.61	4.87
PMMA5/50E	159.4	9.48	6.69
PMMA5/60E	160.0	8.30	5.59
PMMA5/70E	159.4	6.93	4.20
PMMA10/50E	171.0	9.10	6.06
PMMA10/60E	172.7	7.58	5.03
PMMA10/70E	173.1	7.20	4.91

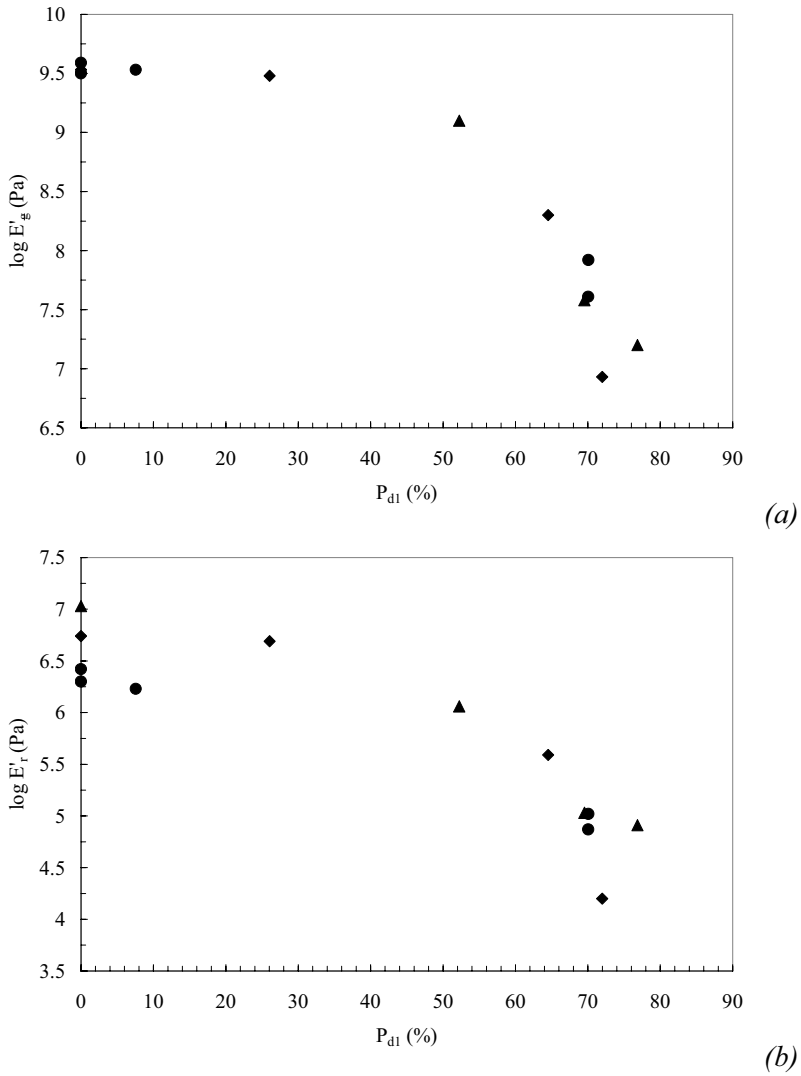

Figure 3.20. Storage modulus in the glassy state at 40ºC *(a)* and in the rubbery state at 210ºC *(b)* as a function of porosity in the dry state (P_{dl}) of macroporous PMMA polymerised with 1 (●), 5(◆) and 10 (▲) wt.% of EGDMA. Values taken from Tables 3.3 and 3.7.

The storage modulus decreases with increasing porosity in both states (glass and rubber). For a given porosity, there are small discrepancies due to the effect of cross-linking.

There is a clear difference between microsyneresis and macrosyneresis. The effect of porosity is more important than the effect of

cross-linking in macrosyneresis because it is more important the way that the PMMA microspheres are packed than the mechanical modulus of the PMMA microspheres. However, the mechanical modulus of bulk PMMA or PMMA with a low degree of porosity (microsyneresis) depend very much on the cross-linking density.

Bulk PMMA and PMMA polymerised with different solvent contents have different effective cross-sections. Therefore, the modulus of the samples was normalised to be compared and see if there is any configuration change for a given EGDMA content. Thus, the DMS spectra shown from Figure 3.14 to 3.16 were normalised dividing E' by the storage modulus measured at 40ºC and shown in Table 3.7 (log E'/(logE'$_g$ at 40ºC)). If the normalised DMS plot of a porous PMMA sample is similar to the DMS spectrum of bulk PMMA, it means that their DMS spectra differ exclusively because they have different effective cross-section. However, if the normalised plots differ, they must have different structure or configuration.

First of all, the normalised storage modulus of bulk PMMA and PMMA polymerised in the presence of different ethanol contents with 1 wt.% of EGDMA are shown in Figure 3.21.

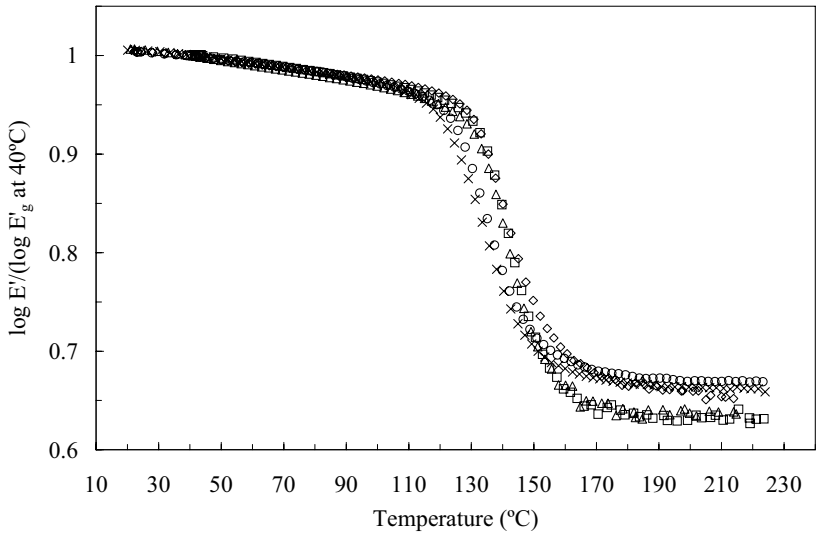

Figure 3.21. Normalised storage modulus of bulk PMMA (○) and PMMA polymerised with 20 (X), 50 (◇), 60(□) and 70 (△) wt. of ethanol. All the samples polymerised with 1 wt.% of EGDMA.

The normalised graph of bulk PMMA and PMMA polymerised with 20 and 50 wt.% of ethanol (microsyneresis) are quite similar, which means that the differences seen in Figure 3.14 were exclusively due to the different effective cross-sections. However, the normalised plots of PMMA polymerised with 60 and 70 wt.% of ethanol (macrosyneresis) are different from bulk PMMA, which means that they must have a different structure.

The normalised DMS plots of bulk PMMA and PMMA polymerised in the presence of different ethanol contents with 5 and 10 wt.% of EGDMA content are plotted together in Figures 3.22 and 3.23 respectively.

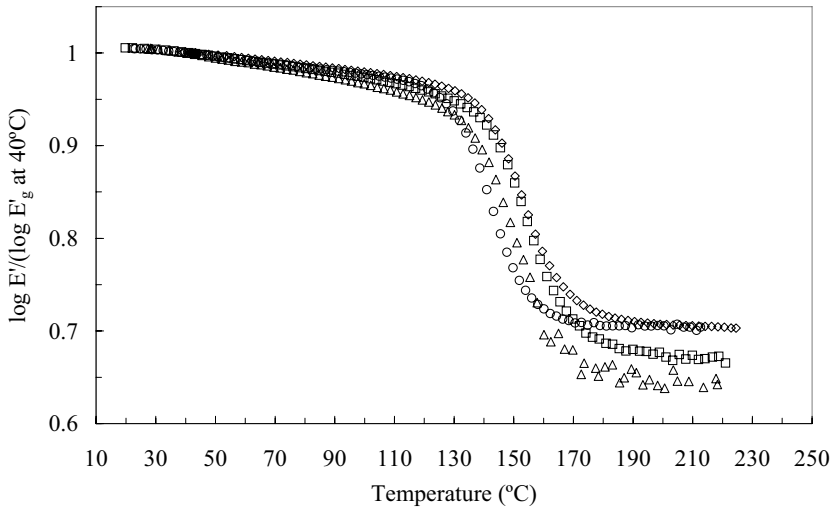

Figure 3.22. Normalised storage modulus of bulk PMMA (○) and PMMA polymerised with 50 (◇), 60(□) and 70 (△) wt.% of ethanol. All of the samples polymerised with 5 wt.% of EGDMA.

The normalised plots of PMMA polymerised with more than 50 wt.% of ethanol are also different from bulk PMMAB5 because of having different structures (see Figure 3.22). The normalised plot of PMMA5/50E is also similar to bulk PMMAB5 because the differences seen in Figure 3.15 were because they have different effective cross-sections as PMMA polymerised with 1 wt.% of EGDMA. Nevertheless, the normalised DMS spectrum of PMMA10/50E is different from bulk PMMAB10 (see Figure 3.23), which is a good indication of the transition limit from microsyneresis to macrosyneresis. The normalised DMS plots of porous PMMA polymerised with high ethanol contents (macrosyneresis) and 10 wt.% of cross-linker are also different from bulk PMMA as seen for porous PMMA polymerised with 1 and 5 wt.% of

EGDMA.

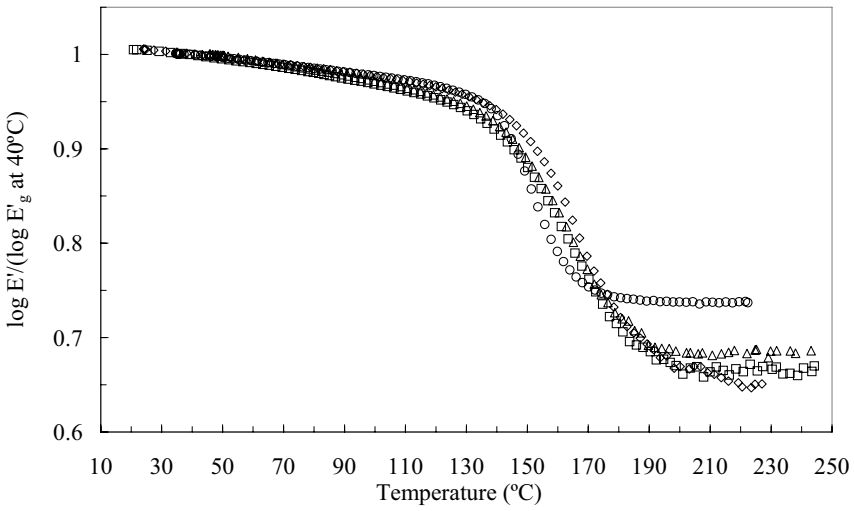

Figure 3.23. Normalised storage modulus of bulk PMMA (○) and PMMA polymerised with 50 (◇), 60 (□) and 70 (△) wt. of ethanol. All of the samples polymerised with 10 wt.% of EGDMA.

Takayanagi's block model was applied in order to see if the DMS differences found between bulk PMMA and PMMA polymerised in the presence of ethanol mainly occurred because these materials have very different structures. The shift of the main relaxation observed between these two PMMA materials could be a consequence of a decrease of material, which keeps the same mechanical behaviour as bulk PMMA.

The dynamic mechanical behaviour of heterogeneous systems can be predicted from the pure phases by means of Takayanagi's block model. Thus, this mechanical model is applied to predict the behaviour of porous PMMA from bulk PMMA (non-porous) and the other phase composed of pores. For example, sample PMMA10/60E is predicted from two phases: PMMAB10 and the porosity of PMMA10/60E in the dry state (P_{d1}).

Takayanagi's block model was explained in section 1.6 (equations 1.1-1.7). This mechanical model has two adjustable parameters (ϕ, λ). However, the only adjustable parameter is the fraction of continuous phase acting in series (λ) because the porosity in the dry state ($\phi = P_{d1}$) was experimentally determined in this thesis (see Table 3.3).

The experimental results of the temperature dependence of the storage modulus for sample PMMA1/50E and its prediction, determined from bulk PMMAB1 and the porosity of PMMA1/50E in the dry state (P_{dl}) with the Takayanagi block model, is shown in Figure 3.24.

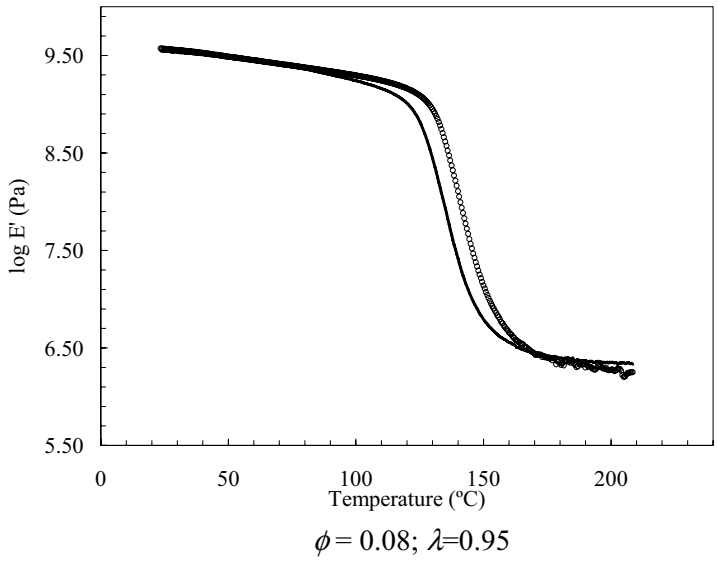

Figure 3.24. Temperature dependence of the storage modulus of PMMA1/50E: experimental values (○) and the Takayanagi block model (continuous line) considering a material composed of two phases: PMMAB1 and the porosity of PMMA1/50E (fraction $\phi = P_{dl}$). The adjustable parameter λ is shown.

Takayanagi's block model predicts very well the storage modulus of PMMA1/50E in the glassy and in the rubbery state (see Figure 3.24). However, the model does not predict well the glass transition but it is parallel to the experimental results in this region. The adjustable parameter λ is close to 1, which makes sense because the small volume fraction of pores.

When the cross-linker content is increased up to 10 wt.% in the same PMMA sample polymerised with 50 wt.% of ethanol, the Takayanagi prediction becomes quite bad (see Figure 3.25). The increase of cross-linking density in these samples has a strong effect because porosity increases very much in the dry state from 8 to 52 % for PMMA1/50E and PMMA10/50E respectively (see Table 3.3).

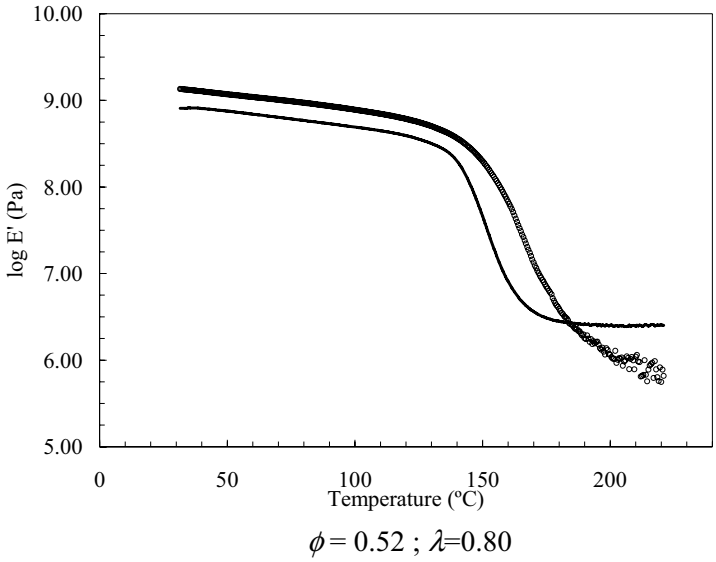

Figure 3.25. Temperature dependence of the storage modulus of PMMA10/50E: experimental values (○) and the Takayanagi block model (continuous line) considering a material composed of two phases: PMMAB10 and the porosity of PMMA10/50E (fraction $\phi = P_{d1}$). The adjustable parameter λ is shown.

Sample PMMA1/50E, in which phase separation occurs as microsyneresis, far from the transition from microsyneresis to macrosyneresis, is well predicted by Takayanagi. However, Sample PMMA10/50E is the previous stage to the transition and it seems very difficult to predict with this model the mechanical properties of these materials near this transition. For this reason, samples PMMA1/60E and PMMA1/70E (macrosyneresis) are also quite well predicted but much worse than sample PMMA1/50E (microsyneresis) (see Figure 3.26).

Increasing the solvent content produces more difficult predictions of the storage modulus of these porous materials from the bulk polymers. The same happens for PMMA polymerised with 5 and 10 wt.% of EGDMA because the PMMA samples polymerised with 60 wt.% of ethanol are always better predicted than those polymerised with 70 wt.% (see Figures 3.27 and 3.28). This means that when macrosyneresis is very far from the transition from microsyneresis to macrosyneresis, the Takayanagi prediction gets worse and worse because the porous polymers have more and more different structure.

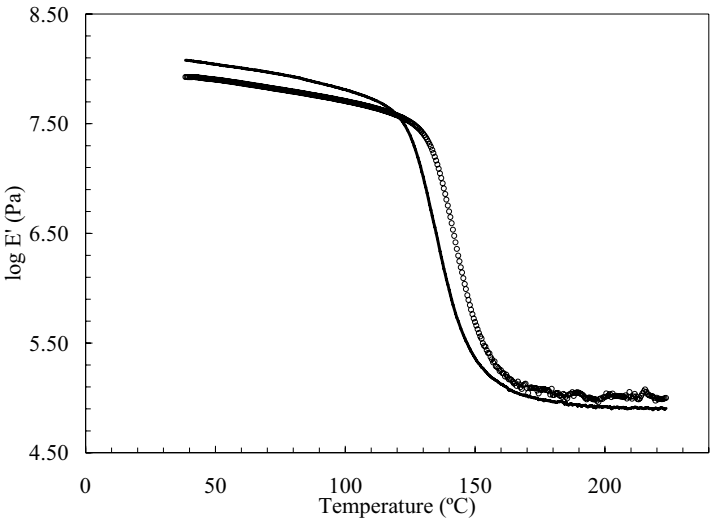

(a)

$\phi = 0.69$; $\lambda = 0.950$

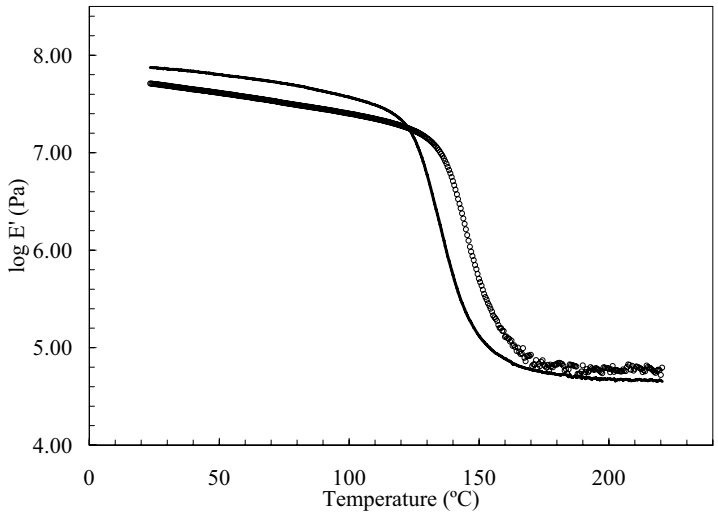

(b)

$\phi = 0.70$; $\lambda = 0.970$

Figure 3.26. Temperature dependence of the storage modulus of PMMA polymerised with 1 wt.% of EGDMA and 60 (*a*) and 70 (*b*) wt.% of ethanol: experimental values (○) and Takayanagi's block model (continuous line) considering a material composed of two phases: PMMAB1 and the porosity of the porous PMMA samples (fraction $\phi = P_{dl}$). The adjustable parameter λ is shown.

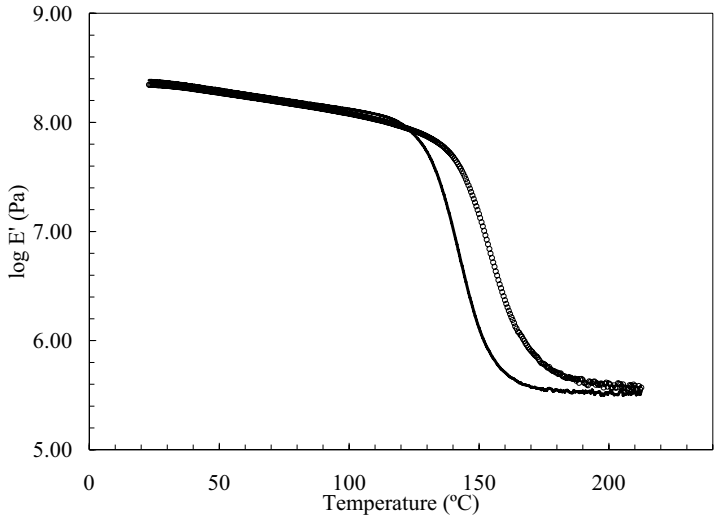

(a)

$\phi = 0.65$; $\lambda = 0.915$

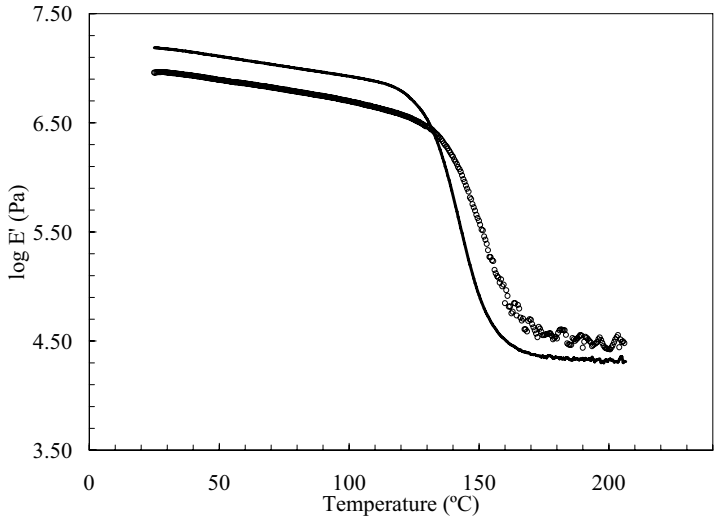

(b)

$\phi = 0.76$; $\lambda = 0.990$

Figure 3.27. Temperature dependence of the storage modulus of PMMA polymerised with 5 wt.% of EGDMA and 60 (*a*) and 70 (*b*) wt.% of ethanol: experimental values (○) and Takayanagi's block model (continuous line) considering a material composed of two phases: PMMAB5 and the porosity of the porous PMMA samples (fraction $\phi = P_{dl}$). The adjustable parameter λ is shown.

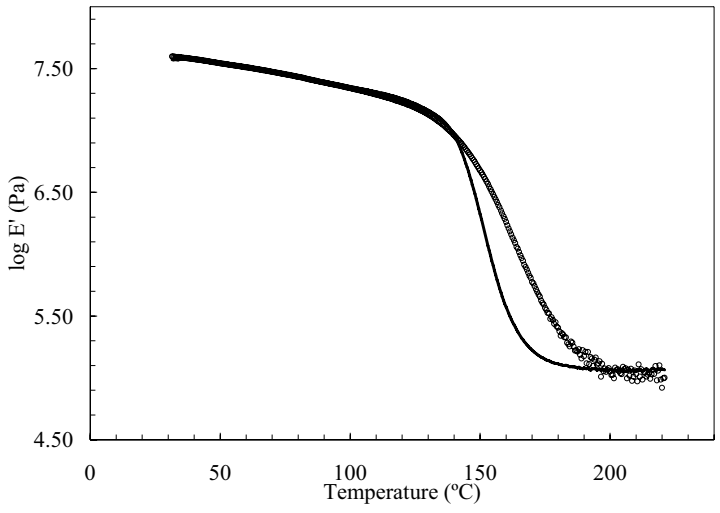

(a)

ϕ=0.70; λ = 0.983

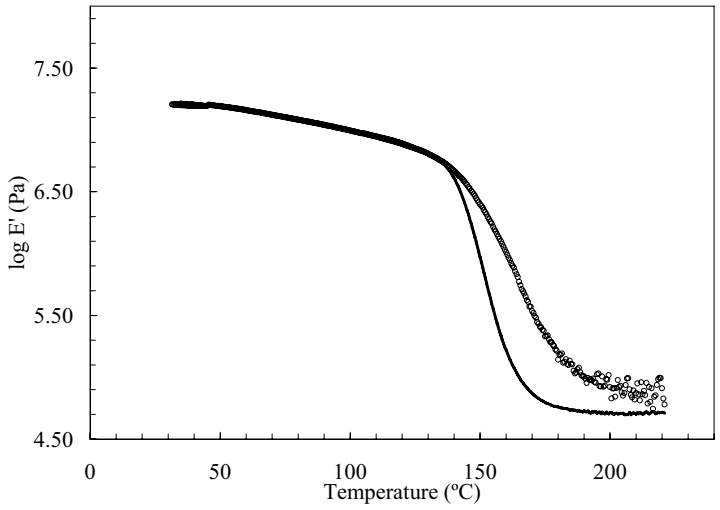

(b)

ϕ=0.77;λ = 0.988

Figure 3.28. Temperature dependence of the storage modulus of PMMA10/60E (*a*) and 10/70E (*b*): experimental values (○) and Takayanagi's block model (continuous line) considering a material composed of two phases: PMMAB10 and the porosity of the porous PMMA samples (fraction $\phi = P_{dl}$). The adjustable parameter λ is shown.

The slope of the glass transition fall cannot be predicted by Takayanagi's model in none of the PMMA samples synthesised in this work. However, the slope of this fall is parallel to the experimental results for all the samples with 1 wt.% of EGDMA. When the cross-linking density is increased, this slope gets less and less parallel to the experimental values. This means that the adhesion between PMMA microspheres depends very much on the cross-linker content and the Takayanagi model does not predict this adhesion, which is very important here. Therefore, the shifting observed of the main relaxation (tan δ) in the DMS results between bulk PMMA and PMMA polymerised in the presence of ethanol cannot be explained under the assumptions of the Takayanagi model, that in this case implies merely the decrease of the amount of PMMA in the porous material, keeping the same properties as bulk PMMA.

3.2. PHEA grafted onto macroporous PMMA.

Macroporous poly(methyl methacrylate) networks with different porosities and cross-linking densities were coated with plasma-polymerised poly(2-hydroxyethyl acrylate) (PMMA-*gr*-*pl*PHEA). In this chapter, the results obtained for the specific volumes, porosities, dynamical-mechanical properties, glass transition, degradation and infrared spectroscopy of these composite materials are presented and discussed. Their porous morphology with the hydrophilic coating was observed by Scanning Electron Microscopy. The *pl*PHEA coating and its interaction with the hydrophobic PMMA substrate are also characterised in this chapter.

3.2.1. Morphology.

Plasma polymerisation is usually a thin film-forming process, where thin films deposit directly on surfaces of the substrates. In this process, the monomer vapour is injected into the plasma chamber and this monomer polymerised onto the substrate with the assistance of the plasma energy, which involves activated electrons, ions, and radicals [51]. Nevertheless, in this work, a different plasma polymerisation method was used. The procedure of this alternative method consisted of allowing the porous PMMA samples to adsorb 2-hydroxyethyl acrylate monomer vapour before the plasma polymerisation. The samples were placed inside a vacuum desiccator on a grid located on the top of a glass with liquid HEA monomer. The air was evacuated from the desiccator with the help of a vacuum pump. After that, this desiccator was placed inside an oven at 50ºC in order to accelerate the adsorption process. Once the samples had adsorbed the desired amount of monomer vapour, they were removed from the desiccator to be treated by plasma right after. The plasma treatment allowed the adsorbed HEA monomer to polymerise onto the macroporous PMMA samples. The spontaneous initiation of the polymerisation process of the adsorbed monomer would be very difficult because of the absence of thermal or photoinitiators. However, by plasma treatment, it is possible to polymerise this monomer. This plasma-polymerised PHEA coating is pure because it is obtained after adsorbing HEA monomer vapour.

The plasma treatment of the Piccolo plasma chamber used in this work started with the evacuation of the air present inside the chamber till achieve a base pressure of 50 *Pa*. After that, 5 seconds of homogenisation and the plasma was generated by a 2.45 *GHz* generator to produce 360 *Watts* during 110 seconds. Finally, the chamber was ventilated to atmospheric pressure in 30 seconds.

Thus, several series of porous PMMA samples with different degrees of porosity and cross-linker contents were prepared with different wt. % of *pl*PHEA simply controlling adsorption time before the plasma polymerisation (see Table 3.8). The *pl*PHEA concentrations were gravimetrically determined with the mass (in the dry state) of the samples before the monomer vapour adsorption and after the plasma treatment. In both cases, the samples were dried at a temperature higher than T_g in vacuo during three days (to constant weight).

Table 3.8. Series of macroporous PMMA prepared with different wt.% of *pl*PHEA controlling adsorption time before the plasma polymerisation. Mass fractions of *pl*PHEA (X_{plPHEA}) determined gravimetrically.

Sample	wt.% of *pl*PHEA (X_{plPHEA})
PMMA1/60E	12.0, 15.0
PMMA1/70E	0.3, 2.8, 11.5, 18.2, 24.8, 26.9, 28.7, 32.1, 35.3
PMMA5/60E	6.7, 15.2
PMMA5/70E	25.3, 55.2

By means of scanning electron microscopy (SEM), it is possible to observe the formation of the hydrophilic coating on a macroporous PMMA1/70E sample after the plasma polymerisation (see Figure 3.29). This macropoporous PMMA sample before the plasma treatment without the hydrophilic coating was shown in Figures 3.3 *(a)* and 3.33 *(a)* at higher magnification.

The *pl*PHEA layer is clearly visible around all of the PMMA microspheres. This hydrophilic coating improves the adhesion between the PMMA microspheres and therefore the mechanical properties of these materials are also improved (see section 3.2.2).

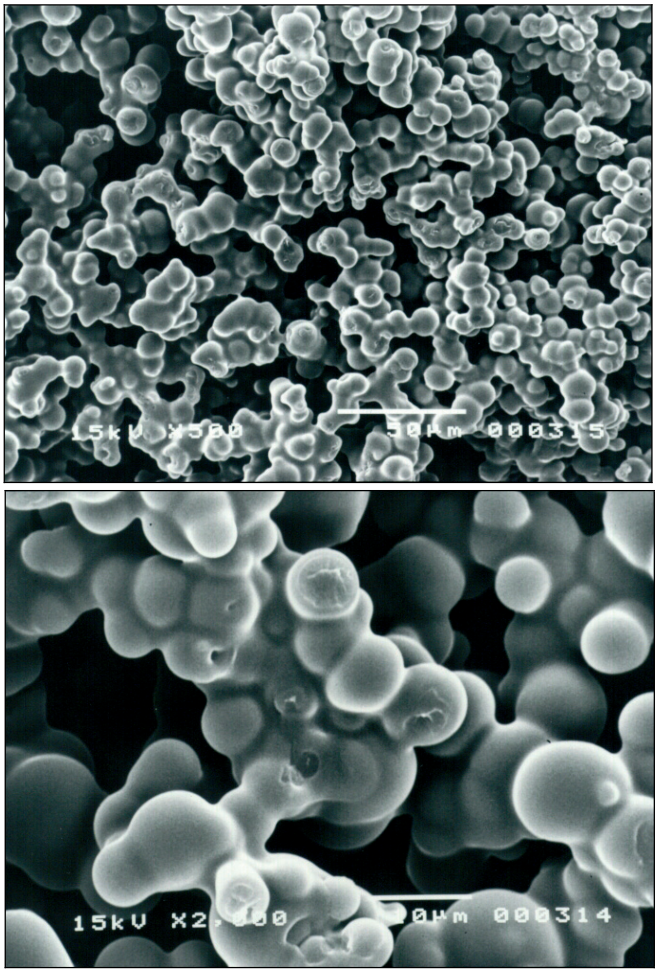

(a)

(b)

Figure 3.29. SEM micrographs of *pl*PHEA grafted onto macroporous PMMA (PMMA1/70E-*gr*-*pl*PHEA(18.2%)) at two different magnifications 500 *(a)* and 2000 *(b)*.

The same plasma treatment was performed in sample PMMA1/70E but without adsorbing any HEA vapour in order to study the effect of the plasma on the morphology of macroporous PMMA. In this case, macroporous PMMA was directly placed into the plasma chamber. Exactly the same experimental conditions were selected in the same Piccolo chamber: 50 Pa of base pressure, 5 seconds of homogenisation, 360 Watts during 110 seconds and 30 seconds of ventilation. The only gas present during the plasma treatment was the small amount of air remaining in the plasma chamber after the evacuation with the vacuum pump. Although the PMMA sample is in different initial conditions (without adsorbed monomer vapour), this experiment can give

additional information about the plasma effect over macroporous PMMA. The SEM micrograph of this sample after the plasma treatment is shown in Figure 3.30. This picture can be compared with the SEM micrograph of the same PMMA sample without plasma treatment shown in Figure 3.33 *(a)* at the same magnification.

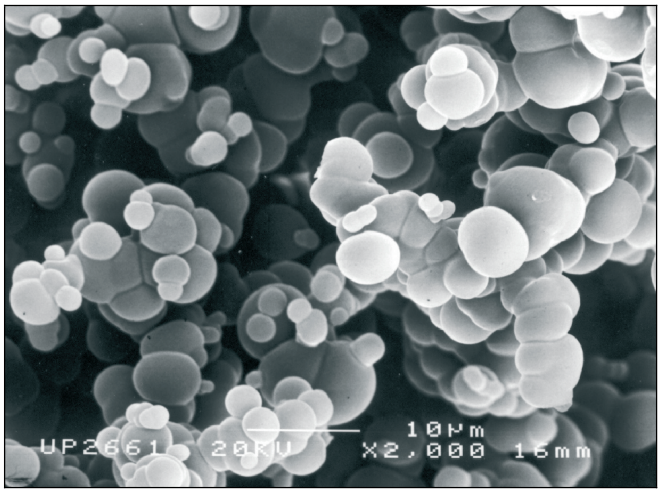

Figure 3.30. SEM micrograph of porous PMMA1/70E treated with plasma during 110 seconds at 360 Watts.

There is no visual change after the plasma treatment. Therefore, the clear change of aspect observed in the PMMA-*gr*-*pl*PHEA samples (see Figure 3.29) was exclusively due to the polymerisation of the HEA monomer and not because of the effect of the plasma treatment on the PMMA sample.

Before the plasma polymerisation, when macroporous PMMA is placed into a desiccator in a saturated monomer vapour atmosphere, the substrate adsorbs HEA vapour, which could make the PMMA microspheres to swell and increase their sizes. Therefore, after the plasma treatment, part of the *pl*PHEA content could be inside the PMMA substrate as Interpenetrated Polymer Network (IPN) and the other part as pure *pl*PHEA coating on the surface. Anyway, this SEM micrograph of sample PMMA1/70E-*gr*-*pl*PHEA(18.2%) was analysed measuring 50 microsphere diameters in order to have an approximated value of the increase of the PMMA microsphere diameter after the plasma polymerisation. A size distribution plot, the mean and the standard deviation were calculated from these measurements for this PMMA-*gr*-*pl*PHEA sample as explained in section 3.1.1 for macroporous PMMA. The number of microspheres of a given size divided by the total number of measured microspheres is represented against microsphere diameter in this size

distribution plot. All these results are shown in Table 3.9 and Figure 3.31.

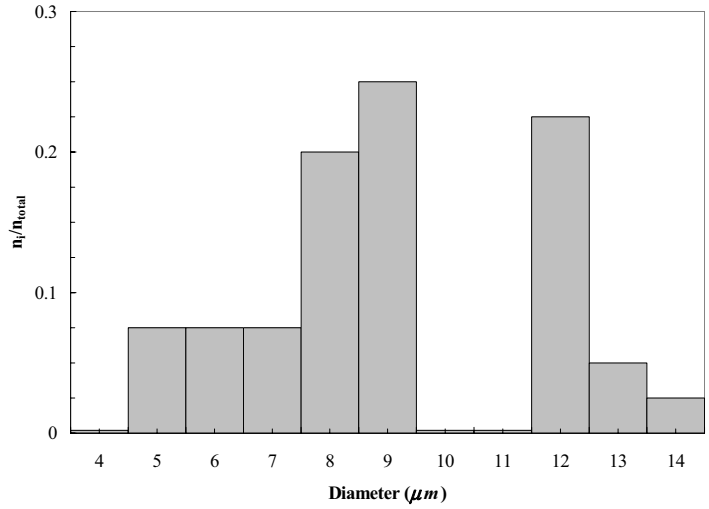

Figure 3.31. Microsphere diameter distribution bar graph of porous PMMA1/70E-*gr*-*pl*PHEA(18.2%).

The microsphere diameter distribution bar graph of porous PMMA1/70E (Figure 3.4 *(b)*) broadens when this sample is covered with 18.2 wt.% of plasma-polymerised PHEA (Figure 3.31). The mean microsphere diameter of sample PMMA1/70E-*gr*-*pl*PHEA(18.2%) is more than two times larger than that of PMMA1/70E (see Table 3.9). Therefore, the *pl*PHEA layer formed onto the macroporous PMMA structure after the plasma polymerisation is approximately 2.5 μm thick for sample PMMA1/70E-*gr*-*pl*PHEA(18.2%).

Table 3.9. Mean microsphere diameters of PMMA1/70E with and without *pl*PHEA (mean microsphere diameter ±standard deviation (ϕ_m)).

Sample	ϕ_m (μm)
PMMA1/70E	4±1
PMMA1/70E-*gr*-*pl*PHEA(18.2%)	9±2

For a higher amount of *pl*PHEA, it is not possible to measure the microsphere diameter because all the PMMA microspheres get covered with the *pl*PHEA coating without keeping their spherical shape. However, a qualitative increase of the *pl*PHEA coating can be observed in the SEM micrographs (Figure 3.33).

Macroporous PMMA samples with the desired amount of *pl*PHEA can be prepared simply controlling adsorption time. Thus, several samples of macroporous PMMA1/70E were placed into a saturated HEA vapour atmosphere during different times before the plasma polymerisation in order to obtain different weight percentages of *pl*PHEA. A graph with the wt.% of *pl*PHEA obtained as a function of adsorption time of the HEA monomer vapour before the plasma treatment is presented in Figure 3.32.

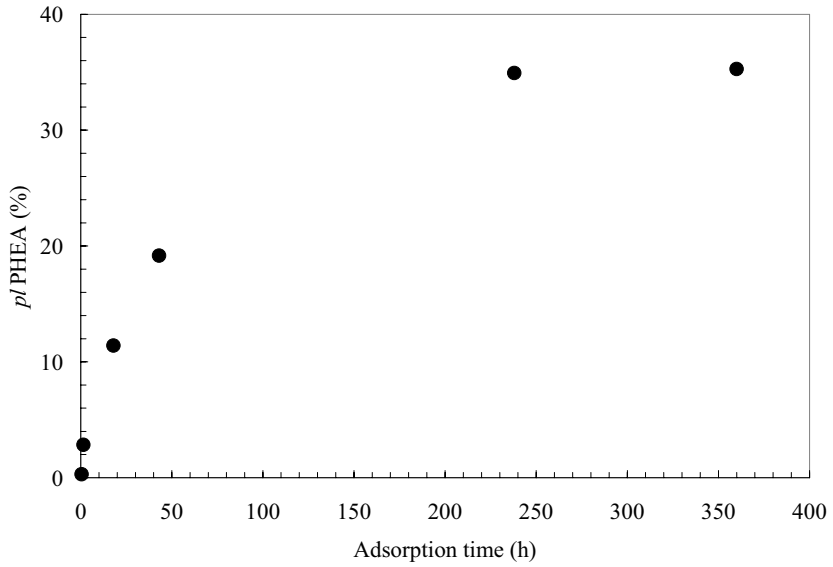

Figure 3.32. Weight percentage of plasma-polymerised PHEA onto macroporous PMMA1/70E as a function of adsorption time of the HEA monomer vapour before the plasma treatment.

After a certain adsorption time, approximately 250 hours, the effect of adsorption time is attenuated because the PMMA network gets saturated of HEA vapour reaching the thermodynamical equilibrium. Figure 3.33 shows how the morphology of sample PMMA1/70E changes as the amount of *pl*PHEA increases.

(a) PMMA1/70E without *pl*PHEA

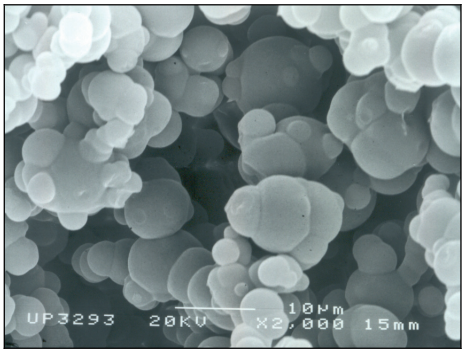

(b) 0.3 wt.% of *pl*PHEA for 30 min.

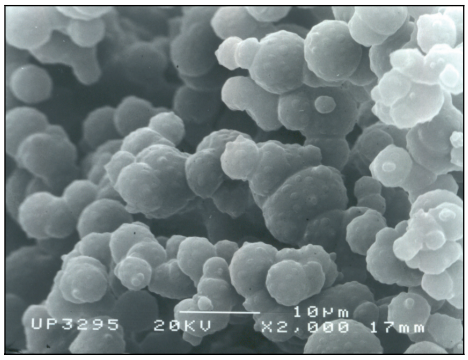

(c) 2.8 wt.% of *pl*PHEA for 1.5 h.

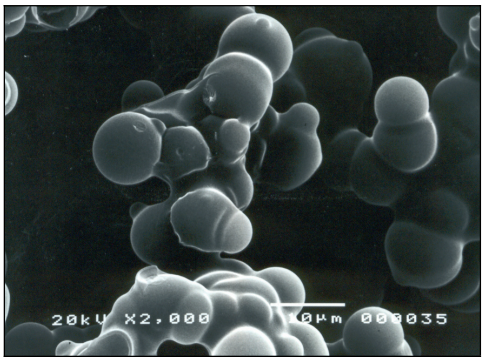

(d) 11.4 wt.% of *pl*PHEA for 18 h.

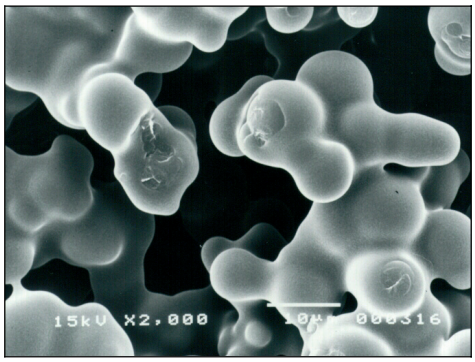

(e) 18.2 wt.% of *pl*PHEA for 40 h.

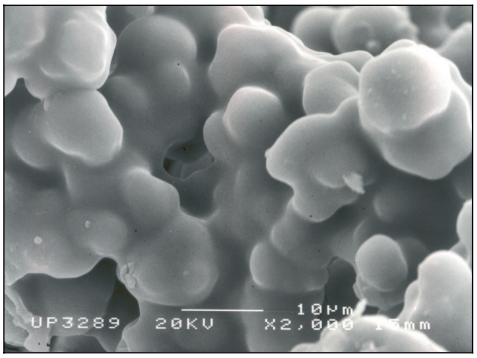

(f) 35.3 wt.% of *pl*PHEA for 360 h.

Figure 3.33. SEM micrographs of PMMA1/70E with different wt.% of *pl*PHEA (0 *(a)*, 0.3 *(b)*, 2.8 (*c)*, 11.4 *(d)*, 18.2 (*e)* and 35.3 *(f)*) obtained controlling adsorption time (0, 0.5, 1.5, 18, 40 and 360 hours respectively). All micrographs have the same magnification (x2000).

For a 0.3 wt.% of *pl*PHEA, there is not a clear visual change in the porous PMMA sample. However, the morphology of the PMMA sample with 2.8 wt.% of *pl*PHEA starts changing superficially. From 11.4 wt.% of *pl*PHEA on, a clear homogeneous hydrophilic layer is observed around all the PMMA microspheres. This thickness of this *pl*PHEA layer increases more and more with increasing the *pl*PHEA content.

The same experiment of controlling adsorption time but only for the two longest times (40 and 360 hours) was performed for a PMMA sample polymerised in the presence of the same ethanol content (70 wt.%) but higher amount of cross-linker (5 wt.%). In this way, the effect of cross-linking on the adsorption process of monomer vapour can be studied. The SEM micrographs of these samples are shown in Figure 3.34.

Almost double amount of *pl*PHEA was obtained in PMMA5/70E than in PMMA1/70E for the same adsorption time.

The plasma treatment takes place only on the surface of the PMMA microspheres. Therefore, the PMMA-*gr*-*pl*PHEA microspheres obtained after the plasma polymerisation are expected to consist of a pure PMMA nucleus, a *pl*PHEA-PMMA interpenetrated polymer layer and a pure *pl*PHEA layer on the surface in both macroporous PMMA samples with different cross-linker contents. In addition, the sorption process was very slow from the surface to the nucleus because the PMMA microspheres were in the glassy state. The glass transition temperature of the PMMA microspheres decreases more and more with increasing the amount of adsorbed HEA vapour, which allows the HEA monomer to go inside the polymer microsphere. The plasma treatment let the HEA monomer polymerise on the surface and only some radicals could achieve to polymerise inside the PMMA network as an interpenetrated polymer network (IPN).

This unexpected effect of increasing so much the amount of *pl*PHEA obtained after the plasma polymerisation with increasing the cross-linking density of the substrate can be better understood paying attention to the specific area and the porosities of these samples with and without *pl*PHEA. Macroporous PMMA polymerised with 70 wt.% of ethanol and 5 wt.% of EGDMA has more porosity than sample PMMA1/70E (see Table 3.10). In addition, in good agreement with the porosity results, Table 3.7 shows that the mechanical modulus of sample PMMA1/70E falls very sharply in both glassy and rubbery state when the cross-linker content is increased up to 5 wt.%. Therefore, PMMA5/70E has more specific area than PMMA1/70E and the HEA vapour has more surfaces to be adsorbed in this sample with more cross-linker. In addition, the polarity of PMMA increases with increasing the EGDMA content (see section 3.3.1).

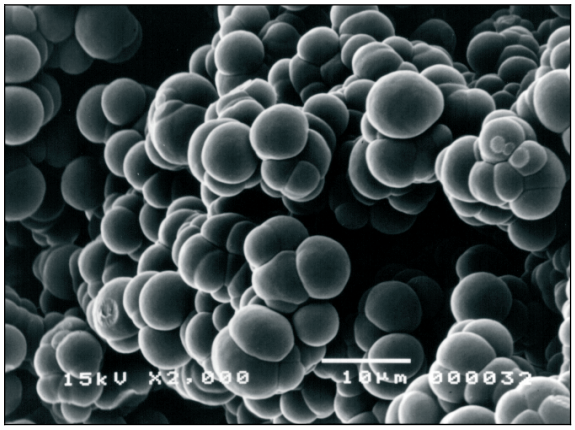

(a) PMMA5/70E without *pl*PHEA

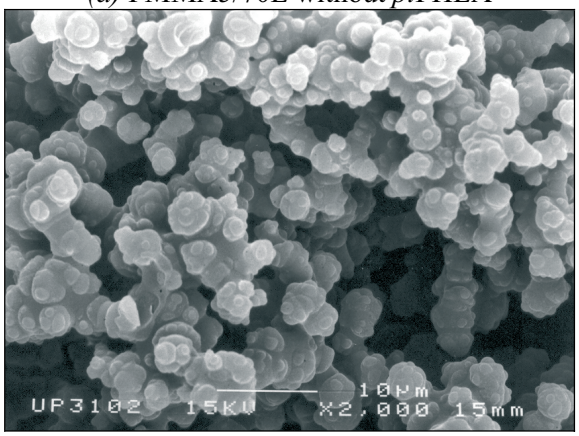

(b) 25.3 wt.% of *pl*PHEA for 40h

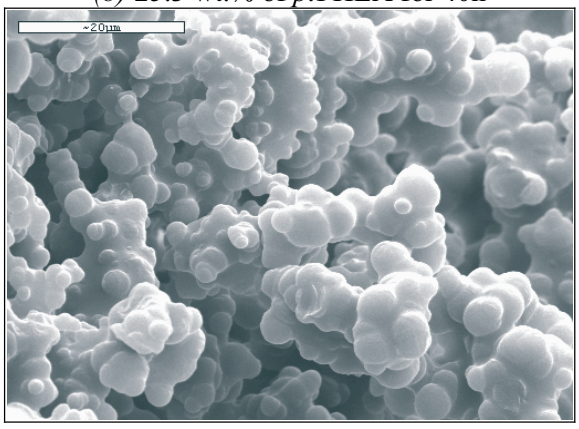

(c) 55.2 wt.% of *pl*PHEA for 360h

Figure 3.34. SEM micrographs of PMMA5/70E with different wt.% of *pl*PHEA (0 *(a)*, 25.3 *(b)* and 55.2 *(c)*) obtained controlling adsorption time (40 and 360 hours respectively). All micrographs have the same magnification (x2000).

The HEA monomer vapour is able to swell more the PMMA microspheres in PMMA5/70E increasing its specific area even more. For this reason, the porosity of PMMA5/70E decreases very little even though there is *pl*PHEA around all of the PMMA microspheres after the plasma polymerisation (see porosities results of sample PMMA5/70E with and without *pl*PHEA in Table 3.10). However, the HEA monomer vapour has less specific area to swell in sample PMMA1/70E and this produces to obtain less amount of *pl*PHEA. Table 3.10 shows that the porosity of this sample polymerised with 1 wt.% of EGDMA considerably decreases after the plasma polymerisation because there is more *pl*PHEA on the surface of this sample.

If the SEM micrographs shown in Figures 3.33 and 3.34 are analysed, the PMMA microspheres coated with *pl*PHEA keep better their shape in PMMA1/70E than in PMMA5/70E. These SEM micrographs of PMMA5/70E with different *pl*PHEA contents show that the PMMA microsphere shapes are very irregular after the polymerisation. They become covered and mixed up with the *pl*PHEA. For this reason, it was not possible to measure the microsphere diameters of sample PMMA5/70E-*gr*-*pl*PHEA(25.3%) and PMMA5/70E-*gr*-*pl*PHEA(55.2%).

The specific volume (v) of bulk PHEA determined through the weight of the sample in air and n-octane is shown in Table 3.10. The apparent specific volumes of PMMA-*gr*-*pl*-PHEA and the porosities (P_{d1}) determined from these apparent specific volumes are also shown in Table 3.10. The equations used for these results were shown in section 2.2.1. In this case, it was not possible to determine the porosity of these samples by swelling in water or ethyl acetate because these methods cannot be applied to a hydrophilic-hydrophobic composite material. The porosities of the macroporous PMMA samples without *pl*PHEA taken from Table 3.3 are also shown in Table 3.10 as reference.

Table 3.10. Specific volume of bulk PHEA and apparent specific volumes at 25ºC±0.5 (v). Porosities of the PMMA networks with *pl*PHEA in the dry state (P_{d1}). The reference porosity of the macroporous PMMA without *pl*PHEA (P_{ref}) is also shown together with each sample.

Sample	v (cm³/g)	P_{d1} (%)	P_{ref} (%)
PHEA	0.754±0.002	-	-
PMMA1/60E-*gr*-*pl*PHEA(12%)	2.045±0.187	58	69
PMMA1/70E-*gr*-*pl*PHEA(18.2%)	2.142±0.221	61	70
PMMA1/70E-*gr*-*pl*PHEA(35.3%)	2.261±0.041	64	70
PMMA5/60E-*gr*-*pl*PHEA(15.2%)	2.561±0.028	67	65
PMMA5/70E-*gr*-*pl*PHEA(25.3%)	3.294±0.048	75	76
PMMA5/70E-*gr*-*pl*PHEA(55.2%)	3.031±0.026	74	76

Bulk PHEA has a lower specific volume than bulk PMMA (see Table 3.3). On the other hand, the apparent specific volumes of PMMA-*gr*-*pl*PHEA logically increases with increasing the amount of solvent used in the polymerisation process. PMMA1/70E-*gr*-*pl*PHEA increases their apparent specific volume with increasing the amount of *pl*PHEA due to the sample becoming more porous after more sorption time. This sample with less specific area needs more time to swell and decreases less its porosity after a longer adsorption time. However, the apparent specific volume of PMMA5/70E-*gr*-*pl*PHEA decreases with increasing the *pl*PHEA content because the sample becomes slightly less porous with increasing the sorption time. It becomes a moment when the PMMA5/70E cannot swell more and part of the *pl*PHEA is polymerised on the surface decreasing a little the porosity.

The same effect of cross-linking can be seen in Table 3.10 for the PMMA samples polymerised with 60 wt.% of ethanol. The porosity of PMMA1/60E considerably decreases after the plasma polymerisation and PMMA5/60 has a very close value before and after the plasma polymerisation.

Table 3.10 show that the porosities of the PMMA1/70E samples decreases very much after the plasma polymerisation. However, the porosities of the PMMA5/70E hardly change. This means that most of the *pl*PHEA is on the surface of PMMA1/70E occupying a part of the volume of pores existing in the uncoated porous sample and the *pl*PHEA is more homogeneously interpenetrated with PMMA5/70E. This is in good agreement with the homogeneous layer of *pl*PHEA observed by SEM onto PMMA1/70E.

3.2.2. Glass transition and dynamic-mechanical relaxation.

Differential Scanning Calorimetry was performed on bulk PHEA and PMMA-*gr*-*pl*PHEA in order to determine the glass transition temperature of the two phases present in these composite materials at a heating rate of 10ºC/min. These results are shown in Table 3.11.

The DSC thermograms of pure PMMA1/70E and PMMA5/70E were shown in Figures 3.10 and 3.11 respectively. The glass transition of pure bulk PHEA is shown in Figure 3.35.

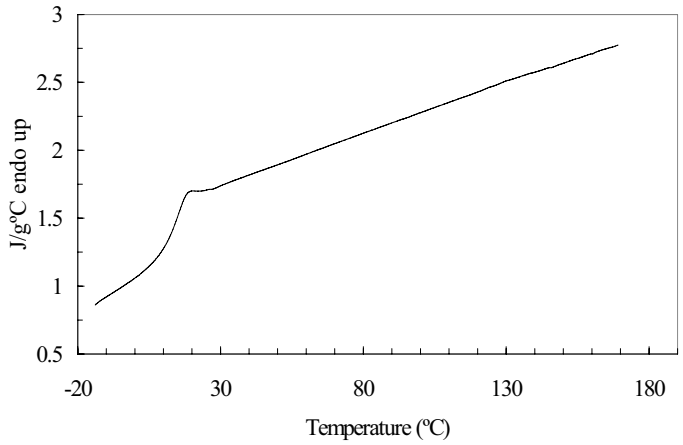

Figure 3.35. DSC heating scans from -20 to 170ºC at a heating rate of 10ºC/min of bulk PHEA.

Heating scans from -20 to 160ºC of the composite material PMMA-*gr-pl*PHEA polymerised with 1 wt.% of cross-linker and different *pl*PHEA contents are shown all together in Figure 3.36 in order to study the effect of the hydrophilic coating content.

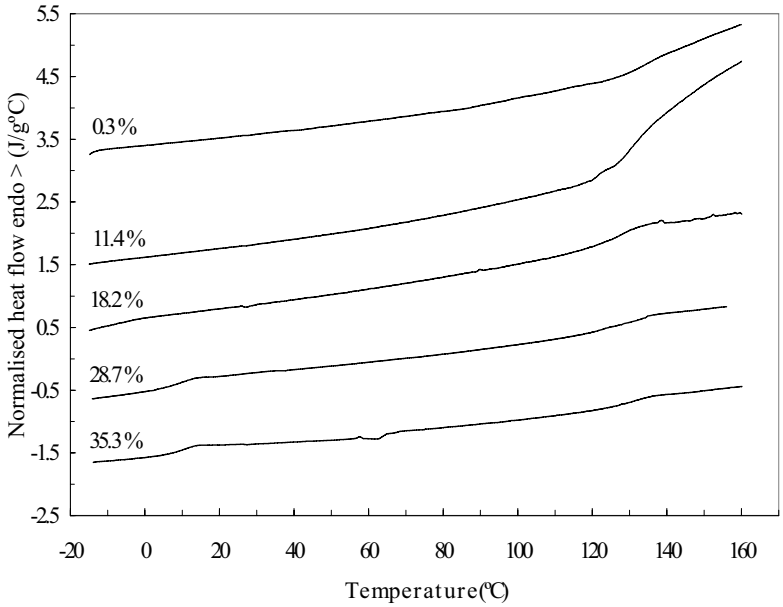

Figure 3.36. DSC heating scans from -20 to 160ºC at a heating rate of 10ºC/min of PMMA1/70E with different wt.% of *pl*PHEA (0.3, 11.4, 18.2, 28.7 and 35.3).

The glass transition temperature (T_g) of the *pl*PHEA is only seen from 28.7 wt.% of *pl*PHEA on. For lower contents, this transition cannot be detected by DSC. There are two glass transition regions due to the presence of *pl*PHEA and PMMA. The T_g of these two samples with 28.7 and 35.3 wt.% of *pl*PHEA are similar (see Table 3.11) because most of the *pl*PHEA is on the surface as seen with the porosity results in section 3.2.1.

The heating scans from -20 to 180ºC of the composite material PMMA-*gr*-*pl*PHEA polymerised with 5 wt.% of cross-linker and different *pl*PHEA contents are shown in Figure 3.37.

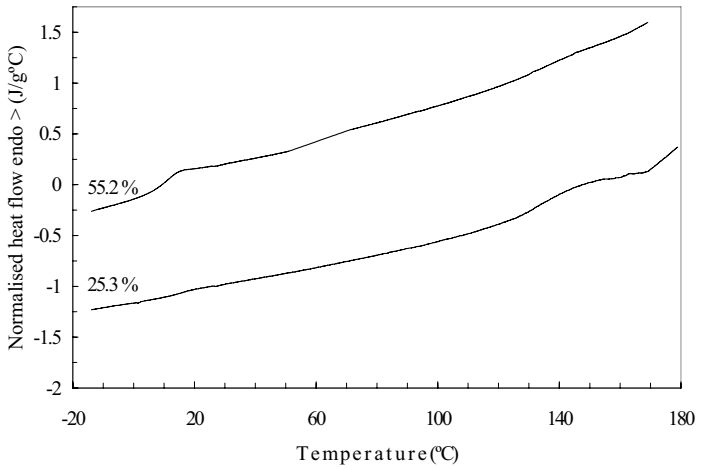

Figure 3.37. DSC heating scans from -20 to 180ºC at a heating rate of 10ºC/min of PMMA5/70E with different wt.% of *pl*PHEA (55.2 and 25.3).

Table 3.11. DSC glass transition temperatures of bulk PHEA and PMMA-*gr*-*pl*PHEA with different ethanol, cross-linker and *pl*PHEA contents in the dry state.

Sample	**T_g (ºC)**	
Bulk PHEA	13.8	
PMMA-*gr*-*pl*PHEA	**Tg_{plPHEA}(ºC)**	**Tg_{PMMA}(ºC)**
PMMA1/60-*gr*-*pl*PHEA(12%)	-	131.0
PMMA1/70E-*gr*-*pl*PHEA(0.3%)	-	130.3
PMMA1/70E-*gr*-*pl*PHEA(11.4%)	-	129.4
PMMA1/70E-*gr*-*pl*PHEA(18.2%)	-	131.3
PMMA1/70E-*gr*-*pl*PHEA(28.7%)	8.3	128.9
PMMA1/70E-*gr*-*pl*PHEA(35.3%)	9.1	129.8
PMMA5/60E-*gr*-*pl*PHEA(15.2%)	-	139.9
PMMA5/70E-*gr*-*pl*PHEA(25.3%)	16.5	137.8
PMMA5/70E-*gr*-*pl*PHEA(55.2%)	10.5	138.7

The DSC thermograms of samples PMMA1/60-*gr*-*pl*PHEA(12%) and PMMA5/60E-*gr*-*pl*PHEA(15.2%) were measured but only the glass transition of PMMA was detected due to the small amount of *pl*PHEA. These results are shown in Table 3.11.

Both PMMA5/70E samples with 25.3 and 55.2 wt.% of *pl*PHEA have two glass transition regions due to the presence of *pl*PHEA and PMMA. The glass transition temperature of *pl*PHEA in these samples slightly decreases from 16.5 to 10.5ºC with increasing the amount of *pl*PHEA (see Table 3.11). Since the glass transition temperature of the PHEA domains interpenetrated with the PMMA network should be higher than in pure PHEA and the glass transition temperature interval should be broader, the shift of the T_g towards lower temperatures with increasing *pl*PHEA content means that the thickness of the coating layer not interpenetrated with PMMA increases, probably PMMA becomes saturated of HEA and new amounts of *pl*PHEA polymerises only at the surface.

The glass transition temperatures of *pl*PHEA in PMMA5/70E with different hydrophilic coatings are higher than those of the samples polymerised with 1 wt.% of cross-linker. This effect of cross-linking could also explain that the *pl*PHEA is more homogeneously interpenetrated in the samples with 5 wt.% of EGDMA.

The heat capacity increments (Δc_p) of the two glass transition regions found in these composite materials were determined from these DSC thermograms and are shown in Table 3.12. The Δc_p of the pure phases are also shown as reference in this table. The composition of PMMA1/70E and PMMA5/70E with different *pl*PHEA contents were determined from the Δc_p of each phase in the composite material ($\Delta c_p PMMA$ and $\Delta c_p plPHEA$) and the Δc_p of the pure phases ($\Delta c_p bulkPHEA$ and $\Delta c_p PMMA1/70E$ or $\Delta c_p PMMA5/70E$) as

$$\%PMMA = \frac{\Delta c_p PMMA}{\Delta c_p PMMA1/70E} \cdot 100 \qquad (3.4)$$

$$\%plPHEA = \frac{\Delta c_p plPHEA}{\Delta c_p bulkPHEA} \cdot 100 \qquad (3.5)$$

The compositions of PMMA1/70 with 28.7 and 35.3 wt.% of *pl*PHEA determined by DSC are very close to those determined gravimetrically. Since the DSC composition is determined from the pure phases, these results give another indication that most of the *pl*PHEA is on the surface of these samples.

The DSC compositions of PMMA5/70E with 25.3 and 55.2 wt.% of *pl*PHEA give lower wt.% of *pl*PHEA than those determined gravimetrically suggesting once again that the *pl*PHEA is more homogeneously interpenetrated in these samples. However, these composition determinations are only an estimation because they are determined from bulk PHEA, which differs chemically from *pl*PHEA.

Table 3.12. Heat capacity increments at the glass transition (Δc_p in J/gK) and composition determination by DSC of PMMA1/70E and PMMA5/70E with different *pl*PHEA contents. Heat capacity increments at the glass transition (Δc_p in J/gK) of the pure phases: bulk PHEA, PMMA1/70E and PMMA5/70E.

SAMPLE	***Δc_p plPHEA***	***Δc_p PMMA***	***%plPHEA***	***%PMMA***
PMMA1/70E-*gr*-*pl*PHEA(28.7%)	0.129	0.15	30.7	69.4
PMMA1/70E-*gr*-*pl*PHEA(35.3%)	0.140	0.130	33.3	60.2
PMMA5/70E-*gr*-*pl*PHEA(25.3%)	0.046	0.309	11.1	68.1
PMMA5/70E-*gr*-*pl*PHEA(55.2%)	0.165	0.165	39.3	50.0
Pure phases	***Δc_p***			
Bulk PHEA	0.420			
PMMA1/70E	0.216			
PMMA5/70E	0.204			

Since different experimental techniques performed in this thesis (SEM, porosimetry, DSC, DMS, FTIR, TGA and water sorption) suggest that most of the *pl*PHEA is on the surface of macroporous PMMA1/70E, the T_g value of sample PMMA1/70E-*gr*-*pl*PHEA(28.7%) could be used as the glass transition temperature of pure *pl*PHEA for comparison with bulk PHEA. Therefore, the glass transition temperature of *pl*PHEA is 5.5ºC lower than bulk PHEA (see Table 3.11). This difference must be attributed to the slight chemical differences between both polymers.

In this work, a PMMA-*gr*-*pl*PHEA hydrogel was synthesised with much better mechanical properties than other porous hydrogels as the poly(2-hydroxyethyl methacrylate) sponges polymerised in the presence of high water contents by Chirila and his research group. Both hydrogels have a similar morphology with microspheres. Although the PHEMA microspheres are not all connected. The mechanical resistance of these PHEMA sponges is extremely poor and they break under their own weight [119,122]. Thus, the dynamical-mechanical properties of these PHEMA sponges cannot be determined. However, the PMMA microspheres coated with *pl*PHEA in the porous PMMA-*gr*-*pl*PHEA composite materials are all connected and their mechanical modulus can be measured in this case.

Thus, the dynamic-mechanical properties of macroporous PMMA with plasma-polymerised coating (PMMA-*gr*-*pl*PHEA) with different porosities, cross-linking densities and *pl*PHEA contents in the dry state are studied. First of all, the DMS spectra of the pure phases (macroporous PMMA and bulk PHEA) are shown in Figures 3.38 and 3.39 respectively. These DMS experimental results of the pure phases served as input for the Takayanagi block model to predict the mechanical behaviour of the composite material.

The dynamic-mechanical properties of macroporous PMMA1/70E were determined from -150 to 250ºC (see Figure 3.38). This spectrum shows the main relaxation at 147.5ºC, which corresponds to the glass transition region. The secondary β relaxation, associated with side-chain motion of the ester group, can also be seen at lower temperatures. The γ relaxation, related to the motion of the methyl groups attached to the main chain, would be seen if this experiment were performed at lower temperatures.

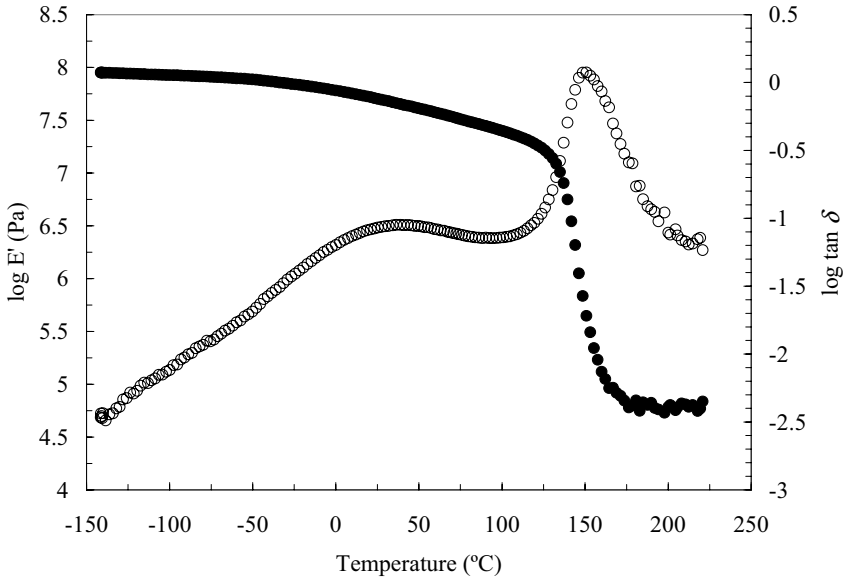

Figure 3.38. Temperature dependence of the storage modulus (solid symbols) and the loss tangent (open symbols) of macroporous PMMA polymerised in the presence of 70 wt.% of ethanol and 1 wt.% of EGDMA. Only one point out of ten is plotted to obtain a clearer representation.

The temperature dependence of the storage modulus and the loss tangent of bulk PHEA is shown in Figure 3.39. The maximum temperature of the main relaxation (α peak) appears around 35ºC. The secondary γ relaxation

, associated to local motions within the side-chain group, appears at lower temperatures in the glassy state (around -75ºC).

All the samples were dried at 90ºC in vacuo during three days (to constant weight) but a small amount of water was sometimes absorbed by the hydrophilic material when the sample was prepared to start the DMS measurement. This presence of very small amounts of water absorbed produces a new relaxation peak, β_{sw}, at temperatures higher than those of the γ relaxation, due to the link of two side-chain groups by a water molecule through hydrogen bonding producing a bulkier molecular group of reduced mobility, whose relaxation takes place at a higher temperature [50 and the references cited therein]. This result is not very different from that shown in Figure 1.5 of bulk PHEA polymerised with 1 wt.% of EGDMA.

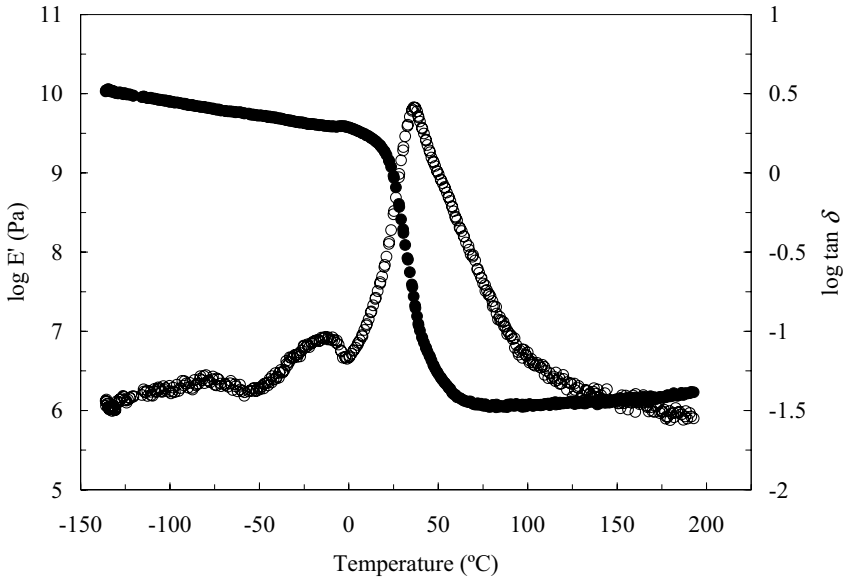

Figure 3.39. Temperature dependence of the storage modulus (solid symbols) and the loss tangent (open symbols) of bulk PHEA. Only one point out of ten is plotted to obtain a clearer representation.

If the DMS spectra of macroporous PMMA and bulk PHEA are compared, the storage modulus in the glassy state of bulk PHEA is much higher. Therefore, the composite PMMA-*gr-pl*PHEA must show an improvement of the dynamic-mechanical properties in the glassy state respect to the macroporous PMMA material without coating. Figure 3.40 shows together the DMS spectra of PMMA1/70E and PMMA1/70E-*gr-pl*PHEA(18.2%).

The storage modulus of PMMA1/70E-*gr*-*pl*PHEA(18.2%) has two main inflection points corresponding to the glass transition region of *pl*PHEA and PMMA1/70E. The loss tangent (tan δ) shows three relaxation peaks: the α peak of PMMA in the region from 150 at 160ºC, the α peak of *pl*PHEA overlapped with the β peak of PMMA1/70E around 19ºC and the γ peak of *pl*PHEA around -75ºC. The fact that the β_{sw} relaxation peak does not appear proves the absence of water in the sample. The γ relaxation of *pl*PHEA appears at the same temperature as seen for bulk PHEA in Figure 3.39. Nevertheless, the main relaxation of *pl*PHEA appears at lower temperature. The storage modulus is higher with the hydrophilic coating from -150ºC to 10ºC at temperatures lower than the main relaxation of *pl*PHEA. The *pl*PHEA coating improves the adhesion between the PMMA microspheres, which is reflected as an important mechanical improvement when the hydrophilic coating is in the glassy state. PMMA1/70E-*gr*-*pl*PHEA(18.2%) is less porous than PMMA1/70E, which also contributes in the increase of the storage modulus in the glassy state. However, the dynamic modulus of the composite material is lower than in macroporous PMMA when the temperature is higher than the glass transition temperature of *pl*PHEA in spite of having less porosity.

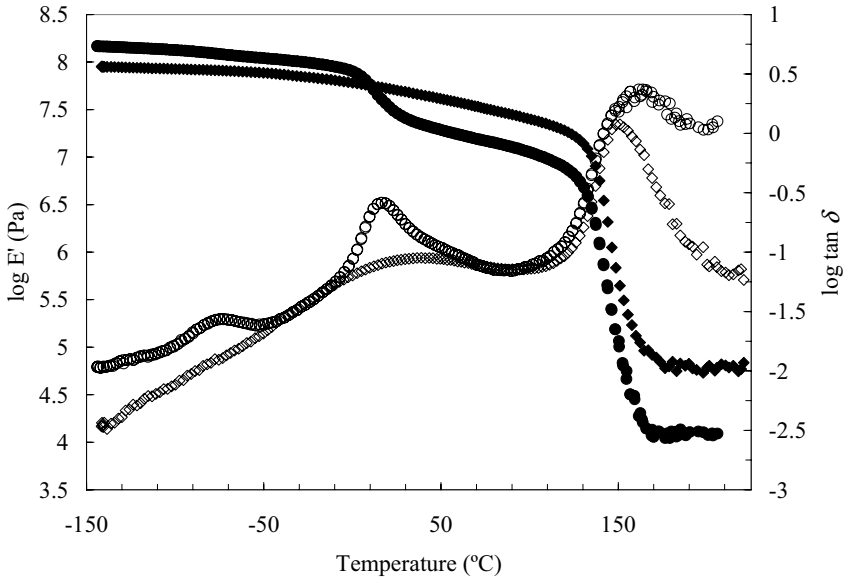

Figure 3.40. Temperature dependence of the storage modulus (solid symbols) and the loss tangent (open symbols) of PMMA1/70E (P_{dl}=70%) (◇) and PMMA1/70E-*gr*-*pl*PHEA(18.2%) (P_{dl}=61%) (○). Only one point out of ten is plotted to obtain a clearer representation.

Nevertheless, macroporous PMMA polymerised with 5 wt.% of EGDMA does not show this behaviour of decreasing the dynamic-mechanical properties after the glass transition of *pl*PHEA. The PMMA5/70E-*gr*-*pl*PHEA(25.3%) composite material have always better mechanical properties than PMMA5/70E from -150 to 250ºC, except during the glass transition of PMMA (from 135 to 170ºC) where both samples present similar storage modulus (see Figure 3.41). Note that these two samples polymerised with 5 wt.% of cross-linker have similar porosities.

Phase separation makes that the main relaxations of the *pl*PHEA and PMMA domains appear clearly apart from each other in both networks cross-linked with 1 or 5 wt.% of EGDMA. Nevertheless, the drop of the elastic modulus in the *pl*PHEA α relaxation is smaller in PMMA5/70E-*gr*-*pl*PHEA(25.3%) than in PMMA1/70E-*gr*-*pl*PHEA(18.2%) in spite of the larger *pl*PHEA content of the former. This means that a part of the PHEA segments does not contribute to the cooperative motions that produce what has to be related to the highest degree of interpenetration of *pl*PHEA in the highly cross-linked PMMA substrate that has been already commented above.

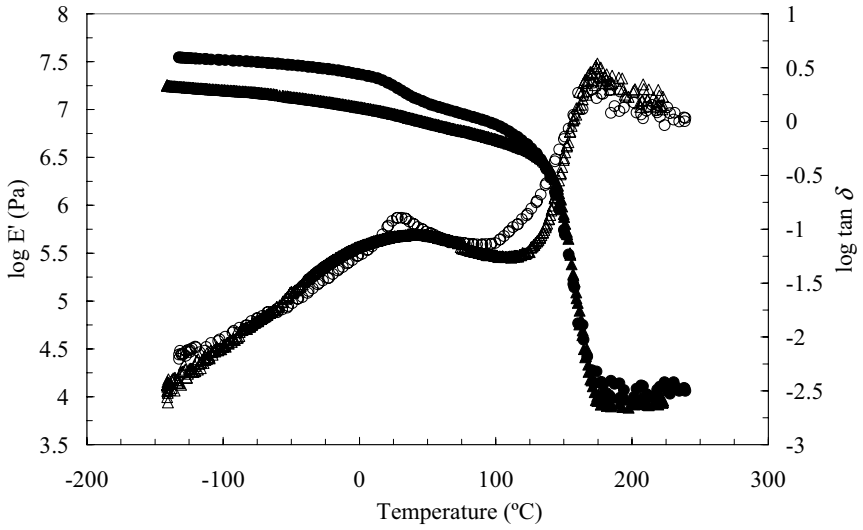

Figure 3.41. Temperature dependence of the storage modulus (solid symbols) and the loss tangent (open symbols) of PMMA5/70E (P_{dl}=76%) (△) and PMMA5/70E-*gr*-*pl*PHEA(25.3%) (P_{dl}=75%) (○). Only one point out of ten is plotted to obtain a clearer representation.

The dynamic-mechanical properties of PMMA1/60E-*gr*-*pl*PHEA(12%) and PMMA1/60E are shown together in Figure 3.42. The damping temperature curve of the composite material shows also three relaxation peaks.

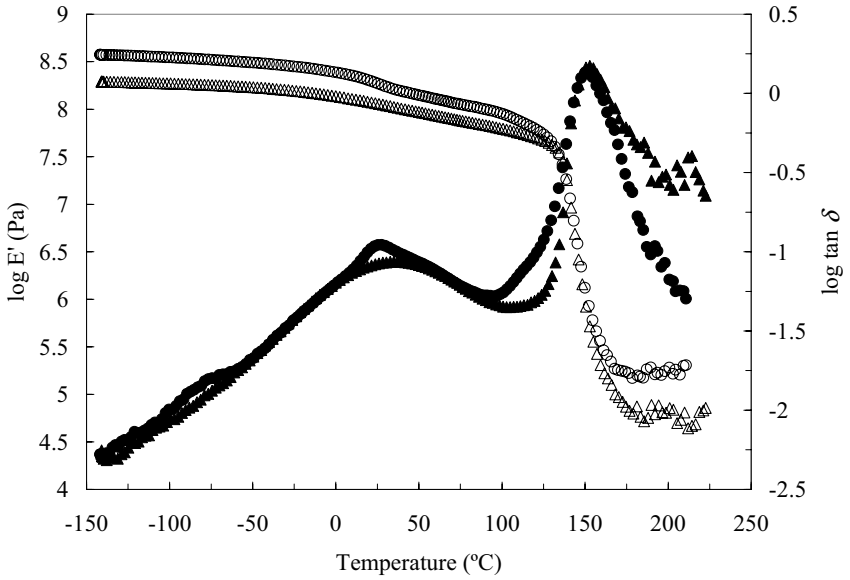

Figure 3.42. Temperature dependence of the storage modulus (open symbols) and the loss tangent (solid symbols) of PMMA1/60E (P_{dl}=69%) (△) and PMMA1/60E-*gr*-*pl*PHEA(12%) (P_{dl}=58%) (○). Only one point out of ten is plotted to obtain a clearer representation.

The mechanical modulus of PMMA1/60E increases after the plasma polymerisation because the *pl*PHEA coating improves the adhesion between the PMMA microspheres and decreases the porosity. The storage modulus of PMMA1/60E-*gr*-*pl*PHEA(12%) is higher than that of PMMA1/60E from -150 to 225ºC.

The DMS spectra of PMMA5/60E-*gr*-*pl*PHEA(15.2%) and PMMA5/60E are shown together in Figure 3.43. Table 3.13 shows the storage modulus of PMMA-*gr*-*pl*PHEA at 25ºC (close to room temperature), -20ºC (PMMA and *pl*PHEA in the glassy state), 70ºC (PMMA in the glassy state and *pl*PHEA in the rubbery state) and 200ºC (PMMA and *pl*PHEA in the rubbery state). The storage modulus of the macroporous PMMA samples without *pl*PHEA at these temperatures are also shown in this table as reference.

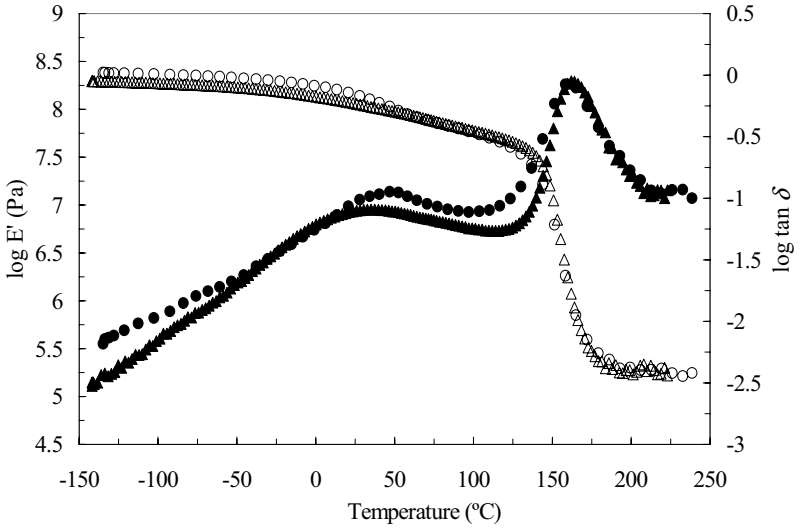

Figure 3.43. Temperature dependence of the storage modulus (open symbols) and the loss tangent (solid symbols) of PMMA5/60E (P_{dl}=67%) (◇) and PMMA5/60E-*gr-pl*PHEA(15.2%) (P_{dl}=65%) (○). Only one point out of ten is plotted to obtain a clearer representation.

Table 3.13. Storage modulus (*log E'(Pa)*) of PMMA-*gr-pl*PHEA with different ethanol, cross-linker and *pl*PHEA contents at 25ºC (room temperature), -20ºC (glass PMMA and glass *pl*PHEA), 70ºC (glass PMMA and rubber *pl*PHEA) and 200ºC (rubber PMMA and rubber *pl*PHEA).

PMMA-*gr-pl*PHEA samples ***PMMA*** ***plPHEA***	***-20ºC*** ***glass*** ***glass***	***25ºC*** ***glass*** ***transition***	***70ºC*** ***glass*** ***rubber***	***200ºC*** ***rubber*** ***rubber***
PMMA1/60E-*gr-pl*PHEA(12%)	8.44	8.27	8.06	5.28
PMMA1/70E-*gr-pl*PHEA(18.2%)	7.98	7.46	7.19	4.10
PMMA5/60E-*gr-pl*PHEA(15.2%)	8.29	8.14	7.88	5.30
PMMA5/70E-*gr-pl*PHEA(25.3%)	7.42	7.26	6.97	4.08
Macroporous PMMA	***-20ºC***	***25ºC***	***70ºC***	***200ºC***
PMMA1/60E	8.18	8.05	7.9	4.85
PMMA1/70E	7.83	7.70	7.53	4.78
PMMA5/60E	8.18	8.05	7.89	5.27
PMMA5/70E	7.07	6.95	6.79	3.93

The storage modulus of PMMA with hydrophilic coating is always higher than without *pl*PHEA at -20ºC (below the main relaxation of *pl*PHEA)

and at room temperature. The hydrophilic coating gives an important reinforcement to the composite material working at these temperatures. However, at 70ºC and 200ºC (above the main relaxation of *pl*PHEA), the storage modulus varies depending on the kind of sample (different porosity, cross-linking density and *pl*PHEA content).

Table 3.13 shows that the PMMA-*gr*-*pl*PHEA synthesised in this work is a hydrophilic porous material with a very high storage modulus at room temperature. These materials can adsorb water because of the hydrophilic *pl*PHEA layer and are able to keep their mechanical properties due to the hydrophobic PMMA structure.

The α relaxation of *pl*PHEA appears overlapped with the β relaxation of PMMA in the DMS spectra of the PMMA-*gr*-*pl*PHEA composite materials. However, it is noteworthy that the position or intensity of the secondary β relaxation of PMMA does not depend on neither ethanol nor cross-linker content added in the polymerisation process as expected since it is due to local non-cooperative motions (see Figure 3.44 and Table 3.14).

The maximum temperature of the α relaxation of *pl*PHEA appears at different temperatures when grafted onto PMMA substrates cross-linked with 1 or 5 wt.% of EGDMA as shown in Table 3.15. As the cross-linking density of PMMA increases, the α relaxation of *pl*PHEA shifts towards high temperatures for a similar ethanol content used in the polymerisation process. These DMS results are in very good agreement with the increase of the glass transition temperature determined by DSC with increasing cross-linker content (see Table 3.11). Table 3.15 shows that for a similar cross-linking density, the temperature $T^{\alpha}_{pl\text{PHEA}}$ decreases with increasing *pl*PHEA content because of the presence of more amount of pure *pl*PHEA.

Table 3.14. Maximum temperature of the PMMA β relaxation (T^{β}_{PMMA}) of macroporous PMMA polymerised with different ethanol and cross-linker contents.

SAMPLE	T^{β}_{PMMA} (ºC)
PMMA1/60E	36.1
PMMA1/70E	37.2
PMMA5/60E	38.8
PMMA5/70E	37.4

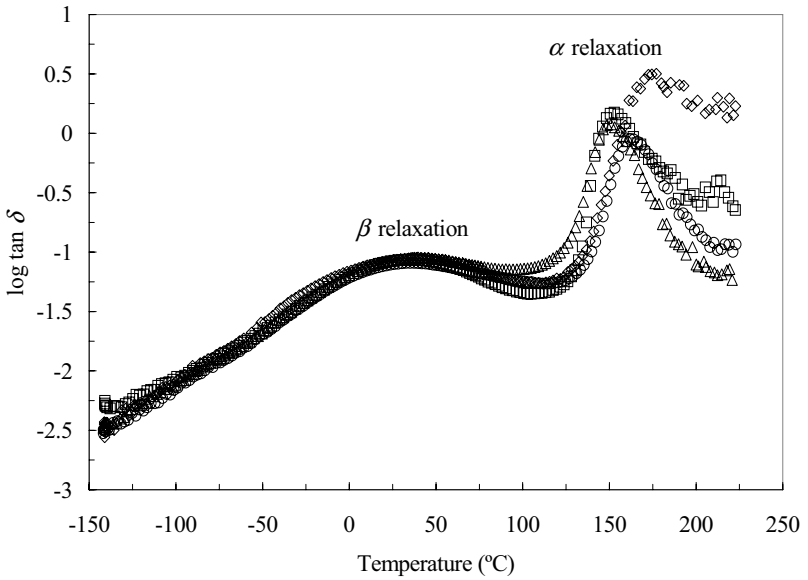

Figure 3.44. β relaxation of macroporous PMMA without *pl*PHEA: PMMA1/60E (□), PMMA1/70E (△), PMMA5/60E (○) and PMMA5/70E (◇). Temperature dependence of the loss tangent. Only one point out of ten is plotted to obtain a clearer representation.

Table 3.15. Maximum temperature of the *pl*PHEA α relaxation ($T^{\alpha}_{pl\text{PHEA}}$) present in PMMA-*gr*-*pl*PHEA with different porosities, cross-linking densities and *pl*PHEA contents.

SAMPLE	**$T^{\alpha}_{pl\text{PHEA}}$ (ºC)**
PMMA1/60E-*gr*-*pl*PHEA(12%)	27.6
PMMA1/70E-*gr*-*pl*PHEA(18.2%)	18.9
PMMA5/60E-*gr*-*pl*PHEA(15.2%)	49.6
PMMA5/70E-*gr*-*pl*PHEA(25.3%)	30.9

A comparison of the experimental values of the dynamic-mechanical properties of PMMA-*gr*-*pl*PHEA with the Takayanagi block model prediction is made considering a material composed of two phases: porous PMMA and bulk PHEA.

This mechanical model has two adjustable parameters (ϕ, λ). However, the volume fraction of the *pl*PHEA phase (ϕ) is well known because it can be determined from the mass fraction of *pl*PHEA in PMMA-*gr*-*pl*PHEA (X_{plPHEA}) as

$$\phi = \frac{X_{plPHEA}}{\frac{v_{app}}{v_{PHEA}} - \frac{v_{app}}{v_{PHEA}} \cdot X_{plPHEA} + X_{plPHEA}} \tag{3.6}$$

where v_{app} is the apparent specific volume of macroporous PMMA (see Table 3.3) and v_{PHEA} is the specific volume of bulk PHEA (see Table 3.10). The X_{plPHEA} values were shown in Table 3.8. Therefore, the only adjustable parameter is the fraction of continuous phase acting in series (λ).

The DMS experimental results of PMMA-*gr*-*pl*PHEA polymerised with 60 wt.% of ethanol and different cross-linking densities (1 and 5 wt.%) are modelled with the aid of the Takayanagi block model and the results are shown in Figure 3.45.

The DMS experimental results of bulk PHEA served as input for the Takayanagi block model to predict the behaviour of *pl*PHEA and it was determined by DSC that *pl*PHEA has a glass transition temperature around 5.5ºC lower than bulk PHEA. Therefore, there must be a little amount of *pl*PHEA interpenetrated in the PMMA1/60E-*gr*-*pl*PHEA(12%) which produces a shift to higher temperatures. This explains why both experimental and predicted PHEA α peaks appear at the same temperature in Figure 3.45 *(a)*. This shift also happened for PMMA1/70E-*gr*-*pl*PHEA(18.2%) and PMMA5/70E-*gr*-*pl*PHEA(25.3%) (see Figure 3.46) but the *pl*PHEA α peak in both samples does not reach the α peak predicted by Takayanagi and appears at lower temperatures because the amount of *pl*PHEA is much larger in these samples. In addition, the shift from lower to higher temperatures is much stronger in PMMA5/70E-*gr*-*pl*PHEA(25.3%) showing once again more homogeneous interpenetration.

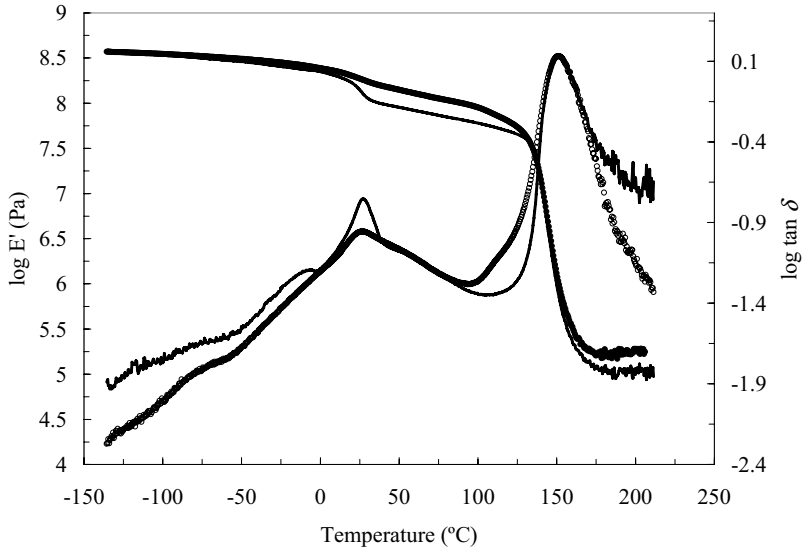

(a) ϕ = 0.0356 ; λ=0.35

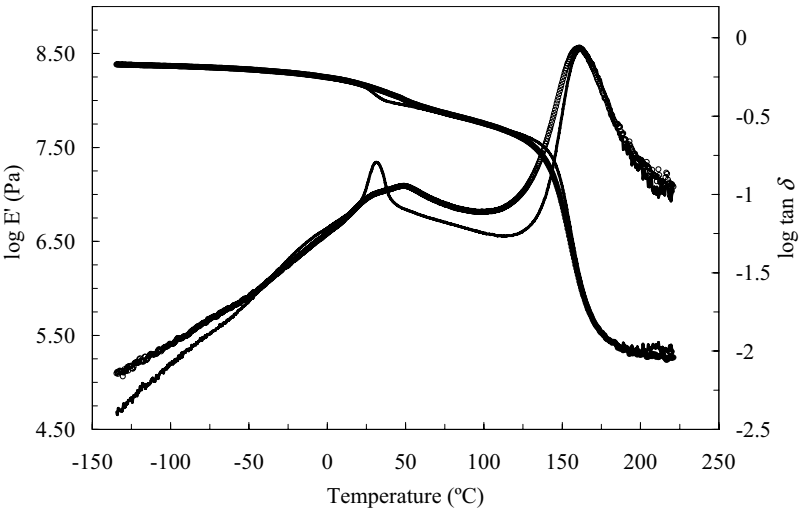

(b) ϕ = 0.0534 ; λ=0.8

Figure 3.45. Experimental results of the Temperature dependence of the storage modulus (●) and loss tangent (○) of PMMA1/60E-*gr*-*pl*PHEA(12%) (*a*) and PMMA5/60E-*gr*-*pl*PHEA(15.2%) (*b*). Takayanagi's block model (continuous line) considering a material composed of two phases: PMMA1/60E or PMMA5/60E and bulk PHEA. The experimentally determined *pl*PHEA content (ϕ) and the Takayanagi adjustable parameter (λ) are shown.

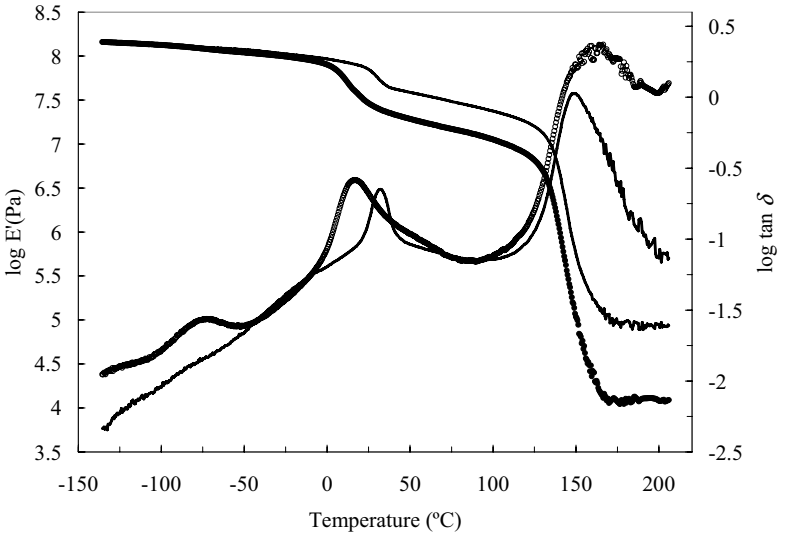

(a) $\phi = 0.0557$; $\lambda = 0.65$

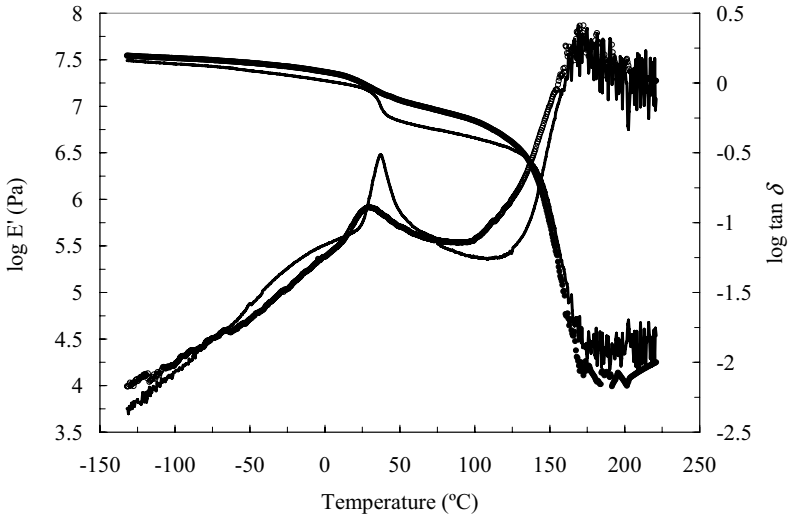

(c) $\phi = 0.0779$; $\lambda = 0.6$

Figure 3.46. Experimental results of the Temperature dependence of the storage modulus (●) and loss tangent (○) of PMMA1/70E-*gr*-*pl*PHEA(18.2%) (*a*) and PMMA5/70E-*gr*-*pl*PHEA(25.3%) (*b*). Takayanagi's block model (continuous line) considering a material composed of two phases: PMMA1/70E or PMMA5/70E and bulk PHEA. The experimentally determined *pl*PHEA content (ϕ) and the Takayanagi adjustable parameter (λ) are shown.

Takayanagi's block model predicts quite badly the DMS experimental results of PMMA-*gr*-*pl*PHEA. No better results are obtained adjusting the Takayanagi parameter (λ). The storage modulus of the composite material cannot be predicted with this mechanical model, not even approximately, in any sample. Takayanagi's block model serves, however, to show the shifts of the expected position of the *pl*PHEA α peak. Thus, the experimental α peak of *pl*PHEA in sample PMMA5/60E-*gr*-*pl*PHEA(15.2%) appears at higher temperature than the α peak of *pl*PHEA predicted by Takayanagi. Since the DMS experimental results of the pure phases served as input for the Takayanagi model calculations, this shift of α peak to higher temperatures shows that this *pl*PHEA is more homogeneously interpenetrated in this sample. However, the α peak of *pl*PHEA predicted by Takayanagi in sample PMMA1/60E-*gr*-*pl*PHEA(12%) appears exactly around the same temperature as the experimental result showing that this sample have its two phases more separated. For this reason, sample PMMA1/60E-*gr*-*pl*PHEA(12%) is better predicted by Takayanagi than PMMA5/60E-*gr*-*pl*PHEA(15.2%).

The small values obtained for the Takayanagi parameter λ indicate that an important fraction of the load is supported by the *pl*PHEA phase.

3.2.3. Infrared Spectroscopy.

ATR FTIR was performed in order to analyse the nature of the *pl*PHEA. The FTIR spectrum of bulk PHEA was also measured in order to see if there are any chemical differences between the plasma polymer and the bulk polymer. Another objective of these FTIR measurements is to study the grafting of the *pl*PHEA coating onto the macroporous PMMA microspheres. The FTIR spectra of the surface and the cross-section were compared to see how homogeneous the hydrophilic coating is. Finally, the FTIR spectrum of macroporous PMMA1/70E treated with plasma with the same experimental conditions as PMMA-*gr*-*pl*PHEA but without adsorbing any HEA vapour is studied in order to see if there is any chemical change in the PMMA network after the plasma treatment.

Before analysing the FTIR spectrum of the PMMA-*gr*-*pl*PHEA composite material, the FTIR spectra of the pure components are studied separately (Figures 3.47 and 3.48).

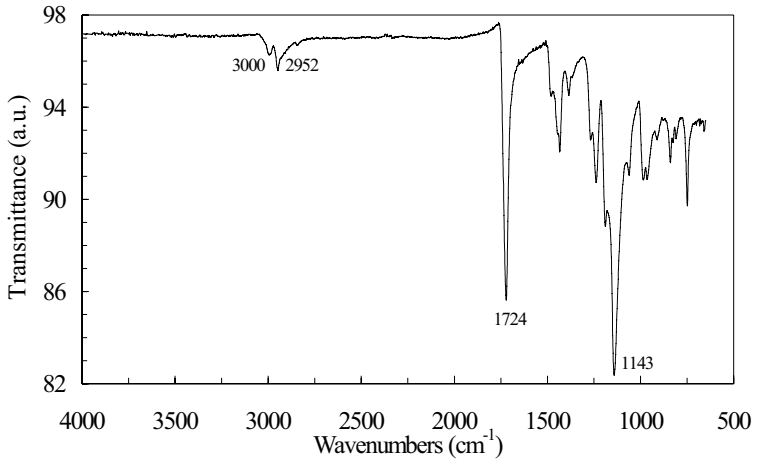

Figure 3.47. ATR FTIR spectrum of macroporous PMMA polymerised in the presence of 70 wt.% and 1 wt.% of EGDMA.

Figure 3.47 shows the FTIR spectrum of PMMA1/70E measured in this work. Similar signals to conventional PMMA (see Figure 1.7) can be identified in this spectrum: the CH_2 and CH_3 stretching vibrations in the region of 2800-3000 cm^{-1} , the stretching of the carbonyl group at 1724 cm^{-1} and the absorption bands characteristic of carboxylic acid esters at ~1143 cm^{-1}[62].

The FTIR spectrum of bulk PHEA without crosslinker was measured as a reference material of the *pl*PHEA coating. This FTIR spectrum is shown in Figure 3.48 and shows similar signals as PMMA because both polymers have similar functional groups: the CH_2 and CH_3 stretching vibrations in the region of 2800-3000 cm^{-1}, the strong band due to the presence of the carbonyl group at 1728 cm^{-1} and the absorption band characteristic of carboxylic acid esters at 1167 cm^{-1}. Nevertheless, a broad absorption can be seen around 3423 cm^{-1} due to the OH stretching vibration and the stretching band of the alcohol group (C–O) at 1076 cm^{-1} present in this PHEA sample. [63, 123]. The FTIR spectrum of bulk PHEA measured in this work is very similar to the spectrum shown in reference [63] (see Figure 1.8).

The FTIR spectra of PMMA1/70E with different *pl*PHEA contents (0, 13.2 and 26.9 wt.%) are shown in Figure 3.49 in order to study the nature of *pl*PHEA coating grafted onto macroporous PMMA.

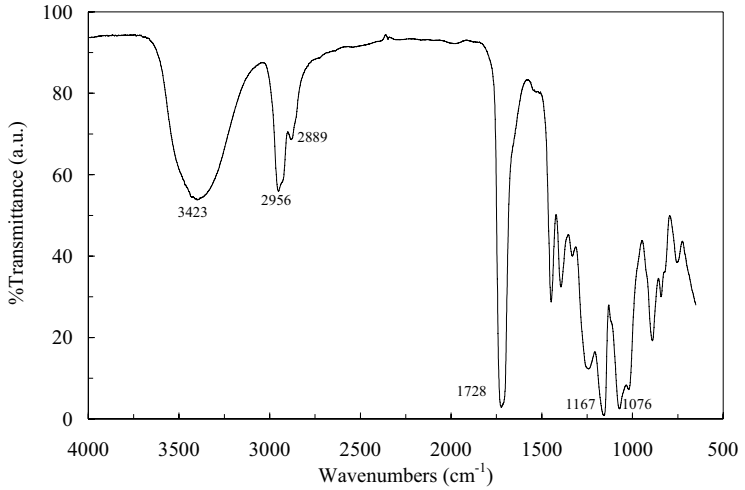

Figure 3.48. ATR FTIR spectrum of bulk PHEA.

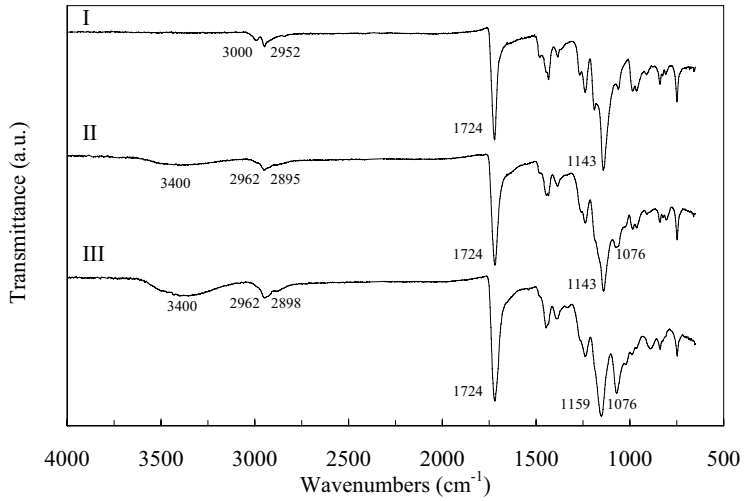

Figure 3.49. ATR FTIR spectra of macroporous PMMA1/70E with 0 (I), 18.2 (II) and 35.3 (III) wt.% of *pl*PHEA.

The main difference between the three spectra is the appearance of two new peaks in the PMMA-*gr*-*pl*PHEA composite material: a broad absorption peak around 3400 cm^{-1} due to the OH stretching vibration and the stretching band of the alcohol group (C–O) at 1076 cm^{-1} [123] (see Figures

3.49 (II and III)). The FTIR spectrum of PMMA1/70E does not show any of these two signals because this polymer has not any OH group in the polymer network (see Figure 3.49 (I)).

The intensity of the absorption peaks at 3400 cm^{-1} (OH stretching) and 1076 cm^{-1} (the alcohol group (C–O)) increases with increasing the amount of the *pl*PHEA present in the composite material. On the other hand, the strong carbonyl stretching vibration at 1724 cm^{-1} appears in all the samples with and without *pl*PHEA because both PMMA and *pl*PHEA have a carbonyl group in their monomeric unit.

The CH_2 and CH_3 stretching vibrations become less clear in coated samples probably because PHEA has a hydrogen atom attached to the chiral carbon atom in the repeat unit instead of a methyl group as PMMA. The different absorption bands found for the CH_2 and CH_3 signal before and after the plasma polymerisation probably occur because of the interaction between *pl*PHEA and PMMA.

The absorption band characteristic of carboxylic acid esters at 1143 cm^{-1} in pure PMMA1/70E and PMMA1/70E-*gr*-*pl*PHEA(18.2%) (Figures 3.49 (I and II)) shifts to higher wavenumbers (1159 cm^{-1}) when a large amount of *pl*PHEA(35.3%) is grafted onto its surface (Figure 3.49 (III)). This effect is the consequence of the increasing presence of *pl*PHEA because the ester peak in pure PHEA appears at a higher wavenumber (1167 cm^{-1}) than pure PMMA1/70E (1143 cm^{-1}) (see Figure 3.48).

Nevertheless, this effect does not happen for macroporous PMMA polymerised with 5 wt.% of EGDMA. The absorption band characteristic of carboxylic acid esters appears at the same wavenumber (1159 cm^{-1}) independently of the amount of *pl*PHEA (see Figure 3.50). All absorption signals in the FTIR spectra of PMMA5/70E-*gr*-*pl*PHEA(25.35%) and PMMA5/70E-*gr*-*pl*PHEA(55.35%) appear at the same wavenumbers. The sample with more *pl*PHEA has more intense OH and C-O alcohol absorption peaks.

These differences observed between macroporous PMMA polymerised with 1 or 5 wt.% of EGDMA must also occur because the *pl*PHEA is more homogeneously interpenetrated with PMMA5/70E than PMMA1/70E as seen with other experimental techniques. Both samples in Figure 3.50 have most of the *pl*PHEA homogeneously interpenetrated in the PMMA network because the HEA vapour is able to swell more PMMA5/70E because it has more specific area and porosity than PMMA1/70E. The HEA vapour needs more time to swell PMMA1/70E with less specific area and less porosity.

Therefore, for a low sorption time (to obtain 18.2 wt.% of *pl*PHEA), most of the *pl*PHEA is separated on the surface of the PMMA microspheres. However, PMMA1/70E-*gr*-*pl*PHEA(35.3%) has more *pl*PHEA as IPN because the HEA vapour had more time to swell this sample and penetrate.

If no molecular interaction took place, the peaks in the spectrum should be a simple summation of the peaks of pure PMMA and pure *pl*PHEA without shifts of the peak wavenumbers. Therefore, this similar shifts found in samples PMMA1/70E-*gr*-*pl*PHEA(35.3%), PMMA5/70E-*gr*-*pl*PHEA(25.35%) and PMMA5/70E-*gr*-*pl*PHEA(55.35%) show that there is molecular interaction between the PMMA and *pl*PHEA in these three samples typical of an Interpenetrated Polymer Network [124].

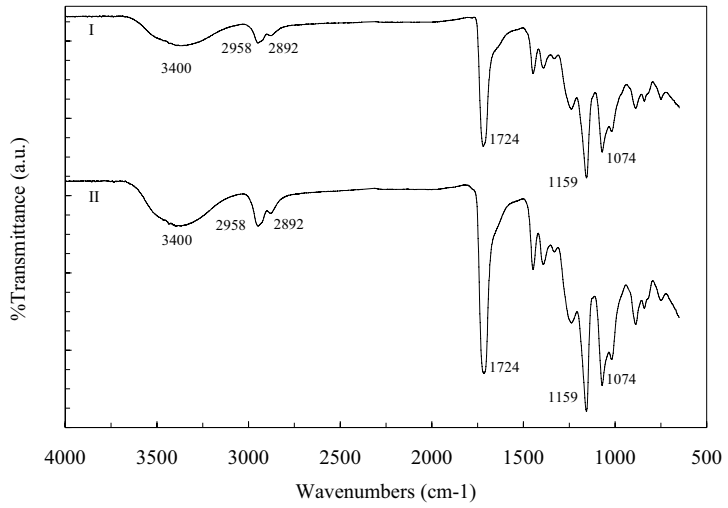

Figure 3.50. ATR FTIR spectra of macroporous PMMA5/70E with 25.3 (I) and 55.2 (II) wt.% of *pl*PHEA.

Significant differences were found between the FTIR spectrum of PMMA and that of *pl*PMMA because the *pl*PMMA is cross-linked in some extent [62]. It is very difficult to compare the FTIR spectrum of *pl*PHEA with that of bulk PHEA because our *pl*PHEA is grafted onto macroporous PMMA. However, the shift of the absorption band characteristic of carboxylic acid esters from 1167 cm^{-1} in bulk PHEA to 1159 cm^{-1} in PMMA-*gr*-*pl*PHEA could occur because a small amount of oxygen is usually incorporated in the plasma polymers [51] which produces to have C-O ether groups located in different places of the polymer network.

Figures 3.51 and 3.52 show the FTIR spectra of the surface and cross-section of PMMA1/70E with two different *pl*PHEA contents (18.2 and 35.3%) in order to prove that the *pl*PHEA coating is formed not only at the skin but also in the core of the macroporous PMMA samples.

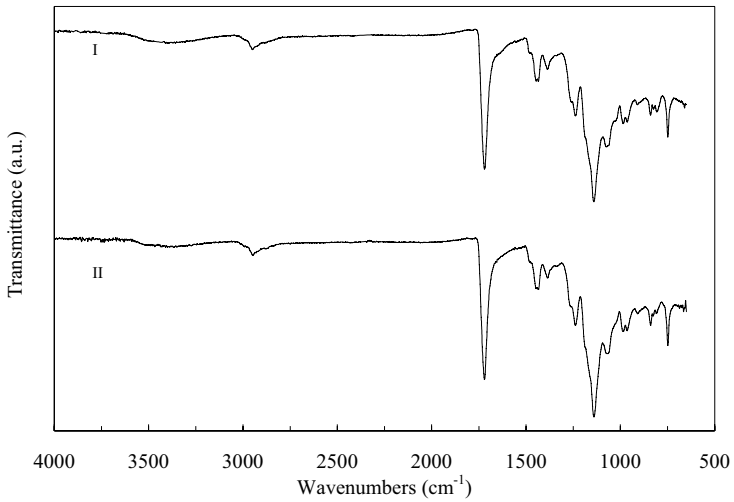

Figure 3.51. Comparison between the ATR FTIR spectrum of the surface (I) and the cross-section (II) of PMMA1/70E-*gr*-*pl*PHEA(18.2%).

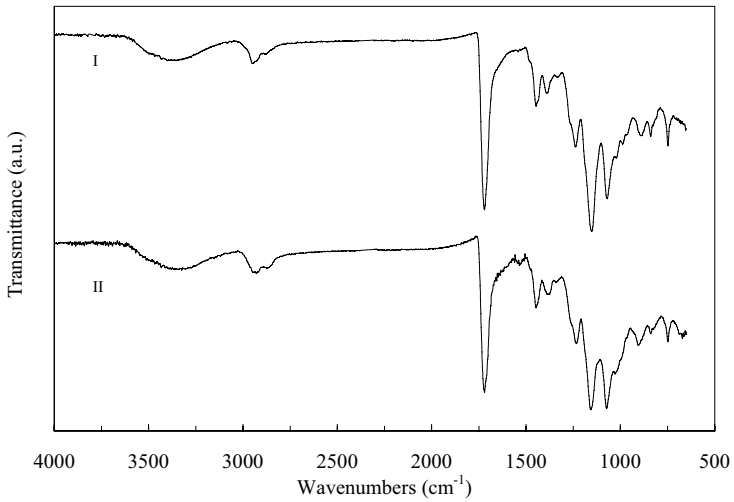

Figure 3.52. Comparison between the ATR FTIR spectrum of the surface (I) and the cross-section (II) of PMMA1/70E-*gr*-*pl*PHEA(35.3%).

It can be concluded from these results that the hydrophilic coating is homogeneous. There is no significant change between the spectrum of the surface and that of the cross-section of the PMMA-*gr*-*pl*PHEA samples. All the absorption peaks appear with similar intensity and around the same wavenumbers. This proves that the *pl*PHEA polymerisation can be initiated by plasma at any point of the porous structure of macroporous PMMA.

Finally, the ATR FTIR spectrum of PMMA1/70E treated with plasma with the same experimental conditions as PMMA-*gr*-*pl*PHEA but without adsorbing any HEA vapour is studied in order to see the effect of the plasma treatment on the PMMA network. The FTIR spectra of PMMA1/70E treated with plasma during 0, 110 and 220 seconds are shown in Figure 3.53. No significant change of the chemical structure of the PMMA substrate during plasma treatment is detected by the FTIR spectra. The same conclusion will be reached below after analysing the thermal degradation of this sample after 110 seconds of plasma treatment (see Figure 3.60).

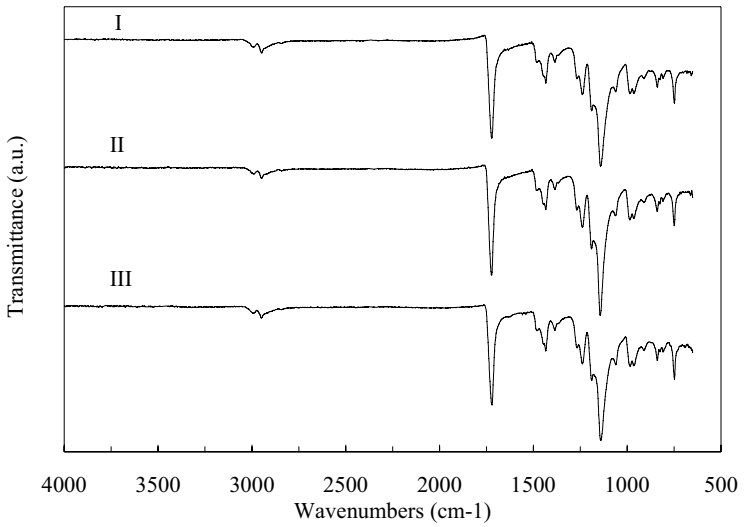

Figure 3.53. ATR FTIR spectra of PMMA1/70E treated with plasma during 0 (I), 110 (II) and 220 (III) seconds.

The spectra of PMMA1/70E treated with plasma during 110 and 220 seconds are similar to PMMA1/70E without plasma treatment. Therefore, it seems that there is not any important chemical change after the plasma treatment.

In conclusion, the shift of the absorption band characteristic of carboxylic acid esters found between *pl*PHEA and bulk PHEA could be because a small amount of oxygen is usually incorporated in the plasma polymers as C-O ether groups. The *pl*PHEA forms an homogeneous hydrophilic coating around all the PMMA microspheres after the plasma polymerisation and the plasma treatment does not affect chemically the PMMA matrix.

3.2.4. Thermal degradation.

Thermogravimetric Analysis (TGA) was performed in order to study the degradation properties of the PMMA-*gr*-*pl*PHEA. Before studying the composite material, the degradation properties of the PMMA networks polymerised in the presence of different solvent and cross-linker contents are analysed.

In the first place, the effect of porosity on the degradation properties of PMMA polymerised in the presence of 50, 60 and 70 wt.% of ethanol and 1 wt.% of EGDMA is shown in Figure 3.54. These three samples present different porosities according to the porosity determination in the dry state (P_{d1} and P_{d2}) with the apparent specific volumes and by swelling in water respectively.

The effect of porosity on the TGA thermogram could come from the different facility for the diffusion of the pyrolisis products through the material to leave the sample. As shown in Figure 3.54, there is no consistent evolution of the slope of the degradation curves with volume fraction of pores. Small differences are found on the initial step of degradation, but in fact the initial weight loss is quicker in PMMA1/60E than in the other two samples. Sample PMMA1/50E has very little porosity in the dry state because most of its pores are collapsed. However, this discontinuity inside the sample makes easier the diffusion of the pyrolisis products and therefore its degradation is not very different from the other two samples with much more porosity.

The effect of cross-linking on the degradation of macroporous PMMA was studied on three PMMA samples with similar porosities but different crosslinking densities and no significant effect was found.

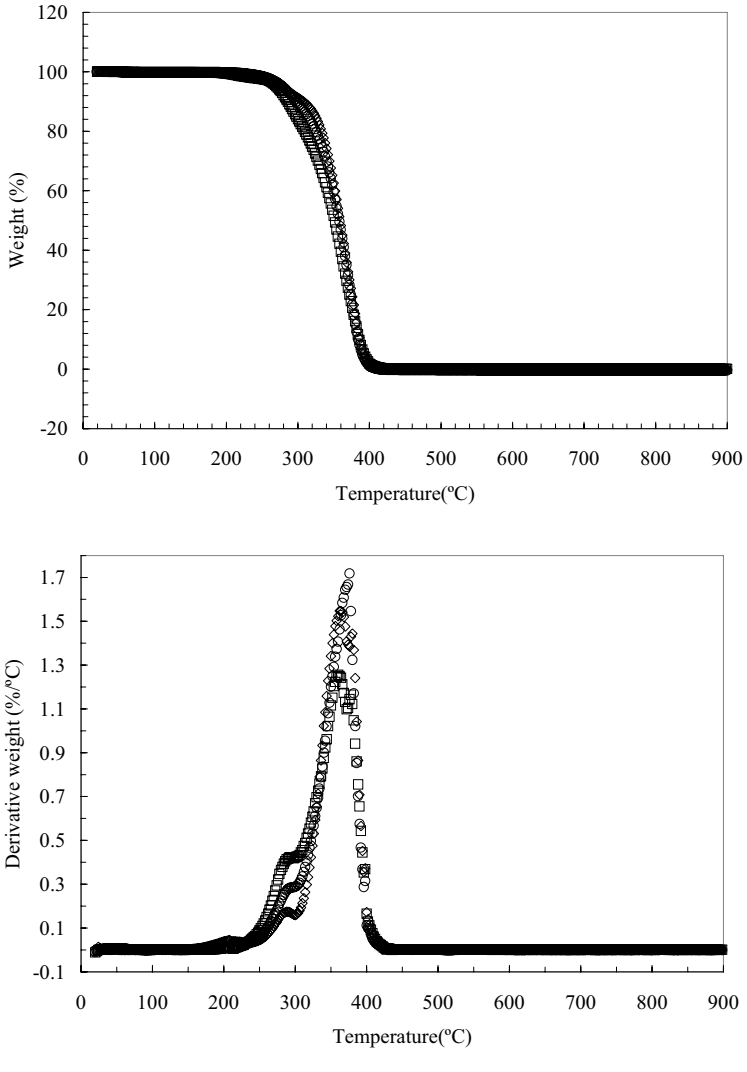

Figure 3.54. Effect of porosity. Thermogravimetric analysis of PMMA1/50E (P_{d1} = 8%) (○), PMMA1/60E (□) (P_{d1} =69% and P_{d2} =63%) and PMMA1/70E (P_{d1} =70% and P_{d2}=70%)(◇). Weight loss *(a)* and derivative *(b)* as a function of temperature. Only one point out of ten is plotted to obtain a clearer representation.

Before studying the degradation properties of the PMMA-*gr-pl*PHEA composite materials, the TGA thermograms of bulk PHEA and PMMA1/70E are analysed (see Figure 3.55).

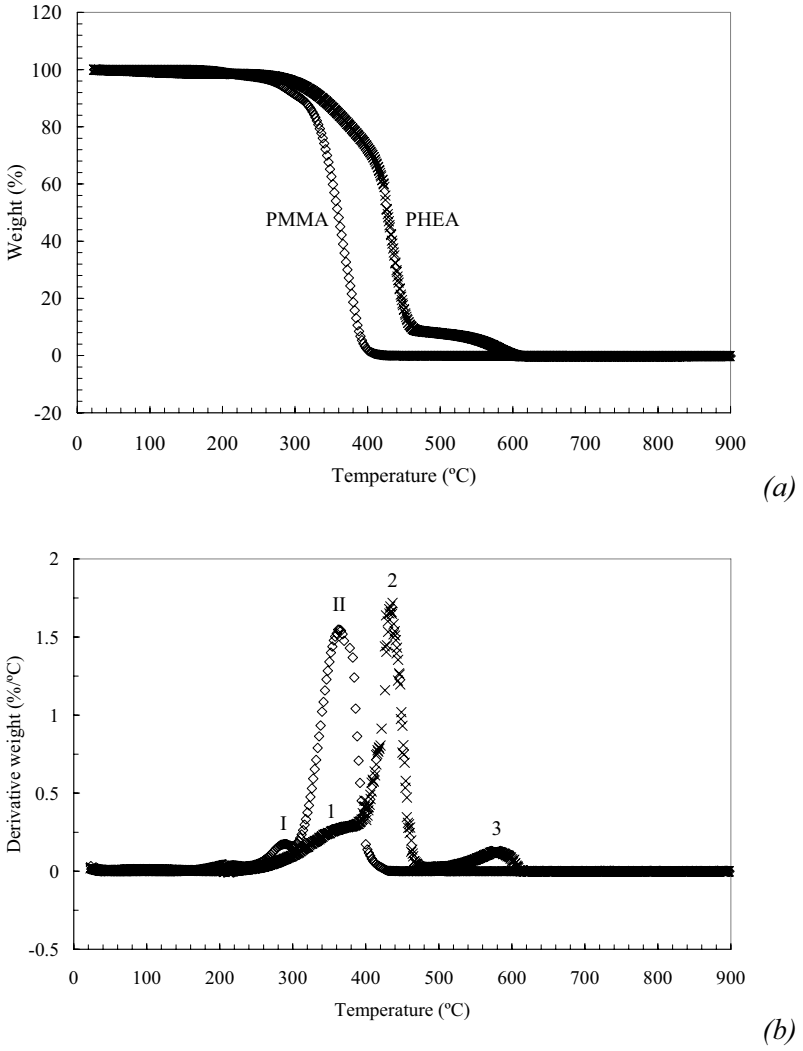

Figure 3.55. TGA of the pure phases: bulk PHEA (X) and PMMA1/70E (◇). Weight loss *(a)* and derivative *(b)* as a function of temperature. The degradation stages of these materials are shown in each degradation peak. Only one point out of ten is plotted to obtain a clearer representation.

The degradation behaviour of bulk PHEA is clearly different than that of macroporous PMMA. Bulk PHEA decomposes in three stages (1, 2 and 3) and macroporous PMMA1/70E in two (I and II) as pure PMMA [71]. PMMA starts decomposing at 220ºC and finish at 430ºC. However, bulk PHEA starts degrading at the same temperature but finish at 620ºC. At 430ºC, when PMMA

is completely degraded, there is still 44.8 wt.% of bulk PHEA.

The TGA spectrum of porous PMMA-*gr*-*pl*PHEA is plotted together with those of the pure components (macroporous PMMA and bulk PHEA) in Figure 3.56.

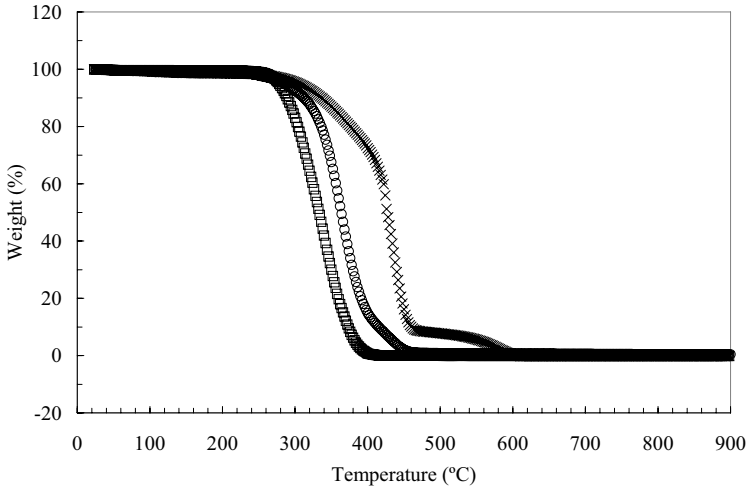

(a)

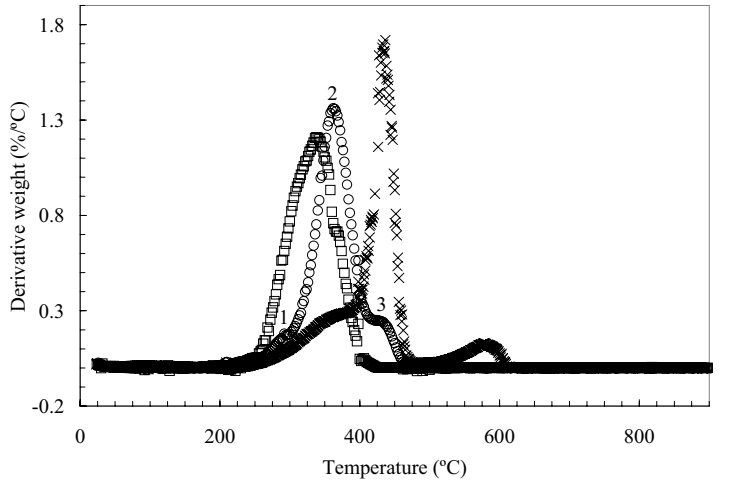

(b)

Figure 3.56. Effect of the *pl*PHEA coating. TGA analysis of bulk PHEA (X), PMMA5/70E (□) and PMMA5/70E-*gr*-*pl*PHEA(25.3%) (○). Weight loss *(a)* and derivative *(b)* as a function of temperature. Only one point out of ten is plotted to obtain a clearer representation.

The weight loss in PMMA-*gr*-*pl*PHEA is slower than in macroporous PMMA without *pl*PHEA coating because bulk PHEA degrades much slower than macroporous PMMA. The hydrophilic coating makes more difficult the diffusion of the degradation products. In addition, PMMA5/70E-*gr*-*pl*PHEA(25.3%) has three degradation stages as bulk PHEA but shifting to lower temperatures due to the presence of PMMA. The main degradation peak of the composite material appears in between the two pure components.

The TGA spectrum of sample PMMA5/70E-*gr*-*pl*PHEA(25.3%) was compared with the lineal prediction made from the TGA results of the pure components (equation (3.7)).

$$\Delta m_{PMMA-PHEA} = 0.25 \cdot \Delta m_{PHEA} + 0.75 \cdot \Delta m_{PMMA} \qquad (3.7)$$

This lineal prediction shows two separated degradation stages typical of an heterogeneous material composed of two separated phases, which is not in good agreement with the experimental result (see Figure 3.57).

The TGA spectrum of PMMA5/70E-*gr*-*pl*PHEA(25.3%) shows that this composite material degrades as an homogeneous material. Therefore, these results also reinforce the idea postulated that the *pl*PHEA is homogeneously interpenetrated in the porous PMMA networks polymerised with 5 wt.% of EGDMA.

The TGA spectra of porous PMMA with different *pl*PHEA contents are shown together in Figure 3.58.

The overall degradation velocity slightly decreases with increasing the *pl*PHEA content (the slope of the graph "weight vs temperature" decreases). This occurs because the more *pl*PHEA present in the macroporous structure of PMMA, the more difficult it is for the degradation products to diffuse. It was seen in Figure 3.55 that bulk PHEA decomposes in three stages (1, 2 and 3) and pure PMMA1/70E in two (I and II). The degradation stage I and II of PMMA1/70E overlap with the first decomposition stage 1 of PHEA (see Figure 3.58). However, the stages 2 and 3 of PHEA increase with increasing the *pl*PHEA content because they take place only in this polymer. All these samples with different *pl*PHEA contents degrades always at lower temperatures than bulk PHEA due to the presence of PMMA.

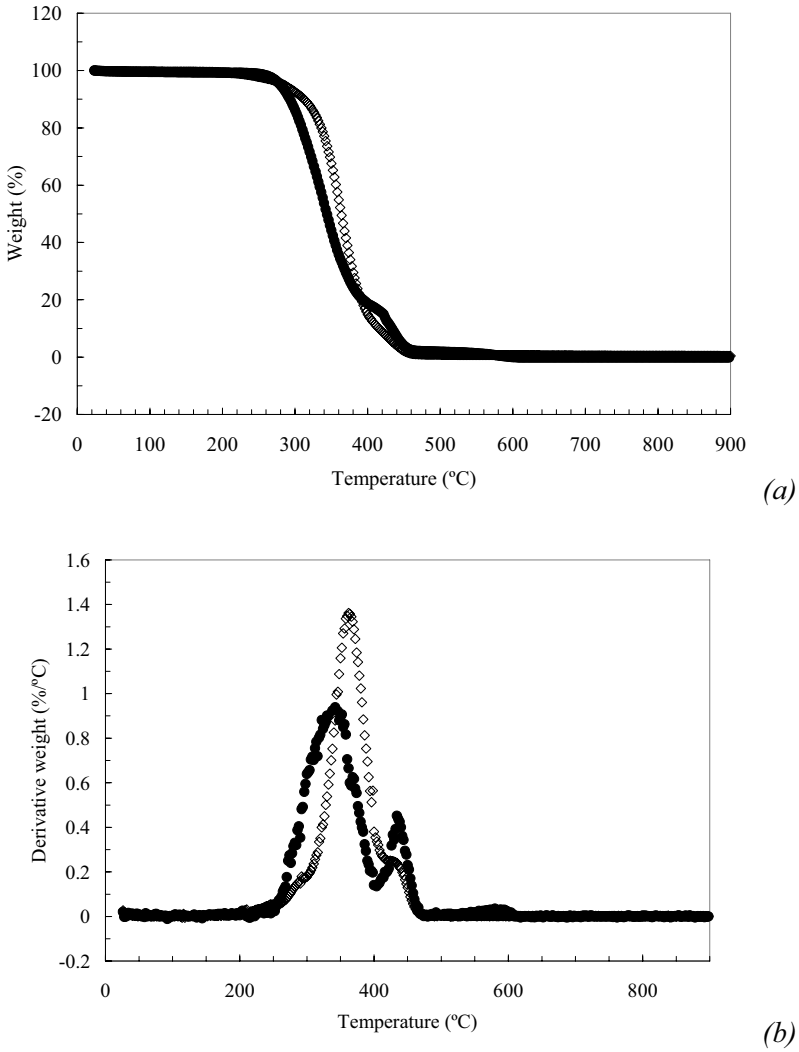

Figure 3.57. TGA analysis of PMMA5/70E-*gr*-*pl*PHEA(25.3%) (◇) and the lineal prediction of equation (3.7) (●). Weight loss *(a)* and derivative *(b)* as a function of temperature. Only one point out of ten is plotted to obtain a clearer representation.

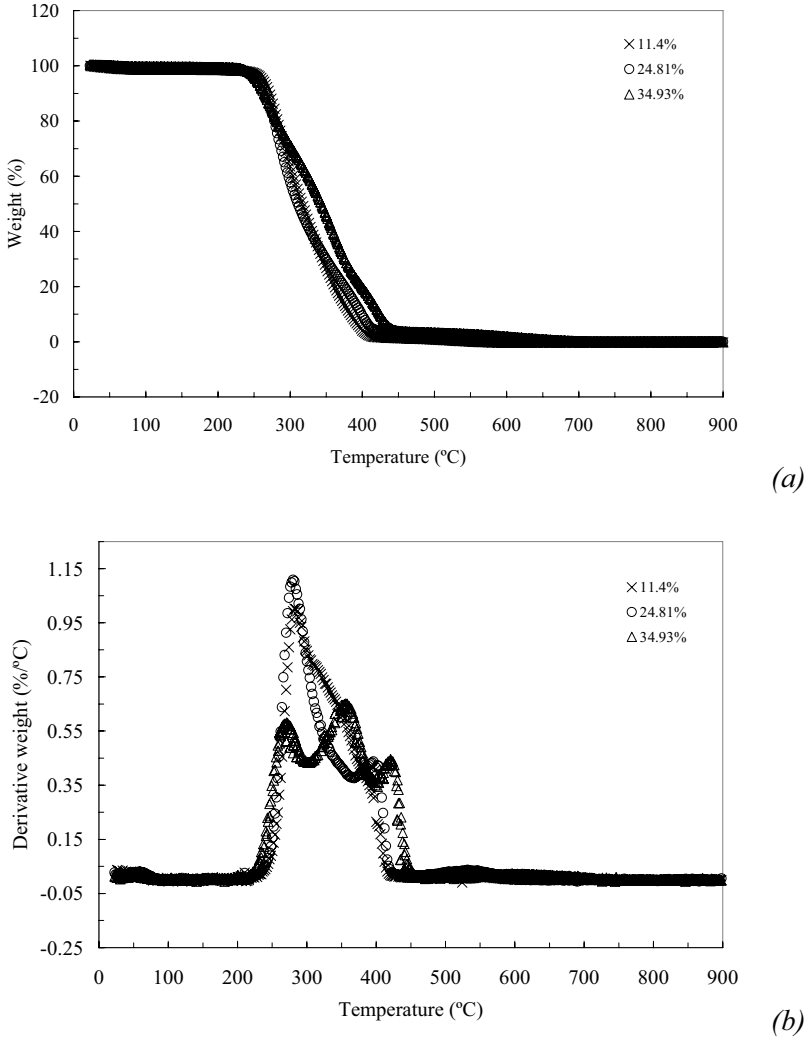

Figure 3.58. Effect of the *pl*PHEA content. TGA analysis of PMMA1/70E with 11.4 (X), 24.8 (○) and 35.3 (△) wt.% of *pl*PHEA. Weight loss *(a)* and derivative *(b)* as a function of temperature. Only one point out of ten is plotted to obtain a clearer representation.

The effect of cross-linking on the degradation temperature and velocity of macroporous PMMA is very little. Nevertheless, the amount of cross-linker used in the polymerisation process has a big influence on macroporous PMMA with hydrophilic coating (see Figure 3.59). Two samples with 1 and 5 wt.% of EGDMA with approximately the same wt.% of *pl*PHEA were chosen to study the effect of cross-linking on PMMA-*gr*-*pl*PHEA. These

results can give additional information about the interaction of the *pl*PHEA coating with the macroporous PMMA matrix.

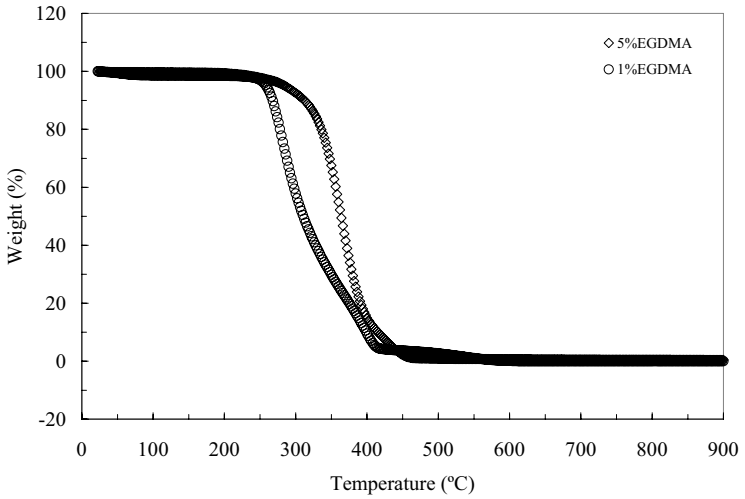

(a)

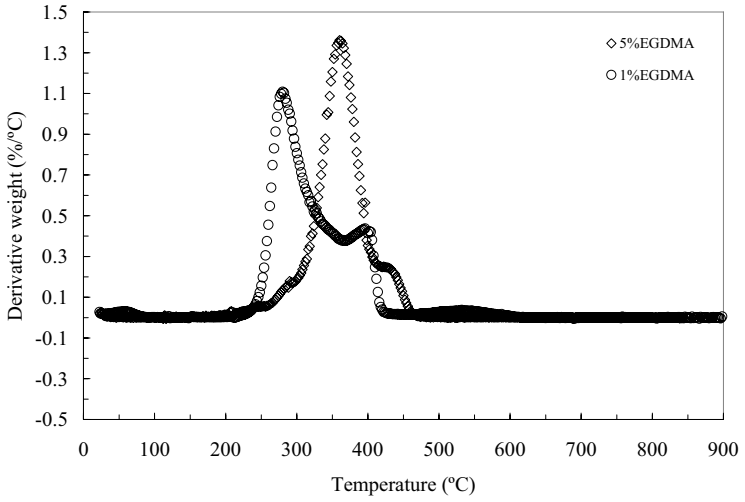

(b)

Figure 3.59. Effect of cross-linking on the degradation of macroporous PMMA with hydrophilic coating. TGA analysis of PMMA1/70E-*gr*-*pl*PHEA(24.8%) (○) and PMMA5/70E-*gr*-*pl*PHEA(25.3%) (◇).Weight loss *(a)* and derivative *(b)* as a function of temperature. Only one point out of ten is plotted to obtain a clearer representation.

Figure 3.59 shows that both samples have three different degradation stages and the PMMA sample polymerised with less cross-linker content degrades faster. The main degradation peak of the composite material polymerised with 5 wt.% of EGDMA appears at higher temperature than the other one. PMMA5/70E-*gr*-*pl*PHEA(25.3%) has more homogeneously interpenetrated *pl*PHEA than PMMA1/70E-*gr*-*pl*PHEA(24.8%) and this interpenetration decreases the degradation velocity of the composite material.

Finally, the thermal degradation of PMMA1/70E treated with plasma with the same experimental conditions as PMMA-*gr*-*pl*PHEA but without adsorbing any HEA vapour is studied in order to see the effect of the plasma treatment on the thermal degradation of macroporous PMMA. Thus, the TGA spectra of PMMA1/70E treated with plasma during 0, 110 and 220 seconds are shown together in Figure 3.60.

These TGA results show significant differences indicating different degradation behaviour of PMMA1/70E when treated with plasma during 220 seconds. After 110 seconds of plasma treatment, the thermal degradation of PMMA1/70E hardly changes. Although, it seems that the plasma treatment increases the degradation velocity in the first stage and decreases in the second stage. This effect increases with increasing the time of the plasma treatment. Thus, after 220 seconds, a strong change is produced appearing two similar degradation peaks for each degradation stage.

Since all the PMMA-*gr*-*pl*PHEA samples synthesised in this thesis were prepared with 110 seconds of plasma treatment, the effect of the plasma treatment on the macroporous PMMA network can be consider negligible. In addition, the FTIR results and the SEM micrograph did not show significant chemical or visual change after 110 seconds of plasma treatment (Figures 3.53 and 3.30).

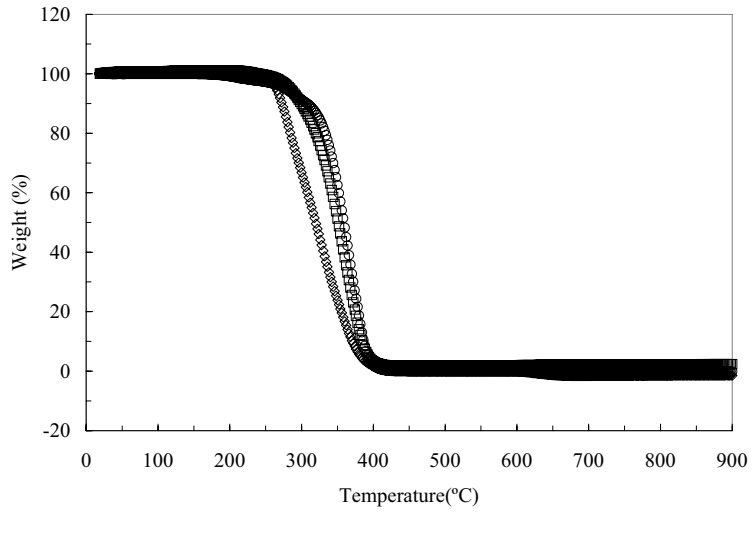

(a)

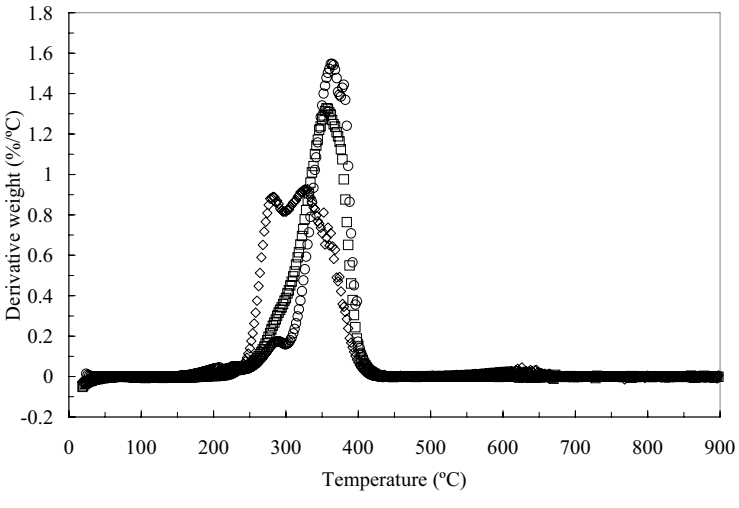

(b)

Figure 3.60. Thermogravimetric analysis of PMMA1/70E treated with plasma during 0 (○), 110 (□) and 220 (◇) seconds. Weight loss *(a)* and derivative *(b)* as a function of temperature.

3.2.5. Stability of the *pl*PHEA coating.

Compared to conventional polymers, plasma polymers generally exhibit superior stability to chemical, thermal, and mechanical stress due to their cross-linked structures [62, 51]. Our *pl*PHEA coating must be cross-linked in some extent and therefore not able to be solved in water according to the literature. Thus, in order to study the stability of the *pl*PHEA coating grafted onto macroporous PMMA, four kinds of PMMA-*gr*-*pl*PHEA samples were immersed in distilled water at 25ºC, 50ºC and 100ºC (boiling water) during 10 days changing water every day. Before the immersion in water, the air present in the samples had to be extracted with a vacuum pump to ensure complete filling of the pores. At the end of the experiment, the samples were dried at 90ºC in vacuo during three days (to constant weight) to determine the weight loss. Three PMMA-*gr*-*pl*PHEA samples with 1 wt.% of EGDMA and different *pl*PHEA contents were used in this experiment. Another composite sample with 5 wt.% of EGDMA was also used. These results are shown in Table 3.16.

Table 3.16. Weight percent of weight loss of the PMMA-*gr*-*pl*PHEA samples after 10 days immersed in distilled water at 25, 50 and 100ºC and dried in vacuo afterwards.

Sample	***25ºC***	***50ºC***	***100ºC***
PMMA1/70E-*gr*-*pl*PHEA(11.4%)	2.7	3.6	9.7
PMMA1/70E-*gr*-*pl*PHEA(24.8%)	4.7	0.01	6.4
PMMA1/70E-*gr*-*pl*PHEA(35.3%)	0.06	0.02	3.7
PMMA5/70E-*gr*-*pl*PHEA(25.3%)	0.03	0.01	2.7

The weight loss is always much smaller than the weight percent of *pl*PHEA present in the samples. Part of this weight loss can be due to a low fraction of the microspheres that are not enough joined to resist the strong push of water. Thus, a small amount of polymer particles could be removed from the sample when filling the pores. In addition, the PMMA-*gr*-*pl*PHEA sample with less *pl*PHEA has the highest weight loss probably because the adhesion between PMMA particles in this sample is poorer than in the rest (see Table 3.16).

Nevertheless, sample 5/70E-*gr*-*pl*PHEA(25.3%) has the lowest weight loss showing again that the *pl*PHEA is more homogeneously interpenetrated in this sample. This composite material losses very few polymer particles because a consistent IPN is formed after the plasma polymerisation.

If the three similar samples with different *pl*PHEA contents are compared, the weight loss decreases with increasing the hydrophilic content at

100ºC. This shows again that the samples with more *pl*PHEA are more consistent and can resist more the strength of water when filling the pores with water. The highest weight loss is achieved at 100ºC because of being in very drastic conditions (boiling water) with possible hydrolytic degradation as well.

From these results, it can be concluded that the *pl*PHEA coating cannot be dissolved in water and must be cross-linked in some extent. The weight losses are much lower than the *pl*PHEA contents and part of these low weight losses occurred because a small fraction of microspheres were not enough joined to support the strong filling of water. Nonetheless, the DSC thermogram, the FTIR spectrum, the thermogravimetric analysis and SEM micrographs of some of these samples were performed in order to study in detail the stability of this *pl*PHEA coating. The DSC thermograms of sample PMMA1/70E-*gr*-*pl*PHEA(35.3%) is shown in Figure 3.61. This kind of PMMA-*gr*-*pl*PHEA sample was chosen because an important amount of *pl*PHEA is necessary to be detectable by DSC as it was seen in section 3.2.2.

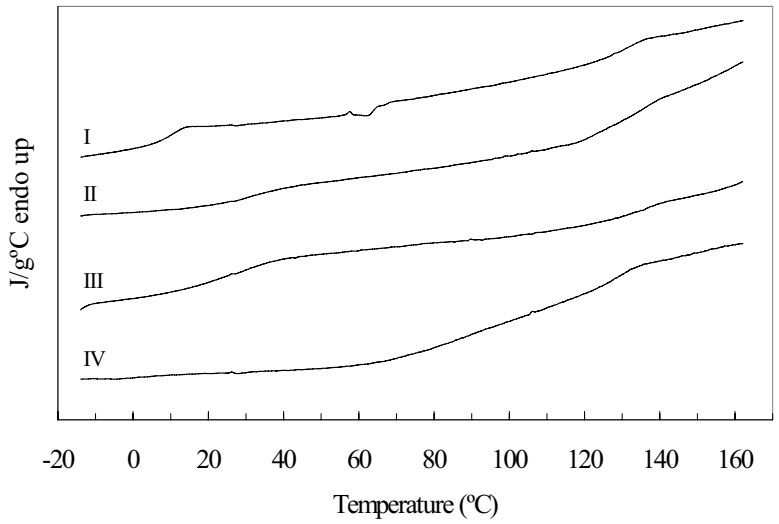

Figure 3.61. DSC thermograms of sample PMMA1/70E-*gr*-*pl*PHEA(35.3%) before (I) and after being immersed in distilled water at 25 (II), 50 (III) and 100ºC (IV) during 10 days and dried in vacuo afterwards.

The glass transition temperatures and the heat capacity increments of these samples were determined from these DSC thermograms and are shown in Tables 3.17 and 3.18. The T_g and Δc_p of the pure components of the composite material are also shown as reference. The composition of samples I, II, III and IV were calculated from the heat capacity increments of each phase in the

composite material and the Δc_p of the pure phases with the equations (3.4) and (3.5).

Table 3.17. Glass transition temperature determined by DSC of bulk PHEA, PMMA1/70E and PMMA1/70E-*gr*-*pl*PHEA(35.3%) before (I) and after being immersed in distilled water at 25 (II), 50 (III) and 100ºC (IV) during 10 days and dried in vacuo afterwards.

SAMPLE	***T_g plPHEA (ºC)***	***T_g PMMA (ºC)***
I	9.1	129.8
II	32.1	125.4
III	28.8	131.6
IV	-	129.5
Pure phases	***T_g (ºC)***	
Bulk PHEA	13.8	
PMMA1/70E	130.8	

Table 3.18. Heat capacity increments at the glass transition and composition determined by DSC of PMMA1/70E-*gr*-*pl*PHEA(35.3%) before (I) and after being immersed in distilled water at 25 (II), 50 (III) and 100ºC (IV) during 10 days and dried in vacuo afterwards. Heat capacity increments at the glass transition of bulk PHEA and PMMA1/70E.

SAMPLE	***Δc_p plPHEA (J/gK)***	***Δc_pPMMA (J/gK)***	***%plPHEA***	***%PMMA***
I	0.140	0.130	33.3	60.2
II	0.102	0.161	24.3	74.5
III	0.197	0.097	46.9	44.7
IV	-	0.134	-	62.0
Pure phases	***Δc_p (J/gK)***			
Bulk PHEA	0.420			
PMMA1/70E	0.216			

The composition of PMMA1/70E-*gr*-*pl*PHEA(35.3%) before immersion, determined by DSC, is practically the same as determined gravimetrically. Nevertheless, after immersion, all the samples show different compositions because the loss of microspheres when filling strongly with water and the hydrolytic degradation at 100ºC produces a change in the initial composition.

The DSC glass transition temperature of *pl*PHEA cannot be detected after immersion at 100ºC. The T_g of PMMA1/70E-*gr*-*pl*PHEA(35.3%) increases

19 and 22ºC after immersion in distilled water at 25 and 50ºC respectively.

The FTIR spectrum of PMMA1/70E-*gr*-*pl*PHEA(35.3%) does not change after immersion in water at 25 and 50ºC (see Figure 3.62). However, this spectrum changes dramatically, showing clearly hydrolytic degradation, after immersion in boiling water (100ºC). The hydrolytic degradation decreases the amount of *pl*PHEA and for that reason, the glass transition of *pl*PHEA becomes non-detectable in this sample.

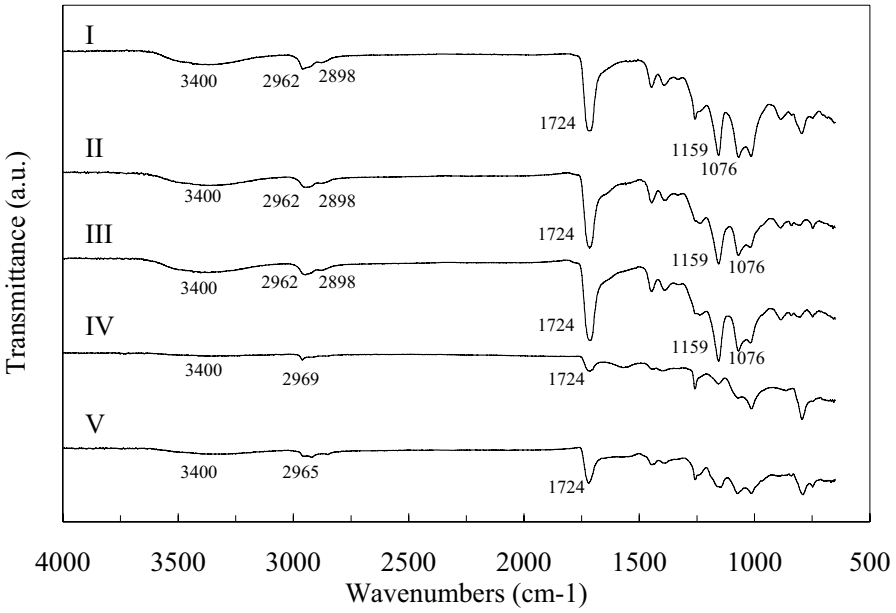

Figure 3.62. FTIR spectra of sample PMMA1/70E-*gr*-*pl*PHEA(35.3%) before (I) and after being immersed in distilled water at 25 (II), 50 (III) and 100ºC (surface (IV) and cross-section(V)) during 10 days and dried in vacuo afterwards.

Hydrolysis mechanisms are the most important degradation reactions involving polyesters, which reverts to the carboxylic acid and alcohol [125]. Figure 3.62 shows that sample IV has suffered a strong hydrolytic degradation because of being in such drastic conditions. The broad absorption around 3423 cm^{-1} due to the OH stretching vibration present in the *pl*PHEA polymer almost disappears completely after immersion in boiling water during 10 days. The strong band present in the PMMA-*gr*-*pl*PHEA samples due to the presence of the carbonyl group at 1724 cm^{-1} loses its typical strong intensity. The CH_2 and CH_3 stretching vibrations in the region of 2800-3000 cm^{-1}, the absorption band

characteristic of carboxylic acid esters at 1167 cm^{-1} and the stretching band of the alcohol group (C–O) suffers strange modifications becoming almost negligible. The bond of the CO-O-CH_2CH_2OH group must break in the hydrolytic degradation at 100ºC during 10 days. For that reason, the intensity of the signs corresponding to all these groups decreases and this explains the high weight losses seen in Table 3.16 for this sample.

Figures 3.62 (IV and V) shows the FTIR spectrum of the surface and cross-section of PMMA1/70E-*gr*-*pl*PHEA(35.3%) respectively after immersion at 100ºC. The surface has more contact with the boiling water and suffers more hydrolytic degradation. The FTIR spectrum of the cross-section shows that the intensity of the functional groups decreases also inside the sample in the same way but to less extent.

Figure 3.63 shows the TGA analysis of dry PMMA5/70E-*gr*-*pl*PHEA(25.3%) after being immersed in distilled water at 25, 50 and 100ºC during 10 days. The TGA spectrum of PMMA5/70E (without hydrophilic coating) is also plotted in this figure for comparison.

If the TGA spectra of pure PMMA5/70E and PMMA5/70E-*gr*-*pl*PHEA(25.3%) after immersion in water at 25, 50 and 100ºC are compared, a strong shift to higher temperatures can be seen due to the presence of *pl*PHEA. In addition, sample PMMA5/70E has only one degradation stage. All these results suggest that the *pl*PHEA is still present in the composite material even after very drastic conditions. Therefore, these results shows once again that the *pl*PHEA cannot be dissolved in water probably because it is cross-linked in some extent and interpenetrated.

Figure 3.64 shows the SEM micrographs of PMMA1/70E-*gr*-*pl*PHEA(35.3%) after being immersed in liquid water at 25, 50 and 100ºC during 10 days. If these micrographs are compared with the SEM picture of the PMMA1/70E without hydrophilic coating shown in Figure 3.3 *(a)*, it can be seen that there is still *pl*PHEA in all of the samples. Analogously, Figure 3.65 shows at higher magnifications that the morphology of PMMA1/70E-*gr*-*pl*PHEA(35.3%) practically does not change after such drastic conditions. The SEM micrograph of this sample before immersion in boiling water is represented in Figure 3.33 *(f)*. These SEM results show once more time that the hydrophilic coating is cross-linked and very stable chemically.

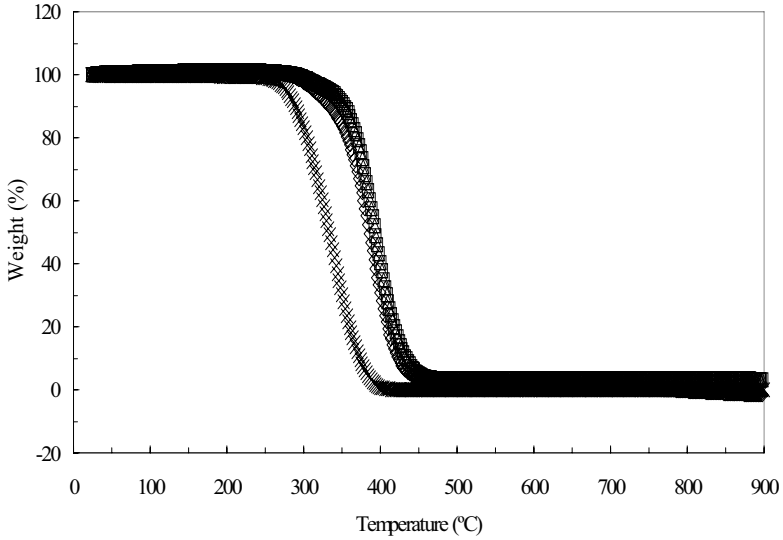

(a)

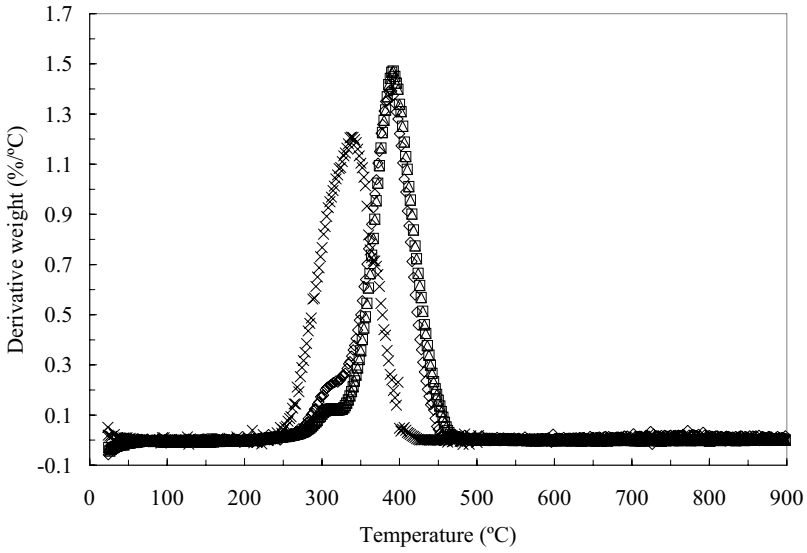

(b)

Figure 3.63. Thermogravimetric analysis of PMMA5/70E (X) and PMMA5/70E-*gr-pl*PHEA(25.3%) before (●) and after being immersed in distilled water at 25 (△), 50 (□) and 100ºC (◇) during 10 days and dried in vacuo afterwards. Weight loss *(a)* and derivative *(b)* as a function of temperature. Only one point out of ten is plotted to obtain a clearer representation.

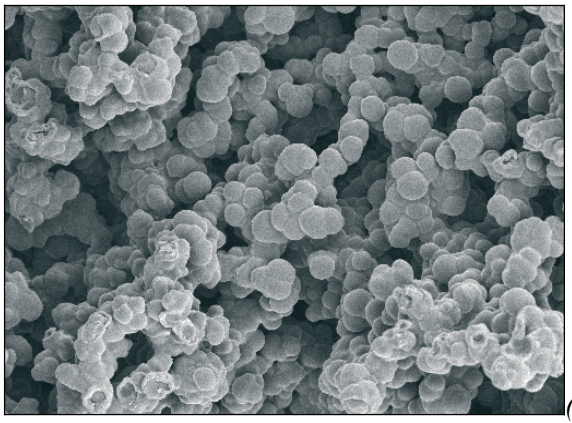

(a)

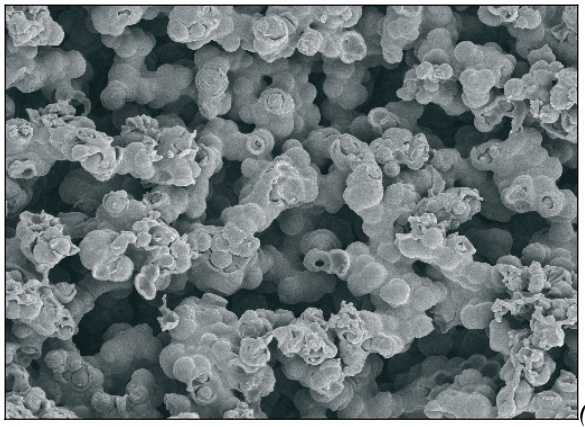

(b)

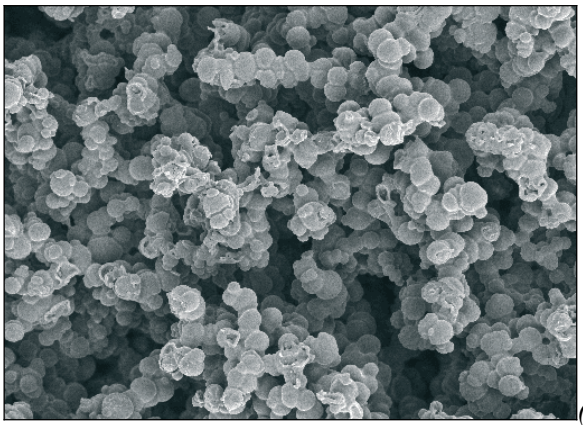

(c)

Figure 3.64. SEM micrographs (x500) of PMMA1/70E-*gr-pl*PHEA(35.3%) after being immersed in liquid water at 25 (*a*), 50 (*b*) and 100ºC *(c)* during 10 days and dried in vacuo afterwards.

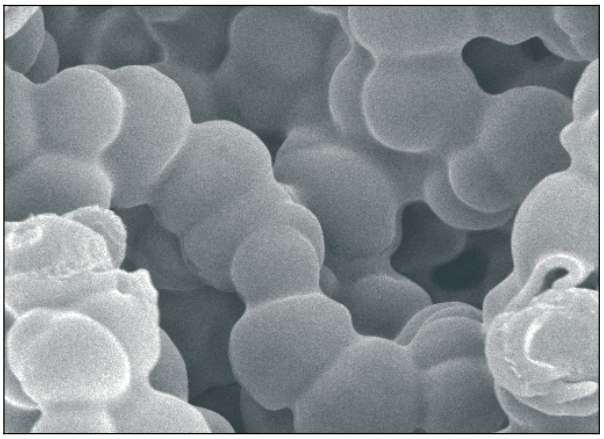

Figure 3.65. SEM micrographs (x4000) of PMMA1/70E-*gr*-*pl*PHEA(35.3%) after being immersed in liquid water at 100ºC during 10 days and dried in vacuo afterwards.

3.3. Water in 'PMMA-*gr*-*pl*PHEA'.

In this chapter, the water properties of PMMA-*gr*-*pl*PHEA are studied. PMMA is very hydrophobic and the *pl*PHEA coating is very hydrophilic. Equilibrium sorption isotherms, desorption after equilibrium in liquid water and water vapour, immersion in water and contact angle measurements were performed. Finally, the results of the thermal analysis of water in the hydrophilic coating are presented and discussed.

3.3.1. Equilibrium sorption isotherms.

The equilibrium sorption isotherms of bulk PMMA with three different EGDMA contents (1, 5 and 10 wt.%) at 50ºC are shown in Figure 3.66.

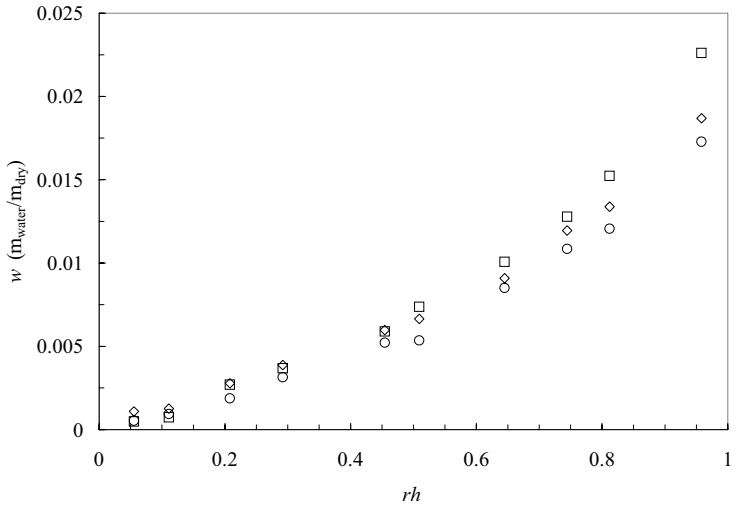

Figure 3.66. Equilibrium water sorption isotherms of PMMAB1 (○), PMMAB5 (◇) and PMMAB10 (□) at 50ºC.

The amount of absorbed water is very low and increases with increasing the EGDMA content. Water sorption usually decreases with increasing cross-linking density, however, the number of polar COO groups increases with increasing the EGDMA content in PMMA, increasing its water sorption capacity.

The moles of COO groups are double in EGDMA than in MMA: $n_{COO}^{MMA} = n_{MMA}$ and $n_{COO}^{EGDMA} = 2 \cdot n_{EGDMA}$. Thus, the moles of COO groups in the

final polymer increase with increasing the moles of EGDMA added in the polymerisation process as

$$\frac{n_{COO}}{n} = \frac{n_{COO}^{EGDMA} + n_{COO}^{MMA}}{n} = 2 \cdot \frac{n_{EGDMA}}{n} + \frac{n_{MMA}}{n} = 1 + \frac{n_{EGDMA}}{n}$$

where n is the total moles of monomers ($n = n_{MMA} + n_{EGDMA}$).

Water sorption at these low water activities (a<1) occurs with no or very small expansion of the polymer network [50, 126]. Thus, the contribution of the elastic energy to water sorption, which is affected by the cross-linking density, is not significant and the contribution of the number of absorption sites determines the amount of water absorbed in equilibrium. This effect of increasing water sorption with increasing cross-linking density was also found in bulk PMMA with different EGDMA contents prepared by thermal polymerisation [127].

The equilibrium water sorption isotherms of macroporous PMMA obtained by polymerisation in the presence of ethanol with different solvent and cross-linker contents at 20, 35 and 50ºC were also determined but much dispersion was found in all the graphs. Only two isotherms of these are going to be shown in order to give an idea of the problem.

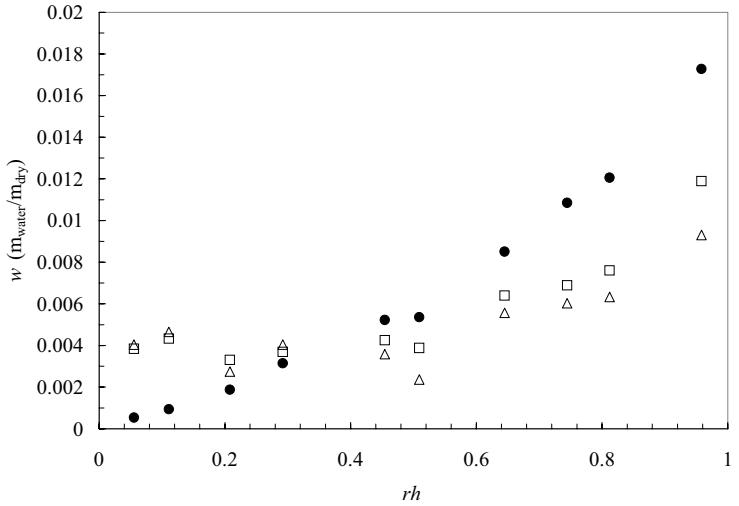

Figure 3.67. Equilibrium water sorption isotherms of non-porous PMMAB1 (●) and macroporous PMMA: PMMA1/60E (△) and PMMA1/70E (□) at 50ºC.

For low water activities or low *rh* values, macroporous PMMA has higher equilibrium water uptakes (*w*) than bulk PMMA. This fast increase of weight for low relative humidities must occur because of porosity, which produces to have a very large specific area where water can be adsorbed. For high water activities, however, the water sorption of bulk PMMA is higher than macroporous PMMA.

When *pl*PHEA is grafted onto macroporous PMMA, water sorption considerably increases, especially for high relative humidities. Figure 3.68 shows the water uptakes of PMMA-*gr*-*pl*PHEA compared with the same kind of sample but without hydrophilic coating.

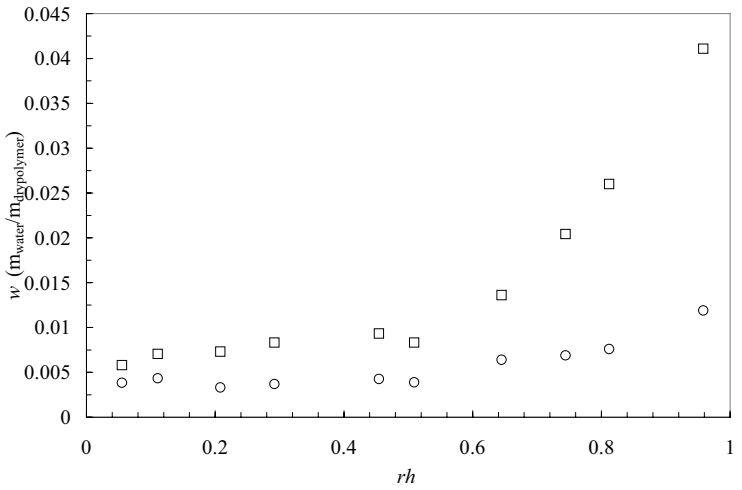

Figure 3.68. Effect of the hydrophilic coating. Equilibrium sorption isotherms of PMMA1/70E (○) and PMMA1/70E-*gr*-*pl*PHEA(18.2%) (□) at 50ºC.

The equilibrium water uptakes at two water activities (*rh*=50.9 and 98.52%) of bulk PMMA and macroporous PMMA with different cross-linker and solvent contents are shown in Table 3.19. The water uptakes of PMMA-*gr*-*pl*PHEA samples and bulk PHEA are also shown in this table in order to study the effect of the *pl*PHEA coating on water sorption.

Contrary to what expected, water sorption decreases with porosity at these water activities. This unexpected phenomenon could be due to water clustering as shown in Figure 3.69, which makes some fraction of the total surface area incapable of lodging water molecules.

Table 3.19. Equilibrium water uptakes ($w=m_{water}/m_{drypolymer}$) of bulk PMMA and macroporous PMMA with different solvent, cross-linker and *pl*PHEA contents at two relative humidities (*rh* = 50.9 and 95.8%) at 50ºC.

SAMPLE	***w*** ***(rh* = 50.9%)**	***w*** ***(rh* = 98.52%)**
PMMAB1	0.00536	0.01728
PMMAB5	0.00665	0.01869
PMMAB10	0.00737	0.02260
PMMA1/60E	0.00236	0.00931
PMMA1/70E	0.00388	0.01189
PMMA5/60E	0.00505	0.01188
PMMA5/70E	0.00507	0.01298
PMMA10/60E	0.00351	0.01208
PMMA10/70E	0.00333	0.01081
PMMA1/60E-*gr-pl*PHEA(12%)	0.00687	0.03406
PMMA1/70E-*gr-pl*PHEA(18.2%)	0.00832	0.04247
PMMA5/60E-*gr-pl*PHEA(15.2%)	0.01097	0.02773
PMMA5/70E-*gr-pl*PHEA(25.3%)	0.01009	0.02459
PHEA	0.07559	0.41424

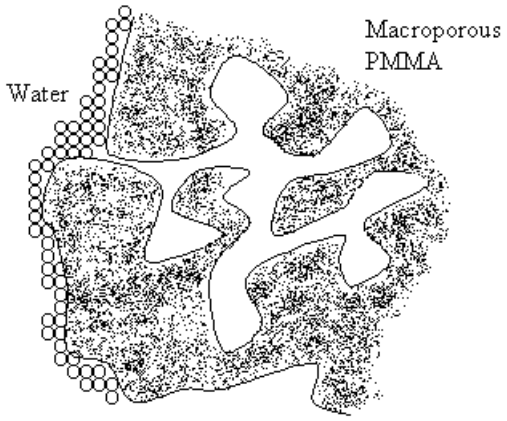

Figure 3.69. Water sorption onto macroporous PMMA.

On the other hand, the equilibrium water uptakes shown in Table 3.19 are much higher when a porous PMMA sample is coated with *pl*PHEA. For example, the water sorption of sample PMMA5/70-*gr-pl*PHEA(25.3 %) is around two times higher than the same porous PMMA but without hydrophilic coating at both water activities.

In order to compare the water sorption properties of bulk PHEA and *pl*PHEA, the equilibrium water sorption isotherms of macroporous PMMA with different EGDMA and *pl*PHEA contents, calculated with the water uptakes referred to the mass of *pl*PHEA present in the composite material, are shown in Figure 3.70. The equilibrium water sorption isotherm of bulk PHEA was also measured and is plotted together with all these curves.

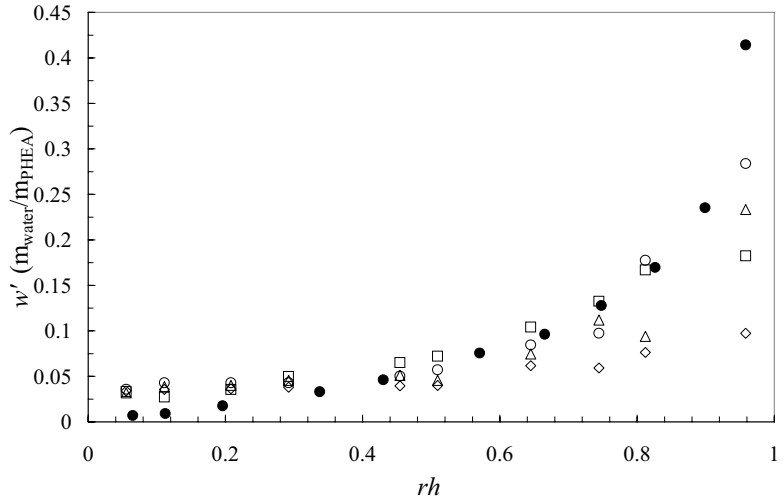

Figure 3.70. Equilibrium water sorption isotherms of PMMA1/60E-*gr-pl*PHEA(12%)(○), PMMA1/70E-*gr-pl*PHEA(18.2%)(△), PMMA5/60E-*gr-pl*PHEA(15.2%)(□), PMMA5/70E-*gr-pl*PHEA(25.3%)(◇) and bulk PHEA(●) at 50ºC. Equilibrium water uptakes referred to the mass of PHEA.

Figure 3.70 shows that from 0 to 40% of relative humidity, *pl*PHEA absorbs more water than bulk PHEA because of the high specific area of these composite materials. For $0.4 < rh < 0.7$, both kinds of PHEA absorbs similar amounts of water. However, for high relative humidities ($0.7 < rh < 1$), the expansion of the polymer network starts having effect on water sorption from the gas phase. The elastic energy of *pl*PHEA interpenetrated in the PMMA network produces a decrease in the water sorption. Bulk PHEA, with respect to that, is not cross-linked nor interpenetrated and can expand its network increasing considerably the amount of absorbed water.

The *pl*PHEA present in PMMA5/70E-*gr*-*pl*PHEA (25.3%) has the lowest water uptake because most of this *pl*PHEA is interpenetrated as seen with other experimental techniques. For that reason, the PMMA-*gr*-*pl*PHEA samples with 5 wt.% of EGDMA have lower water uptakes than those with 1 wt.%. On the other hand, the *pl*PHEA present in PMMA1/60E-*gr*-*pl*PHEA(12%) has the highest water uptake because most of this *pl*PHEA is on the surface of PMMA separated from the PMMA network. This amount of water (w'=0.2840) is still lower than that of bulk PHEA (w'=0.4142) because part of this *pl*PHEA could be interpenetrated. In addition, *pl*PHEA and bulk PHEA differ chemically and plasma polymers are always cross-linked in some extent [62, 51].

3.3.2. Water diffusion.

In this section, the results obtained from dynamic desorption after equilibrium in water vapour, dynamic desorption after equilibrium in liquid water and contact angle measurements are presented and discussed in order to study water diffusion in PMMA-*gr*-*pl*PHEA.

Dynamic desorption after equilibrium in water vapour, in an atmosphere with a relative humidity of 97%, is shown for macroporous PMMA with and without *pl*PHEA coating. These results are shown as normalised mass against normalised time: $\Delta m_{1,t} / \Delta m_{1,\infty}$ *vs* $t^{0.5}/l$ (see equation (1.18)).

Figure 3.71 shows the effect of porosity on the desorption after equilibrium in water vapour for macroporous PMMA. Thus, porosity increases the speed of the desorption process (increase of the slope) independently of the cross-linking density. The less porosity, the more difficult is for water to diffuse out of the sample.

The normalised dynamic water desorption results of macroporous PMMA with plasma-polymerised hydrophilic coating are shown in Figure 3.72. The diffusion coefficients (D) of macroporous PMMA and PMMA-*gr*-*pl*PHEA, determined from the normalised graphs with equation (1.22), are shown in Table 3.20.

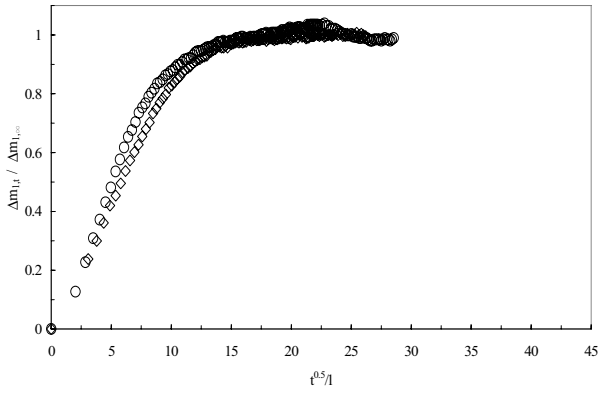

(a)

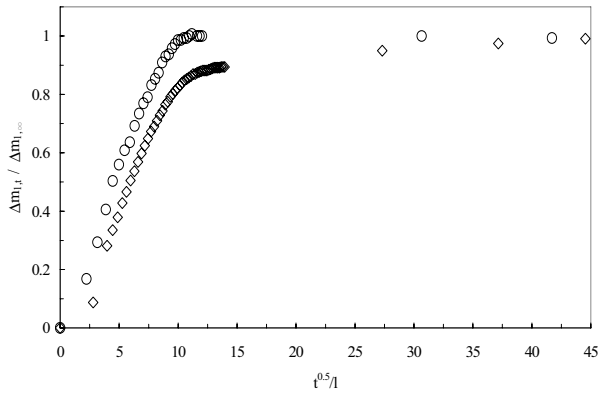

(b)

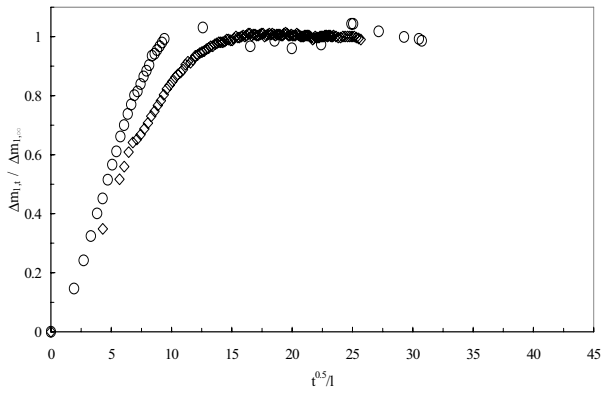

(c)

Figure 3.71. Effect of porosity. Normalised dynamic water desorption of PMMA1/70E (P_{dl}=70) (○) and PMMA1/60E (P_{dl}=69) (◇) *(a)*; PMMA5/70E (P_{dl}=76) (○) and PMMA5/60E (P_{dl}=65) (◇) *(b)*; PMMA10/70E (P_{dl}=77) (○) and PMMA10/60E (P_{dl}=70) (◇) *(c)*.

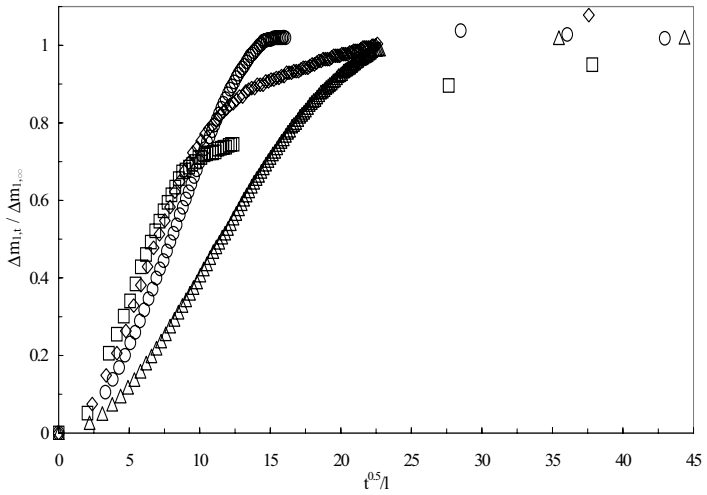

Figure 3.72. Normalised dynamic desorption experiments of PMMA-*gr-pl*PHEA: PMMA1/70E-*gr-pl*PHEA(18.2%) (○), PMMA1/60E-*gr-pl*PHEA(12%) (△), PMMA5/70E-*gr-pl*PHEA(25.3%) (◇) and PMMA5/60E-*gr-pl*PHEA(15.2%) (□).

Table 3.20. Desorption diffusion coefficients of macroporous PMMA and PMMA-*gr-pl*PHEA.

SAMPLE	***Dx10^5 (cm^2/s)***
PMMA1/60E	1.45
PMMA1/70E	1.95
PMMA5/60E	1.48
PMMA5/70E	2.03
PMMA10/60E	1.54
PMMA10/70E	2.43
PMMA1/60E-*gr-pl*PHEA(12%)	0.481
PMMA1/70E-*gr-pl*PHEA(18.2%)	0.913
PMMA5/60E-*gr-pl*PHEA(15.2%)	1.27
PMMA5/70E-*gr-pl*PHEA(25.3%)	1.16

All these diffusion coefficients shown in Table 3.20 are plotted against porosity (P_{dl}) in Figure 3.73 to study the effect of porosity and cross-linking density .

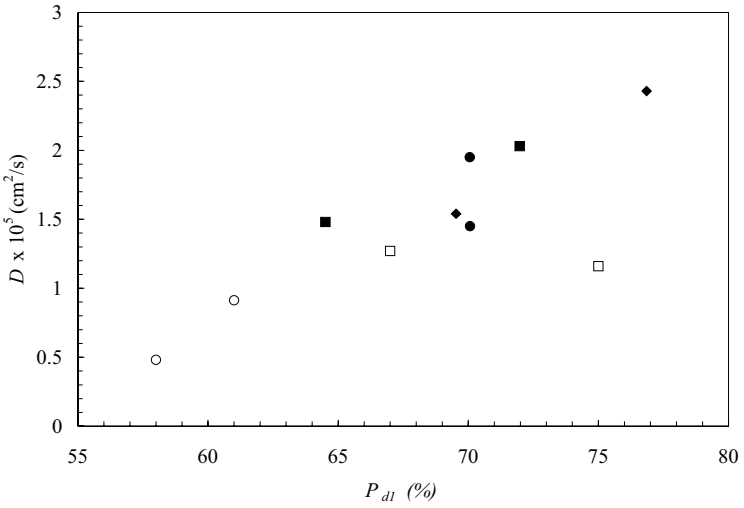

Figure 3.73. Water desorption diffusion coefficients of macroporous PMMA with 1 (○), 5 (□) and 10 (◇) wt.% of EGDMA with (open symbols) and without (solid symbols) *pl*PHEA as a function of porosity (P_{dl}).

The diffusion coefficients increases with increasing porosity or cross-linking density. On the other hand, the *pl*PHEA coating decreases the speed of the desorption process. Even though there is much less PHEA than PMMA, the diffusion coefficient decreases very sharply when a macroporous PMMA sample is coated with this hydrogel. This is an expected result because hydrophilic polymers show lower diffusion coefficients than hydrophobic polymers due to the effect of hydrogen bonding of water molecules to the hydrophilic chains on their mobility through the polymer matrix [126,128]. The *pl*PHEA coating has OH functional groups, which retain more time the water molecules by hydrogen bonding and decrease the velocity of the desorption process.

When a hydrophilic polymer is interpenetrated in a hydrophobic polymer, its diffusion coefficient increases due to the presence of the hydrophobic material [128]. Therefore, these results also prove that the *pl*PHEA coating is more homogeneously interpenetrated with the macroporous PMMA polymerised with 5 than with 1 wt.% of EGDMA because lower diffusion coefficients are found in the two samples with less amount of cross-linker (see

Table 3.20). PMMA1/60E-*gr*-*pl*PHEA(12%) and PMMA1/70E-*gr*-*pl*PHEA(18.2%) have most of its *pl*PHEA on the surface and there are more OH groups in contact with the water vapour. However, samples PMMA5/60E-*gr*-*pl*PHEA(15.2%) and PMMA5/70E-*gr*-*pl*PHEA(25.3%) have most of the *pl*PHEA interpenetrated.

The desorption diffusion coefficients of the PMMA-*gr*-*pl*PHEA samples are much higher (~ 10^{-5} cm^2/s, Table 3.20) than bulk PHEA (~ 10^{-7} cm^2/s, Table 3.21) due to the presence of the macroporous PMMA matrix.

An estimation of the diffusion coefficient of *pl*PHEA can be achieved on the basis of the assumption that the diffusion process of the composite is mostly controlled by the desorption kinetics in a layer of *pl*PHEA with an effective thickness l_{plPHEA} corresponding to the thickness of an homogeneous coating of *pl*PHEA on the surface of the PMMA microspheres. Thus, these results were recalculated to estimate the diffusion coefficient of the *pl*PHEA coating (see Table 3.21). The effective *pl*PHEA thickness (l_{plPHEA}) was determined considering $V_{plPHEA}=A\cdot l_{plPHEA}$ (V_{plPHEA} is the volume of *pl*PHEA and A is the surface of the microspheres in PMMA-*gr*-*pl*PHEA) and $V=A\cdot l$ (V is the volume, A is the surface and l the thickness of the PMMA-*gr*-*pl*PHEA sample). Thus, with the total mass of the PMMA-*gr*-*pl*PHEA sample (m),

$$V_{plPHEA} = m_{plPHEA} \cdot v_{plPHEA} = m \cdot X_{plPHEA} \cdot v_{plPHEA} \qquad (3.8)$$

where m_{plPHEA} , v_{plPHEA} and X_{plPHEA} are the mass, the specific volume and the mass fraction of the *pl*PHEA in the macroporous PMMA matrix. The specific volume of bulk PHEA was taken in this estimation ($v_{plPHEA} \approx 0.754\ cm^3/g$). Therefore,

$$l_{plPHEA} = \frac{V_{plPHEA}}{A} = \frac{m \cdot X_{plPHEA} \cdot v_{plPHEA}}{V / l} \qquad (3.9)$$

Finally,

$$l_{plPHEA} = \rho \cdot X_{plPHEA} \cdot v_{plPHEA} \cdot l \qquad (3.10)$$

where ρ is the apparent density and l is the thickness of the PMMA-*gr*-*pl*PHEA sample. With this value of the effective *pl*PHEA thickness (l_{plPHEA}), in the same way, representing '$\Delta m_{1,t} / \Delta m_{1,\infty}$' vs '$t^{0.5}/l_{plPHEA}$', the diffusion coefficient of the *pl*PHEA can be calculated as the slope of the linear plot.

Table 3.21 shows the diffusion coefficients of the *pl*PHEA present in the different macroporous PMMA structures, estimated from the effective *pl*PHEA thickness. The diffusion coefficient of bulk PHEA taken from reference [10] is also shown in this table as reference. Although, this *D* of PHEA was determined in this work with different experimental conditions.

Table 3.21. Diffusion coefficients (*D*) of bulk PHEA[10] and the *pl*PHEA in the PMMA-*gr*-*pl*PHEA composite materials calculated from the effective *pl*PHEA thickness (l_{plPHEA}). The porosities in the dry state of state (P_{dl}) of these samples are also indicated.

SAMPLE	P_{dl} (%)	Dx10^8 (cm^2/s)
PMMA1/60E-*gr*-*pl*PHEA(12%)	58	0.71
PMMA1/70E-*gr*-*pl*PHEA(18.2%)	61	1.43
PMMA5/60E-gr-*pl*PHEA(15.2%)	67	3.63
PMMA5/70E-*gr*-*pl*PHEA(25.3%)	75	4.34
Bulk PHEA	-	14

The diffusion coefficients of *pl*PHEA get closer to that of bulk PHEA with this estimation. Here again the diffusion coefficients of the *pl*PHEA present in the PMMA-*gr*-*pl*PHEA composites with 5 wt.% of EGDMA are higher due to the high interpenetration of the *pl*PHEA. The diffusion coefficient of *pl*PHEA in PMMA1/60E-*gr*-*pl*PHEA(122) is the lowest because the *pl*PHEA is more separated from the PMMA matrix in this sample. The diffusion coefficients increase with increasing porosity and cross-linking density as it occurred with macroporous PMMA.

Dynamic water desorption after equilibrium in liquid water at 25ºC is shown and discussed for bulk PHEA, macroporous PMMA and PMMA-gr-*pl*PHEA. The samples were immersed in liquid water to equilibrate to constant weight. Then, after drying their surfaces with filter paper, they were placed on the stage of a balance in an atmosphere with a relative humidity of 19% and their weight was recorded continuously with the help of a computer. These results are shown as normalised water mass loss per total water mass loss against time: $(m(t)-m_\infty)/(m(t=0)-m_\infty)$ *vs time*.

Water sorption from a vapour phase containing water swells the polymer agregates but no liquid water condense into the pores because pure liquid water would not be in equilibrium with water in the water phase. In principle, the equilibrium water sorption on the polymer in an atmosphere with saturated air should be the same than in immersion in liquid water because in

both cases the activity of water outside the polymer sample is the unity. The difference is obviously the amount of liquid filling the pores when the sample is immersed in liquid water.

The dynamic water desorption result after equilibrium in liquid water for bulk PHEA is shown in Figure 3.74. This plot is also represented as normalised mass against normalised time: $\Delta m_{1,t} / \Delta m_{1,\infty}$ *vs* $t^{0.5}/l$ (equation (1.18)) in Figure 3.75.

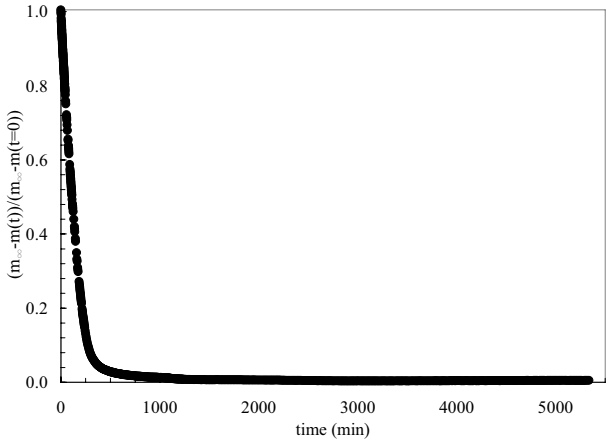

Figure 3.74. Dynamic water desorption after equilibrium in liquid water for bulk PHEA. Weight loss as a function of time at 25ºC and 19% of relative humidity.

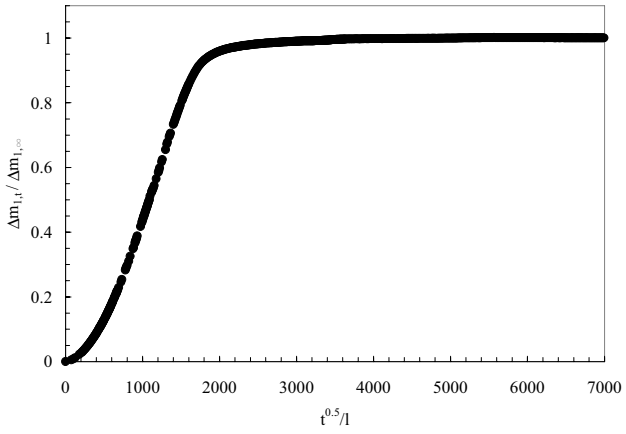

Figure 3.75. Normalised dynamic desorption after equilibrium in liquid water for bulk PHEA. Desorption at 25ºC and 19% of relative humidity.

This normalised graph clearly shows that the desorption process of water in bulk PHEA is not Fickian because this plot is not linear for low desorption times. Therefore, there is not only diffusion in the desorption process of water in bulk PHEA.

The maximum water uptake of bulk PHEA after immersion in liquid water is 2.5 grams of water per gram of dry polymer (see Table 3.24). However, the maximum water uptake of bulk PHEA after sorption from the vapour phase is only 0.41 grams of water per gram of dry polymer (see Table 3.19). The amount of liquid water present in the pores of swollen PHEA is approximately the difference between these two water uptakes. This amount of water is very large and must evaporate in the desorption process. The same applies for the PMMA-*gr*-*pl*PHEA composite materials.

Bulk PHEA and PMMA-*gr*-*pl*PHEA are hydrophilic materials. However, macroporous PMMA is very hydrophobic and the amount of water absorbed by the polymer matrix could be considered negligible in comparison with the large amount of water present in the pores.

Therefore, the desorption process of water in bulk PHEA, macroporous PMMA and PMMA-*gr*-*pl*PHEA after equilibrium in liquid water consists of diffusion of water adsorbed in the polymer matrix and evaporation of water present in the pores. Once the pores are empty, there must be diffusion exclusively. However, diffusion could be negligible in comparison with evaporation because of the large amount of water filling the pores.

In order to quantify the importance of evaporation against diffusion, the mass fraction of water in the pores was estimated as the difference between the water uptakes from the liquid and from the gas phase (Tables 3.24 and 3.19 respectively) divided by the water uptake from the liquid phase: $(w_{\text{liquid phase}} - w_{\text{gas phase}})/w_{\text{liquid phase}} = m_{\text{water in pores}}/m_{\text{total water}}$. From these results shown in Table 3.22, it can be concluded that the desorption process after equilibrium in liquid water for macroporous PMMA and PMMA-*gr*-*pl*PHEA can be considered to consist almost exclusively of evaporation because the mass fraction of water in the pores is close to unity and the diffusion contribution is negligible. Water diffusion is more important in bulk PHEA but still much less important than evaporation.

Table 3.22. Mass fraction of water in the pores of macroporous PMMA, PMMA-*gr-pl*PHEA and bulk PHEA.

Sample	$m_{water\ in\ pores}/m_{total\ water}$
PMMA1/60E	0.995
PMMA1/70E	0.996
PMMA5/60E	0.994
PMMA5/70E	0.995
PMMA10/60E	0.995
PMMA10/70E	0.995
PMMA1/60E-*gr-pl*PHEA(12%)	0.983
PMMA1/70E-*gr-pl*PHEA(18.2%)	0.988
PMMA5/60E-*gr-pl*PHEA(15.2%)	0.987
PMMA5/70E-*gr-pl*PHEA(25.3%)	0.992
Bulk PHEA	0.834

Evaporation can be predicted by Dalton's equation. Evaporation takes place when the saturation pressure of water (p_w^v) is higher than the partial pressure of water in air (p_a^v) [129]. Dalton's equation considers that *dm/dt*,

$$\frac{dm}{dt} = k \cdot (p_w^v - p_a^v) \tag{3.11}$$

where *k* is the mass transfer coefficient. The partial pressure of water in air (p_a^v) may be expressed as

$$p_a^v = rh \cdot p_w^v \tag{3.12}$$

where *rh* is the relative humidity. Therefore, substituting 3.12 in the Dalton equation,

$$\frac{dm}{dt} = K \cdot (1 - rh) \tag{3.13}$$

where the evaporation constant *K* is $k \cdot p_w^v$. Evaporation and *K* will be expressed in *g/s*. Since *K* and *rh* are constant, *dm/dt* is also constant and can be easily determined as the slope of the normalised linear plot: *$(m(t)-m_\infty)/(m(t=0)-m_\infty)$ vs time*.

The desorption results after equilibrium in liquid water for macroporous PMMA and PMMA-*gr*-*pl*PHEA are shown in Figures 3.76 and 3.77 respectively. The evaporation constants of these samples, determined with the slope of the normalised linear plot (*(m(t)-m∞)/(m(t=0)-m∞) vs time*) and the Dalton equation (3.13), are shown in Table 3.23. The evaporation constant of bulk PHEA is also shown in this table.

Table 3.23 shows no significant differences between all the evaporation constants ($\sim \cdot 10^{-5}$ g/s). The evaporation process seems to be very similar for macroporous PMMA, PMMA-*gr*-*pl*PHEA and bulk PHEA. This means that the liquid water phase inside the swollen PHEA network behaves as if it were a macroporous material with interconnected pores like macroporous PMMA. In addition, the evaporation process is very similar in all these materials even though PMMA is hydrophobic and PHEA is hydrophilic. This is very different from diffusion where the OH functional groups produces a decrease in the speed of the desorption process [126]. There is not a clear influence of the cross-linking density or porosity on the evaporation constant of these samples. The *pl*PHEA coating has not influence at all on the evaporation process. Even sample PMMA5/70E has the same evaporation constant with and without *pl*PHEA.

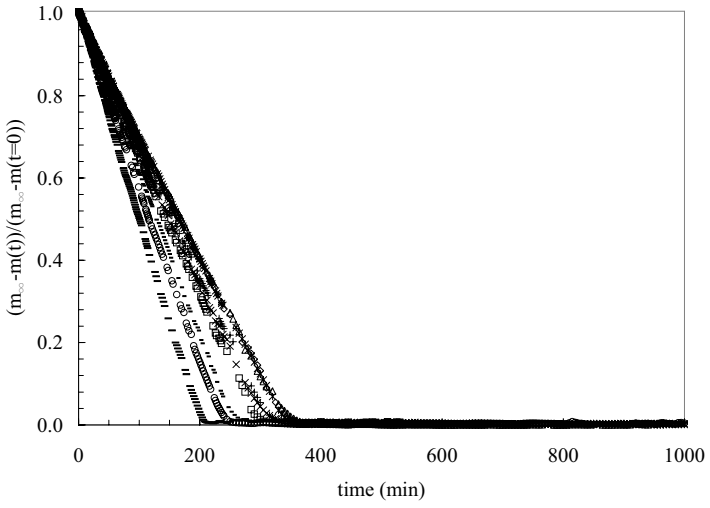

Figure 3.76. Desorption after equilibrium in liquid water for macroporous PMMA with different solvent and cross-linker contents: PMMA1/60E (X), PMMA1/70E, (∗), PMMA1/80E (○), PMMA5/60E (△), PMMA5/70E (□), PMMA5/80E (◇), PMMA10/60E (+), PMMA10/70E(-) and PMMA10/80E(—). Desorption at 25ºC and 19% of relative humidity

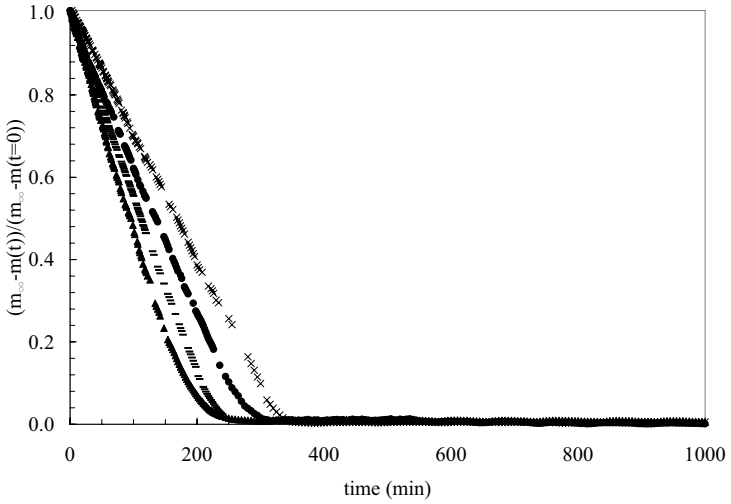

Figure 3.77. Desorption after equilibrium in liquid water for PMMA1/60E-*gr-pl*PHEA(12%) (△), PMMA1/70E-*gr-pl*PHEA(18.2%) (○), PMMA5/60E-*gr-pl*PHEA(15.2%) (-), PMMA5/70E-*gr-pl*PHEA(25.3%)(X). Desorption at 25ºC and 19% of relative humidity

Table 3.23. Evaporation constants of bulk PHEA and macroporous PMMA with different solvent, cross-linker and *pl*PHEA contents. Desorption after equilibrium in liquid water at 25ºC and 19% of relative humidity.

SAMPLE	**K x 10^5 (g/s)**
Bulk PHEA	1.44
PMMA1/60E	1.23
PMMA1/70E	1.44
PMMA1/80E	1.03
PMMA5/60E	1.23
PMMA5/70E	1.23
PMMA5/80E	1.44
PMMA10/60E	1.03
PMMA10/70E	1.23
PMMA10/80E	0.823
PMMA1/60E-*gr-pl*PHEA(12%)	1.03
PMMA1/70E-*gr-pl*PHEA(18.2%)	1.03
PMMA5/60E-*gr-pl*PHEA(15.2%)	1.44
PMMA5/70E-*gr-pl*PHEA(25.3%)	1.23

Contact angle of water on macroporous PMMA with and without *pl*PHEA were measured in air at room temperature (close to 25ºC) in order to study the water diffusion on the surfaces of these materials. The experiment consisted of placing a small drop of water on the macroporous material and taking pictures every several seconds to measure how the contact angle changes as a function of time.

First of all, this experiment of contact angle was performed on macroporous PMMA without *pl*PHEA coating. Thus, the contact angle as a function of time is shown in Figure 3.78 for PMMA1/70E. This contact angle value is the mean of the left and right contact angles.

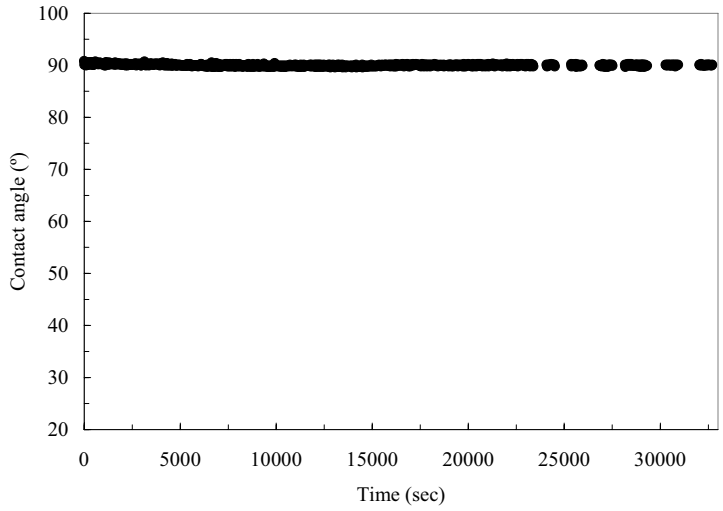

Figure 3.78. Contact angle of water on macroporous PMMA (sample PMMA1/70E) as a function of time. The contact angle values are the mean of the left and right contact angles.

The contact angle of water hardly changes on macroporous PMMA without hydrophilic coating because the drop does not go into this hydrophobic material, even though it is very porous. However, when the same experiment is performed on the same macroporous PMMA sample but with *pl*PHEA coating, the contact angle of water starts with a much lower value and it decreases dramatically as a function of time because water diffuses into this material. Thus, water on PMMA1/70E-*gr*-*pl*PHEA(18.2%) starts with a contact angle of 15º lower than on PMMA1/70 and it gets very close to 0º in less than 50 seconds (see Figure 3.79).

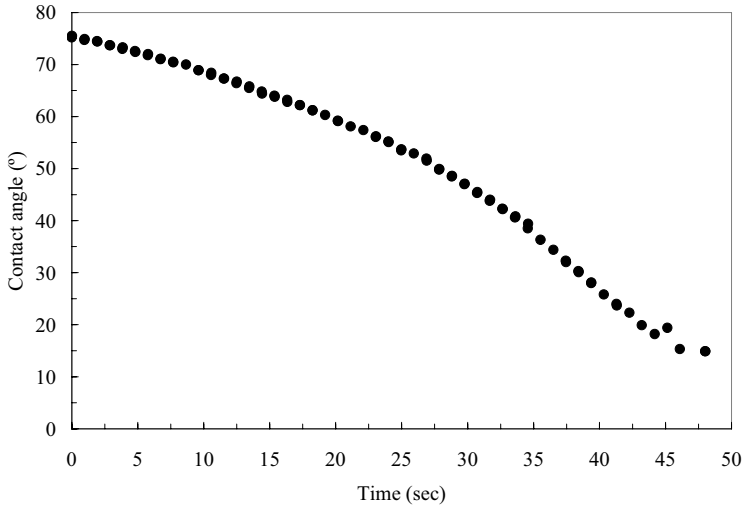

Figure 3.79. Contact angle of water on macroporous PMMA-*gr-pl*PHEA (sample PMMA1/70E-*gr-pl*PHEA(18.2%)) as a function of time. The contact angle values are the mean of the left and right contact angles.

3.3.3. Immersion in liquid water.

Equilibrium water uptakes (*w*) were determined at 25±0.5ºC by immersion in liquid water during two days (to constant weight) after extracting the air in the pores of the samples with a vacuum pump to ensure complete filling of the pores. The equilibrium water uptake of bulk PHEA was also determined by immersion in water during two days (to constant weight). These values are shown in Table 3.24 together with the porosities of the samples in the dry state (P_{d1} and P_{d2}).

SAMPLE	*w*	P_{d1}	P_{d2}
PMMA1/60E	1.76	69	63
PMMA1/70E	3.45	70	70
PMMA1/80E	3.11	80	75
PMMA5/60E	1.86	65	60
PMMA5/70E	2.56	76	68
PMMA5/80E	4.80	80	81
PMMA10/60E	2.40	70	72
PMMA10/70E	2.36	77	72
PMMA10/80E	4.57	81	83
PMMA1/60E-*gr-pl*PHEA(12%)	1.90	58	-
PMMA1/70E-*gr-pl*PHEA(18.2%)	3.53	61	-
PMMA5/60E-*gr-pl*PHEA(15.2%)	2.15	67	-
PMMA5/70E-*gr-pl*PHEA(25.3%)	3.12	75	-
Bulk PHEA	2.5	-	-

Table 3.24. Equilibrium water uptakes (*w*) determined by immersion in water after extracting the air in the pores with a vacuum pump at 25±0.5ºC.

In general, the equilibrium water uptakes of macroporous PMMA logically increase with increasing porosity. There are some exceptions because the structures of the macroporous PMMA samples are not homogeneous.

Equilibrium water uptakes of PMMA-*gr-pl*PHEA polymerised with 5 wt.% of EGDMA were expected to be similar to those of macroporous PMMA polymerised with the same cross-linking density because all these samples have

similar porosities. On the other hand, equilibrium water uptakes of PMMA-*gr*-*pl*PHEA polymerised with 1 wt.% of EGDMA were expected to be lower than those of macroporous PMMA polymerised with the same cross-linking density because these composite materials are less porous. However, contrary to what expected, the hydrophilic coating increases the equilibrium water uptakes of all macroporous PMMA samples. These increases can be seen more clearly in the bar graph of Figure 3.80.

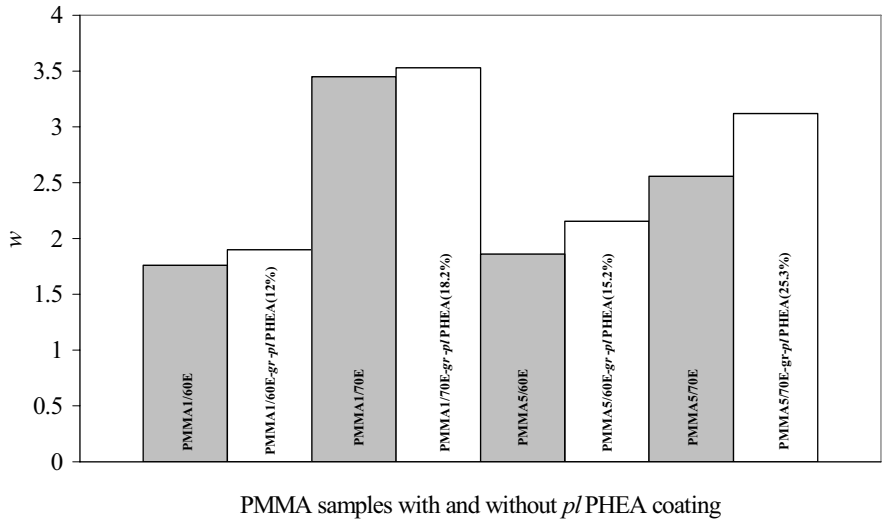

Figure 3.80. Effect of the hydrophilic coating. Equilibrium water uptakes of macroporous PMMA with different porosities, cross-linking densities and *pl*PHEA contents at 25±0.5ºC.

An explanation of this phenomenon could be that the swelling of the *pl*PHEA coating deforms the porous structure creating new pores and thus increasing porosity. The increase of the water uptakes is higher in PMMA-*gr*-*pl*PHEA polymerised with 5 wt.% than in those polymerised with 1 wt.% of EGDMA probably because the swollen *pl*PHEA deforms more the porous structure when is more homogeneously interpenetrated. Besides, before the swelling in water, the samples polymerised with 1 wt.% of EGDMA have lower porosities than those without *pl*PHEA.

Another explanation of this increase of the water uptakes could be that the *pl*PHEA coating improves the water transport inside the pores of the samples. It was seen in section 3.1.1 that the porosity determination by swelling in water could give lower values than those determined from the apparent specific volumes because there were pores in macroporous PMMA where water was not able to penetrate. This phenomenon of water not being able to penetrate

in some of the pores of macroporous PMMA was shown in Figure 3.69 for water sorption from the gas phase. However, when macroporous PMMA is coated with *pl*PHEA, water is then able to penetrate in all the pores increasing the water uptake.

An estimation of the water sorption of the plasma-polymerised PHEA can be obtained subtracting the amount of water absorbed by macroporous PMMA (m_w^{PMMA}) to that absorbed by macroporous PMMA coated with *pl*PHEA ($m_w^{composite}$). However, this is only an estimation because the porosity of the samples decreases or not depending on the cross-linking density as it was seen in Table 3.24. Thus, the water uptake of *pl*PHEA (*w'*) can be determined as

$$w' = \frac{m_{water}}{m_{plPHEA}} = \frac{m_w^{composite} - m_w^{PMMA}}{X_{plPHEA} \cdot (m_{PMMA} + m_{plPHEA})} \qquad (3.14)$$

where m_{PMMA} and m_{plPHEA} are the mass of the dry pure polymers and X_{plPHEA} is the mass fraction of *pl*PHEA in the composite material. Thus, with the water uptakes of macroporous PMMA (w^{PMMA}) and the composite material ($w^{composite}$) shown in Table 3.24,

$$w' = \frac{(m_{PMMA} + m_{plPHEA}) \cdot w^{composite} - m_{PMMA} \cdot w^{PMMA}}{X_{plPHEA} \cdot (m_{PMMA} + m_{plPHEA})} \qquad (3.15)$$

Therefore,

$$w' = \frac{w^{composite} - (1 - X_{plPHEA}) \cdot w^{PMMA}}{X_{plPHEA}} \qquad (3.16)$$

Thus, the equilibrium water uptakes of plasma-polymerised PHEA grafted onto macroporous PMMA can be determined with this equation (3.16). Figure 3.81 shows the equilibrium water uptakes of *pl*PHEA as a function of the mass fraction of *pl*PHEA in the composite material. The water uptake of bulk PHEA (straight line) is also shown in this figure for comparison.

All the equilibrium water uptakes of *pl*PHEA are higher than that of bulk PHEA. The equilibrium water uptake of the *pl*PHEA grafted onto PMMA1/60E-*gr*-*pl*PHEA(12%) must be very close to that of bulk PHEA because most of the *pl*PHEA is on the surface of this sample and there is not a strong modification of the porous structure after the equilibrium in liquid water. This is the closest situation to the water uptake of pure *pl*PHEA. However, the

water uptake of the *pl*PHEA grafted onto PMMA5/70E-*gr*-*pl*PHEA(25.3%) is much higher than that of bulk PHEA because there is a strong modification of the initial porous structure after the equilibrium in liquid water.

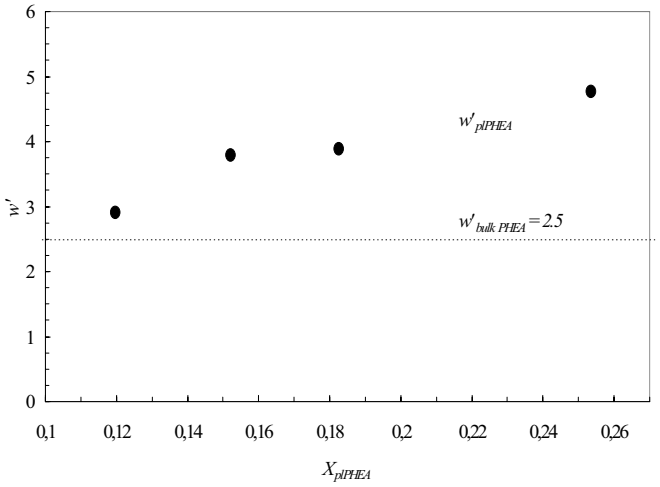

Figure 3.81. Equilibrium water uptakes of *pl*PHEA grafted onto macroporous PMMA (●), determined with equation (3.16), after immersion in liquid water during 2 days (to constant weight) at 25±0.5ºC as a function of the mass fraction of *pl*PHEA in the composite material. For comparison, the dotted line shows the equilibrium water uptake of bulk PHEA after immersion in liquid water during 2 days (to constant weight) at 25±0.5ºC (Table 3.24).

The more amount of *pl*PHEA grafted onto macroporous PMMA, the better water transports to the pores, which could not be filled in the macroporous network without hydrophilic coating. This argument could explain why the equilibrium water uptake of *pl*PHEA clearly increases with increasing the amount of *pl*PHEA.

3.3.4. Thermal transitions of water in the *pl*PHEA coating.

Thermal transitions of water in the *pl*PHEA coating and bulk PHEA are explained in a simple thermodynamic framework based on the transition diagram. Macroporous PMMA with 28.7 wt.% of *pl*PHEA was chosen for this kind of measurements because an important amount of *pl*PHEA is necessary to be detectable by DSC as seen in section 3.2.2. Bulk PHEA was also studied for comparison with *pl*PHEA.

The DSC thermograms of these two samples (bulk PHEA and PMMA-*gr*-*pl*PHEA(28.7%)) in the dry state were shown in Figures 3.35 and 3.36 respectively. From these thermograms, the glass transition temperatures of dry *pl*PHEA and bulk PHEA (8.3ºC and 13.8ºC respectively) were determined (see Table 3.11). These glass transition temperatures decrease very sharply when these hydrogels absorb a little amount of water.

These two hydrophilic polymers were equilibrated in liquid water to constant weight for two days. After that, they were dried at room temperature in order to perform several DSC measurements with a broad range of water mass fractions (ω'= 0.05, 0.10, 0.15, 0.20, 0.30, 0.40, 0.50 and 0.72).

The samples were subjected to a cooling scan from room temperature down to -120°C at 10°C/min, followed by a heating scan from that temperature up to 35°C at 10°C/min.

The DSC thermograms on heating and on cooling of bulk PHEA and the *pl*PHEA present in the PMMA-*gr*-*pl*PHEA(28.7%) composite material with different water mass fractions are shown in Figures 3.82 to 3.86.

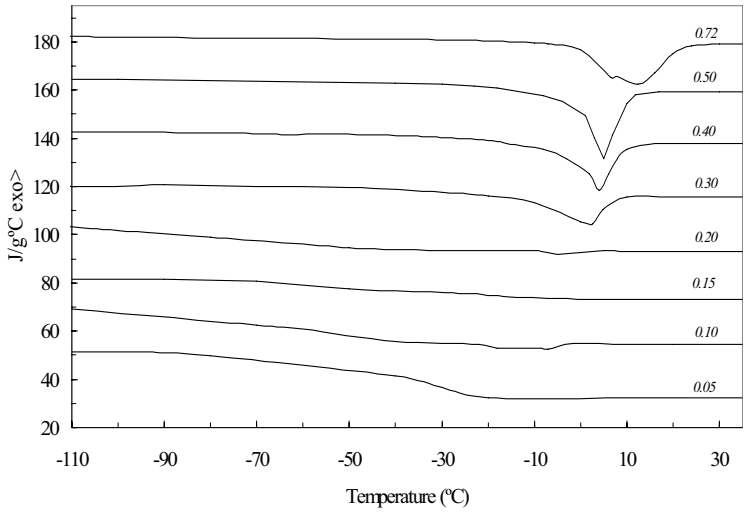

Figure 3.82. DSC thermograms at a heating rate of 10ºC/min of bulk PHEA with different water mass fractions (ω'=0.05, 0.10, 0.15, 0.20, 0.30, 0.40, 0.50 and 0.72). Exothermic heat flow calculated per gram of water.

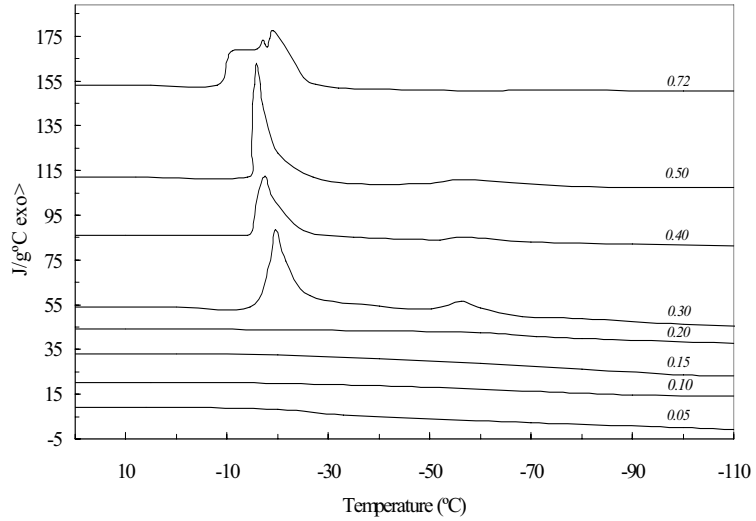

Figure 3.83. DSC thermograms at a cooling rate of 10ºC/min of bulk PHEA with different water mass fractions (ω'=0.05, 0.10, 0.15, 0.20, 0.30, 0.40, 0.50 and 0.72). Exothermic heat flow calculated per gram of water.

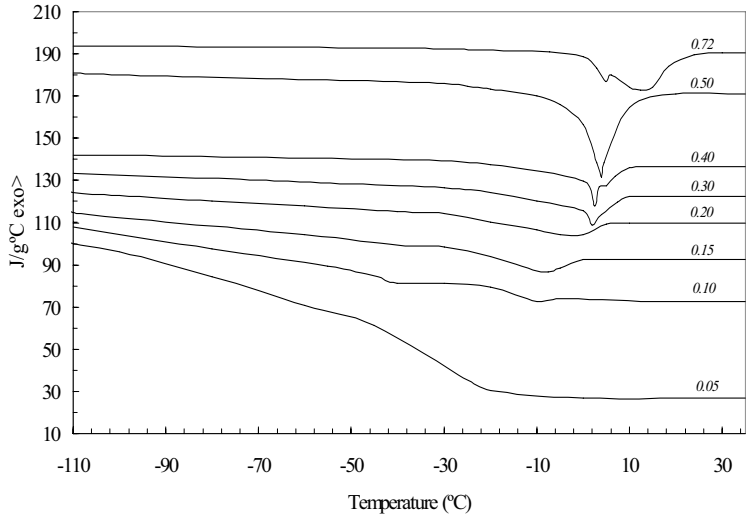

Figure 3.84. DSC thermograms at a heating rate of 10ºC/min of the *pl*PHEA present in the macroporous structure of PMMA (sample PMMA1/70E-*gr*-*pl*PHEA(28.7%)) with different water mass fractions (ω'=0.05, 0.10, 0.15, 0.20, 0.30, 0.40, 0.50 and 0.72). Exothermic heat flow calculated per gram of water.

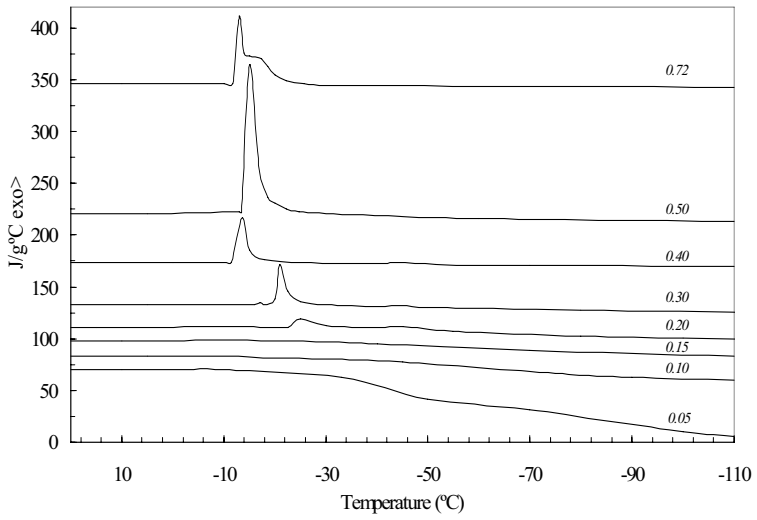

Figure 3.85. DSC thermograms at a cooling rate of 10ºC/min of the *pl*PHEA present in the macroporous structure of PMMA (sample PMMA1/70E-*gr*-*pl*PHEA(28.7%)) with different water mass fractions (ω'=0.05, 0.10, 0.15, 0.20, 0.30, 0.40, 0.50 and 0.72). Exothermic heat flow calculated per gram of water.

As explained in section 1.12, the intersection of T_g with T_m and T_c defines the compositions ω'^{**} and ω'^{*} respectively. The T_g, T_m and T_c found for bulk PHEA and *pl*PHEA are represented in Figure 3.91. These two values divide the transition diagram in three concentration domains: $\omega'<\omega'^{**}$, $\omega'^{**}<\omega'<\omega'^{*}$ and $\omega'>\omega'^{*}$. For solvent concentrations $\omega' < \omega'^{**}$, only the glass transition of the swollen network occurs on cooling and heating without any sign of water crystallisation. All water remains non-crystallisable for low water mass fractions. For solvent concentrations $\omega'^{**} < \omega' < \omega'^{*}$, only the glass transition occurs on cooling without any sign of crystallisation. However, crystallisation and subsequent melting of water must be expected upon heating. The glass transition of the swollen network is not clearly visible in this concentration domain because of the other thermal transitions. For solvent concentrations $\omega' > \omega'^{*}$, after a certain supercooling, the solvent crystallises on cooling. Crystallisation is arrested by the glass transition of the system. On the subsequent heating scan, the solvent will crystallise while the composition and glass transition temperature of the gel changes continuously. From $T_g(\omega'^{**})$ on, the solvent will melt and diffuse following the T_m curve until the initial composition is reached.

Three DSC thermograms were selected to show more clearly the three water concentration domains in bulk PHEA (see Figure 3.86). The bulk PHEA sample with ω'=0.05 is representative of the thermograms in which only the glass transition is observed both on cooling and heating (Figure 3.86 *(a)*). At intermediate water mass fractions (the thermograms of the sample with ω'=0.2 is shown in Figure 3.86 *(b)*) only the glass transition is observed on cooling. In the subsequent heating scan, contrary to what expected, there is not a clear crystallisation peak. However, there is a clear melting of water, which must has crystallised before on heating because no sign of crystallisation appears on cooling as expected. Finally, for high water mass fractions (the sample with ω'=0.3 shown in Figure 3.86 *(c)*), water crystallises on cooling appearing two crystallisation peaks. The first sharp peak at higher temperatures corresponds to free water and the second one at lower temperatures due to the crystallisation of water homogeneously mixed with the hydrogel. For these water concentrations, the glass transition is no longer visible due to the other thermal transitions. However, a change in the baseline from the start to the end can be identified.

Three DSC thermograms were also selected to show the three water concentration domains in the *pl*PHEA present in sample PMMA1/70E-*gr*-*pl*PHEA(28.7%)) (see Figure 3.87). In this case, at intermediate water mass fractions (Figure 3.87 (*b*) shows the thermograms for ω'=0.15), a crystallisation exotherm is clearly seen on heating after the cooling scan in which only the glass transition is shown.

All water remains non-crystallisable as well for *pl*PHEA in the first concentration domain ($\omega' < \omega'^{**}$). Thus, only the glass transition of the swollen network appears both on cooling and heating. For water mass fractions $\omega'^{**} < \omega' < \omega'^{*}$, no crystallisation is seen on cooling. Finally, for water mass fractions higher than ω'^{*}, water crystallises on cooling showing two crystallisation peaks as bulk PHEA. The peak at the highest temperature, which appears around the crystallisation temperature of pure water, is associated with free water present in the swollen system. The peak appearing at lower temperature is related to water homogeneously mixed with the hydrogel. This second peak is much smaller than the first one. This means that at room temperature, before the start of cooling, phase separation takes place between pure water and swollen polymer domains. Water domains crystallise at a temperature close to that of pure water whereas the crystallisation from the homogeneous mixture of polymer segments and water molecules take place at a lower temperature as explained in section 1.12. The amount of bulk water at high water mass fractions can be much higher than that of water mixed with polymer segments. At these high water mass fractions, the glass transition is no longer visible on cooling or heating but a change in the baseline from the start to the end can be identified (see Figure 3.87).

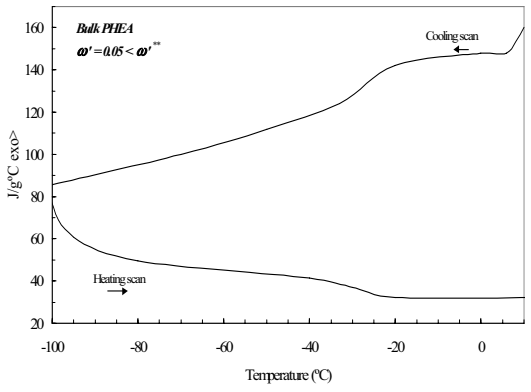

(a)

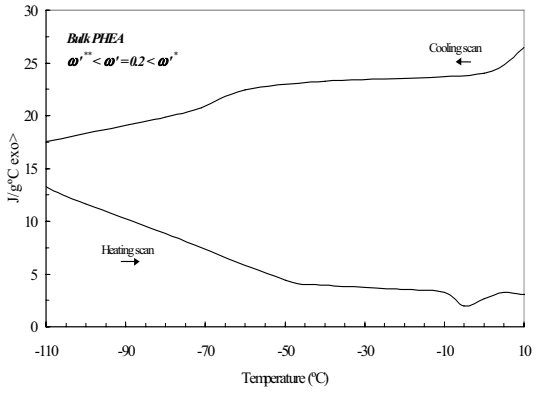

(b)

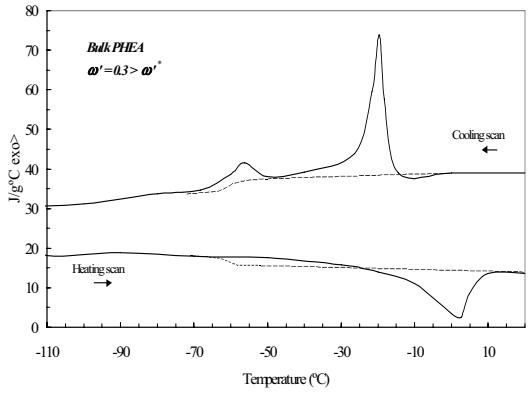

(c)

Figure 3.86. Three qualitatively kinds of thermograms, obtained after cooling and heating at 10ºC/min for three different concentration ranges of water in bulk PHEA : *(a)* $\omega'=0.05<\omega'^{**}$, *(b)* $\omega'^{**}<\omega'=0.2<\omega'^{*}$ and *(c)* $\omega'=0.3>\omega'^{*}$. Baseline approximately drawn with the T_g predicted by the Couchman-Karasz equation (---). Exothermic heat flow calculated per gram of water.

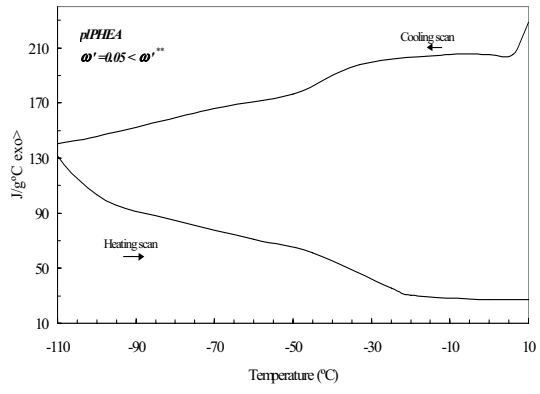

(a)

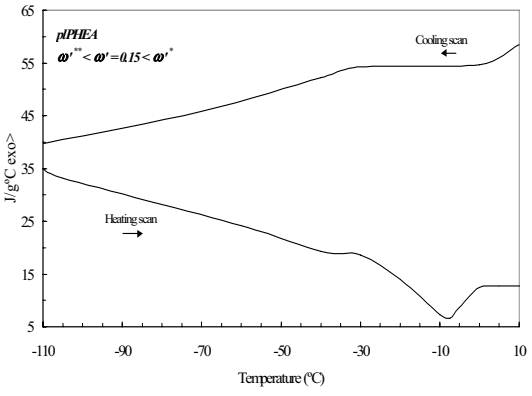

(b)

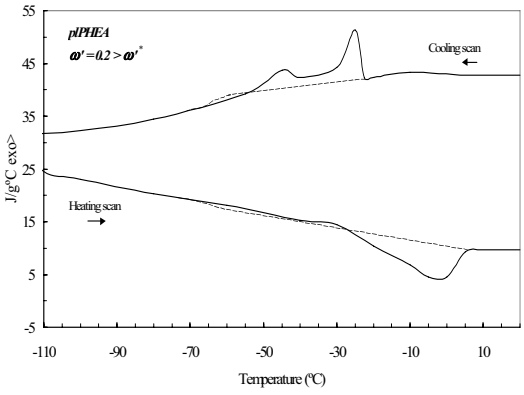

(c)

Figure 3.87. Three qualitatively kinds of thermograms at 10ºC/min for three different concentration ranges of water (*(a)* $\omega'=0.05<\omega'^{**}$, *(b)* $\omega'^{**}<\omega'=0.15<\omega'^{*}$ and *(c)* $\omega'=0.2>\omega'^{*}$) in *pl*PHEA present in sample PMMA1/70E-*gr*-*pl*PHEA(28.7%). Baseline approximately drawn with the T_g predicted by the Couchman-Karasz equation (---). Exothermic heat flow calculated per gram of water.

The thermal transitions in the two kinds of PHEA are quite similar but with several differences. Bulk PHEA with water concentrations up to 0.2 shows only, on cooling and heating a single transition, which corresponds to the glass transition of the hydrogel. Nevertheless, this range of water concentration decreases down to 0.15 for *pl*PHEA. Water crystallises on cooling from $\omega' = 0.3$ for bulk PHEA and from $\omega' = 0.2$ for *pl*PHEA.

The temperature-composition diagram for each kind of PHEA can be drawn from these series of DSC thermograms representing the crystallisation, melting and glass transition temperatures as a function of water mass fraction (see Figure 3.88). The temperature of the inflection point of the heating thermogram was taken to determine the glass transition temperature (T_g). The temperature of the maximum of the melting peak appearing on heating was taken to determine the melting temperature of water (T_m). The temperature of the maximum of the crystallisation peak, which appears on cooling at lower temperature and is related to water homogeneously mixed with the hydrogel, was taken to obtain the crystallisation temperature of water (T_c) in the temperature-composition diagram. These temperature-composition diagrams show that there is less undercooling of water crystallisation in the *pl*PHEA present in the PMMA-*gr*-*pl*PHEA(28.7%) composite material than in bulk PHEA.

This representation qualitatively corresponds to our discussion held in 1.12 where there were three different intervals in the x-axis of the transition diagram defined by the intersection of the T_g and T_m curves (ω'^{**}) and the intersection of the T_g and T_c curves (ω'^{*}). A mean value of ω'^{**} and ω'^{*} can be determined analysing the cooling and heating DSC thermograms with different water mass fractions of the transition diagrams of bulk PHEA and *pl*PHEA. Thus, for bulk PHEA: $\omega'^{**} \approx 0.17$ (mean value of the water mass fractions ω'=0.15 and 0.20 of the measured DSC thermograms) and $\omega'^{*} \approx 0.25$ (mean value of the water mass fractions ω'=0.20 and 0.30 of the measured DSC thermograms). Therefore, water remains always homogeneously mixed with the hydrogel phase for water mass fractions lower than 0.17, water does not crystallise on cooling but does so on heating for compositions between 0.17 and 0.25 and first order transitions are present both on cooling and on heating for water mass fractions higher than 0.25. These values are very close to those obtained in reference [109] for bulk PHEA polymerised with 1 wt.% of ethylene glycol dimethacrylate (EGDMA) ($\omega'^{**} \approx 0.20$ and $\omega'^{*} \approx 0.30$).

In the same way, analysing the cooling and heating DSC thermograms of *pl*PHEA with different water mass fractions: $\omega'^{**} \approx 0.12$ (mean value of the water mass fractions ω'=0.10 and 0.15 of the measured DSC

thermograms) and $\omega'^{*} \approx 0.17$ (mean value of the water mass fractions ω'=0.15 and 0.20 of the measured DSC thermograms).

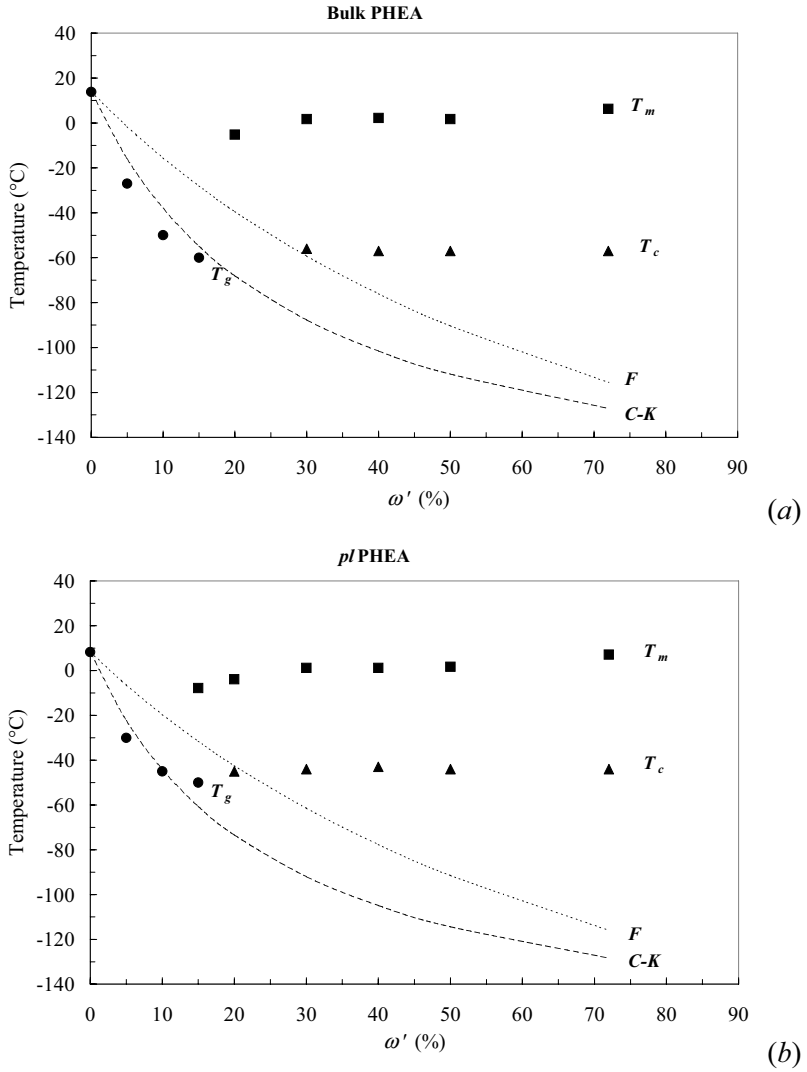

Figure 3.88. Experimental temperature-composition diagram of swollen bulk PHEA (*a*) and swollen *pl*PHEA present in macroporous PMMA (sample PMMA1/70E-*gr*-*pl*PHEA(28.7%)) (*b*): glass transition temperature on heating (T_g) (●), melting temperature of water on heating (T_m) (■), crystallisation temperature on cooling of water homogeneously mixed with the hydrogel (T_c) (▲), glass transition temperature predicted by the Fox equation (*F*) (---) and the Couchman-Karasz equation (*C-K*) (————).

Table 3.25. Critical water mass fractions of bulk PHEA and *pl*PHEA present in sample PMMA1/70E-*gr*-*pl*PHEA(28.7%).

Sample	ω'^{**}	ω'^{*}
Bulk PHEA	0.17	0.25
*pl*PHEA	0.12	0.17

The values ω'^{**} and ω'^{*} are often obtained from a direct inspection of the transition diagram. To determine ω'^{**} and ω'^{*}, the experimental T_m and T_c curves must be extrapolated to lower concentrations to obtain the intersection with the T_g curve respectively. However, it must be taken into account that at these low concentrations, the T_m and T_c curves are almost vertical [130,131]. Unfortunately, this zone is not experimentally accessible in our systems and it is not possible to determine these values with this method.

The glass transition temperature curve predicted by the Fox and Couchman-Karasz equations were determined with T_{gw} =134 K and $\Delta c_{pw}(T_g)$ = 1.94 *J/gK* taken from reference [133]. These values of bulk PHEA (T_{g0} = 287 K and Δc_{p0} = 0.42 *J/gK*) and those of the *pl*PHEA present in the PMMA-*gr*-*pl*PHEA(28.7%) sample (T_{g0} = 281.4 K and Δc_{p0} = 0.39 *J/gK*) were determined from the DSC thermograms shown in Figures 3.35 and 3.36 respectively (Δc_{p0} = 0.112·100/28.7=0.39 *J/gK*). The prediction of Fox equation is far from the experimental results in both types of PHEA but the Couchman-Karasz equation fits very well the experimental results and supports the hypothesis of an homogeneous mixture water/polymer as the basic physical picture of a hydrogel.

3.3.5. Kinetics of crystallisation for high and low water contents.

For water mass fractions higher than ω'^{*}, water crystallises on cooling and an exothermic peak followed by an endothermic peak shows up on heating, indicating the occurrence of first-order phase transitions of water (crystallisation and melting). The glass transition of the hydrogel is no longer visible in these cooling and heating thermograms. However, a change of baseline from the start to the end of the scan is clearly noticeable. Bulk PHEA and PMMA1/70E-*gr-pl*PHEA(28.7 wt.%) were swollen in liquid water to obtain a water composition belonging to this domain $\omega' > \omega'^{*}$ (ω'=0.3).

These samples were subjected to two different thermal treatments, which will be called hereafter experiences A and B. The first one consisted of quenching to a determined temperature T_{hold} (-10, -30, -40, -50, -65 and -70ºC) and holding at this selected T_{hold} for 15 minutes. After that, the samples were quenched to -120ºC and subsequently heated from that temperature up to 20ºC at 10 *K/min*. On the other hand, the experience B consisted of quenching to -120ºC, heating from that temperature up to a determined T_{hold} (-10, -30, -40, -50, -65 and -70ºC) at 10 *K/min* and holding at this selected T_{hold} for 15 minutes. After that, the samples were quenched from T_{hold} to -120ºC. Finally, a heating scan from -120ºC up to 20ºC at 10 *K/min* was performed.

These DSC experiences study the influence of performing or not an extensive nucleation and growth in bulk PHEA and *pl*PHEA with high water contents. In order to understand better these experiments, Figure 3.89 shows these thermal treatments A and B taking in account T_m, T_c and T_g. The main difference between the two experiences is the total time that the samples stay at a temperature lower than T_c in the whole experience. The more time the samples are at temperatures lower than T_c, the more nucleation and growth are expected to occur.

The thermal paths of experience A and B for T_{hold} = -10ºC and -70ºC are drawn on the transition diagram of bulk PHEA (see Figure 3.90). This figure shows that T_{hold} can be higher or lower than the crystallisation temperature depending on the selected temperature. When T_{hold} = -10ºC, the temperature of the sample is hold at a temperature higher than T_c and the last heating scan of experience A shows a strong crystallisation peak followed by a melting peak (see Figure 3.91) because only nucleation without crystal growth occurs in this experience. However, the same thermal treatment cooling down to -120ºC at 10 *K/min* instead of quenching did not show this strong crystallisation peak on heating because most water had crystallised before on cooling (see Figure 3.86 *(c))*. The sample spends much more time at a temperature lower

than T_c in experience B (see Figure 3.89) and only a melting peak appears on the last heating scan of experience B. Most water crystallises before due to the extensive nucleation and growth obtained with this thermal treatment.

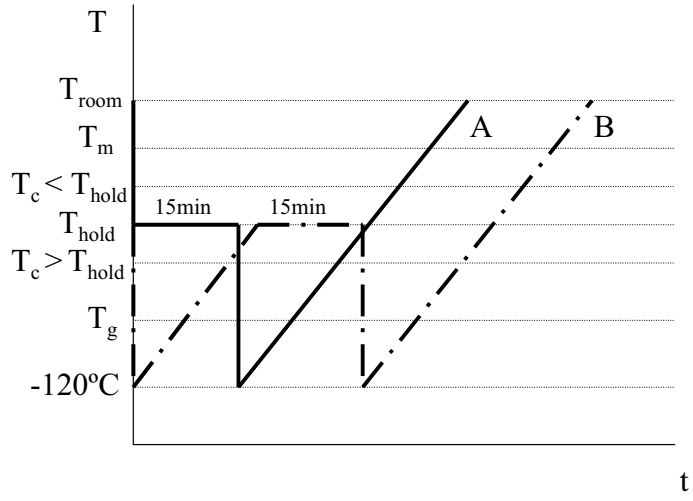

Figure 3.89. Thermal treatment followed in experiences A and B taking into account T_m, T_c and T_g.

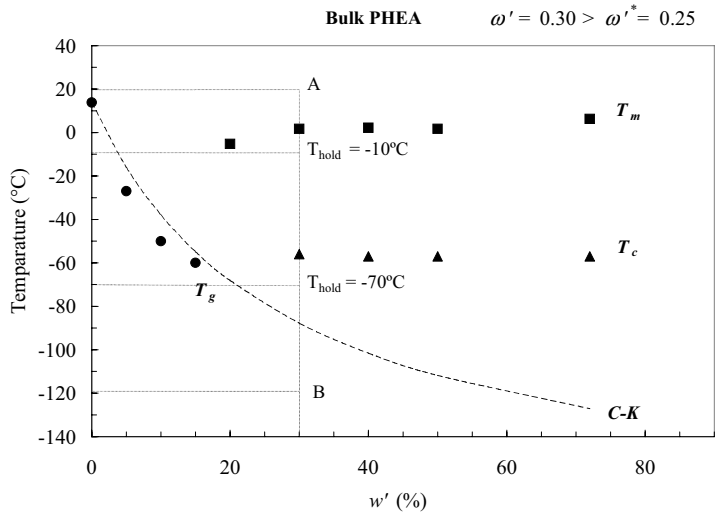

Figure 3.90. Experience A (thermal path AT_{hold}BA) and experience B (thermal path ABT_{hold}BA) for T_{hold} = -10ºC and -70ºC for bulk PHEA with high water mass fractions (ω' = 0.3).

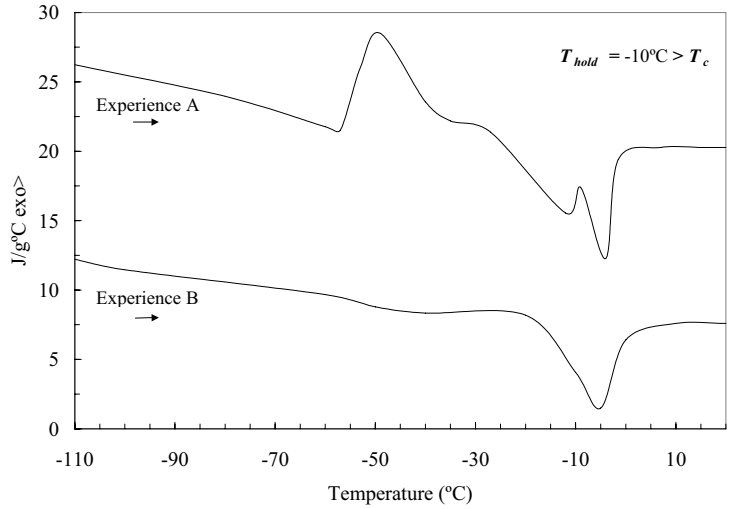

Figure 3.91. DSC heating scans of bulk PHEA with high water mass fractions (ω' = 0.3) following experience A and B with T_{hold} = -10ºC. Exothermic heat flow calculated per gram of water.

The same behaviour is observed when T_{hold} is also higher than T_c (T_{hold} = -30 and -50ºC).

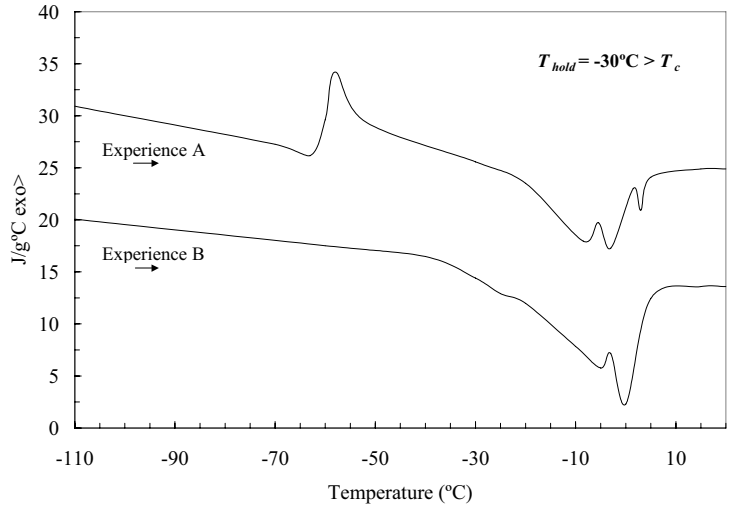

Figure 3.92. DSC heating scans of bulk PHEA with high water mass fractions (ω' = 0.3) following experience A and B with T_{hold} = -30ºC. Exothermic heat flow calculated per gram of water.

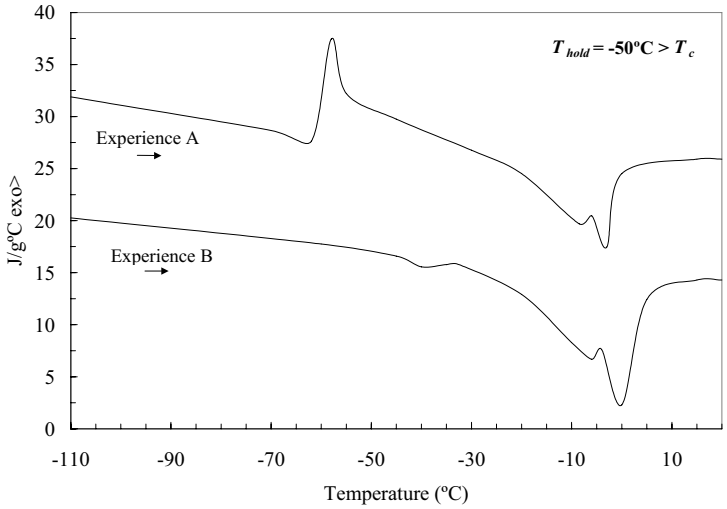

Figure 3.93. DSC heating scans of bulk PHEA with high water mass fractions (ω' = 0.3) following experience A and B with T_{hold} = -50ºC. Exothermic heat flow calculated per gram of water.

However, both heating scans start looking the same for T_{hold} = -60, although less crystallisation of water appears still in experience B (see Figure 3.94). Now, T_{hold} is lower than the crystallisation temperature (T_c) (see Figure 3.90).

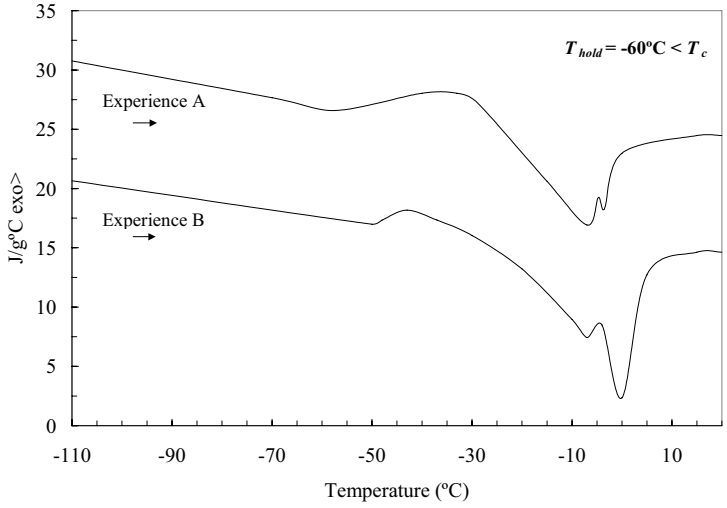

Figure 3.94. DSC heating scans of bulk PHEA with high water mass fractions (ω' = 0.3) following experience A and B with T_{hold} = -60ºC. Exothermic heat flow calculated per gram of water.

Finally, from T_{hold} = -65ºC on, both heating scans are exactly the same for experiences A and B (see Figure 3.95). The same amount of water crystallises on heating in both experiences A and B.

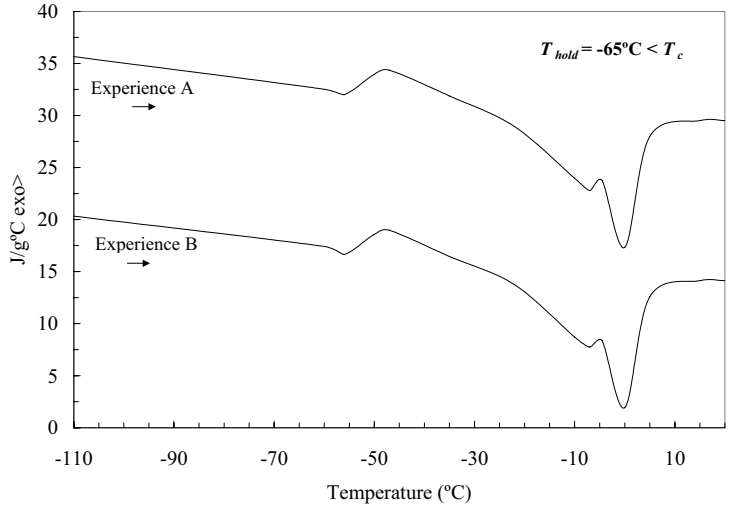

Figure 3.95. DSC heating scans of bulkPHEA with high water mass fractions (ω' = 0.3) following experience A and B with T_{hold} = -65ºC. Exothermic heat flow calculated per gram of water.

Nucleation always occurs at low temperatures independently of having crystallisation or not in the cooling scan. Experience B shows the crystallisation capacity at different temperatures once nucleation is produced. Holding during 15 minutes at temperatures between -10 and -50ºC clearly makes water to crystallise in bulk PHEA and practically there is not residual crystallisation on the subsequent heating scan. However, when T_{hold} is from -60 to -70ºC, crystallisation is slower and water does not crystallise completely holding at this temperature for 15 minutes. Water begins to crystallise on the following heating scan from T_{hold} showing clearly its existence. Experience A show the nucleation capacity at different temperatures. Water does not crystallise or only a small amount does during all the thermal steps before the last heating scan from -120ºC to 20ºC in spite of holding during 15 minutes at T_{hold}. The shape of the crystallisation peak appearing on the heating scan is related to the kinetics of crystallisation, which enormously depends on the number of nucleus of crystallisation. The more number of nucleus, the faster is the growth process of the water mass crystallised in bulk PHEA and this gives a higher initial slope of the exothermic peak. Thus, this slope significantly increases when T_{hold} decreases from -10 to -50ºC. However, from -50 to -70ºC,

this slope markedly decreases. This gives an idea of the form of the distribution graph of the nucleation velocity of water in the mixture with the polymer segments with a maximum around -50ºC. The probability of occurring also crystal growth during the isotherm step for 15 minutes could be analysed with the areas of the crystallisation peaks appearing on heating but it clearly seems to be very small.

Another explanation of these results can be carried out comparing the time spent by the samples at low temperatures in experiences A and B (see Figure 3.89). Thus, the samples always spend more time at low temperatures in experience B. The lower T_{hold}, the shorter difference of time spent by the samples at low temperatures in experiences A and B. When T_{hold} is -10ºC, the samples spend much more time at low temperatures in experience B. For this reason, the thermograms of these two thermal treatments are very different occurring extensive nucleation and crystal growth in experience B before the last heating scan.

The same thermal treatments were performed with sample PMMA1/70E-*gr*-*pl*PHEA(28.7 wt.%) with ω' = 0.3. The thermal paths followed in experiences A and B are drawn on the transition diagram of this sample (Figure 3.96).

The last heating scan of the experience A shows crystallisation on heating followed by a melting peak when T_{hold} = -10ºC for *pl*PHEA (see Figure 3.97). This crystallisation peak is much smaller than that found for bulk PHEA. No crystallisation peak appears on heating in experience B, only a melting peak.

A similar behaviour is observed when T_{hold} is still higher than the crystallisation temperature (T_{hold} = -30ºC). Experience A shows a slight crystallisation on heating followed by a strong melting peak for *pl*PHEA (see Figure 3.98).

The temperature-composition diagrams showed that there is less undercooling of water crystallisation in the *pl*PHEA than in bulk PHEA (Figures 3.96 and 3.90). For this reason, T_{hold} is lower than T_c when T_{hold} = -50ºC and exactly the same heating scan for experiences A and B are obtained (see Figure 3.99) as it occurred for T_{hold} = -65ºC in bulk PHEA. Thus, for T_{hold} = -60, -65 and -70ºC, exactly the same heating scans are obtained for experiences A and B.

All these experiments show a clear difference between the kinetics of water crystallisation for high water contents in bulk PHEA and *pl*PHEA. Experience A shows that water crystallises very fast in *pl*PHEA. An appreciable

crystallisation at the same time as nucleation occurs during the 15 minutes of the isothermal step. Although, a small amount of residual water crystallises on the last heating scan.

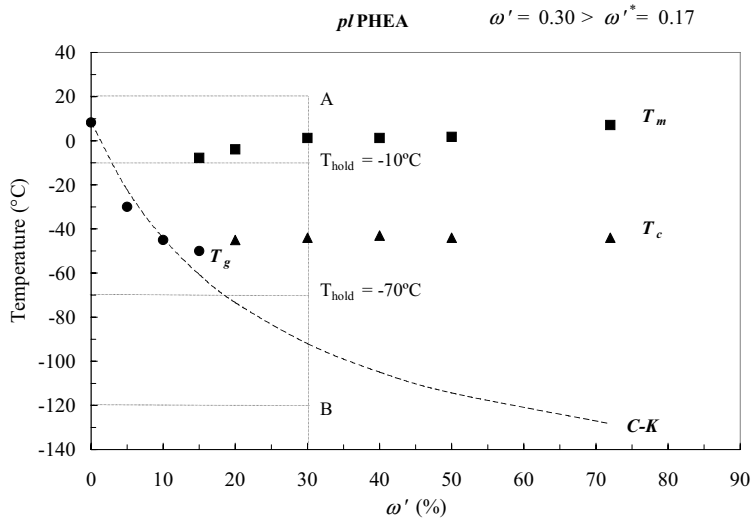

Figure 3.96. Experience A (thermal path AT_{hold}BA) and experience B (thermal path ABT_{hold}BA) for T_{hold} = -10ºC and -70ºC for *pl*PHEA present in sample PMMA1/70E-*gr*-*pl*PHEA(28.7 wt.%) for high water mass fractions (ω' = 0.3).

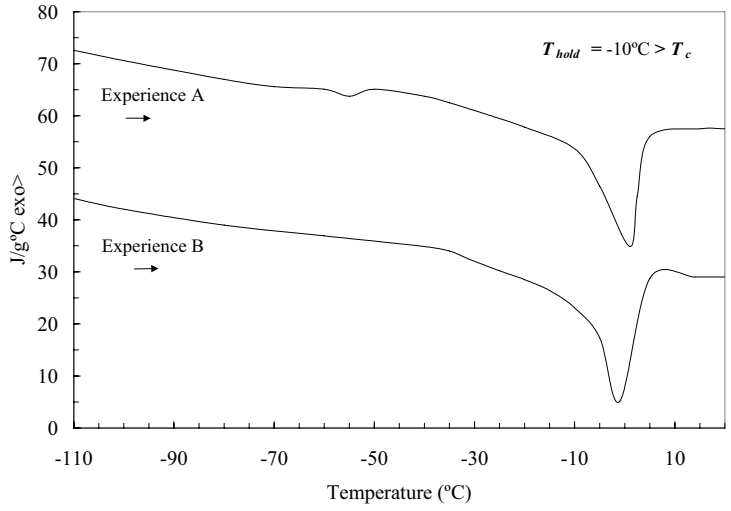

Figure 3.97. DSC heating scans of the *pl*PHEA present in sample PMMA1/70E-*gr*-*pl*PHEA(28.7 wt.%) with high water mass fractions (ω' = 0.3) following experience A and B with T_{hold} = -10ºC. Exothermic heat flow calculated per gram of water.

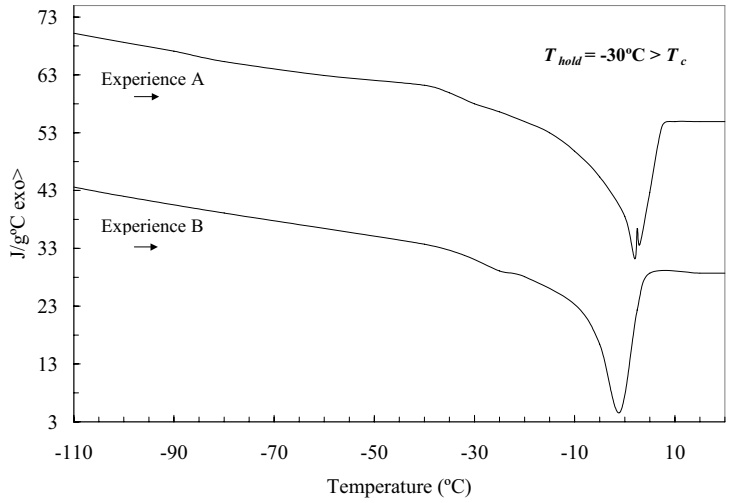

Figure 3.98. DSC heating scans of the *pl*PHEA present in sample PMMA1/70E-*gr*-*pl*PHEA(28.7 wt.%) with high water mass fractions (ω' = 0.3) following experience A and B with T_{hold} = -30ºC. Exothermic heat flow calculated per gram of water.

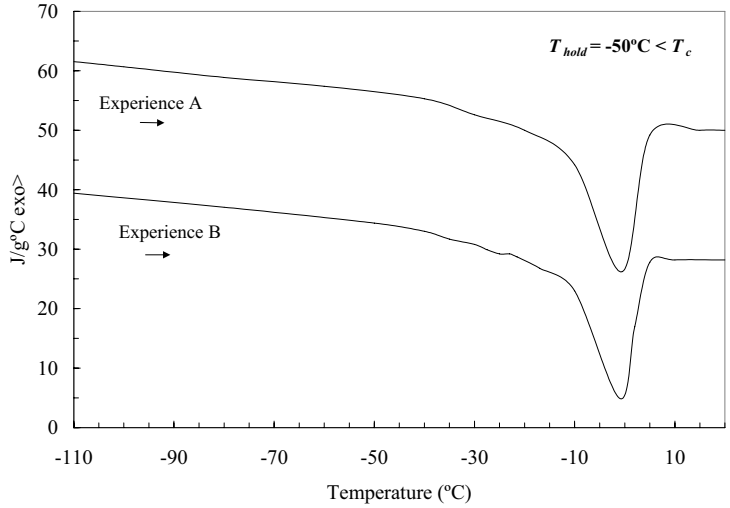

Figure 3.99. DSC heating scans of the *pl*PHEA present in PMMA1/70E-*gr*-*pl*PHEA(28.7 wt.%) with high water mass fractions (ω' = 0.3) following experience A and B with T_{hold} = -50ºC. Exothermic heat flow calculated per gram of water.

In order to study the kinetics of crystallisation for low water contents, bulk PHEA and PMMA1/70E-*gr*-*pl*PHEA(28.7%) were swollen in liquid water to obtain a water mass fraction ω'=0.10. This low water mass fraction belongs to the first domain ($\omega' < \omega'^{**}$) and only the glass transition of the swollen hydrogel without any sign of water crystallisation is seen on cooling. Only the glass transition of the swollen network is also seen on heating in the same interval, shifting towards lower temperatures as water mass fraction increases, without any sign of first-order phase transitions of water. Thus, all water remains non-crystallisable for this water mass fraction. Nevertheless, in the experiments now under consideration, it was demonstrated that holding at -30ºC during a certain amount of time, crystallisation of water becomes possible. In addition, the longer isothermal step at T_{hold}=-30ºC, the more water crystallises. The total amount of water that crystallises was calculated through the melting enthalpies of the heating scans.

These DSC measurements consisted of holding at -30ºC during several times (1, 2, 16.7, 33.3 and 61.7 hours). After that, two consecutive heating scans were performed from -50 to 10ºC at 10 *K/min* (see Figure 3.100).

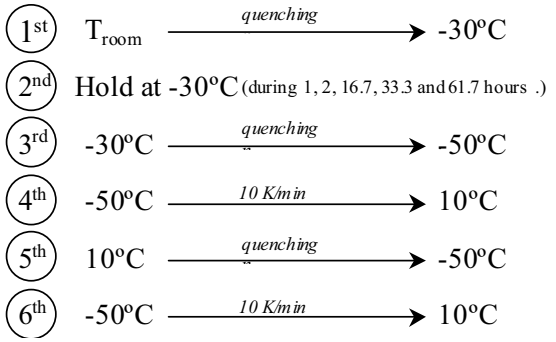

Figure 3.100. DSC method applied to bulk PHEA and *pl*PHEA present in sample PMMA1/70E-*gr*-*pl*PHEA(28.7%) to study the kinetics of crystallisation for low water mass fractions (ω'=0.10).

This thermal treatment is drawn on the transition diagram of bulk PHEA in Figure 3.101.

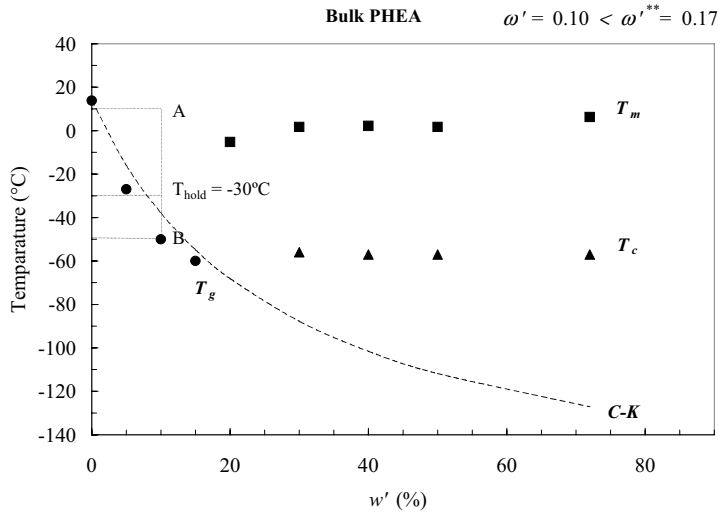

Figure 3.101. DSC experimental method (thermal path AT_{hold}BABA) drawn on the transition diagram of bulk PHEA for low water mass fractions (ω' = 0.10).

The first heating scans from -50 to 10ºC after holding at -30ºC during several times are shown in Figure 3.102 for bulk PHEA. The melting area of water (water which had crystallised before) increases with increasing holding time.

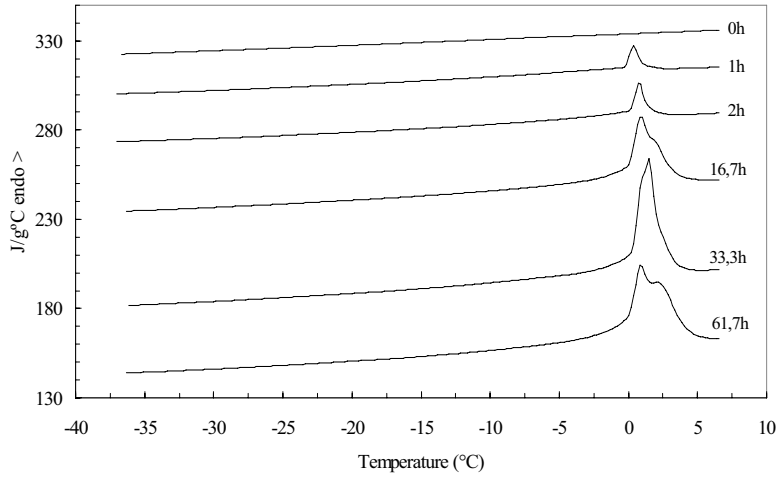

Figure 3.102. First DSC heating scans from -50 to 10ºC after holding at -30ºC during several times (0, 1, 2, 16.7, 33.3 and 61.7 hours) of bulk PHEA with low water mass fractions (ω' = 0.10). Exothermic heat flow calculated per gram of water.

For these low water mass fractions (ω' = 0.10) lower than the critical concentration (ω'^{**} = 0.17), water cannot crystallise without the isothermal step at -30ºC. However, this experiment demonstrates that when the temperature is cooled down to -30ºC and the sample is kept at this temperature for some time, crystallisation of water becomes possible even though having a water mass fraction lower than the critical one (ω'^{**}). In addition, the more time holding at -30ºC, the more amount of water crystallises. Figure 3.104 shows that an equilibrium value of crystallised water must be achieved after a certain amount of time. Crystal nucleus are formed in the isothermal step at this low temperature and the longer is this step, the more nucleation and subsequent growth are obtained until a maximum equilibrium amount of water.

All the melting peaks of water in bulk PHEA appear around 0ºC (see Figure 3.102). This unexpected result can be clearly understood because when the temperature is cooled down to -30ºC and kept at this temperature, water does not crystallise and is segregated from the water-PHEA mixture because the solubility of water in the PHEA hydrogel is lower at this temperature. This water melts around 0ºC as free water on the subsequent heating scan after the isothermal step.

The second heating scans from -50 to 10ºC show smaller peaks of melting but they follow the same tendency. Less water crystallises because the second heating scan is performed right after the first one and it is only seen the free water that has not had enough time to mix homogeneously with the polymer matrix. If the sample is kept at 10ºC for a long time after the first heating scan, water has time to mix homogeneously with the hydrogel and no phase transition appears on the last heating scan, only the glass transition.

The second heating scans from -50 to 10ºC performed right after the first ones are shown in Figure 3.103 for bulk PHEA. In the same way, the melting area of water (water which had crystallised before) increases with increasing the holding time.

Figure 3.104 shows the melting enthalpy and the amount of crystallised water as a function of the holding time at -30ºC after the first and the second heating scan from -50 to 10ºC for bulk PHEA with low water mass fractions (ω' = 0.10). The amount of crystallised water is around two times lower after the second heating.

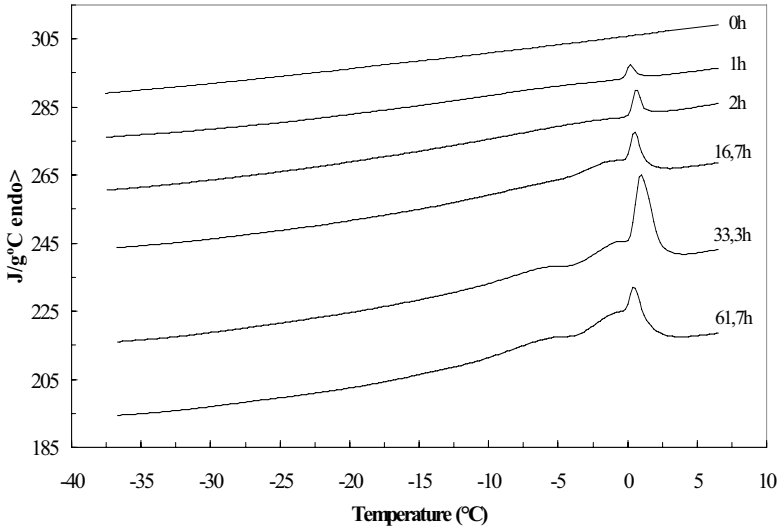

Figure 3.103. Second DSC heating scans from -50 to 10ºC after the first ones and after holding at -30ºC during several times (0, 1, 2, 16.7, 33.3 and 61.7 hours) for bulk PHEA with low water mass fractions (ω' = 0.10). Exothermic heat flow calculated per gram of water.

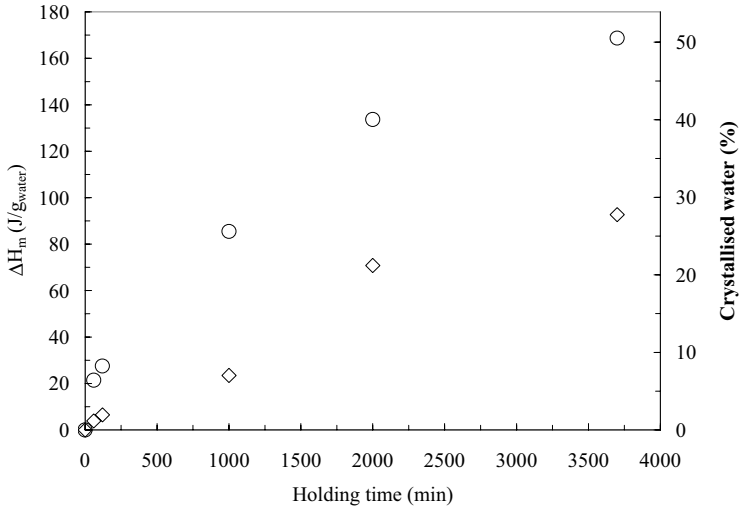

Figure 3.104. Melting enthalpy (ΔH_m) and wt.% of crystallised water as a function of the holding time at -30ºC after the first (○) and the second (◇) heating scans from -50 to 10ºC for bulk PHEA with low water mass fractions (ω' = 0.10).

The same tendency of water crystallisation was observed in the *pl*PHEA present in the PMMA-*gr*-*pl*PHEA(28.7%) composite material. Nevertheless, much less water crystallises in this kind of PHEA and holding for 2 hours at -30ºC is not enough time to crystallise water. The thermal treatment shown in Figure 3.100 can be seen drawn on the transition diagram of *pl*PHEA in Figure 3.105.

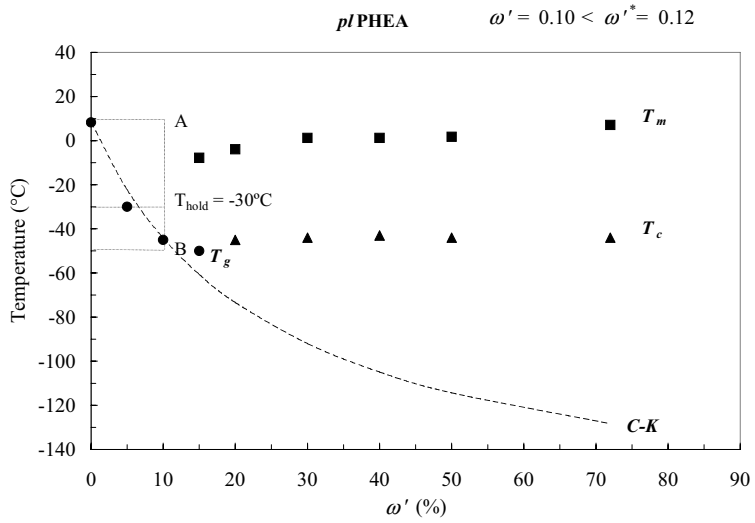

Figure 3.105. DSC experimental method (thermal path AT_{hold}BABA) drawn on the transition diagram of the *pl*PHEA present in PMMA1/70E-*gr*-*pl*PHEA(28.7%) for low water mass fractions (ω' = 0.10).

The first and second DSC heating scans from -50 to 10ºC after holding at -30ºC during several times are shown in Figures 3.106 and 3.107 respectively for *pl*PHEA. Since no sign of water melting for 1 hour of holding time at -30ºC, only the first DSC heating scans for 2 or more hours are shown. In the same way, only the second DSC heating scans for 16.7, 33.3 and 61,7 hours are shown due to no sign of melting was found from 0 to 33.3 hours of holding time.

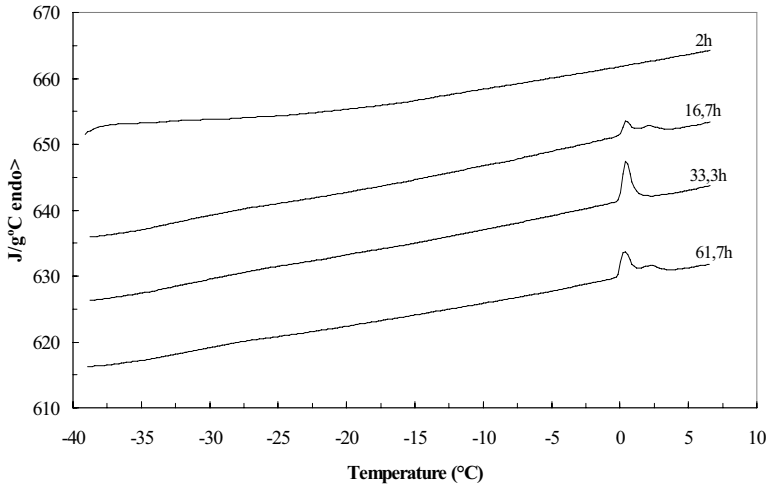

Figure 3.106. First DSC heating scans from -50 to 10ºC after holding at -30ºC for several times (2, 16.7, 33.3 and 61.7 hours) of the *pl*PHEA present in PMMA1/70E-*gr*-*pl*PHEA(28.7%) with low water mass fractions (ω' = 0.10). Exothermic heat flow calculated per gram of water.

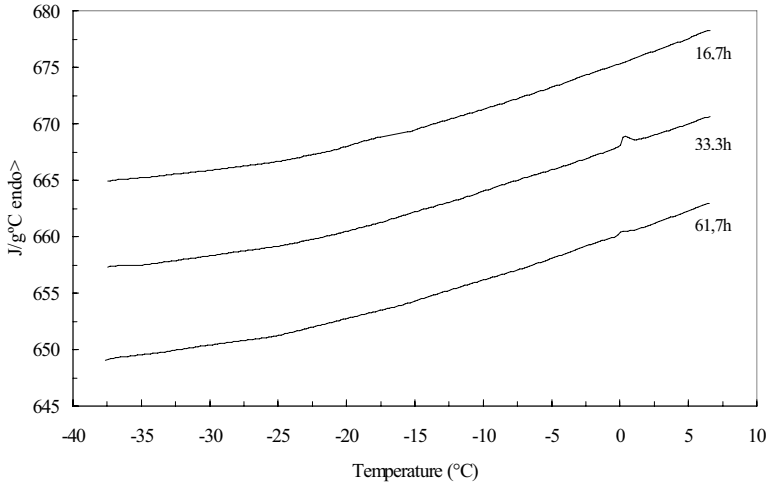

Figure 3.107. Second DSC heating scans from -50 to 10ºC after the first one and after holding at -30ºC for several times (16.7, 33.3 and 61.7 hours) of the *pl*PHEA present in PMMA1/70E-*gr*-*pl*PHEA(28.7%) with low water mass fractions (ω' = 0.10). Exothermic heat flow calculated per gram of water.

Figure 3.108 shows how the melting enthalpy of water also increases with increasing holding time for *pl*PHEA after the first heating scan. However,

after the second scan, the amount of crystallised water is close to 0%. After the first heating scan, there is very little free water (1.48% after 33.3 hours) which has time to mix with the *pl*PHEA.

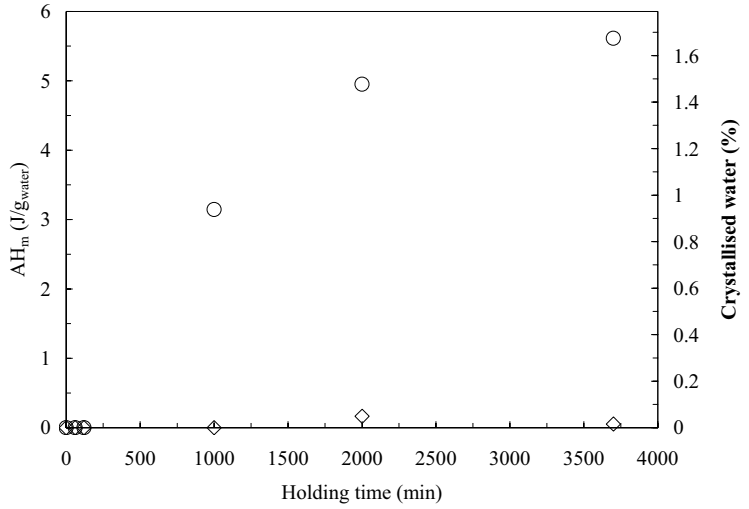

Figure 3.108. Melting enthalpy (ΔH_m) and wt.% of crystallised water as a function of the holding time at -30ºC after the first (○) and the second (◇) heating scans of the *pl*PHEA present in PMMA1/70E-*gr*-*pl*PHEA(28.7%) with low water mass fractions (ω' = 0.10).

For these low water mass fractions (ω' = 0.10) lower than the critical concentration (ω'^{**} = 0.12), water cannot crystallise without the isothermal step at -30ºC. However, this experiment demonstrates that when the temperature is cooled down to -30ºC and the sample is kept at this temperature for some time, crystallisation of water becomes possible again for this kind of PHEA even though having a water mass fraction lower than the critical one (ω'^{**}). In addition, the more time holding at -30ºC, the more amount of water crystallises and an equilibrium value of crystallised water must be achieved after a certain amount of time. All the melting peaks of water in *pl*PHEA appear also around 0ºC as free water (see Figure 3.106) because when the temperature is cooled down to -30ºC and kept at this temperature, water is segregated from the water-*pl*PHEA mixture as it occurred with bulk PHEA.

These results show a very important difference in the crystallisation of water for low water contents in bulk PHEA and *pl*PHEA. Much less amount of water is segregated from the water-*pl*PHEA mixture (1.68% after 61.7 hours) than from the water-bulk PHEA one (50.5% after 61.7 hours). This significant difference could be due to the influence of the hydrophobic polymer in the PMMA1/70E-*gr*-*pl*PHEA(28.7%) composite material.

4. Conclusions.

1. Poly(methyl methacrylate) polymerised under UV light with EGDMA as crosslinker and in the presence of 60 or more wt.% of ethanol gives rise to a structure of spherical polymer particles typical of macrosyneresis. For low ethanol contents, microsyneresis takes control in the phase separation process and the porous PMMA structures have part of the pores collapsed. This collapsed pores open when the samples are swollen in ethyl acetate increasing very much the porosity of the sample. For high ethanol contents, however, the porosity of the samples decreases in the swollen state because the PMMA microspheres swell occupying volume of pores. The cross-linker content has a strong influence in the transition from microsyneresis to macrosyneresis and PMMA10/50E shows the previous stage to this transition. The effect of cross-linking is more important when low solvent contents are added in the polymerisation process increasing porosity very much in microsyneresis. Nevertheless, for high solvent contents, in macrosyneresis, the effect of cross-linking is attenuated. The effect of the solvent content is very strong on the synthesis of macroporous PMMA. The increase of the ethanol content in the polymerisation process produces smaller PMMA microspheres with narrower diameter dispersion and more porosity.

2. The effect of porosity on the mechanical behaviour of the scaffold produced by macrosyneresis is more important than the effect of cross-linking. However, the storage modulus of the porous samples produced by microsyneresis depends on the crosslinking density very much. The storage modulus decreases very sharply with increasing porosity for ethanol contents greater than the critical one (60 wt.%) because the microspheres are more and more separated and the effective cross-section decreases. The main relaxation seems not to be influenced by the porosity appearing always at the same temperature for PMMA polymerised with 50, 60, 70 wt.% of ethanol. However, comparing samples with the same cross-linking density, bulk PMMA has the maximum of the main relaxation always at higher temperatures than macroporous PMMA. This feature must be due to the presence of ethanol in the polymerisation process, which helps cyclation producing a different chemical network or could be the effect of the surface energy due to the increase of specific area. The glass transition temperature measured by DSC is also higher for PMMA polymerised in the presence of 50 or more wt.% of ethanol than for bulk PMMA.

3. The slope of the log E' against temperature plot in the temperature range of the main relaxation, measured by DMS on PMMA scaffolds obtained by

macrosyneresis, decreases as the cross-linking density increases. This feature cannot be reproduced using the block model of Takayanagi in which the pores are considered as a dispersed phase. This means that the adhesion between PMMA microspheres depends very much on the cross-linker content and the Takayanagi model does not predict this adhesion, which is essential here.

4. Poly(2-hydroxyethyl acrylate) hydrophilic coatings can be grafted onto macroporous poly(methyl methacrylate) by adsorbing monomer vapour and subsequent plasma polymerisation without the need of thermal or photoinitiators. The amount of grafted *pl*PHEA can be controlled with the sorption time of HEA vapour. An homogeneous coating is formed around all the PMMA microspheres inside and on the surface of macroporous PMMA according to the FTIR measurements. This plasma-polymerised PHEA coating is pure because it is obtained after adsorbing HEA monomer vapour. The plasma-polymerised PHEA cannot be dissolved in water probably because it is cross-linked in some extent and interpenetrated. It is very stable chemically and only in very drastic conditions (immersion in boiling water for 10 days) can it suffer hydrolytic degradation. The formation of the hydrophilic coating can be clearly observed by scanning electron microscopy.

5. The *pl*PHEA coating is more homogeneously interpenetrated with macroporous PMMA polymerised with 5 wt.% of EGDMA because there is more cross-linker. The *pl*PHEA grafted onto macroporous PMMA with 1 wt.% of EGDMA is less homogeneously interpenetrated (mostly on the surface of the PMMA microspheres). Thus, the porosity of macroporous PMMA polymerised with 1 wt.% of EGDMA decreases after plasma polymerisation and hardly changes in macroporous PMMA with 5 wt.% of EGDMA.

6. The *pl*PHEA coating improves the mechanical properties of macroporous PMMA because it produces a better adhesion between the PMMA microspheres. Thus, the PMMA-*gr*-*pl*PHEA hydrogels synthesised in this work are hydrophilic porous materials with a very high storage modulus at room temperature. These composite materials can absorb water because of the hydrophilic *pl*PHEA layer and keep their mechanical properties due to the hydrophobic PMMA structure. Their dynamic-mechanical properties are much better than those of other macroporous hydrogels due to the connection obtained between all the PMMA-*gr*-*pl*PHEA microspheres.

7. The effect of porosity or crosslinking density on the thermal degradation of macroporous PMMA is very low. However, the effect of crosslinking is

very significant on the thermal degradation of PMMA-*gr*-*pl*PHEA because of the more or less homogeneous interpenetration. The degradation velocity of PMMA-*gr*-*pl*PHEA slightly decreases with increasing the *pl*PHEA content because the more *pl*PHEA present in the macroporous structure of PMMA, the more difficult it is for the degradation products to diffuse because of hydrogen bonding. PMMA-*gr*-*pl*PHEA degrades at lower temperatures than bulk PHEA due to the presence of PMMA.

8. The water sorption capacity from the gas phase of bulk PMMA increases with increasing EGDMA content because the number of polar COO groups increases with increasing EGDMA content. For low water activities, macroporous PMMA has higher equilibrium water uptakes from the gas phase than bulk PMMA because it has a very large specific area where water can be adsorbed. For high water activities, however, water sorption of bulk PMMA is higher than macroporous PMMA due to water clusters, which impede water sorption inside the pores. After grafting *pl*PHEA onto macroporous PMMA, water sorption considerably increases. From 0 to 40% of relative humidity, *pl*PHEA absorbs more water than bulk PHEA because of the high specific area of these composite materials. For $0.4 < rh < 0.7$, both kinds of PHEA absorbs similar amounts of water. However, for high relative humidities ($0.7 < rh < 1$), the expansion of the polymer network starts having effect on the water sorption from the gas phase. The elastic energy of *pl*PHEA interpenetrated in the PMMA network produces a decrease in the water sorption. However, bulk PHEA is neither cross-linked nor interpenetrated and can expand its network increasing considerably the amount of absorbed water.

9. Porosity and cross-linking density have a similar effect of increasing the desorption diffusion coefficient of macroporous PMMA. On the other hand, the *pl*PHEA coating decreases the speed of the desorption process. The diffusion coefficient decreases very sharply after the plasma polymerisation because hydrophilic polymers show lower diffusion coefficients due to hydrogen bonding. The desorption diffusion coefficients of *pl*PHEA present in PMMA-*gr*-*pl*PHEA polymerised with 5 wt.% of EGDMA are higher due to the homogeneous interpenetration of the *pl*PHEA. The desorption diffusion coefficients of PMMA-*gr*-*pl*PHEA also increase with increasing porosity and cross-linking density. After immersion in liquid water, most water suffers evaporation in the desorption process because there is free water inside the pores of macroporous PMMA and PMMA-*gr*-*pl*PHEA. Water diffusion necessarily occurs after evaporation is completed but is negligible in comparison with the large amount of water present in the pores. This diffusion contribution is more important in bulk PHEA but still much less important than evaporation. The water uptakes obtained after

equilibrium in liquid water are higher in PMMA-gr-*pl*PHEA than in macroporous PMMA even though the *pl*PHEA coating decreases the porosity of the PMMA samples polymerised with 1 wt.% of EGDMA. The swollen *pl*PHEA must deform the porous PMMA structure increasing porosity. This increase of water sorption could also occur because the *pl*PHEA coating allows water to penetrate in pores, which were inaccessible without the hydrophilic coating.

10. The kinetics of water crystallisation for high water contents in bulk PHEA and *pl*PHEA are quite different. Water crystallises much faster in *pl*PHEA than in bulk PHEA. The transition diagrams of water/PHEA and water/*pl*PHEA have been determined. They show less undercooling of water crystallisation in *pl*PHEA than in bulk PHEA. When swollen bulk PHEA and swollen *pl*PHEA (both with $\omega' = 0.10$) are kept at -30ºC for some time, crystallisation of water becomes possible even though with this low water mass fraction no crystallisation can be observed in the cooling or heating DSC thermograms. Crystallisation occurs because water is segregated from the water/polymer mixture in the isothermal step at -30ºC. All the melting peaks of water in bulk PHEA and *pl*PHEA appear around 0ºC as free water. Much less water is segregated from the water-*pl*PHEA mixture (1.68% after 61.7 hours) than from the water-bulk PHEA one (50.5% after 61.7 hours) probably due to the influence of the hydrophobic polymer in the PMMA1/70E-*gr*-*pl*PHEA(28.7%) composite material.

Glossary

a	activity
rh	relative humidity
v	specific volume
v_b	specific volume of bulk polymers
$v_{swollenb}$	specific volume of bulk polymers after immersion
v_{app}	apparent specific volume
v_{PHEA}	specific volume of bulk PHEA
V_b	volume of bulk polymers
ρ	density
$\rho_{n\text{-}octane}$	density of n-octane
m	mass
m_{air}	mass of a sample in air
$m_{n\text{-}octane}$	mass of a sample immersed in n-octane
P_{d1}	porosity in the dry state determined from v_{app}
P_{d2}	porosity in the dry state determined by swelling in water
P_s	porosity in the swollen state determined by swelling in ethyl acetate
w	solvent content
w_b	solvent content of bulk polymers
w'	solvent content referred to the dry mass of the hydrophilic component
ω	mass fraction of solvent
ω_b	mass fraction of solvent in bulk polymers
ω'	mass fraction of solvent in the hydrophilic component
T_{gh}	glass transition temperature curve of hydrogels
E'	storage modulus
E''	loss modulus
$tan\ \delta$	loss tangent
E'_g	storage modulus in the glassy state
E'_r	storage modulus in the rubbery state
$\phi_{solvent}$	volume fraction of solvent
T_g	glass transition temperature
T_m	melting temperature
T_c	crystallisation temperature
$\overline{Me}$	mean molecular weight between cross-links of the elastically active chains.
α	expansion coefficient

α_g	expansion coefficient in the glassy state
α_r	expansion coefficient in the rubbery state
ϕ	volume fraction of the disperse phase in the Takayanagi block model (*pl*PHEA in the PMMA-*gr*-*pl*PHEA composite material).
λ	volume fraction of the continuous phase in series in the Takayanagi block model
X_{plPHEA}	mass fraction of *pl*PHEA in the PMMA-gr-*pl*PHEA composite material
T^{α}_{plPHEA}	maximum temperature of the α relaxation of *pl*PHEA
T^{α}	maximum temperature of the α relaxation of polymers
T^{β}_{PMMA}	maximum temperature of the β relaxation of PMMA
T_{g0}	glass transition temperature of dry polymers
T_{gw}	glass transition temperature of water
Δc_p	Heat capacity increment at T_g and constant pressure
Δc_{pw}	Heat capacity increment of water at T_g and constant pressure
Δc_{p0}	Heat capacity increment of dry polymers at T_g and constant pressure
D	diffusion coefficient
bulk polymer	non-porous polymer
SEM	scanning electron microscopy
DMS	dynamic-mechanical spectroscopy
DSC	differential scanning calorimetry
TGA	thermogravimetric analysis
TG	thermogravimetry
FTIR	fourier transform infrared spectroscopy
ATR	attenuated total reflectance spectroscopy
PMMA	poly(methyl methacrylate)
PMMABx	bulk PMMA polymerised with x% of EGDMA
PHEA	poly(2-hydroxyethyl acrylate)
EGDMA	ethylene glycol dimethacrylate
IPN	interpenetrated polymer network
PMMAx/yE	PMMA polymerised with x% of EGDMA and y% of ethanol
plPHEA	plasma-polymerised PHEA
PMMA-gr-plPHEA	PMMA with grafted *pl*PHEA coating
PMMAx/yE-gr-plPHEA(z%)	PMMAx/yE with z% of *pl*PHEA

References

[1] Dimitriu S. (ed.), *Polymeric Biomaterials*, Marcel Dekker, N.Y. (1994)
[2] Szycher M. (ed.), *High Performance Biomaterials*, Technomic Pu., Lancaster (1991)
[3] Vallet Regi M., Munera L. (ed.), *Biomateriales aqui y ahora*, Dykinson, Madrid (2000)
[4] Peppas N. A. (ed.), *Hydrogels in medicine and pharmacy*, vol. 3., CRC Press, Boca Raton, Fl. (1987)
[5] Hoffman A. S., *Hydrogels-a broad class of biomaterials*. In: Kronenthal, Oser, Martin, editors., *Polymers in medicine and surgery*, New York, Plenum Press, 33-43 (1975)
[6] Tanzawa H., Nagaoka S., Suzuki J., Kobayashi S., Masubuchi Y., Kikuchi T., *Cell adhesion and growth on the surface of synthetic hydrogels*, In: Goldberg E, Nakajima A., editors. Biomedical polymers, Academic Press, 189-211 (1980)
[7] Peppas N. A., Langer R., Science, 263:1715 (1994)
[8] Bell C. L., Peppas N. A., Adv. Polym. Sci., 122:125 (1995)
[9] Ozawa H., Hosaka S., Kuminoto T., Tanzawa H., *Biomaterials*, 5:170 (1988)
[10] Monleón Pradas M., Gómez Ribelles J. L., Serrano Aroca A., Gallego Ferrer G., Suay Anton J., Pissis P., Colloid Polym. Sci. 279, 323-330 (2001)
[11] LaPorte R. J., *Hydrophilic polymer coatings for medical devices,* Technomic Pub., Basel (1997)
[12] Kroschwitz J. I. (ed.), Encyclpedia of Polymer Science and Engineering, vol 7. Wiley-Interscience, N. Y.,article 'Hydrogels' (1987)
[13] AB Ferrosan, European Patent 41934
[14] Fulmer Yarsley Ltd., European Patent 301753
[15] Kazanskii K. S., Dubrovskii S. A., *Adv. Polym. Sci.*, 104, 97 (1992)
[16] Hwang J. R., Sefton M. V., *J. Membr. Sci.*, 108, 257 (1995)
[17] Yan Q., Hoffman A. S., *Polymer*, 36, 887 (1995)
[18] Haldon R. A., Lee B. E., *Br. Polym. J.*, 4, 491 (1972)
[19] Park Y. J., Lee Y. M., Park S. N., Sheen S. Y., Chung C. P., Lee S. J., *Biomaterials*, 21, 153 (2000)
[20] Shapiro L., Cohen S., *Biomaterials*, 18, 583 (1997).
[21] Thomson R. C., Yaszemski M. J., Powers J. M., Mikos A. G., *J. Biomater. Sci. Polymer Edn.*, 7; 23 (1995)
[22] Plant G. W., Harvey A. R., Chirila T. V., *Brain Res.*, 671, 119 (1995)
[23] Chirila T. V., Constable I. J., Crawford G. J., Vijayasekaran S., Tompson D. E., Chen Y., -C., Fletcher W. A., Biomaterials, 14, 26 (1993)
[24] Crawford G. J., Constable I. J., Chirila T. V., Vijayasekaran S., Thompson

D. E., *Cornea*, 12, 348 (1993)
[25] Corkhill P. H., Fitton J. H., Tighe B. J., *Biomater. Sci.*, *Polym. Ed.*, 4, 615 (1993)
[26] Soichet M. S, Hubbell J. A., *Polymers for Tissue Engineering.* VPS, Utrecht (1998)
[27] Naraghi K., Soussand J., Félix J. M., Schimshowisch S., Lutz P. J., *Polym. Prepr.*, 39, 196 (1998)
[28] Kang H. W., Tabata Y., Ikada Y., *Biomaterials*, 20, 1339 (1999)
[29] Chen Y. S., Hsieh C. L., Tsai C. C., Chen T. H., Cheng W. C., Hu C. L., Yao C. H., *Biomaterials*, 21, 1541 (2000)
[30] Miyoshi H., Yanagi K., Fukuda H., Ohsima N., *Artif. Organs*, 20, 803 (1996)
[31] Wyre R. M., Downes S., *Biomaterials*, 21, 335 (2000)
[32] Rosen J. J., Schway M. B., *Polym. Sci. Technol*., 12, 667 (1980)
[33] Horbett T. A., Schway M. B., Ratner B. D., *J. Colloid Interf. Sci.*, 104, 28 (1985)
[34] Lyndon M. J., *Br. Polym. J*., 18, 22 (1986)
[35] Altankov G., Groth T.H., *J. Mater. Sci.: Materials in Medicine*, 5, 732 (1994)
[36]Kiremitçi M., Gürhan I., Pişkin E., *Biotech. and Appl. Biochem.*, 14, 170 (1991)
[37] Arora K. A., Lesser A. J., McCarthy T. J., *Polym Engng Sci.*, 38, 2055 (1998)
[38] Thomson R. C., Wake M. C., Yaszemski M. J., Mikos A. G., *Adv. Polym. Sci.*, 122, 245 (1995)
[39] Arica M. Y., Hasirci V. N., *Polymer International*, 32, 177 (1993)
[40] Chen J. H., Ruckenstein E., *J. Appl. Polym. Sci.*, 45, 377 (1992)
[41] Adrianova G. P., Parkhomov S. I., *Polym. Engng Sci.*, 37, 1367 (1997)
[42] Murphy S. M., Skelly P. J., Tighe B. J., *J. Mater. Chem., Chem.*, 2, 1007 (1992)
[43] Shapiro L., Cohen S., *Biomaterials*, 18, 583 (1997)
[44] Song S. W., Torkelson J. M., *Macromolecules*, 27, 6389 (1994)
[45] Bennett D. J., Burford R. P., Davis T. P., Tilley H. J., *Polymer International*, 36, 219 (1995)
[46] Dietmar W. Hutmacher, *Biomaterials*, 21, 2529 (2000)
[47] Okay O., *J. Appl. Polym. Sci.*, 74, 2181 (1999)
[48] Dušek K., *J. Polym. Sci. C.*, 16, 1289 (1967)
[49] Dušek K., *Polymer Networks-Structure and Mechanical Properties*, Chompff A. J.,Newman S., (eds.). Plenum Press, N. Y. (1971)
[50] Monleón Pradas M., Gómez Ribelles J. L., Serrano Aroca A., Gallego Ferrer G., Suay Anton J., Pissis P., *Polymer*, 42, 4667-4674 (2001)
[51] Inagaki N., *Plasma surface modification and plasma polymerisation*,

Technomic Publishing Company, Inc. (1996)
[52] Kroschwitz, Jaqueline I*, Polymers: An encyclopedic sourcebook of engineering properties*, John Wiley&Sons, Inc., Encyclopedia reprint series (1987)
[53] Espadero Berzosa A., Gómez Ribelles J. L., Kripotou S., Pissis. P, *Macromolecules*, 37, 6472 (2004)
[54] Takayanagi M., *Memoirs of the Faculty of Engineering Kyushu Univ.*, 20, 2691 (1976)
[55] Dickie R. A., *Polymer blends*, (ed. Paul D. R. and Newman S.), Vol.1, 353-388; San Diego, Academic Press (1978)
[56] Ouali N., Cavaillé J. Y., Perez J., *Plast. Rubber Compos. Process. Appl.*, 16, 55 (1991)
[57] Torregrosa Lopez J.I., Escoto Palacios M. J., Martinez Sanchez M. A., Verdú Sanchez E., Gómez Ribelles J. L., Monleón Pradas M., Meseguer Duenyas J. M., Romero Colomer F., *Plast. Rubber Compos. Process. Appl.*, 25, 427 (1996)
[58] Gómez Ribelles J. L., Manyo Sebastia J.,Marti Soler R., Monleón Pradas M., Ribes Greus A., Suay Anton J., *J. Appl. Polym. Sci.*, 42, 1647 (1991).
[59] Díaz Calleja R., Gómez Ribelles J. L., Monleón Pradas M., Ribes Greus A., Romero Colomer F., *Polym. Compos*., 12, 428 (1991)
[60] Gómez Ribelles J. L., Monleón Pradas M., Más Estellés J., Meseguer Dueñas J. M., Romero Colomer F., *Plast. Rubber Compos. Process. Appl.*, **18**, 169 (1992)
[61] Iisaka K., Shibayama K., *J. Appl. Polym. Sci.*, 22, 1321 (1978)
[62] Denes F., Sarmadi A. M., Hop C. E. C. A., Young R. A., *Journal of Applied Polymer Science: Applied Polymer Symposium,* 54, 55 (1994)
[63] Iizawa T., Morimoto T., Yamaguchi T., Kato S., *Polymer*, 45, 5077 (2004)
[64] Hajji P., David L., Gerard J. F., Pascault J. P., Vigier G., *Journal of Polymer Science: Part B: Polymer Physics*, 37, 3172 (1999)
[65] Perova T. S., Vij J. K., Xu H., *Colloid Polym Sci*, 275, 323 (1997)
[66] Bill George, Peter McIntyre, *Infrared Spectroscopy*, Analytical Chemistry by open learning, John Wiley&Sons, London (1987).
[67] Jack L. Koening, *Spectroscopy of Polymers*, Case Western Reserve University, American Chemical Society, Washington, DC (1992)
[68] Keattch C. J., Dollimore D., *Introduction to thermogravimetry*, Ch.1, Heyden, London (1975)
[69] Rodigrez F., *Principles of Polymer Systems* (2^{nd} edn), Ch. 11, McGraw-Hill, Singapore (1983)
[70] Haines P. J., *Thermal methods of analysis: Principles, applications and problems*, Blackie Academic & Professional, Capman & Hall, Great Britain (1995)
[71] Yu-Hsiang H., Chuh-Yung C., Cheng-Chien W., *Polymer Degradation and*

Stability, 84, 545 (2004)
[72] Arisawa H., Brill T. B., *Combustion and Flame*, 109, 415 (1997)
[73] Demirelli K., Coşkun M., Kaya E., *Polymer Degradation and Stability*, 72, 75 (2001)
[74] Çaykara T., Özyürek C., Kantoğlu Ö., Erdoğan B., *Polymer Degradation and Stability*, 80, 339 (2003)
[75] Adamson A. W., *Physical Chemistry of Surfaces*, 5th ed. J. Wiley & Sons (1990)
[76]Gregg S. J., Sing K. S. W., *Adsorption , surface area and porosity*, 2nd ed., Academic Press, London (1982)
[77] IUPAC Report, *Pure & Appl. Chem.*, 57, 603 (1985)
[78] Altankov G., Groth T. H., *J. Mater. Sci.: Materials in Medicine*, 5, 732 (1994)
[79] Guggenhein E. A., *Applications of Statical Mechanics*, Clarendon Press, Oxford (1966)
[80] Timmermann E. O., *J. Chem. Soc., Faraday Trans. 1*, 85, 1631 (1989)
[81] Gallego Ferrer G., Monleón Pradas M., Gómez Ribelles J. L., Salmerón Sánchez M., *Polymer*, 45, 6207 (2004).
[82] Světlík J., Pouchlý J., *Eur. Polym. J.*, 12, 123 (1976)
[83] Pouchlý J., Biroš J., Beneš S., *Makromol. Chem.*, 180, 745 (1979)
[84] Galin J. C., Galin M., *J. Polym. Sci. B: Polym. Phys.*, 30, 1113 (1992)
[85] Lewicki P. P., *Int. J. Food Sci. Technol.*, 32, 553 (1997)
[86]Wolf W., Spiess W. E. L., Jung G., *J. Food Engng.*, 3, 51 (1984)
[87] Crank J., Park G. S. (eds.), *Diffusion in Polymers*, Academic Press, London (1968)
[88] Peppas N. A., Brannon-Peppas L., *J. Food Engng.*, 22, 189 (1994)
[89] Crank J., *The Mathematics of Diffusion*, Clarendon Press, Oxford (1975)
[90] Van Krevelen D. W., Properties of polymers, 3rd ed. Elsevier, Amsterdam (1990)
[91] George S. C., Thomas S., *Prog. Polym. Sci.*, 26, 985 (2001)
[92] Zisman, W. A., Influence of Constitution on Adhesion from *Handbook of Adhesives*, edited by Skeist, Irving, New York: Van Nostrand Reinhold, p.37 (1977)
[93]Andrade J. D., Nagoaka S., Cooper S., Okano T., Kim S. W., *Surface and blood compatibility*, from ASAIO, 10, pp. 75-76 (1987)
[94] John M. S., Andrade J. D., Water and Hydrogels from *J. Biomed. Mater. Res.* (1973)
[95] Van Blitterwijk C. A., Bakker D., Hesseling S. C., Koerten H. K., Reaction of cells and implant surfaces from *Biomaterials*, 12, pp. 187-193 (1991)
[96] Young T., *Philos. Trans. Roy. Soc. London*, 95, p. 65 (1805)
[97] Höhne G., Hemminger W., Flammersheim H.-J., *Differential Scanning Calorimetry: an introduction for Practitioners.*, Springer-Verlag Berlin

Heidelberg (1996)
[98] Bershtein V.A., Egorov V.M., *Differential Scanning Calorimetry of polymers*., Ellis Horwood Limited (1994)
[99] Pedley D.G., Tighe B.J., *Br Polym. J.*, 11, 130 (1979)
[100] Nakamura K., Hatakeyama T., Hatakeyama H., *Polymer*, 24, 871 (1983)
[101] Burghoff H.G., Pusch W., *J. Appl. Polym. Sci.*, 23, 473 (1979)
[102] Sivashinsky N., Tanny G.B., *J. Appl. Polym. Sci.*, 26, 2625 (1981)

[103] Higuchi A., Komiyama J., Iijima T., *Polym. Bull.*, 11; 203 (1984)
[104] Rault J., Lucas A., Neffati R., Monleón Pradas M., *Macromolecules*, 30, 7866 (1997)
[105] Rault J., Gref R., Ping Z.H., Nguyen Q.T., Néel J., Polymer, 36, 1655 (1995)
[106] Rault J., Ping Z.H., Nguyen Q.T., *J. Non-Cryst. Solids*, 172/174, 733 (1994)
[107] Rault J., *Makromol. Chem.*, 31, 100 (1995)
[108] Rault J., Ping Z.H., Nguyen Q.T., *Poymer Bull.*, 35, 649 (1995)
[109] Salmerón Sánchez M., *On the nature of thermal transitions in acrylic polymer gels, Dr. Eng. Sci. Thesis*, Ed. ProQuest Information and Learning Company, ISBN 0-493-232-79-6 (2003)
[110] Rault J., *Les polymères solides. Amorphes, élastomères, semi-cristallins. Propiétés microscopiques et macroscopiques*, Cépaduès-Éditions (2002)
[111] Fox T.G., *Bull. Am. Phys. Soc*., 1, 123 (1953)
[112] Couchman P.R., *Macromolecules*, 11, 1156 (1978)
[113] Couchman P.R., *Macromolecules*, 20, 1712 (1987)
[114] Pouchlý J., Biroš J., Beneš S., *Makromol. Chem.*, 180, 745 (1979)
[115] Molyneux P., in: *Water. A Comprehensive Treatise*., vol. 4, F. Franks (ed.), Plenum Press, New York (1971)
[116] Warren T. C., Pims W., *Macromolecules*, 5, 506 (1972)
[117] Greenspan L., J Res Natl Bur Stand, US, 81:89 (1977)
[118] Serrano Aroca A., Campillo Fernández A. J., Gómez Ribelles J. L., Monleón Pradas M, Gallego Ferrer G., Pissis P., *Polymer, 45*, 8949 (2004)
[119] Chirila T. V., Chen Y. C., Griffin B. J., Constable I. J., *Polymer International*, 32, 221 (1993)
[120] Brandrup J. (ed.), Immergut E. H. (ed.), *Polymer Handbook*, John Wiley&Sons, Inc. (1975)
[121] Erman B., Mark J. E., Structure and properties of rubberlike networks. Oxford University Press, Oxford (1997)
[122] Anthony B. C., Chirila T. V., Dalton P. D., *Polymer International*, 42, 45 (1997)
[123] Martins M. C. L., Wang D., Ji J., Feng L., Barbosa M. A., *Biomaterials*, 24, 2067 (2003)

[124] Zhang J, Peppas N. A., *Journal of Applied Polymer Science*, 82, 1077 (2001)
[125] Amass W., Amass A., Tighe B., *Polym. Int.*, 47, 89 (1998)
[126] Gallego Ferrer, G., *Structure and properties of polymer hydrogels based on interpenetration of a hydrophilic and a hydrophobic network Dr. Eng. Sci. Thesis*, Ed. ProQuest Information and Learning Company, UMI number: 3041278, ISBN 0-493-54613-8 (2002)
[127] Bajpai R., Krishna Kumar M., Datt S. C., Reddy B. S. R., *J. Polym. Mater.*, 13, 147 (1996)
[128] Gómez Ribelles J. L., Monleón Pradas M., Gallego Ferrer G., Peidro Torres N., Pérez Giménez V., Pissis P., Kyritsis A., *Journal of Polymer Science: Part B: Polymer Physics*, 37, 1587 (1999)
[129] Sánchez-Moral S., Ordóñez S., Benavente D., García del Cura M. A., *Sedimentary Geology*, 148,221 (2002)
[130] Franks F., in: *Thermal Analysis, vol 2.* W. Hemminger (ed.) (1980)
[131] Mackenzie A. P., Rasmussen D. H., in [132]. P. 146
[132] Yasuda H., Olf H. G., Crist B., Lamaze C. E., Peterlin A., in: *Water Structure at the Water-Polymer Interface.* Jellinek H. H. G. (ed.), Plenum Press, N. Y. (1973)
[133] Johari G. P., Hallbrucker A., Mayer E., *Nature,* 330, 552 (1987)